S. Kim R. Williams
Karin D. Caldwell *Editors*

Field-Flow Fractionation in Biopolymer Analysis

Springer

Field-Flow Fractionation in Biopolymer Analysis

S. Kim R. Williams • Karin D. Caldwell
Editors

Field-Flow Fractionation in Biopolymer Analysis

Springer

Editors
Prof. S. Kim R. Williams
Laboratory for Advanced Separations Technologies
Department of Chemistry and Geochemistry
Colorado School of Mines
Golden, CO 80401
USA
krwillia@mines.edu

Prof. Karin D. Caldwell
Department of Physical and Analytical Chemistry
Section of Surface Biotechnology
Uppsala University
75123, Uppsala
Sweden
karin.caldwell@biorg.uu.se

SpringerWienNewYork is a part of Springer Science+Business Media
springer.at

Typesetting: SPi, Pondicherry, India

Printed on acid-free and chlorine-free bleached paper
SPIN: 12803026

With 93 Figures

Library of Congress Control Number: 2011944221

ISBN 978-3-7091-0153-7 e-ISBN 978-3-7091-0154-4
DOI 10.1007/978-3-7091-0154-4
SpringerWienNewYork

Preface

The collection of analytical techniques suitable for separation and characterization of fragile biopolymers contains, among many others, a group of methods collectively referred to as Field-Flow Fractionation (FFF). Common to these methods is that they are liquid phase elution techniques, in which the separation is executed in open channels unobstructed by solid packing materials, and that they offer a wide resolution range particularly well suited for macromolecules and particles. Recently, these techniques have had a strong upswing in use, especially due to the increased availability of convenient–to-handle commercial instrumentation. The FFF techniques differ from each other in terms of the field chosen to accomplish selectivity, e.g. thermal, gravitational, electrical, etc. Today, the hydrodynamic "flow field" is most commonly used, and hence the present collection of articles focuses extensively, although not exclusively, on a number of attractive applications of flow FFF to problem solving in the biomedical field. The growth of a technique brings with it nonuniformity in terminology. For example, asymmetrical flow FFF is commonly designated as AsFlFFF or AF4. This variation is apparent in the published literature and was purposefully maintained in this book.

Chapter 1 describes the theory of flow FFF, both in the symmetric and asymmetric channels presently in use. The evolution and fine-tuning of the technique is discussed in conjunction with the effects of channel dimensions and operating conditions on retention and resolution.

Chapter 2 discusses the choice of membrane to serve as sample accumulation wall in the flow FFF channel. The discussion leads to a scrutiny of sample recovery in relationship to membrane composition and zonal compression (retention).

Chapter 3 introduces the tubular, hollow fiber flow FFF channel which provides the advantage of being easy to replace, as one eliminates cross-over between runs. Through this approach sample volumes can be kept low to allow for MS-analysis on line.

Chapter 4 advances the technique into the 2D domain, where the first dimension is an isoelectric focusing and the second is a size-based separation accomplished by

asymmetric flow FFF. The system design is described and the technique is proven amply suited for problem-solving in proteomics.

Chapter 5 illustrates the use of flow FFF in pharmaceutical problem solving. Target identification and development of production processes are discussed in conjunction with process analytical technology formulation (PAT) and use in the discovery phase of protein therapeutic development.

Chapter 6 is another pharmaceutical application. It examines the analytical reliability of flow FFF and compares it to the performance of AUC and the work horse SEC in characterizing pharmaceutical proteins in terms of purity and aggregation.

Chapter 7 constitutes a detailed study on protein aggregate formation in the flow FFF channel, with or without crossflow.

Chapter 8 illustrates how the flow FFF technique, unlike the packed bed based SEC, can demonstrate weak protein interaction ($K_D > \mu M$) and analyze the components participating in complex formation under different conditions.

Chapter 9 examines the wide resolution range of the FFF techniques and demonstrates its particular value for particles produced for drug delivery and as an on-line sample clean-up tool to remove non-specific background molecules and enhance signal-to-noise ratio in immunoassays.

Chapter 10 demonstrates how highly complex protein structures, such as prions, can be purified and analyzed using flow FFF thus allowing correlation of protein aggregate size and structure to infectivity.

Chapter 11 presents the sedimentation FFF technique in its capacity as a sensitive mass balance which allows an exact and reproducible determination of the number of molecules – be it proteins or synthetic polymers- that are introduced to a nanoparticle surface during modification. This quantification allows a determination to be made e.g. of the specific binding of a protein to its substrate.

Chapter 12 gives a polymer chemist's use of the combination Flow FFF/MALS in the analysis of a range of starches and other polysaccharides in terms of e.g. molecular weight, size, and branching.

Chapter 13 addresses nanoparticles used for drug and gene delivery and the required evaluation of size as well as load. The AF4 is shown to be invaluable in determination of both size and size distribution, comparing favorably with DLS, AUC, and a number of microscopic techniques. The chapter contains an extensive literature review of FFF analyses of drug and gene delivery systems.

Chapter 14 discusses the studies of size and size distribution of liposomes, especially those intended for drug delivery purposes. The Flow FFF /MALS is shown to provide detailed insight into shifts in these parameters caused by shifts in fabrication conditions.

Chapter 15 demonstrates the ability of sedimentation FFF to sort populations of mammalian cells in terms of degree of maturation, differentiation and apoptosis. The cells remain undamaged by the sorting, which does not require binding of markers or specific identifiers to the cell surfaces.

Chapter 16 cells can be typed and enriched in miniaturized flow channels by dielectrophoretic FFF for which a theory is outlined in this chapter. The technique is

highly specific and does not require the binding of antibodies or other marker identifiers.

Chapter 17 reviews the use of flow and sedimentation FFF to determine size distributions of environmental and engineered nanoparticles. Nanoecotoxicity is an emerging field. Here size is an obvious characteristic of importance, as it relates to uptake and organ penetration. Hyphenation of the FFF channels with the element sensitive ICP-MS is shown to be of unique value in pinpointing environmental metal transport and understanding toxicity.

Golden, CO, USA *S. Kim R. Williams*
Uppsala, Sweden *Karin D. Caldwell*

Contents

Chapter 1
Flow FFF – Basics and Key Applications

Karl-Gustav Wahlund and Lars Nilsson

Abstract The 1990s and 2000s have seen a rapidly growing use of flow field-flow fractionation (flow FFF, FlFFF). As of today hundreds of publications in many different application areas are presented each year in which flow FFF has been used or is referred to. In this chapter a brief historical overview of flow FFF is given. Channel designs and basic principles are discussed as well as approaches to development of rapid high resolution separations. Finally, an overview of key applications is included with pioneering and ground-breaking papers from literature.

Keywords Flow field-flow fractionation • Flow FFF • Trapezoidal asymmetrical channel • Asymmetrical flow FFF • Protein aggregates • Plasmids • High resolution • Rapid separations • H-value • Time-average velocity • Velocity gradient • Polysaccharides • Ultra-high molar mass • Zone broadening

1.1 Flow Field-Flow Fractionation

The 1990s and 2000s have seen a rapidly growing use of flow field-flow fractionation (flow FFF, FlFFF). As of today hundreds of publications in many different application areas are presented each year in which flow FFF has been used or is referred to. Such growth is necessarily dependent on the introduction of commercial equipment.

The development of flow FFF to its present state can be can be traced back to the theories and research by the late J. Calvin Giddings [1, 2] and his group and has

K.-G. Wahlund (✉)
Unit for Analysis and Synthesis, Department of Chemistry, Lund University, Lund, SE, Sweden
e-mail: Karl-Gustav.Wahlund@organic.lu.se

L. Nilsson
Department of Food Technology, Engineering and Nutrition, Lund University, Lund, Sweden

S.K.R. Williams and K.D. Caldwell (eds.), *Field-Flow Fractionation in Biopolymer Analysis*, DOI 10.1007/978-3-7091-0154-4_1,

taken place in four development steps. The *first* step is represented by the first publication on flow FFF 1976 [3], tightly followed by several more [4–7]. The *second* step was the introduction of high-flow fractionations in 1986 to increase the separation speed [8]. The *third* step started in the mid-1980s also, still using high-flow fractionations, when a significant change of the construction of the flow FFF channel rendered the term asymmetrical flow FFF (AsFlFFF) [9]. The *fourth* step occurred in 1991 when the trapezoidal AsFlFFF channel was introduced [10–12]. This design has since been used in very successful commercial instrumentations.

The *first* step publications used separation channels that nowadays are often termed symmetrical flow FFF channels. They were of the parallel plate rectangular design using two permeable walls. The delivery of the carrier flow was obtained by peristaltic pumps. This necessarily led to using low flow rates ($<$ 1 ml/min), low migration velocities, and therefore very long retention times, typically many hours (1–5 h). Technically, the separations can be characterized as low-speed fractionations. Yet, because of the slow migration, excellent resolution between components was obtained. Applications were explored for many important sample types such as proteins [3, 5].

To obtain the same resolution, but with higher speed, it was necessary to go to the *second* development step. This utilized standard HPLC pumps capable of delivering flow rates in the range 0.5–10 ml/min, still using the parallel plate rectangular symmetrical channels. Thus the separation speed was increased so that the retention times were reduced to values within a 5–50 min range. This also eliminated a common adverse effect that was caused by sample immobilisation on the membrane when the crossflow velocity was high relative to the channel flow velocity [8]. Basically, this seems to have been caused by the limited channel flow rates that peristaltic pumps could create.

In the *third* development step the parallel plate rectangular design was again used but with only one permeable wall, i.e. the rectangular asymmetrical flow FFF channel. This offered a significant technical simplification. Again, separations were performed in 5–50 min. Later on, when experimental conditions were fine-tuned by further technical improvements (downstream central injection) and optimization of flow rates, the separation speed and resolution was much improved [13, 14]. High-speed high-resolution separations of a protein and its dimer was obtained in 15 min [13], then in 10 min, and even 3 min [14]. These advances made the way for AsFlFFF in a broader scientific community.

The *fourth* step introduced the trapezoidal geometry. Theoretical work showed that this design will give improved performance, as compared to the rectangular symmetrical channel and the rectangular asymmetrical channel, regarding peak dilution, which can be reduced by a factor of 4. Therefore the detection limit can be decreased and this makes it possible to decrease the sample load on the channel thus having better chances to avoid sample mass overloading and to reach lower mass detection limits. Further fine tuning of flow conditions and channel thickness made it possible to separate five components with complete resolution in 7 min, i.e. roughly one peak per minute [10]. This channel design is today used in all commercial instruments for flow FFF.

It may be mentioned that other scientists suggested flow FFF to be performed in cylindrical hollow fibers [15, 16] and parallel plate channels [17] and worked out complete theories. However, this never turned into experimentally useful separations. Full theoretical work on symmetrical and asymmetrical flow FFF with parallel plates was presented [18–20] but no useful experiments were demonstrated. Renewed interest and much improved experimental design of hollow fiber FFF took place in the late 1980s [21–23] but problems with the technical quality and stability of the fibers seem to have halted further work. Hollow fiber FFF was again revived in early 2000s [24–27] and later on excellent results were demonstrated especially as a pre-separation tool to proteomics analysis [28].

The work referred to above represents the so-called normal mode [29], which is applicable to submicron particles and macromolecules (5 to ~500 nm diameter). When sample components are micron-sized particles or macromolecules (~0.5–50 μm diameter) the fractionation mechanism can change into so called steric [30], hyperlayer, steric-hyperlayer, or focusing mode, which experimentally are nearly the same, and can result in high-speed particle separations (4 sec–2 min) sometimes effected by using extremely high flow rates (38 ml/min) [31–33]. However, the remainder of this chapter will only deal with normal mode separation since this is the mode that is useful for most biopolymer separations.

1.2 Basics

1.2.1 Principle

The principle of trapezoidal asymmetrical flow FFF is illustrated in Fig. 1.1. The crossflow drives sample components towards the ultrafiltration membrane, the accumulation wall, where they are confined to a thin concentrated layer [34, 35]. The Brownian motion yielding a transport in the opposite direction, away from the membrane, simultaneously causes a steady-state concentration distribution, i.e. the sample components will, after some time, have become relaxed in relation to the transport caused by the crossflow. The concentration distribution is exponential which means that the highest concentration is found at the wall whereas the concentration decreases exponentially with increasing distance from the wall. The thickness of the layer is characterized by the centre of gravity, l, of the concentration distribution. This can be thought of as a kind of mean distance from the wall and is under common experimental conditions of the order of a few micrometers. The relative distance from the wall, l divided by the channel thickness, w, is the most important retention parameter, symbolized by λ (see more below), since it directly governs the retention time and the zone broadening. Any decrease of the retention parameter λ contributes to increased retention time and increased resolution between components. Of course, the retention time can be modulated by the carrier flow velocity, which also however effects the resolution. Generally, it should be preferred to use as low λ as possible in combination with as

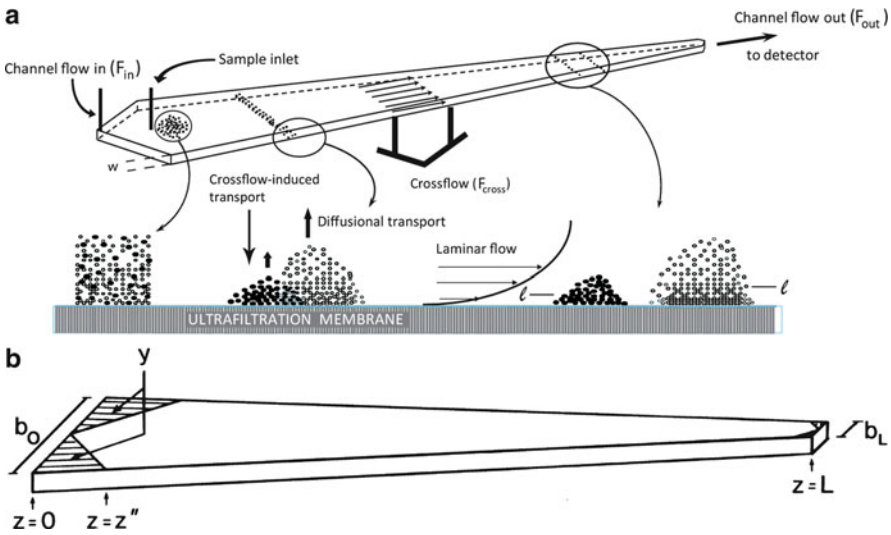

Fig. 1.1 The principle of trapezoidal asymmetrical flow FFF. (**a**) Illustration of the separation of two particles of different size. A homogeneous mixture was loaded through the sample inlet tube, then relaxed and focused at a short distance downstream from the sample inlet. When the elution flow starts the two particle populations start to migrate with different velocities. At the end of the channel the two zones have become resolved. Filled symbol = large particle. Open symbol = small particle. w = channel thickness. l = the centre of gravity distances of particle populations from the ultrafiltration accumulation wall. (**b**) The geometry of the trapezoidal channel. b_0 and b_L are the breadths of the trapezoid at the inlet and outlet ends. z denotes the distance along the length axis. z'' defines the length of the two cuts making up the area y. L is the channel length (Reproduced with permission from [10], © 1991, American Chemical Society)

high carrier velocity as possible in order to maximize resolution and minimize retention time. This is obtained by high crossflow velocity together with high carrier channel flow velocity [8]. The benefit of high crossflow velocity comes from its effect on a component's centre of gravity distance from the accumulation wall, i.e. the thickness of the component layer. The thinner the layer is, the lesser will be the contribution of non-equilibrium zone broadening. The reason is that the sample component's transversal Brownian motion is confined to a thinner layer, that is over a shorter distance. This contributes to decreased zone broadening as expressed by decreased H-value, and therefore increased resolution.

1.2.2 Channel Designs

1.2.2.1 Parallel Plate – Symmetrical

In the parallel plate symmetrical flow FFF the depletion wall ("top" plate) is a porous frit preferably made of porous ceramic [36]. The accumulation wall ("bottom" plate) has a semi-permeable ultrafiltration membrane supported by a

porous frit that is similar to the top wall. The separation channel is created by cutting out a suitable area in a spacer material, which then is squeezed between the top and bottom walls. The carrier liquid enters the so formed channel in one end (inlet end) and leaves through the other end (outlet end). Sample solutions or dispersions are introduced at the inlet end and separated sample components will exit the channel through the outlet end to be carried into a suitable flow-through detector.

Sample introduction has been performed by various techniques. A sample injection valve inserted in the inlet flow line is the simplest way and is combined with a stop-flow period immediately after the total sample volume has been displaced in order to let the relaxation take place. The frit inlet technique gives an improved starting distribution of the sample and takes care of the relaxation without using stop-flow.

1.2.2.2 Parallel Plate – Asymmetrical, Rectangular

The asymmetrical flow FFF channel was invented in order to simplify the channel construction and eliminate a potential negative influence of the presence of the upper wall frit. The latter was replaced by a solid non-porous material such as glass or PMMA [9] (Fig. 1.1). This channel rapidly gained acceptance since it gave results of higher resolution and speed than the symmetrical channel [9, 13, 14]. With the introduction of the focusing technique for sample introduction and relaxation together with shifting the sample injection point from the channel inlet tip to a few cm downstream the channel (downstream central injection, DCI) very time-efficient sample injection/relaxation could be made without any disturbing zone broadening [11, 13].

1.2.2.3 Parallel Plate – Asymmetrical, Trapezoidal

The trapezoidal version was introduced [10, 11] as a response to a specific limitation of the rectangular channel. When the crossflow rate was needed to be high (for relatively low molar mass or small nanoparticles) and therefore often constituting a large fraction of the channel inlet flowrate, the remaining channel flowrate at the channel outlet end was very low and consequently also the channel flow velocity. This can potentially lead to adverse effects. One was suspected to be a notable contribution from longitudinal diffusional zone broadening, the other a possible retardation or even immobilization due to a low ratio of channel flow velocity to crossflow velocity. The remedy to this was the invention of a channel that has a linearly decreasing breadth. This “trapezoidal” channel will naturally have a decreasing gradient in the longitudinal flow velocity, but sometimes a minimum [10] so that the velocity increases on approaching the channel outlet. A positive effect of the trapezoidal channels is that the detection sensitivity could be increased by at least a factor of 4 due to the low channel flowrate at the channel outlet end, so

that sample components were less diluted when entering the detector than in a rectangular channel. The trapezoidal channel is standard today.

1.2.3 Retention Parameters and Zone Broadening

For experimental purposes [37] it is most useful to consider retention in terms of the retention level, *RL*, which is defined as

$$RL = \frac{t_r}{t^0} \tag{1.1}$$

where t_r is the retention time and t^0 is the void time. Equation 1.1 expresses the number of void times in the retention time. This corresponds in some way to the retention factor used in chromatography. The importance of knowing the retention level is because it has a direct effect on the separation efficiency and then on the resolution, R_S. The resolution can be calculated [38] by

$$R_S = \frac{\Delta t_r}{\bar{w}_b} \tag{1.2}$$

where Δt_r is the difference in retention time between two peaks and $\bar{w}_b$ is the average of their base widths, which each are four standard deviations projected onto the baseline.

In fact, it is through proper choice of the retention level that the resolution between peaks can be optimized since the base width is strongly dependent on the retention level. When publishing fractograms it is therefore a good habit to mark or give the value of t^0 so that it can be easily concluded which retention level has been used.

For the trapezoidal channel the calculation of t^0 is made [10] by

$$t^0 = \frac{V^0}{F_{cross}} \ln\left[1 + \frac{F_{cross}}{F_{out}}\left(1 - \frac{w\left(b_o z' - \frac{b_o - b_L}{2L} z'^2 - y\right)}{V^0}\right)\right] \tag{1.3}$$

where V^0 is the volume of the channel (void volume) and w its thickness. The symbols b_0, b_L, z', y, and L, further define the geometry of the channel as explained in Fig. 1.1. F_{cross} is the crossflow volume rate and F_{out} the channel outlet flowrate.

The retention time can be directly measured in the fractogram whereas the void time should preferably be calculated directly from Eq. 1.3 [9, 10, 12–14, 37]. The reason to use Eq. 1.3 is that it is hardly possible to find an "unretained" sample component that is carried through the channel with the true void time although this has sometimes been practiced [9, 13]. Moreover, for accurate experimental measurement of the retention level, and parameters derived from it, any so called

"void peaks" in the most early part of the fractogram should not be used since their origin and migration character are not well defined.

The retention level can be directly related to the retention parameter λ by

$$RL = \frac{1}{6\lambda} \tag{1.4}$$

This is an approximation which is valid for most practical purposes [9, 12, 37], for example when $RL \geq 5.3$, if a 5% relative error is accepted [37]. Therefore it applies to nearly all relevant experimental conditions since good-resolution separations in any case requires much higher retention levels than 5 [7, 39].

Now, the retention parameter λ is defined by

$$\lambda = \frac{l}{w} \tag{1.5}$$

where l is the centre of gravity distance from the accumulation of the exponential sample component concentration distribution at the wall, as illustrated in Fig. 1.1. In this way λ becomes dimensionless and expresses the relative distance from the wall instead of the absolute (l).

Next, the centre of gravity distance is governed by

$$l = \frac{D}{u_0} \tag{1.6}$$

in which D is the diffusion coefficient of a sample component and u_0 is the crossflow velocity at the membrane surface. Then, the retention level can be expressed as

$$RL = \frac{wu_0}{6D} = \frac{wF_{cross}}{6AD} \tag{1.7}$$

which shows how it can be controlled by the experimental conditions, w and F_{cross}, if it is assumed that the area A of the accumulation wall membrane through which the crossflow passes is constant. Clearly, any increase of the crossflow rate will increase the retention level. Alternatively, increasing the channel thickness will also increase the retention level.

Finally, Eq. 1.7 shows also how the retention level depends on the property of sample components through their diffusion coefficients. Therefore the retention level increases in direct proportion to increasing molecular size (decreasing diffusion coefficients or increasing hydrodynamic diameters). Equations 1.2–1.4 demonstrate the importance of understanding the role of the retention parameters l and λ and how they can be regulated by the experimental conditions and therefore used to predict and control the retention level by Eq. 1.7.

Finally, the retention time can be predicted [9] by

$$t_r = \frac{w^2}{6V^o D} F_{cross} t^o \tag{1.8}$$

which means that for a given channel geometry (w, V^O) and a specified sample component of diffusion coefficient D only the crossflow rate remains to be adjusted except that this also will affect the void time. When this is accounted for by substitution for (1.3) the retention time expression becomes [12]

$$t_r = \frac{w^2}{6D} \ln\left(1 + \frac{F_{cross}}{F_{out}} B\right) \tag{1.9}$$

where B is the expression within square brackets in Eq. 1.3 and describes the channel geometry. Hence, for a given channel geometry and sample component diffusion coefficient the retention time can be simply controlled and adjusted by the ratio F_{cross}/F_{out}. If retention time prediction rather would be made based on a component's hydrodynamic diameter (d_h) the diffusion coefficient can be substituted for an expression based on the Stokes-Einstein equation.

The separation efficiency in an asymmetrical flow FFF channel is related to the H-value which expresses the zone variance per length unit as observed at the outlet end of the channel [40]. It is given [10–12, 14] by

$$\bar{H} = \frac{24\lambda^3 w^2}{D} \bar{v} = \frac{24\lambda^3 w^2}{D} \frac{(L - z')}{t^0} \tag{1.10}$$

where $\bar{H}$ is the average H-value as observed at the channel outlet, $\bar{v}$ is the time-average carrier velocity, and L-z' the effective channel length. This equation has the same mathematical form as that for symmetrical flow FFF channels [8] but there the carrier velocity and therefore the local H-value is constant throughout the channel length. Experimental determination of the $\bar{H}$-value can be based on [10–12, 14, 41]

$$\bar{H} = \frac{L\sigma_t^2}{t_r^2} \tag{1.11}$$

where σ_t is the peak standard deviation in time units.

1.3 Asymmetrical Flow FFF – Working Out Separations

The successful flow FFF separation of a multicomponent sample may have to reach several criteria. Firstly, of course, the resolution between peaks needs to be sufficient and this is fulfilled by $R_S \geq 1.5$. This corresponds to "complete" resolution between two sample component zones meaning that each zone is pure by 98% if

their concentration peak heights are equal. Sometimes a resolution value of about 1.0 may suffice. Another parameter is the separation speed, which directly relates to the retention time. Some users prefer high-speed separations for which a minimization of retention times is necessary. Another pre-requisite may be the peak concentration, which is of importance when the detection sensitivity is low or when sample mass is limited. The latter can happen when overloading phenomena occur such as for ultra-high molar mass polymers [42, 43].

As opposed to the situation in column chromatography, optimisation of separation experiments in AsFlFFF is not straight-forward. In chromatography there is a direct dependence of separation time on the reciprocal of the flowrate and the outlet flowrate will of course be identical to the inlet flowrate. The flowrate also determines the separation efficiency, N (plate number), by way of the H-value of the van Deemter equation, so that the efficiency can be improved by reducing the flowrate. Then, the effect of flowrate on the analysis time and efficiency is straightforward. The challenge in AsFlFFF is that there are three flowrates to operate but they are interdependent: the inlet flowrate, the outlet flowrate, and the crossflow rate as illustrated in Fig. 1.1. These flowrates depend on each other since the sum of the two outlet flowrates have to be identical to the single inlet flowrate,

$$F_{in} = F_{out} + F_{cross} \tag{1.12}$$

F_{in} being determined by the flow delivery from a pump. Once two of the flowrates have been fixed the third is given. Moreover, if one of the flowrates is changed, at least one of the other two also has to change. Since the retention time and the separation efficiency depend on both the transport flow velocity through the channel and the crossflow velocity they are governed by all three flowrates, the crossflow rate influencing the retention level.

The optimisation of AsFlFFF separations has the goal to obtain enough resolution between peaks in a reasonable time as decided by the user and the analytical problem. As in chromatography, if the resolution is more than necessary it is possible to decrease analysis time (retention times) by choosing flowrate conditions that decrease the resolution. The other way around, if the resolution is not enough it can be increased at the cost of longer analysis time.

1.3.1 Retention Time and Separation Speed

The way to adjust the retention time is explained by Eq. 1.9 which shows that for a given channel geometry (length, breadth, thickness) the retention time can be regulated by the ratio F_{cross}/F_{out}. For preliminary experiments it is recommended to calculate the necessary ratio with a 5 min retention time as goal [44], provided that short analysis time is prioritized. With less demands on analysis time any longer retention time can be chosen.

If F_{cross} has some upper limit so that RL has to be sacrificed it can be compensated for by sacrificing analysis time through increasing t_r. If necessary, thicker channels can be used to compensate for the loss in RL.

1.3.2 Retention Level and Resolution

To obtain the desired resolution [45] (usually $R_S \geq 1.5$) F_{in} should be increased as much as is needed while keeping the ratio F_{cross}/F_{out} constant. The result will be a successive narrowing of the sample component zone widths while keeping retention times constant [11]. Hence an increase of the resolution. The source for this effect is the increase of F_{cross} in proportion to the increase of F_{in}. As F_{cross} increases the sample components are more compressed to the ultrafiltration membrane so that the centre of gravity distance, l, becomes shorter and so also the λ. Smaller λ means that the H-value decreases impacting both separation efficiency and the zone widths.

1.3.3 Development of a Separation

Comprehensive descriptions on how to develop AsFlFFF separations has been the subject of many publications [8–14, 37, 44]. The primary parameter to regulate is the retention level. It should be in the range 5–40. Below 5 the resolution rapidly deteriorates. Any increase of the retention level contributes to increased resolution but when approaching 40 some declination of peak symmetry and efficiency have been observed for monoclonal antibodies [12]. The way to choose the retention level is by adjusting the crossflow rate according to Eq. 1.8. For this, two different approaches can be used. The first one is to be used if the retention time already is adequate. F_{cross} is then increased while keeping the ratio F_{cross}/F_{out} constant. This is simply effected by increasing F_{in} as much as possible. If analysis time can be sacrificed, leading to higher retention times, a second approach is to increase F_{cross} at constant F_{in} by increasing the ratio F_{cross}/F_{out}, i.e. by decreasing F_{out}.

For some instruments there are upper limitations in the available crossflow rates due to the pumping system and/or flow regulators. This can limit the available retention levels and resolution. Thus, if the retention level has to be sacrificed this can be compensated by a decreased separation speed, i.e. higher retention times, through a decreased time-average carrier velocity. This helps to decrease the $\overline{H}$-value and keep up the resolution. A further way to keep up the resolution is to increase the channel thickness since this increases the retention level according to Eq. 1.7. In addition, it decreases the $\bar{H}$-value according to Eq. 1.10, which further helps to increase the resolution. The reason is that a thicker channel contributes to a decrease in the retention parameter λ according to Eq. 1.5. Because of the cubic dependence of the $\bar{H}$-value on λ this dominates over the square dependence on channel thickness.

The F_{cross}/F_{out} ratio can also be used to improve the peak height, i.e. decrease the sample dilution in the channel. Because of the continuous loss of flow through the accumulation wall in AsFlFFF, an increase of F_{cross}/F_{out} results in the sample components being eluted in smaller volumes. This decrease in eluted sample volume counteracts the dilution of the samples due to zone broadening and may very efficiently effect the sample concentration of the effluent. The maximum peak height is usually obtained at a short, but for the resolution necessary, retention time.

1.3.4 Programmed Crossflow

Crossflow programming (crossflow gradient) is used to continuously decrease the retention level during a separation. Two common types are linear decays and exponential decays [46]. Sometimes there is a short period of constant (isocratic) crossflow before the decay sets in.

One reason for using crossflow gradients is when the sample contains components of widely different sizes. Then a constant crossflow separation may not resolve the smallest and largest components in one single experiment if they would fall outside the operative range of retention levels, i.e. 5–40 (see below). Of course, if it is acceptable to make several experiments they can be performed with different constant crossflows, each to fit a certain size fraction in the sample. Since a crossflow gradient squeezes differently sized components into smaller retention time increments it may give lower size resolution than an isocratic run. This should be considered in determinations of molar mass and size distributions since the accuracy increases with the resolution.

Another reason for using crossflow gradients is when analyzing an unknown sample so as to quickly get a first idea of the various component sizes that are present. For this purpose the exponential decay should be preferred since the crossflow never reaches zero. This avoids the possibility that the very largest sample components are eluted without any crossflow acting on them.

A study was made of crossflow programming for size separation of very polydisperse hydroxypropyl cellulose and a set of pullulan standards of widely different molar masses [47]. For the pullulans the exponentially decaying crossflow was more beneficial since it gave a higher molar mass selectivity in the high molar mass range and a more uniform selectivity across the whole fractogram.

1.4 Biopolymer Characterization – Molar Mass, Hydrodynamic Diameter (Stokes Diameter), Root-Mean-Square Radius, Conformation, Shape

A strong property of flow FFF and the other kinds of FFF is that, since they are based on first principles in physical chemistry, the experimental results in terms of for example retention time, retention level, and other, can be used to back-calculate

to basic physico-chemical properties of the separated components. This results in characterization of the components. In flow FFF the characterized property is the diffusion coefficient which can be transformed to the hydrodynamic diameter (Stokes diameter). Hence, results can be used to obtain macromolecular hydrodynamic diameter and hydrodynamic diameter distribution. Another possibility for this is to couple a flow-through dynamic light scattering detector to the channel outlet.

If the effluent from the channel is coupled on-line to special detectors, further characteristics can be obtained. When a multiangle light scattering (MALS) detector is used in combination with a refractive index (RI) or UV/Vis detector, the molar mass (M) can be directly measured as well as the root-mean-square radius. This gives highly important characterization data for biopolymers that even can be used to measure biopolymer conformation and shape. Further shape information can be obtained by relating the root-mean-square radius to the hydrodynamic radius.

1.4.1 Determination of the Hydrodynamic Diameter (Stokes Diameter) and the Apparent Density

Under conditions of high retention, where Eq. 1.8 is valid, the diffusion coefficient of a sample component can be measured from the retention time according to

$$D = \frac{t^0 F_{cross} w^2}{6V^0} \frac{1}{t_r} \tag{1.13}$$

which is a transformation of Eq. 1.8. Using the Stokes-Einstein equation the diffusion coefficient can be transformed into the hydrodynamic diameter, d_h, by

$$d_h = \frac{2V^0 kT}{w^2 \pi \eta t^0 F_{cross}} t_r \tag{1.14}$$

where k is the Boltzmann constant, T the temperature and η the dynamic viscosity of the solvent. A fractogram from an FFF analysis may therefore be presented as the detector response plotted against a time scale or a size (hydrodynamic diameter) scale. The transformation of the time scale into a size scale is linear to within 10% relative error at retention levels >2.3 [37] and starts at t^0 where the hydrodynamic size is 0.

An interesting property of a macromolecule is its apparent density distribution. The apparent density is defined as the average molecular mass, numerically identical to the molar mass obtained from MALS-RI detection data, of a component divided by its molecular volume. The volume can be defined as that for a sphere having a radius equal to either the experimental root-mean-square radius [48] as determined by MALS detection or the hydrodynamic radius [49] as determined from observed retention times. The apparent density has been shown to

systematically change as a function of the molecular size which indicates changes in structural distributions within the biopolymer [48–52].

1.5 Key Applications

Below are reported some pioneering and ground-breaking studies using AsFlFFF.

1.5.1 Proteins – Covalent/Non-covalent Aggregates, Antibody Aggregates

Some of the earliest examples of the power of AsFlFFF as a fractionation technique for biopolymers were fractionation of proteins and aggregates. Rapid high resolution ($R_s = 2.0$) fractionation of human serum albumin (HSA) monomer and dimer was achieved in 15 min utilizing a channel with 300 μm thickness [13] as illustrated in Fig. 1.2. Nearly the same high resolution ($R_s = 1.8$) was achieved, and with five times higher separation speed (separation time 3 min), by a much thinner channel, 120 μm, and a higher F_{in} [14]. This approach was further refined in the pioneering paper [12] on high-speed high-resolution separation of a monoclonal antibody monomer and dimer ($R_s = 1.5$) as well as higher aggregates, see Fig. 1.3. The same thin channel was used, however, with even much higher F_{in}. These ground-breaking papers on AsFlFFF introduced high-speed high-resolution separation of proteins by flow FFF.

AsFlFFF has also shown its power in the fractionation of ultra-high molar mass proteins such as glutenin, which is a polymeric protein, i.e. a covalent aggregate of subunits. Glutenin molar mass was estimated from calibration with standards to be in range of $4.4{\cdot}10^5$ and $1.1{\cdot}10^7$ g/mol [53]. It was shown that glutenin, as many ultra-high molar mass macromolecules, was sensitive to overloading in the separation channel, calling for a careful optimization of experimental conditions such as the mass load [54]. In a following paper MALS-RI detection was utilized, allowing for direct molar mass determination [55]. The glutenins covered a wide molar mass range (10^4–10^8 g/mol) and the results showed that gentle stirring under long dissolution time enabled the characterization of undegraded glutenins while sonication caused degradation.

Casein micelles are ultra-large protein aggregates and were characterized with AsFlFFF-MALS-RI [49]. Aggregates up to a mass of approximately 10^{10} g/mol were fractionated and analyzed. Experimental data suggested strategies to distinguish between individual casein micelles and aggregates of casein micelles within a population.

Other applications to proteins but obtained in symmetrical channels have been reported [56].

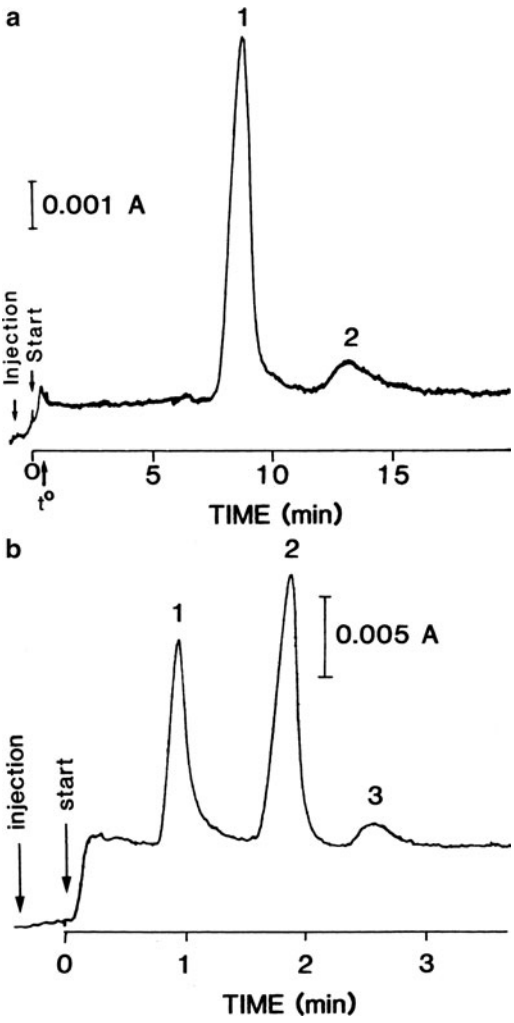

Fig. 1.2 High-resolution separations of the monomer and dimer of HSA in rectangular asymmetrical flow FFF channels of different thicknesses. $L = 28.50$ cm. (**a**) Low-speed high-resolution separation in a thick channel, $w = 300$ μm. Peaks: 1 = monomer (retention level = 27); 2 = dimer (retention level = 43). Sample: HSA 10 mg/ml, ≈1 μl. Relaxation/focusing: focusing point (distance from inlet, z´) = 4.1 cm, $F_{cross} = 4.00$ ml/min. Elution: $F_{in} = 6.09$, $F_{cross} = 5.37$, $F_{out} = 0.72$ ml/min, $t^o = 0.30$ min. Observed diffusion coefficient for peak 1 is $5.8{\cdot}10^{-7}$ cm^2/s (Reproduced from [13], © 1989, with permission from Elsevier). (**b**) High-speed high-resolution separation in a thin channel, $w = 120$ μm. Peaks: 1 = cytochromeC (retention level = 10); 2 = HSA monomer (retention level = 21); 3 = HSA dimer (retention level = 29). Sample: cytochromeC 10 mg/ml, 1 μl; HSA, 1.25 mg/ml, 9 μl. Sample loading: flowrate = 0.1 ml/min, loop volume = 10 μl, time = 1 min. Relaxation/focusing: focusing point (distance from inlet, z´) = 5.0 cm, $F_{cross} = 5$ ml/min during 1 min and 9.9 ml/min during 15 s. Elution: $F_{in} = 9.7$, $F_{cross} = 8.9$, $F_{out} = 0.8$ ml/min, $t^o = 0.09$ min (Reproduced from [14], © 1989, with permission from Elsevier)

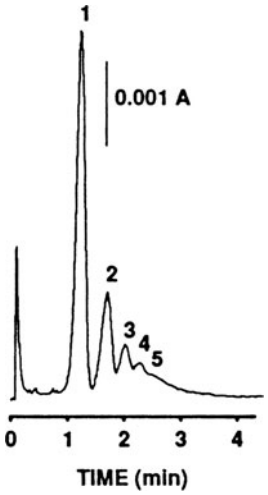

Fig. 1.3 High-speed high-resolution separation of a monoclonal antibody and aggregates in a thin trapezoidal asymmetrical channel. Peaks: 1 = monomer (retention level = 13), 2 = dimer (retention level = 19), 3–5 = higher aggregates. Sample: 0.2 mg/ml, 20 µl. Channel geometry: $w = 130$ µm, $L = 28.50$ cm, $b_0 = 2.12$ cm, $b_L = 0.47$ cm, focusing point = 2.50 cm. Elution: $F_{in} = 10.00$, $F_{cross} = 8.19$, $F_{out} = 1.81$ ml/min, $t^0 = 0.09$ min (Reproduced from [12], © 1993, with permission from Elsevier)

1.5.2 Polysaccharides

Characterization of polysaccharides and derivatives with AsFlFFF is attractive due to the often highly polydisperse nature of these substances. Furthermore, many polysaccharides contain ultra-high molar mass components and can sometimes be prone to aggregate formation. The first work on polysaccharides with AsFlFFF was performed on dextran and hyaluronan [13]. True size fractionation was achieved.

Starch is a typical example of a polysaccharide mixture which is demanding to fractionate and to which AsFlFFF is the only nearly ideal fractionation method that exists. Early attempts displayed the demanding nature of starch fractionation due to the sensitivity of ultra-high molar mass biopolymers to sample mass overloading [57]. A comprehensive study of native starch from many different botanical sources demonstrated the high potential of AsFlFFF for starch characterization [58].

Starch derivatives are different to natural starches since the derivatization often causes partial degradation. An AsFlFFF study on hydroxypropyl and hydroxyethyl starch showed that good size separation in the range $4{\cdot}10^4$–$6{\cdot}10^6$ g/mol could be achieved in 3 min [59]. Other starch derivatives such as the surface active octenyl succinic anhydride (OSA) starch [48, 60, 61] and cationic starch [42, 43] were successfully characterized in terms of molar mass and radius distributions.

Extensive work with AsFlFFF has been performed on various cellulose derivatives. Optimization of injected amounts and flow conditions were of outmost

importance in order to obtain adequate analysis [62]. High crossflows could lead to decreased recoveries while high mass loads caused loss in recovery as well as insufficient size separation. It has also been shown that AsFlFFF enables the detection of ultra-high molar mass components in cellulose derivatives, most likely representing supramolecular aggregates [63].

In the early work on cellulose derivatives it could be observed that beneficial effects on the separation, i.e. more even selectivity over the size distribution, could possibly be achieved by utilizing programmed crossflows which decay with time. This concept was successfully demonstrated [47] for cellulose derivatives as well as pullulan.

1.5.3 Polynucleotides – DNA, RNA, Viruses

Certainly, the linear biopolymers DNA and RNA have been subject to attempts to separate by flow FFF according to chain length, for separation from other biopolymers, or for characterization purposes. The crossflow rate of flow FFF is easily adjusted to cover the molecular size of a specific polynucleotide. The two plasmids pGL 101 (2,390 base pairs) and pBR 322 (4,360 base pairs) obtained the expected order in retention times, 10 and 15 min, respectively, when run under identical conditions [13] in a rather thick channel, 300 μm. The loaded DNA mass had to be low, 1–2 μg, to avoid asymmetric (fronting) peaks at higher loads. At that time there was a fast growing need to preparatively isolate DNA fragments of different sizes after for example cleavage of plasmids by restriction enzymes into two fragments, one small and one large, both of which needed to be collected. A 1.6 μg sample of plasmid pTL 830 (5,300 base pairs) was treated separately with three different enzymes to give three sets of plasmid fragments, 1,200 + 4,100 base pairs, 200 + 5,100 base pairs, and 700 + 4,600 base pairs, respectively. In all three cases the small and large fragments were separated with very high resolution over a retention time scale of about 60 min or less permitting easy collection of each.

Further optimization of the flow rates together with a reduction of channel thickness to 120 μm, brought down the separation time to 12 min for pGL 101 and pBR 322 with more than complete resolution [14]. Sample mass load had to be in the sub-micron range, 0.1 μg, since the thinner channel was more easily overloaded by the large plasmid leading to shifts in peak retention time and skewed (fronting) peaks. Very rapid high-resolution separation of three “small” plasmid fragments (200, 700, and 1200 base pairs respectively) were obtained. For “large” plasmids and fragments the peaks were very broad due to the lower diffusion coefficients. Yet, successful micropreparative separation of the small and large fragments of 16 μg of the plasmid pTL830 was carried out in 30 min.

Hence, whereas very large DNAs can be difficult to resolve from each other their hydrodynamic properties can be characterized by flow FFF based on their observed retention time and its transformation to the translational diffusion coefficient [39]. A variety of linear and both single- and double-stranded circular DNA chains

covering a molar mass range of (0.4–4.8) $\times$ 10^6 g/mole gave measured diffusion coefficients that compared favorably with predictions from various theoretical models for different conformations of DNA. For such ultra-high molar mass linear biopolymers care must be taken to avoid mass overloading by chain entanglement and shear degradation.

For much smaller polynucleotides such as tRNA the flow FFF experiments are straight-forward since mass overloading does not occur easily. This was utilized in determinations of tRNA and ribosome levels in genetically engineered bacterial cells [64] by injecting the cell lysate directly on the flow FFF channel (thickness 165 μm). In a single experiment, tRNA and all three ribosome particles could be resolved allowing their quantification in the different growth phases of the cell culture. The very rapid separation was completed in 6 min as illustrated in Fig. 1.4. The tRNA was eluted at 1.2 min (retention level = 8) followed by intracellular proteins at 2.8 min (retention level = 19) and finally the 30S, 50S, and 70S ribosomes in 4–6 min (RL = 27–41) thus covering a retention level range of 3–40 and a hydrodynamic diameter range of 4–24 nm.

Being condense biopolymers containing RNA, virus particles are easily subjected to flow FFF separations without causing mass overloading. Flowrates can be chosen straight-forwardly for rapid elution [14]. Satellite tobacco necrosis (STNV) virus (6 μg; $M = 1.8 \times 10^6$) and Semliki forest virus (0.5 μg; $M = 50 \times 10^6$) gave efficient peaks at retention times of 2.5 (retention level = 19) and 5 (retention level = 23) min, respectively, in a thin channel (120 μm). In a different STNV sample [10] it was easy to rapidly separate the monomer (t_r = 1.3 min; retention level = 8), the dodecamer (t_r = 4 min; retention level = 25) and three

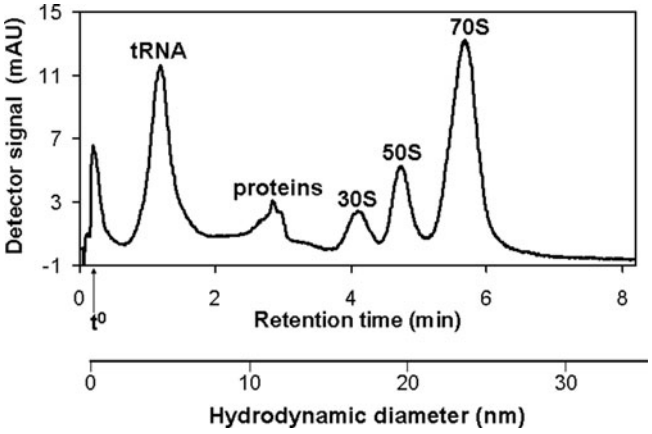

Fig. 1.4 High-speed high-resolution separation of bacterial t-RNA from intracellular proteins and ribosomal particles in a thin trapezoidal asymmetrical channel. Sample: lysate of *E. coli* taken in the exponential growth phase. 30S, 50S, and 70S are the ribosomal subunits and the complete ribosome, respectively. Channel geometry: L = 28.4 cm, w = 165 μm, b_0 = 1.9 cm, b_L = 0.5 cm. Elution: F_{in} = 7.86, F_{cross} = 6.39, F_{out} = 1.47 ml/min, t^0 = 0.146 min (Reproduced from [64], © 2003, with permission from Elsevier)

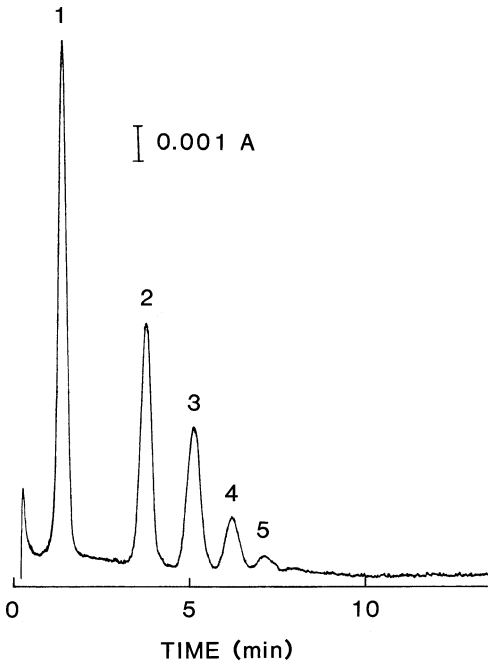

Fig. 1.5 High-speed high-resolution separation of a virus (STNV) and its aggregates in a thin rectangular asymmetrical channel. Peaks: 1 = monomer, 2 = dodecamer, 3–5 = higher aggregates. Channel geometry: $w = 130$ μm, $L = 28.5$ cm, breadth = 1.0 cm. Relaxation/focusing: focusing point = 2.5 cm, $F_{cross} = 3.0$ ml/min, time = 1 min. Elution: $F_{in} = 4.0$, $F_{cross} = 3.0$, $F_{out} = 1.0$ mL/min, $t^0 = 0.16$ min (Reproduced with permission from [10], © 1991, American Chemical Society)

aggregates of the latter ($t_r = 5$–7 min; retention level = 31–44) as illustrated in Fig. 1.5. Virus particles can be regarded as models for nanoparticles carrying DNA for gene therapy.

References

1. Giddings JC (1966) A new separation concept based on a coupling of concentration and flow nonuniformities. Sep Sci 1(1):123–125
2. Giddings JC (2000) The field-flow fractionation family: underlying principles. In: Schimpf M, Caldwell K, Giddings JC (eds) Field-flow fractionation handbook. Wiley-Interscience, New York, pp 3–30
3. Giddings JC, Yang FJ, Myers MN (1976) Flow field-flow fractionation: a versatile new separation method. Science 193(4259):1244–1245
4. Giddings JC, Yang FJ, Myers MN (1976) Theoretical and experimental characterization of flow field-flow fractionation. Anal Chem 48(8):1126–1132
5. Giddings JC, Yang FJ, Myers MN (1977) Flow field-flow fractionation as a methodology for protein separation and characterization. Anal Biochem 81(2):395–407

6. Giddings JC, Lin G-C, Myers MN (1978) Fractionation and size distribution of water soluble polymers by flow field-flow fractionation. J Liq Chromatogr 1(1):1–20
7. Giddings JC, Lin G-C, Myers MN (1978) Fractionation and size analysis of colloidal silica by flow field-flow fractionation. J Colloid Interf Sci 65:67–78
8. Wahlund KG, Winegarner HS, Caldwell KD, Giddings JC (1986) Improved flow field-flow fractionation system applied to water-soluble polymers: programming, outlet stream splitting, and flow optimization. Anal Chem 58(3):573–578
9. Wahlund KG, Giddings JC (1987) Properties of an asymmetrical flow field-flow fractionation channel having one permeable wall. Anal Chem 59(9):1332–1339
10. Litzén A, Wahlund KG (1991) Zone broadening and dilution in rectangular and trapezoidal asymmetrical flow field-flow fractionation channels. Anal Chem 63(10):1001–1007
11. Litzen A (1993) Separation speed, retention, and dispersion in asymmetrical flow field-flow fractionation as functions of channel dimensions and flow-rates. Anal Chem 65(4):461–470
12. Litzen A, Walter JK, Krischollek H, Wahlund KG (1993) Separation and quantitation of monoclonal antibody aggregates by asymmetrical flow field-flow fractionation and comparison to gel permeation chromatography. Anal Biochem 212(2):469–480
13. Wahlund KG, Litzen A (1989) Application of an asymmetrical flow field-flow fractionation channel to the separation and characterization of proteins, plasmids, plasmid fragments, polysaccharides and unicellular algae. J Chromatogr 461:73–87
14. Litzen A, Wahlund KG (1989) Improved separation speed and efficiency for proteins, nucleic-acids and viruses in asymmetrical flow field-flow fractionation. J Chromatogr 476:413–421
15. Lee HL, Reis JFG, Dohner J, Lightfoot EN (1974) Single-phase chromatography - solute retardation by ultrafiltration and electrophoresis. AIChE J 20(4):776–784
16. Doshi MR, Gill WN (1979) Pressure field-flow fractionation or polarization chromatography. Chem Eng Sci 34(5):725–731
17. Lightfoot EN, Chiang AS, Noble PT (1981) Field-flow fractionation (polarization chromatography). Annu Rev Fluid Mech 13:351–378
18. Granger J, Dodds J, Leclerc D, Midoux N (1986) Flow and diffusion of particles in a channel with One porous wall - polarization chromatography. Chem Eng Sci 41(12):3119–3128
19. Granger J, Dodds J (1992) 2 Different configurations of flow field-flow fractionation for size analysis of colloids. Sep Sci Technol 27(13):1691–1709
20. Granger J, Dodds J, Midoux N (1989) Laminar-flow in channels with porous walls. Chem Eng J 42(3):193–204
21. Jonsson JA, Carlshaf A (1989) Flow field-flow fractionation in hollow cylindrical fibers. Anal Chem 61(1):11–18
22. Carlshaf A, Jonsson JA (1991) Effects of ionic-strength of eluent on retention behavior and on the peak broadening process in hollow fiber flow field-flow fractionation. J Microcolumn Sep 3(5): 411–416
23. Carlshaf A, Jonsson JA (1993) Properties of hollow fibers used for flow field-flow fractionation. Sep Sci Technol 28(4):1031–1042
24. Lee WJ, Min BR, Moon MH (1999) Improvement in particle separation by hollow fiber flow field-flow fractionation and the potential use in obtaining particle site distribution. Anal Chem 71(16):3446–3452
25. Kang D, Moon MH (2005) Hollow fiber flow field-flow fractionation of proteins using a microbore channel. Anal Chem 77(13):4207–4212. doi:10.1021/ac050301x
26. Park Y, Paeng KJ, Kang D, Moon MH (2005) Performance of hollow-fiber flow field-flow fractionation in protein separation. J Sep Sci 28(16):2043–2049. doi:10.1002/jssc.200500125
27. Reschiglian P, Zattoni A, Roda B, Cinque L, Parisi D, Roda A, Dal Piaz F, Moon MH, Min BR (2005) On-line hollow-fiber flow field-flow fractionation-electrospray ionization/time-of-flight mass spectrometry of intact proteins. Anal Chem 77(1):47–56. doi:10.1021/ac048898o
28. Lee JY, Min HK, Choi D, Moon MH (2010) Profiling of phospholipids in lipoproteins by multiplexed hollow fiber flow field-flow fractionation and nanoflow liquid chromatography-tandem mass spectrometry. J Chromatogr A 1217(10):1660–1666. doi:10.1016/j.chroma. 2010.01.006

29. Schure MR, Schimpf ME, Schettler PD (2000) Retention-normal mode. In: Schimpf M, Caldwell K, Giddings JC (eds) Field-flow fractionation handbook. Wiley-Interscience, New York, p 31
30. Caldwell KD (2000) Steric field-flow fractionation and the steric transition. In: Schimpf M, Caldwell K, Giddings JC (eds) Field-flow fractionation handbook. Wiley-Interscience, New York, pp 79–94
31. Giddings JC, Chen XR, Wahlund KG, Myers MN (1987) Fast particle separation by flow steric field-flow fractionation. Anal Chem 59(15):1957–1962
32. Chen XR, Wahlund KG, Giddings JC (1988) Gravity-augmented high-speed flow steric field-flow fractionation - simultaneous use of 2 fields. Anal Chem 60(4):362–365
33. Wahlund K-G, Zattoni A (2002) Size separation of supermicrometer particles in asymmetrical flow field-flow fractionation. Flow conditions for rapid elution. Anal Chem 74(21):5621–5628
34. Giddings JC (1973) Conceptual basis of field-flow fractionation. J Chem Educ 50:667
35. Giddings JC (1993) Field-flow fractionation: analysis of macromolecular, colloidal, and particulate materials. Science 260:1456–1465
36. Ratanathanawongs-Williams SK (2000) Flow field-flow fractionation. In: Schimpf M, Caldwell K, Giddings JC (eds) Field-flow fractionation handbook. Wiley-Interscience, New York, pp 257–277
37. Wittgren B, Wahlund KG, Derand H, Wesslen B (1996) Aggregation behavior of an amphiphilic graft copolymer in aqueous medium studied by asymmetrical flow field-flow fractionation. Macromolecules 29(1):268–276
38. Giddings JC (1979) Field-flow fractionation of polymers: one-phase chromatography. Pure Appl Chem 51:1459–1471
39. Liu MK, Giddings JC (1993) Separation and measurement of diffusion coefficients of linear and circular DNAs by flow field-flow fractionation. Macromolecules 26(14):3576–3588
40. Davis JM (2000) Band broadening and plate height. In: Schimpf M, Caldwell K, Giddings JC (eds) Field-flow fractionation handbook. Wiley-Interscience, New York, pp 49–70
41. Giddings JC (1963) Plate height of nonuniform chromatographic columns - Gas compression effects, coupled columns, and analogous systems. Anal Chem 35(3):353–356
42. Lee S, Nilsson PO, Nilsson GS, Wahlund KG (2003) Development of asymmetrical flow field-flow fractionation-multi angle laser light scattering analysis for molecular mass characterization of cationic potato amylopectin. J Chromatogr A 1011(1–2):111–123. doi:10.1016/s0021-9673(03)01144-0
43. Modig G, Nilsson PO, Wahlund KG (2006) Influence of jet-cooking temperature and ionic strength on size and structure of cationic potato amylopectin starch as measured by asymmetrical flow field-flow fractionation multi-angle light scattering. Starch-Starke 58(2):55–65
44. Wahlund K-G (2000) Asymmetrical flow field-flow fractionation. In: Schimpf M, Caldwell K, Giddings JC (eds) Field-flow fractionation handbook. Wiley-Interscience, New York, pp 279–294
45. Schimpf ME (2000) Resolution and fractionating power. In: Schimpf M, Caldwell K, Giddings JC (eds) Field-flow fractionation handbook. Wiley-Interscience, New York, pp 71–77
46. Kirkland JJ, Dilks CH, Rementer SW, Yau WW (1992) Asymmetric-channel flow field-flow fractionation with exponential force-field programming. J Chromatogr 593(1–2):339–355
47. Leeman M, Wahlund KG, Wittgren B (2006) Programmed cross flow asymmetrical flow field-flow fractionation for the size separation of pullulans and hydroxypropyl cellulose. J Chromatogr A 1134(1–2):236–245. doi:10.1016/j.chroma.2006.08.065
48. Nilsson L, Leeman M, Wahlund KG, Bergenståhl B (2006) Mechanical degradation and changes in conformation of hydrophobically modified starch. Biomacromolecules 7:2671–2679
49. Glantz M, Håkansson A, Lindmark-Månsson H, Paulsson M, Nilsson L (2010) Revealing the size, conformation and shape of bovine casein micelles and aggregates with asymmetrical flow field-flow fractionation and multi-angle light scattering. Langmuir 26(15):12585–12591
50. Rojas CC, Wahlund KG, Bergenstahl B, Nilsson L (2008) Macromolecular geometries determined with field-flow fractionation and their impact on the overlap concentration. Biomacromolecules 9(6):1684–1690. doi:10.1021/bm800127n

51. Alftrén J, Penarrieta JM, Bergenståhl B, Nilsson L (2011) Comparison of molecular and emulsifying properties of gum arabic and mesquite gum using asymmetrical flow field-flow fractionation. Food Hydrocolloids (in press)
52. Fernandez C, Rojas CC, Nilsson L (2010) Size, structure and scaling relationships in glycogen from various sources investigated with asymmetrical flow field-flow fractionation and 1H-NMR. Int J Biol Macromol (in press)
53. Wahlund KG, Gustavsson M, MacRitchie F, Nylander T, Wannerberger L (1996) Size characterisation of wheat proteins, particularly glutenin, by asymmetrical flow field-flow fractionation. J Cereal Sci 23(2):113–119
54. Arfvidsson C, Wahlund KG (2003) Mass overloading in the flow field-flow fractionation channel studied by the behaviour of the ultra-large wheat protein glutenin. J Chromatogr A 1011(1–2):99–109. doi:10.1016/s0021-9673(03)01145-2
55. Arfvidsson C, Wahlund KG, Eliasson AC (2004) Direct molecular weight determination in the evaluation of dissolution methods for unreduced glutenin. J Cereal Sci 39(1):1–8. doi:10.1016/s0733-5210(03)00038-9
56. Li P, Hansen M (2000) Protein complexes and lipoproteins. In: Schimpf M, Caldwell K, Giddings JC (eds) Field-flow fractionation handbook. Wiley-Interscience, New York, pp 433–470
57. van Bruijnsvoort M, Wahlund KG, Nilsson G, Kok WT (2001) Retention behaviour of amylopectins in asymmetrical flow field-flow fractionation studied by multi-angle light scattering detection. J Chromatogr A 925(1–2):171–182
58. Wahlund KG, Leeman M, Santacruz S (2011) Size separations of starch of different botanical origin studied by asymmetrical-flow field-flow fractionation and multiangle light scattering. Anal Bioanal Chem 399(4):1455–1465. doi:10.1007/s00216-010-4438-5
59. Wittgren B, Wahlund K-G, Andersson M, Arfvidsson C (2002) Polysaccharide characterization by flow field-flow fractionation-multiangle light scattering: initial studies of modified starches. Int J Poly Anal Charact 7(1–2):19–40
60. Nilsson L, Leeman M, Wahlund K-G, Bergenståhl B (2007) Competitive adsorption of a polydisperse polymer during emulsification: experiments and modeling. Langmuir 23:2346–2351
61. Modig G, Nilsson L, Bergenståhl B, Wahlund KG (2006) Homogenization induced disruption of hydrophobically modified starch as measured by FFF-MALS. Food Hydrocolloids 20(7): 1087–1095
62. Andersson M, Wittgren B, Schagerloef H, Momcilovic D, Wahlund K-G (2004) Size and structure characterization of ethyl hydroxyethyl cellulose by the combination of field - flow fractionation with other techniques. Investigation of ultralarge components. Biomacromolecules 5(1):97–105
63. Andersson M, Wittgren B, Wahlund K-G (2001) Ultrahigh molar mass component detected in ethyl hydroxyethyl cellulose by asymmetrical flow field - flow fractionation coupled to multi-angle light scattering. Anal Chem 73(20):4852–4861
64. Arfvidsson C, Wahlund K-G (2003) Time-minimized determination of ribosome and tRNA levels in bacterial cells using flow field-flow fractionation. Anal Biochem 313(1):76–85

Chapter 2
Assessing Protein-Ultrafiltration Membrane Interactions Using Flow Field-Flow Fractionation

Galina E. Kassalainen and S. Kim Ratanathanawongs Williams

Abstract Flow FFF (FlFFF) is used to rapidly and conveniently measure initial stage protein fouling on ultrafiltration membranes. The procedures and findings are applicable to both ultrafiltration processes and flow FFF analyses. UV detector peak areas representing analytes eluting from the FlFFF channel are used to determine the amount of sample recovered. It was observed that compositionally similar membranes from different companies exhibited significantly different sample recoveries. The measured FlFFF retention times provided insights into the relationship between sample recovery and proximity of the sample layer to the membrane wall. Increasingly large amounts of bovine serum albumin were adsorbed when the average distance of the sample layer was less than 11 μm. This information can be used to establish guidelines for flowrates that should be used to minimize sample adsorption and membrane fouling. The methods described here also provide a means to rapidly test membranes when developing a new FlFFF analysis, evaluating membranes from different manufacturers, and testing batch-to-batch membrane reproducibility.

Keywords Flow FFF • Protein-membrane interactions • Membrane fouling • Adsorption • Ultrafiltration • Membrane performance • Membrane evaluation • Lactate dehydrogenase

G.E. Kassalainen • S.K.R. Williams (✉)
Laboratory for Advanced Separations Technologies, Department of Chemistry and Geochemistry, Colorado School of Mines, Golden, CO, USA
e-mail: krwillia@mines.edu

S.K.R. Williams and K.D. Caldwell (eds.), *Field-Flow Fractionation in Biopolymer Analysis*, DOI 10.1007/978-3-7091-0154-4_2,

2.1 Introduction

Flow field-flow fractionation (FlFFF) has become the most widely used technique of the FFF family [1–5]. Reasons include the need for a low shear rate size-based separation for fragile and/or large analytes such as protein aggregates and complexes, the wide applicable size range that is ideal for polydisperse samples, and the straightforward relationship between retention time and hydrodynamic diameter [6–14]. These advantageous features originate from the open channel design intrinsic to FFF and the crossflow of fluid that is used to retain sample in FlFFF. This crossflow necessitates the use of semipermeable walls that allow permeation of fluid out of the channel in a direction perpendicular to the separation axis. Membranes are used to fulfill this function and present both challenges and opportunities. The selection of a suitable membrane is critical to the success of an FlFFF analysis. The ideal membrane would exhibit no undesirable interactions with the sample, the sample would be completely recovered, and accurate physicochemical properties would be calculated from the measured retention times using FFF theory. This is often not the case particularly when the samples analyzed have wide distributions of chemistries, charges, etc. The challenge is to identify the membrane and experimental conditions for optimum resolution and sample recovery. The use of a membrane in FlFFF channels also opens up new opportunities that have remained largely untapped. Primary among these is the role of FlFFF in studying analyte-membrane interactions. Since the separation process occurs at the surface of the membrane, FlFFF can be used as a sensitive probe to study interactions. Such studies can shed invaluable insights into membrane fouling in ultrafiltration (UF) processes and help establish guidelines for operational conditions. Furthermore, the short analysis times and the small amount of sample injected makes FlFFF an ideal method for quality control of UF membranes that are used for filtration and FlFFF.

This chapter commences with an example study of enzyme dissociation that highlights many of the advantages of FlFFF. The focus then shifts to the use of FlFFF to assess protein-ultrafiltration membrane interactions and the description of a simple method to test membrane suitability and select experimental conditions. This method for evaluating membrane performance is suitable for UF processes, FlFFF, and FFF in general.

2.2 Theory

Differential retention in FFF is based on the formation of equilibrium distributions of different sample components in different flow velocity streamlines of a parabolic flow (see Fig. 2.1). These equilibrium distributions are formed when sample is transported by an applied field U towards a so-called accumulation wall and the subsequent concentration build-up results in sample diffusion away from the wall

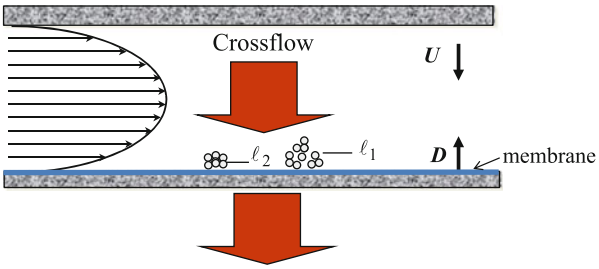

Fig. 2.1 FlFFF channel and separation mechanism

[1–5]. Each distribution can be described by an exponential concentration gradient and a unique mean layer thickness ℓ.

Figure 2.1 shows the distribution of two components in different velocity streamlines, as represented by ℓ_1 and ℓ_2 and the faster displacement of component 1. In the case of flow FFF, the field is provided by a second flow of fluid or crossflow that is driven perpendicular to the separation axis and exits through a semipermeable membrane situated on a porous frit panel. Since all components are positively displaced to this membrane wall irrespective of physicochemical properties, the differentiating sample property that leads to different equilibrium positions in the parabolic flow profile (and thus retention) is the diffusion coefficient D. The D and ℓ terms are related to experimental parameters by Eq. 2.1 which can be derived from the equations in Chap. 1.

$$t_r = \frac{wt^0}{6\ell} = \frac{w^2\dot{V}_c}{6D\dot{V}} \tag{2.1}$$

The t_r is measured retention time, $\dot{V}_c$ is cross flowrate, $\dot{V}$ is channel flowrate, w is channel thickness, and t^0 is void time. Hydrodynamic diameters can be calculated from D via the Stokes-Einstein equation ($D = kT/3\pi\eta d$ where k is the Boltzmann constant, T is temperature, η is carrier liquid viscosity, and d is hydrodynamic diameter). The basic principles of flow FFF are fully described in Chap. 1. Only aspects that are directly relevant to this chapter will be further highlighted.

2.3 Experimental

The FlFFF systems consisted of a channel (symmetric and asymmetric), two pumps for supplying the liquid flows (Model 414 HPLC, Kontron Electrolab, London, U.K. and Model HPLC 420, ESA Inc., Bedford, MA), a 25-μL loop injector (Model 7010, Rheodyne, Inc., Cotati, CA), and a UV-detector (Model 757, Applied Biosystems, Ramsey, NJ). The flowrates were measured using two electronic balances (Model TS4000S, Ohaus, Florham Park, NJ) connected to the RS-232 ports of a PC computer. Inlet and outlet flow rates were equalized using a flow restrictor (Upchurch Scientific, Oak Harbor, CA) located at the detector outlet.

A three-way valve (Hamilton, Reno, NV) and a six-port valve (Valco E36, Chrom Tech, Apple Valley, MN) were used for changing flow paths during stop-flow relaxation and channel rinsing. The channel volume, cut out from the Mylar spacer, had a length of 28.5 cm tip-to-tip and a breadth of 2.0 cm. The UF membrane cross-section area inside the FlFFF channel was 53 cm^2 unless otherwise specified. The spacer thickness was 254 μm but the actual thickness ranged between 210 and 245 μm (measured using calipers). This smaller channel thickness is due to membrane compression in areas of contact with the spacer.

2.3.1 Lactate Dehydrogenase Study

The LDH-5 sample (6.7 mg/mL in 2.1 M $(NH_4)SO_4$, pH 6.0) was obtained from Sigma (St. Louis, MO, USA). Repeated dialysis was carried out with 0.2 M phosphate buffer at pH 7.6 to obtain the enzyme suspension subsequently used in AsFlFFF experiments. The LDH-5 concentration after dialysis and filtration of the precipitate was determined by UV absorbance at 280 nm and literature data (10 mg/mL gives A = 14.6 [15]) to be ~3 mg/mL. A regenerated cellulose membrane with a 5 kDa molecular weight cut-off (Nadir, Wiesbaden, Germany) was used.

2.3.2 Sample Adsorption Study

Six commercial UF membranes composed of regenerated cellulose (RC) and poly (ethersulfone) (PES) were studied. They are designated as RC1(30 kDa), RC2 (110 kDa), RC3 (10 kDa), RC4 (5 kDa), PES1 (10 kDa), and PES2 (10 kDa) where the numbers in parenthesis are the nominal molecular weight cut-offs (MWCO). The carrier liquid was a 0.01 M Tham-boric acid buffer having a pH in the range of 7.3–9.0. Tham, or tris-(hydroxymethyl)aminomethane, was obtained from Fisher Scientific (Fair Lawn, NJ), and boric acid was obtained from VWR Scientific (Chicago, IL). All solutions were prepared with distilled deionized water. The channel flowrate, $\dot{V}$, was 0.5 mL/min and the cross flowrate, $\dot{V}_c$, was 3.2 mL/min.

The purified proteins BSA (98% monomer, MW = 67 kDa, pI 4.8) and γ-globulin (human, from Cohn Fraction II, III; 99% purity, MW = 156 kDa, pI 6.85–6.95) were obtained from Sigma Chemical Co (St. Louis, MO). Sample concentrations were 1.9 mg/mL for BSA and 2.7 mg/mL for γ-globulin. All protein solutions were prefiltered through 0.22 μm membranes (Millipore, Billerica, MA). The injected sample volume was 10–20 μL. The eluted proteins were monitored using a UV detector set at a wavelength of 280 nm. The relative standard deviation of the retention time and peak area measurements did not exceed 3% and 10%, respectively.

Absolute sample recovery was calculated from the ratio of the protein amount eluted from the FlFFF channel to the protein amount injected [16, 17]. The latter

was determined from the peak area of a sample injected into the detector. A ~ 1 mL dilution tube was used in lieu of the FlFFF channel to maintain the same injected sample concentration as that used in a FlFFF analysis and obtain on-scale detector peaks. The resulting peak area represents the protein amount *injected* or 100% sample recovery. The protein amount *eluted* was calculated from the area of the sample peak that was retained and eluted from the FlFFF channel.

2.4 Results and Discussion

2.4.1 Asymmetric FlFFF (AsFlFFF) of Lactate Dehydrogenase

Flow FFF comes in different variants that include the original symmetrical channel, the most frequently used asymmetric channel, and the most recently introduced hollow fiber channel. Numerous papers have been published on the application of these different variants to proteins and complexes, polysaccharides, nanoparticles, cellular components, cells, and micron-sized particulates [1–14].

Lactate dehydrogenase (LDH) is a good sample for illustrating the use of AsFlFFF to monitor relative changes. LDH-5 is an isoenzyme derived from the rabbit skeletal muscle. It consists of four similar polypeptide chains (M_4) with a total molecular weight of 140,000 Da (4 × 35,000 Da) and an isoelectric point of ~7.5. Figure 2.2 shows the effect of pH on the dissociation of LDH-5. At pH 7.6, the

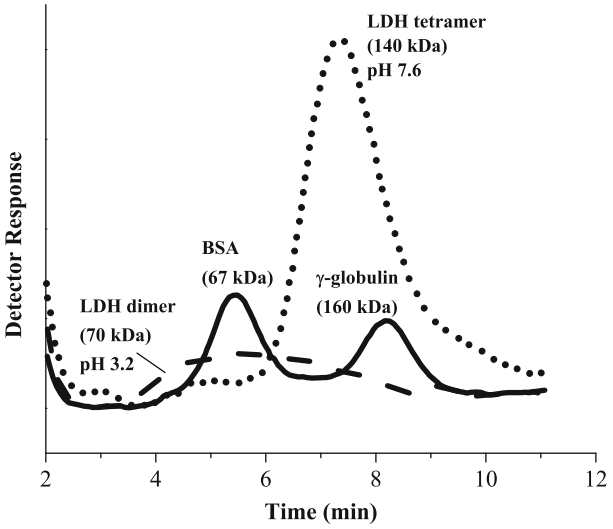

Fig. 2.2 AsFlFFF fractograms showing effect of pH on the formation of lactate dehydrogenase dimers and tetramers

tetramer form of LDH dominates and a large peak is observed at approximately 7.5 min. After suspending the LDH-5 in pH 3.2 buffer for 72 min, the enzyme has mostly dissociated into dimers and a broad fractogram with a peak maximum at ~5.5 min is obtained. The bovine serum albumin (BSA) and γ-globulin fractogram shown superimposed in Fig. 2.2 confirm the elution positions for the LDH-5 dimer (70 kDa) and tetramer (140 kDa).

The rate at which dissociation occurs was dependent on pH with faster dissociation under increasingly acidic conditions. At pH 5.0, the tetramer peak does not show any significant change at the 37 min mark. However, a significant shift in retention time is observed in pH 3.2 buffer after the same amount of time had elapsed. The LDH dissociation was also observed to be a reversible process with reformation of the tetramer when the pH was increased from 4.0 to 6.7. This example demonstrates the gentleness of FlFFF and its suitability for monitoring changes in protein complexes.

2.4.2 Evaluating Membrane Performance Using FlFFF

Controlling protein–membrane interaction is a critical component in the optimization of ultrafiltration (UF) processes [18] and flow FFF analyses. The strength (intensity) of the interaction is a complex function of many parameters such as membrane chemistry and morphology [19], protein structure [20], solution composition [21], and mechanism of protein transport to the membrane surface [22]. Due to this complexity, each protein–membrane pair would ideally be experimentally studied individually. In the case of ultrafiltration with fully retentive membranes, one has to also deal with several concurrent processes causing progressive reduction in system performance, e.g., concentration polarization, deposition of protein aggregates onto the membrane surface, and membrane pore constriction and blockage [23]. As a consequence, UF optimization experiments are very time and sample consuming, and data are difficult to correlate with original parameters affecting protein–membrane interaction.

A number of studies have evaluated other techniques, which are capable of providing more direct information about protein–membrane interaction, as tools for UF optimization. For instance, the study of protein adsorption on the membrane in static conditions [24] and direct measurements of intermolecular forces between a protein and a surface [25] have allowed the comparison of different UF membranes and showed good agreement with UF experiments. The limitation of these approaches as tools for UF optimization is the absence of UF hydrodynamic conditions. During UF, trans-membrane and tangential flow streams affect protein transport to a membrane surface, and hence, the strength of protein–membrane interactions [26]. This is analogous to the effect of cross and channel flowrates in FlFFF [16, 17].

One approach to the study of protein-membrane interactions is to examine the initial stage of protein adsorption onto a pristine membrane. It has previously been

observed that protein membrane interactions during the initial stage of UF have dramatic influence on long-term membrane performance [21]. At this initial stage, the main characteristic of protein–membrane interaction that should be measured is the amount of protein attached to the membrane surface or the initial protein surface coverage. On-line measurements have been made using a stirred cell UF module that was installed into a liquid chromatography system in place of a column [27]. A protein sample was injected and protein passing through a membrane was registered with an UV detector. Unfortunately, the enormous sample dilution experienced in the UF module resulted in very broad UV signals, making it difficult to determine the protein quantities.

This work describes an alternative approach to studying protein-membrane interactions, namely flow field-flow fractionation (FlFFF). During the FFF process, the protein sample moves along the membrane length and undergoes multiple interactions with the membrane surface. Repulsive interactions lead to shorter retention times t_r than theoretically predicted [16]. The opposite is true for attractive interactions, which in the extreme case results in irreversible sample adsorption. FlFFF can thus be used to study a range of weak to strong analyte-membrane interactions. The FlFFF channel hydrodynamics resembles that of a flat cross-flow UF module and the interactions that occur between a protein and a clean membrane can be associated with the very initial stage of UF. The advantage of this method compared to the method of [27] is that the sample dilution is sufficiently lower and protein signals are well-shaped peaks that can be easily characterized.

The application of FlFFF for studying analyte-membrane interactions is not yet widely recognized by FFF practitioners but has made inroads in the membrane filtration community. Published UF papers have demonstrated quantitative measurements of membrane fouling by organics, colloids, and microorganisms present in natural and waste waters and experimental verification of theoretical models [28–36]. To date, no UF publication has addressed quantitating protein fouling on membranes using FlFFF. Although a number of FlFFF papers have discussed approaches to reducing sample adsorption to the membrane as part of methods development [16, 17, 37–42], there has been no report of the purposeful use of FlFFF to quantitate protein recovery. The objectives of this study are to demonstrate the suitability of FlFFF as a tool to rapidly evaluate membrane performance. The results can then be applied to the optimization of FlFFF, UF, and other techniques where protein-membrane interactions must be controlled.

2.4.2.1 Effect of pH

FlFFF experiments were carried out for two globular proteins, six UF membranes, and six solution pHs in the range of 7.3–9.0. The same flowrates $\dot{V}$and $\dot{V}_c$were used for all experiments unless otherwise specified. The diluted 0.01 M Tham-boric acid buffer was chosen to reduce hydrophobic interactions between the membrane surface and protein molecules [21]. The pH of this buffer can be varied in the range of 7.3–9.0. Extension of pH range $<$7.3 would require the addition of

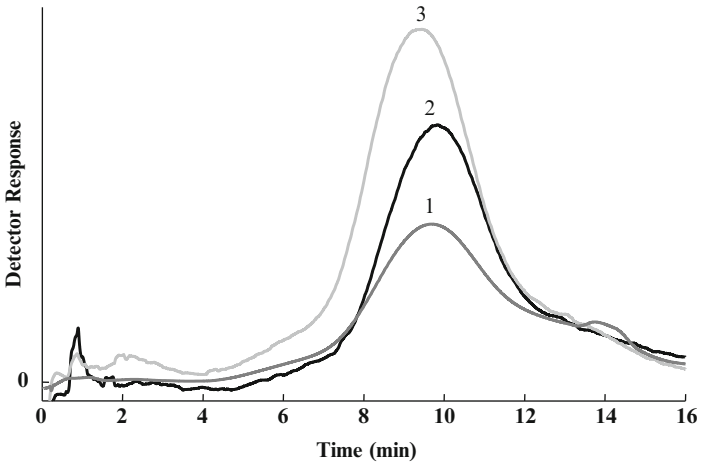

Fig. 2.3 FlFFF fractograms showing peak areas of γ-globulin obtained at different carrier liquid pH using the RC1 membrane

other chemicals, which would introduce new variables affecting the adsorption mechanism.

Typical FlFFF fractograms obtained for γ-globulin at different carrier liquid pHs are presented in Fig. 2.3. Each run was completed within 20 min.

The peak areas are equated to sample recovery as described in the experimental section. Data obtained for the recovery of BSA and γ-globulin at different pH solutions (constant flowrates) are presented in Fig. 2.4. It is evident that sample loss occurred at most pHs studied.

The isoelectric points (pI) of the PES and RC UF membranes are about 3.1 and 3.4, respectively [43, 44]. The isoelectric point of BSA, (pI = 4.8), is sufficiently far from the studied pH range for one to expect strong electrostatic repulsion between protein molecules and both types of membrane. But even for these conditions, BSA recovery did not usually reach 100% (Fig. 2.4a). The isoelectric point of γ-globulin is in the range of 6.85–6.95. For all membranes, a decreasing γ-globulin recovery was observed as the pH approached the pI (Fig. 2.4b). This result is as expected. Structurally "soft" proteins, e.g., globular proteins BSA and γ-globulin, tend to have the highest adsorption onto various surfaces at a pH close to pI [20]. This phenomenon was also observed in UF experiments [21, 45].

2.4.2.2 Membrane Composition

In addition to the effect of solution pH, a significant influence of membrane chemistry on recovery was observed. The PES membranes tested in this study yielded substantially lower sample recoveries than the RC membranes for both BSA and γ-globulin. A similar result was also observed in UF studies [44]. This effect was likely caused by

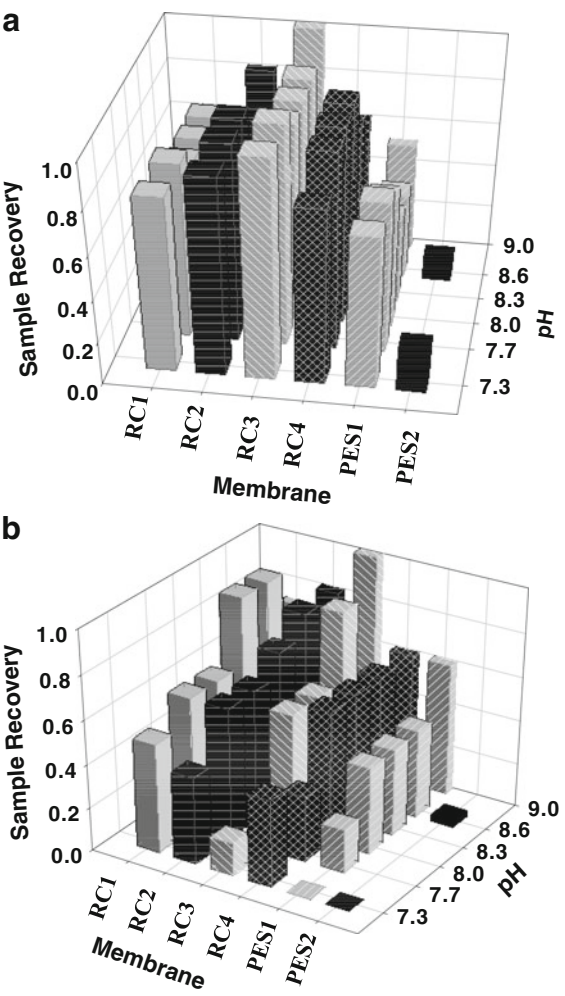

Fig. 2.4 Recovery of (**a**) BSA and (**b**) γ-globulin from a FlFFF channel assembled with UF membranes of different chemistries and obtained from different sources. RC is regenerated cellulose and PES is polyethersulfone. $\dot{V} = 0.5$ mL/min, $\dot{V}_c = 3.2$ mL/min

the higher hydrophobicity of PES membranes. The PES repeat unit contains hydrophobic aromatic groups whereas the RC is more hydrophilic due to presence of hydroxyl groups. The increase in protein adsorption with increasing membrane hydrophobicity was also observed in a number of UF studies [26, 45].

Figure 2.4 also demonstrates that membranes with the same nominal surface chemistry from different suppliers can yield dramatically different protein recoveries. This is likely due to different membrane fabrication processes that result in different residual chemical functionalities at the surface, layered constructions, and surface roughness [16, 46]. These results emphasize the importance of performing preliminary experiments such as those described here to evaluate and establish a baseline for membrane performance and as part of methods development.

2.4.2.3 Proximity of Sample to Membrane Surface

Additional insights can be extracted from FlFFF fractograms. The measured retention time at peak maximum is related to the equilibrium mean layer thickness ℓ and flowrates as stated in Eq. 2.1. The higher the $\dot{V}_c$, the higher the t_r, the smaller the ℓ, the closer the analyte is to the membrane during the FlFFF separation. The opposite relationship holds for $\dot{V}$. Figure 2.5 is a plot of relative sample recovery versus ℓ. Here, the relative sample recovery is defined as the peak area relative to that measured for $\dot{V}_c = 2.75$ mL. $D_{BSA} = 6 \times 10^{-7}$ cm^2/s [47] was used in calculating ℓ. Different t_rs and ℓs were obtained when $\dot{V}_c$ was varied (2.75, 3.21, 3.82, and 4.20 mL/min) while keeping $\dot{V}$ constant at 0.5 mL/min. The data shows the highest sample recovery for $\ell > \sim$11 μm and complete sample loss for ℓ of 8 μm. This set of experiments suggests that a threshold ℓ exists (for a specific analyte, solution, FlFFF channel dimensions, and membrane) and that ℓcan be used as a guide for selecting a $\dot{V}$and $\dot{V}_c$combination that is optimized for both resolution and sample recovery. Since ℓ is proportional to the ratio of the channel flowrate to cross flowrate, this ratio or the flow velocity equivalent $< v > / v_c$ can also be used to establish a threshold for optimized sample recovery as shown in Fig. 2.5b. Since sample recovery is dependent on both the channel and crossflows, a more complete picture can be obtained when their flowrate or flow velocity ratio is varied. The use of flow velocities removes the dependence on channel dimensions. Finally, since ℓ is proportional to D and D is temperature dependent, temperature may also play a role in controlling sample-membrane interactions.

2.4.2.4 Sample Deposition Along Channel length

The total amount of sample deposited per unit area on the membrane is readily calculated from the measured FlFFF sample recovery (amount of protein deposited = amount protein injected – amount protein eluted). However, this quantity does not give information about the rate of sample deposition or its distribution on the membrane. The deposition rate can be estimated using semi-empirical equations developed for UF [48, 49] and modifying the FlFFF mass flux equation. Experimentally, the deposition rate has been observed to decrease as the sample progresses along the membrane due to sample loss and the associated decrease in sample concentration. A fluorescence analysis of n-benzoyl-staurosporine, adsorbed on an UF membrane during FlFFF and then extracted from different pieces of the membrane, showed a gradual decrease in the adsorbed drug amount along the membrane length [37]. No drug adsorption was evident beyond the first half of the FlFFF channel.

The results of the previous study may partially explain the constant BSA recovery measured for five hollow fiber channels with lengths between 15 and 47 cm [40]. If BSA mainly adsorbs to the first part of the channel and saturates available sites, increasing the channel length (keeping all else constant) would not have a significant effect in the amount recovered. Pre-saturating the membrane with at least 2 μg egg phosphatidylcholine of liposomes was reported to yield ~100% sample recovery and negligible carry-over [41].

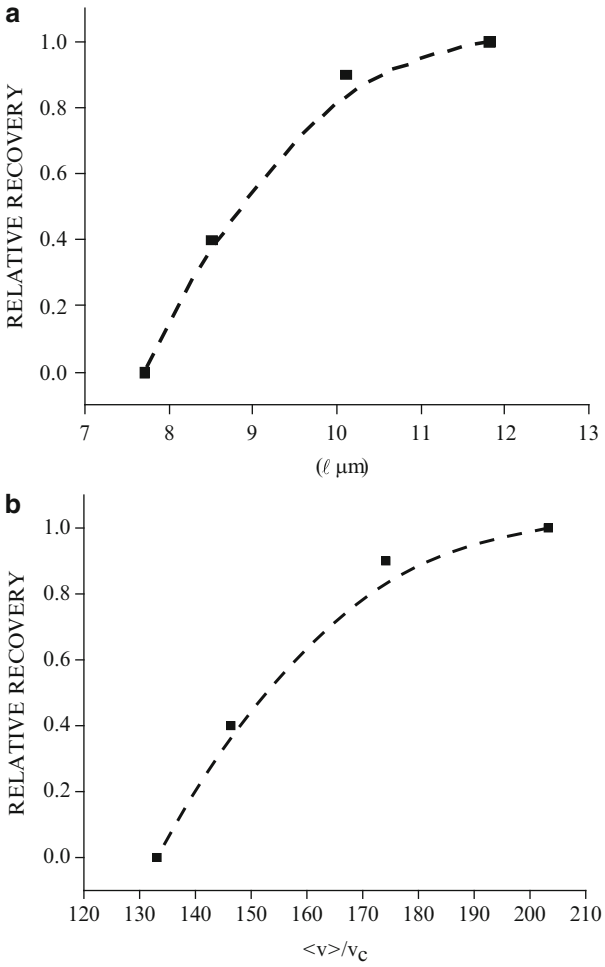

Fig. 2.5 Relative recovery of BSA as a function of (**a**) mean equilibrium distance ℓ from the regenerated cellulose wall and (**b**) the ratio of channel flow velocity $< v >$ to crossflow velocity v_c. Channel dimensions are 28.4 × 3.5 × ~0.0254 cm; carrier liquid is 0.01 M Tris-HCl, pH 7.2; $\dot{V} = 0.5$ mL/min. $<v> = \dot{V}/bw$ and $v_c = \dot{V}_c/bL$ where b is channel breadth and L is length

2.5 Conclusion

Simple experiments have been described to study initial stage fouling on ultrafiltration membranes and to evaluate membrane performance for FlFFF. The pIs of the membrane and proteins and the pH of the solution should be taken in to consideration when selecting a carrier liquid. Other important factors such as membrane hydrophobicity, surface roughness, and batch-to-batch reproducibility are more difficult to control as these depend on the membrane manufacturers. However,

these parameters all culminate in the observed relationship between sample recovery and average distance of sample cloud to the membrane wall. The determination of a threshold ℓ can provide useful guidelines for selecting operating flowrates for both ultrafiltration and FlFFF analyses.

Acknowledgments The authors gratefully acknowledge support from the National Science Foundation CHE-1013029 and CBET-0968042.

References

1. Williams SKR, Runyon JR, Ashames AA (2011) Field-flow fractionation: addressing the nano challenge. Anal Chem 83:634–642
2. Yohannes G, Jussila M, Hartonen K, Riekkola ML (2011) Asymmetrical flow field-flow fractionation technique for separation and characterization of biopolymers and bioparticles. J Chromatogr 1218:4104–4116
3. Qureshi RN, Kok WT (2011) Application of flow field-flow fractionation for the characterization of macromolecules of biological interest: a review. Anal Bioanal Chem 399:1401–1411
4. Roda B, Zattoni A, Reschiglian P et al (2009) Field-flow fractionation in bioanalysis:a review of recent trends. Anal Chim Acta 635:132–143
5. Williams SKR, Lee D (2006) Field-flow fractionation of proteins, polysaccharides, synthetic polymers, and supramolecular assemblies. J Sep Sci 29:1720–1732
6. Andersson CI, Arfvidsson C, Kallio PT et al (2003) Enhanced ribosome and tRNA contents in Escherichia coli expressing a truncated Vitreoscilla hemoglobin mutant analyzed by flow field-flow fractionation. Biotechnol Lett 25:1499–1504
7. Lee H, Williams SKR, Allison SD et al (2001) Analysis of self-assembled cationic lipid-DNA gene carrier complexes using flow field-flow fractionation and light scattering. Anal Chem 73:837–843
8. Silveira JR, Raymond GJ, Hughson AG et al (2005) The most infectious prion protein particles. Nature 437:257–261
9. Yohannes G, Wiedmer SK, Hiidenhovi J et al (2007) Comprehensive two-dimensional field-flow fractionation-liquid chromatography in the analysis of large molecules. Anal Chem 79:3091–3098
10. Kim KH, Moon MH (2009) High speed two dimensional protein separation without gel by isoelectric focusing-asymmetrical flow field-flow fractionation: application to urinary proteome. J Proteome Res 8:4272–4278
11. McEvoy M, Razinkov V, Wei Z (2011) Improved particle counting and size distribution determination of aggregated virus populations by asymmetric flow field-flow fractionation and multiangle light scattering techniques. Biotechnol Prog 27:547–554
12. Arosio P, Barolo G, Muller-Spath T et al (2011) Aggregation stability of a monoclonal antibody during downstream processing. Pharm Res 28:1884–1894
13. Wahlund KG, Leeman M, Santacruz S (2011) Size separations of starch of different botanical origin studied by asymmetrical-flow field-flow fractionation and multiangle light scattering. Anal Bioanal Chem 399:1455–1465
14. Dubascoux S, Von Der Kammer F, Hecho L et al (2008) Optimisation of asymmetrical flow field-flow fractionation for environmental nanoparticles separation. J Chromatogr 1206: 160–165
15. Lundblad RL (2010) Handbook of biochemistry and molecular biology, 4th edn. CRC, Florida
16. Hartmann RL, Williams SKR (2002) Flow field-flow fractionation as an analytical technique to rapidly quantitate membrane fouling. J Membr Sci 209:93–106

17. Williams SKR, Giddings JC (2000) Sample recovery. In: Schimpf M, Caldwell K, Giddings JC (eds) FFF handbook. Wiley, New York
18. Zeman LJ, Zydney AL (1996) Microfiltration and ultrafiltration principles and applications. Marcel Dekker, Inc, New York
19. Matthiasson E (1983) The role of macromolecular adsorption in fouling of ultrafiltration membranes. J Membr Sci 16:23–36
20. Lyklema J, Norde W (1996) Interfacial behaviour of biomacromolecules. Progr Colloid Polym Sci 101:9–17
21. Fane AG, Fell CJD, Suki A (1983) The effect of pH and ionic environment on the ultrafiltration of protein solutions with retentive membranes. J Membr Sci 16:195–210
22. Cohen Stuart MA (1998) Chapter 1. In: Malmsten M (ed) Biopolymers at interfaces, vol 75, Surfactant science series. Marcel Dekker, New York, pp 1–25
23. Belfort G, Zydney AL (1998) Chapter 15. In: Malmsten M (ed) Biopolymers at interfaces, vol 75, Surfactant science series. Marcel Dekker, New York, pp 513–559
24. Amanda A, Mallapragada SK (2001) Comparison of protein fouling on heat-treated poly(vinyl alcohol), poly(ether sulfone) and regenerated cellulose membranes using diffuse reflectance infrared Fourier transform spectroscopy. Biotechnol Prog 17:917–923
25. Koehler JA, Ulbricht M, Belfort G (2000) Intermolecular forces between a protein and a hydrophilic modified polysulfone film with relevance to filtration. Langmuir 16:10419–10427
26. Marshall AD, Munro PA, Tragardh G (1993) The effect of protein fouling in microfiltration and ultrafiltration on permeate flux, protein retention and selectivity: A literature review. Desalination 91:65–108
27. Ghosh R, Cui Z (2000) Analysis of protein transport and polarization through membranes using pulsed sample injection technique. J Membr Sci 175:75–84
28. Kim S, Lee S, Kim CH, Cho J (2009) A new membrane performance index using flow-field-flow fractionation (fl-FFF). Desalination 247:169–179
29. Moon J, Lee S, Song J, Cho J (2010) Membrane fouling indicator of effluent organic matter with nanofiltration for wastewater reclamation, as obtained from flow field-flow fractionation. Sep Purif Technol 73:164–172
30. Pellegrino J, Wright S, Ranvill J, Amy G (2005) Predicting membrane flux decline from complex mixtures using flow-field-flow fractionation measurements and semi-empirical theory. Water Sci Technol 51:85–92
31. Moon J, Cho J (2005) Investigation of nano-colloid transport in UF membrane using flow field-flow fractionation (flow FFF) and an irreversible thermodynamic transport model. Desalination 179:151–159
32. Shon HK, Puntsho S, Chon K, Aryal R, Vigneswaran KIS, Cho J (2009) A study of the influence of ionic strength on thee elution behaviour of membrane organic foulant using advanced separation tools. Desalination Water Treat 11:38–45
33. Kim DH, Moon J, Cho J (2005) Identification of natural organic matter (NOM) transport behavior near the membrane surface using flow field-flow-flow-fractionation (fl-FFF) micro channel. J Water Supply Res T 54:249–259
34. Lim SB, Lee SY, Choi S, Moon J, Hong SK (2010) Evaluation of biofouling potential of microorganism using flow field-flow fractionation (Fl-FFF). Desalination 264:236–242
35. Lee E, Shon HK, Cho J (2010) biofouling characteristics using flow field-flow fractionation: effect of bacteria and membrane properties. Bioresource Technol 101:1487–1493
36. Phuntsho S, Shon HK, Vigneswaran S et al (2011) Assessing membrane fouling potential of humic acid using flow field-flow fractionation. J Membr Sci 373:64–73
37. Madorin M, Van Hoogevest P, Hilfiker R et al (1997) Analysis of drug/plasma interactions by means of asymmetrical flow field-flow fractionation. Pharm Res 14:1706–1712
38. Li P, Hansen M, Giddings JC (1997) Separation of lipoproteins from human plasma by flow field-flow fractionation. J Liq Chromatogr Relat Technol 20:2777–2802
39. Lang R, Vogt L, Zurcher A et al (2009) Asymmetrical flow FFF as an analytical tool for the investigation of the physical stability of virus-like particles. LC GC North Am 27:844–852

40. Park I, Paeng KJ, Kang D et al (2005) Performance of hollow-fiber flow field-flow fractionation in protein separation. J Sep Sci 28:2043–2049
41. Hupfeld S, Ausbacher D, Brandl M (2009) Asymmetric flow field-flow fractionation of liposomes: 2. Concentration detection and adsorptive loss phenomena. J Sep Sci 32:3555–3561
42. Cao S, Pollastrini J, Jiang YJ (2009) Separation and characterization of protein aggregates and particles by field-flow fractionation. Curr Pharm Biotechnol 10:382–390
43. Pontie M, Chasseray X, Lemordant D, Laine MJ (1997) The streaming potential method for the characterization of ultrafiltration organic membranes and the control of cleaning treatments. J Membr Sci 129:125–134
44. Pontie M (1999) Effect of aging on UF membranes by a streaming potential (SP) method. J Membr Sci 154:213–220
45. Mockel D, Staude E, Guiver MD (1999) Static protein adsorption ultrafiltration behavior and cleanability of hydrophilized polysulfone membranes. J Membr Sci 158:63–75
46. Tsuyuhara T, Hanamoto Y, Miyoshi T et al (2010) Influence of membrane properties on physically reversible and irreversible fouling in membrane bioreactors. Water Sci Technol 61:2235–2240
47. Liu M-K, Li P, Giddings JC (1993) Rapid protein separation and diffusion coefficient measurement by frit inlet flow field-flow fractionation. Protein Sci 2:1520–1531
48. Ko MK, Pellegrino JJ, Nassimbene R, Marko P (1993) Characterization of the adsorption-fouling layer using globular proteins on ultrafiltration membranes. J Membr Sci 76:101–120
49. Ruiz-Bevia F, Gomis-Yagues V, Fernandez-Sempere J, Fernandez-Torres MJ (1997) An improved model with time-dependent adsorption for simulating protein ultrafiltration. Chem Eng Sci 52:2343–2352

Chapter 3
Hollow-Fiber Flow Field-Flow Fractionation: A Pipeline to Scale Down Separation and Enhance Detection of Proteins and Cells

Pierluigi Reschiglian, Andrea Zattoni, Barbara Roda, Diana C. Rambaldi, and Myeong Hee Moon

Abstract Commercial flow field-flow fractionation (FlFFF) employs macro-scale, flat-type channels. The idea of hollow-fiber (HF) membranes as tubular, micro-column channels for FlFFF (HF FlFFF or, more shortly, HF5) dates back to 1974, with fundamentals on HF5 given in the late 1980s, and outstanding applications reported only over the last 15 years. Compared to flat-channel FlFFF, the key aspect of HF5 lies in the downscaling of the fractionation channel. This implies low-cost, possible disposable usage, and low volume of the channel that allows on-line coupling with highly sensitive detection and characterization techniques. The use of coupled techniques enhances the analysis of macromolecules and micron-sized particles such as intact proteins and whole cells. In this chapter we first report a few basics on HF5 theory and instrumentation. We then focus on technical and methodological developments that have made HF5 reach a performance normally achieved by flat-channel FlFFF. We finally focus on the enhancements obtained by coupling HF5 with powerful methods for detection and characterization of intact proteins and whole cells such as multi-angle light scattering (MALS), time-of-flight (TOF) mass spectrometry (MS), chemiluminescence (CL), and UV/Vis turbidity diode-array detection (DAD).

Keywords Flow field-flow fractionation • FlFFF • Hollow fiber flow field-flow fractionation • HF FlFFF • HF5 • Miniaturized channel • Detection • Mass spectrometry • Light scattering • Chemiluminescence • Turbidimetric detection • High-molar mass protein separation • Whole cell separation

P. Reschiglian (✉) • A. Zattoni • B. Roda
Department of Chemistry "G. Ciamician", Bologna, Italy

byFlow Srl, Bologna, Italy
e-mail: pierluigi.reschiglian@unibo.it

D.C. Rambaldi
byFlow Srl, Bologna, Italy

M.H. Moon
Department of Chemistry, Yonsei University, Seoul, South Korea

S.K.R. Williams and K.D. Caldwell (eds.), *Field-Flow Fractionation in Biopolymer Analysis*, DOI 10.1007/978-3-7091-0154-4_3,

3.1 Introduction

The commercial, standard ("flat") FlFFF channels have been made of two machined blocks that clamp together around a foil (the spacer) from which the flat type, ribbon-like channel profile is cut out. One or more inset frit panels are inserted in one (asymmetrical FlFFF, AsFlFFF) or both (symmetrical FlFFF) blocks to allow for the required cross-flow of mobile phase. An ultrafiltration membrane is usually placed on the frit where the sample accumulates under the action of the cross-flow. Because of possible interaction between the sample components and the membrane, possible run-to-run sample carry-over due to incomplete sample recovery can occur. Moreover, the typical FlFFF channel volumes are as large as 1 mL. Consequently, a relatively high sample dilution occurs at the FlFFF outlet. These aspects can affect reproducibility, sensitivity, and accuracy, particularly if further characterization of the fractionated analytes is to be performed by coupling FlFFF with orthogonal detection/characterization methods. In the case of biological samples, moreover, contamination of the fractionated analytes can also occur, which may affect their viability or functionality (e.g. in the case of biopolymers or living cells). These issues have been faced following an alternative approach to FlFFF since HF filtration membranes have been effectively exploited as potentially disposable, micro-volume channels. The idea of HF5 indeed dates back to 1974 [1]. Quite surprisingly, only in relatively recent years a significant effort on the development of HF5 fundamentals started [2], which has consequently improved the applications.

3.2 HF5 Basics

3.2.1 Theory

In a typical HF5 arrangement, a HF is connected to a pump that generates inside the HF channel a flowrate F_{in} of a liquid flow in the longitudinal direction. A pressure drop is also generated between the inner and outer wall of the HF, either by a second pump that aspirates the liquid across the HF, or by the application/generation of a backpressure at the HF longitudinal outlet. Due to the pressure difference, also a radial flow F_{rad} is generated through the HF. Consequently, the longitudinal flowrate decreases along the HF from the initial value F_{in} to a lower, outlet value F_{out}, where $F_{out} = F_{in} - F_{rad}$. Since a uniform radial flow velocity can be assumed along the HF length [3], assuming also a laminar flow profile along the HF, the transport time of an unretained species in the HF, i.e. the void time t_0, can be calculated as [4]

$$t_0 = \frac{V^0}{F_{rad}} \ln\left(\frac{F_{in}}{F_{out}}\right) \tag{3.1}$$

where V^0 is the channel void volume ($\pi R^2 L$, with R and L the HF radius and length, respectively), and the average flow rates in the HF (F_{in}, F_{out}, F_{rad}) are expressed in terms of volumetric flowrates.

3.2.1.1 Normal Mode

Based on a simplified treatment [3, 4], the practical expression for retention time (t_r) in normal HF5, which is the elution mode of macromolecules and relatively small (e.g. nanosized) particles, can be given as

$$t_r = \frac{R^2}{8D} \ln\left(\frac{F_{in}}{F_{out}}\right) \tag{3.2}$$

where D is the analyte diffusion coefficient.

Separation performance in normal HF5 can be expressed in terms of maximum number of theoretical plates per unit time, which is related to the limit analyte concentration at the detector which does not induce overloading (c^*), and to the minimum detectable concentration c_{LOD} as [5]

$$\left(\frac{N}{t_r}\right)_{\max} = 2\frac{Dc^*}{R^2 c_{LOD}} \tag{3.3}$$

Equation 3.3 indicates that the maximum efficiency per unit time can be determined by the physical and chemical characteristics of the analytes, in particular by their detectability and susceptibility to overloading. This is a key aspect for HF5 applications. Performance is expected to decrease with increasing the analyte molar mass (M_r) not only because of a decrease of the analyte D, but also because c^* is expected to decrease with increasing the analyte M_r [6]. The expression also shows that miniaturization can boost HF5 performance. With narrower HFs, less dilution of the sample occurs so that higher crossflow rate values can be applied on smaller amounts of sample [7].

3.2.1.2 Hyperlayer Mode

This elution mode governs retention of particles the size of which is sufficiently high to make negligible the effect of diffusion on the sample concentration profile [8]. It is the case, for instance, of whole cells. In this mode, the HF5 retention can be expressed as [9]

$$t_r = \frac{t^0}{2\gamma}\frac{R}{d} \tag{3.4}$$

where γ is a correction factor that depends on the physical features of sample particles, and on the experimental conditions. The relationship between particle size and retention time can be determined by calibration with standard particles of known size [9]

$$\log t_r = \log t_{r1} - S_d \log d \tag{3.5}$$

where S_d is the diameter-based selectivity, and t_{r1} is the extrapolated retention time for a particle of unit diameter. Experimental values of S_d in hyperlayer (Hyp) HF5 were calculated from the retention time of standard beads [10], and they were found comparable, or slightly higher than the values typically found in flat-type, Hyp FlFFF [11].

3.2.2 Instrumentation

Because of the radial symmetry of the cross-flow stream, HF5 can be considered a one permeable-wall, symmetrical FlFFF methodology. This allows using the same operation conditions commonly employed in one permeable-wall, flat-channel for AsFlFFF. Typical HF5 runs then need a system design and configuration to carry on at least two steps: sample injection/focusing/relaxation, and sample elution. Different system and channel configurations have been proposed. Over more than 20 years, their developments have made HF5 evolve from an early-prototype to a ready-to-market technology the fractionation performance of which today is comparable to or already higher than that of commercial AsFlFFF.

3.2.2.1 Systems

The described systems differentiate in the use of one or two pumps to generate the axial and radial flow streams. In the firstly developed system [2], a first pump delivered the mobile phase fluid inside the HF5 channel at a given flow rate, and a second pump was connected to the radial flow outlet of the HF5 channel to work in "unpump" mode, that is it drew in the mobile phase fluid from the inner wall of the HF channel through the HF pores. This arrangement showed that a two-pump arrangement can give sufficiently accurate and independent control of the flows to properly perform the required sample injection/focusing/relaxation and elution steps. An evolved, two-pump system was then presented to permit easier management of the complete run cycle [12]. In that system, an HPLC pump was employed to generate the required flow rate during sample elution, and a syringe pump to generate, in combination with the first pump, two opposite flows for the necessary injection/focusing/relaxation step of the sample.

The use of a single pump can however give significant advantages in terms of simplicity in system operations, and lower costs. Therefore, an instrumental scheme

using a single pump was proposed [3]. The injection/focusing/relaxation step was carried out by splitting the pump flow into the two streams applied in opposite direction to the inlet and outlet extremities of the HF5 module. Using a single pump however required fine control and setting of the flow rates by metering valves, and multiple-way switching valves to convert the flow patterns. With respect to two-pump configurations, method control and operation accuracy in one-pump configuration then require highly-specialized skills, high-quality devices, and possibly automated procedures. Work on progress to implement HF5 operation in commercial systems for AsFlFFF is showing significant improvements in one-pump HF5 operations, and this ultimate HF5 technology has been recently released to the market.

UV/Vis spectrophotometric detection has been proposed in all HF5 systems. This is however a concentration-dependent detection method. As in the cases of other separation techniques, compared to standard, flat-channel FlFFF the lower amount of sample loaded in HF5 could induce a reduction in sensitivity, and an increase of the limit of detection if sample dilution during retention is not sufficiently reduced. When a UV/vis diode-array detector (DAD) equipped with a fiber-optic guided, 5 cm light-pipe cell has been employed in a HF5 system, an increase in detection sensitivity has been observed because of the fivefold increase in optical path length compared to standard 1 cm, Z-type cells. Improved retention reproducibility has also been observed, because the low back-pressure generated by such a light-pipe cell reduces polymeric HF deformation during usage [12].

3.2.2.2 Channel Modules

Many efforts have been focused on the optimization of the HF5 module design and construction. More than 10 years ago, a HF5 module consisting of a piece of polymeric HF inserted into two 1/8″-O.D. (outer diameter) Teflon sleeves of equal length was for the first time proposed [3]. The sleeves were connected by a tee-union to make the radial flow exit. The extremities of the HF were glued to the inner wall of the Teflon sleeves, where standard plastic fittings were placed to make inlet and outlet connections. This module design had the advantage to employ commercially-available and relatively inexpensive components, and to standardize connections to a liquid chromatography-like system. Gluing does not however permit replacement of the HF inside the module. Moreover, it can cause interferences due to possible glue bleeding during usage. A glue-free connection design based on the polymeric HF anchor to the Teflon sleeve was then proposed [13, 14]. The anchor was realized by compression of the Teflon sleeve at the inlet and outlet ends of the module using hand-tight ferrule/nut plastic fittings. This channel design is schematized in Fig. 3.1.

Current work aims to further optimize a glue-free connection design to make easier replacement of the used HF. The most recent channel design has a new sealing mechanism that allows for effective and straightforward sealing of the HF

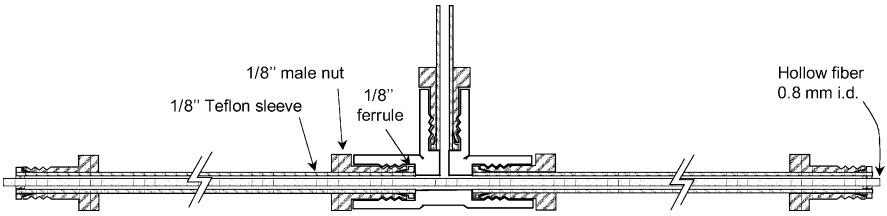

Fig. 3.1 Most employed, glue-free connection design for the prototype channel module using polymeric HF membranes (Adapted with permission from [15], © 2006, American Chemical Society)

into a rigid tube housing. This has been a necessary requirement for actual disposable usage of the channel and for the release of HF5 technology to the market.

Common channel dimensions have been about 20 cm in length and 0.80–1 mm I.D. As demonstrated above in 2.1.1, miniaturization boosts the HF5 performance through decrease in sample injection amount, and increase in efficiency and detection limit. Using microbore, polymeric HF channels with geometrical volumes around 40 μL, HF5 was scaled down to a microflow rate regime [7].

3.2.2.3 Membranes

Two classes of membranes have been used for HF5 channels: ceramic and polymeric membranes. Ceramic HFs have shown high robustness and chemical inertness [16], and promising results in terms of recovery, run-to-run repeatability, and long-term stability [17]. However, polymeric membranes have been mostly employed. They generally have been in the 6–100 KDa pore cut-off range, and made of polysulphone (PSf), polyacrylonitrile (PAN) or chlorinated polyvinylchloride (cPVC).

Size and chemical properties of the analytes influence the choice for the best pore cut-off value and surface composition of the HF membrane. Best fractionation performance is of course achieved if interactions between analytes and the membrane inner wall are minimized. As in the case of AsFlFFF, relatively polar membranes are advised for nonpolar analytes, while membranes of moderate polarity should be preferred for polar analytes. Most proper choice of the membrane type can be eventually assisted by analyzing the membrane inner surface after the runs [18].

PSf HFs are massively produced for applications in hemodialysis and cell ultrafiltration. They are, therefore, ideal candidates to make HF5 channels optimized for protein and cell separation, but they are relatively soft, and they can be deformed during usage [3, 19]. HF channel deformation can be particularly serious in Hyp HF5 because of the relatively high flowrate conditions required. Because of their rigidity, PAN HFs were used for Hyp HF5 of micron-sized particles [10]. PAN HFs also show chemical resistance to different organic

solvents. For this reason, they were employed for the analysis of organic-soluble polymers [5]. Recently, PAN HFs were used also for proteins and airborne particulate analysis [20].

3.3 Applications

Although HF5 has shown a singularly slow, multi-step evolution process, and despite the fact that it has only recently been commercialized, it has over the last 10 years already found sound applications to a very broad range of samples. Most recent technical developments have made HF5 increasingly effective in life science, particularly in intact protein and whole cell separation. When HF5 is coupled with detection/characterization methods such as multi-angle light scattering (MALS), soft-impact mass spectrometry (MS), chemiluminescence (CL), and UV/vis turbidity detection, it shows the ability to increase the amount of analytical information that could otherwise be obtained only if the methods were applied stand-alone.

3.3.1 Proteins

When it is applied to high-molar mass analytes, HF5 shows itself competitive with respect to other flow-assisted separation methods such as flat-type FlFFF. Over 15 years ago, HF5 of standard, relatively high-molar mass proteins such as horse ferritin was for the first time presented [21]. Because of the subsequent boom of protein analysis methods, different HF5 applications to proteins have been developed, and the HF5 performance in protein separation has been systematically studied [13].

3.3.1.1 HF5-MALS

Determination of protein size and, then, M_r is possible from the retention time. However, the relationship between the hydrodynamic radius (r_h) and the M_r of proteins depends on protein conformation. Moreover, the accuracy of M_r determination via retention time might be affected by non-ideality effects on retention, which can be due, for instance, to analyte/HF membrane interaction.

A flow-through, MALS detector measures the light scattered at multiple angles from the separated analytes. In combination with a concentration-based (UV/vis or refractive index) detector, MALS detection gives absolute, uncorrelated size and M_r values of the fractionated proteins. MALS can directly provide the root-mean-square (r.m.s.) radius (or gyration radius, r_g) of the analyte. The r_g values represent the mass-average distance of each point in the analyte molecule/particle from the

center of gravity. As expressed in Eq. 3.2, retention is in principle related to the protein diffusion coefficient, which is related to the hydrodynamic size that is the diameter of a sphere with the same diffusion coefficient or viscosity of the protein molecule. As a consequence, by comparing the r_g values measured by MALS to the r_h values measured by HF5, HF5-MALS allows obtaining information on the protein shape and/or on the mass distribution inside the protein molecule/particle. It must be also noted that HF5 retention is independent of the analyte density. HF5-MALS then yields results of great interest for the biophysical characterization of protein complexes, particularly in the case of high or very-high M_r species for which FlFFF and MALS are characterized by high size-based selectivity and sensitivity, respectively.

HF5-MALS of proteins was for the first time described for the analysis of β-lactoglobulin (β-LG) aggregates, and it made use of a ceramic HF channel [17]. MALS detection was used to accurately estimate the M_r and size values of the aggregates. Because of the relationship existing between the apparent diffusion coefficient and M_r values of the protein aggregates, from the ratio of the experimentally-measured values of r_g (from MALS detection) and r_h (from HF5 retention) it was concluded that the largest β-LG aggregates behaved as though they were flexible chains in solution. Such a study showed the importance of coupling two techniques that are able to independently measure the r_g/r_h value. This ratio is known to be a very important parameter for conformational characterization of proteins. More recently, a polymeric HF5 channel inserted into a commercial flow control unit for AsFlFFF (Eclipse 3, from Wyatt Technology Europe GmbH, Dernbach, Germany) was online coupled to MALS detection for r_g/r_h characterization of the low-density lipoprotein (LDL) class in human blood serum [22]. The results showed that, because of the core-shell nature of the LDL particles, the obtained r_g/r_h values could not be compared with the reference values for either homogeneous spheres or disk-like particles. Most recent improvements on HF5-MALS coupling using the commercial flow control unit Eclipse have been showing a performance comparable to that obtained by AsFlFFF-MALS. A representative example is shown in Fig. 3.2, where the fractogram and the M_r distribution of a mixture of bovine serum albumin (BSA) and horse spleen ferritin are reported. Peak efficiency and resolution between different oligomeric forms are comparable to flat-type FlFFF. Accurate molar mass values obtained from MALS detection confirm HF5 mass selectivity in a molar mass range from 66 to 1,350 KDa.

3.3.1.2 HF5-MS

HF5 shows unique, intrinsic features for online coupling to MS: (a) low channel volume (in the order of 100 μL) which reduces sample dilution; (b) low flowrate conditions (as low as 200 μL/min) which, in case of on-line coupling to MS, do not require high split ratios between the channel outlet and the ionization source; (c) possible disposable usage which eliminates the risk of run-to-run sample carry-over and, then, spectra contamination; (d) on-the-fly sample desalting.

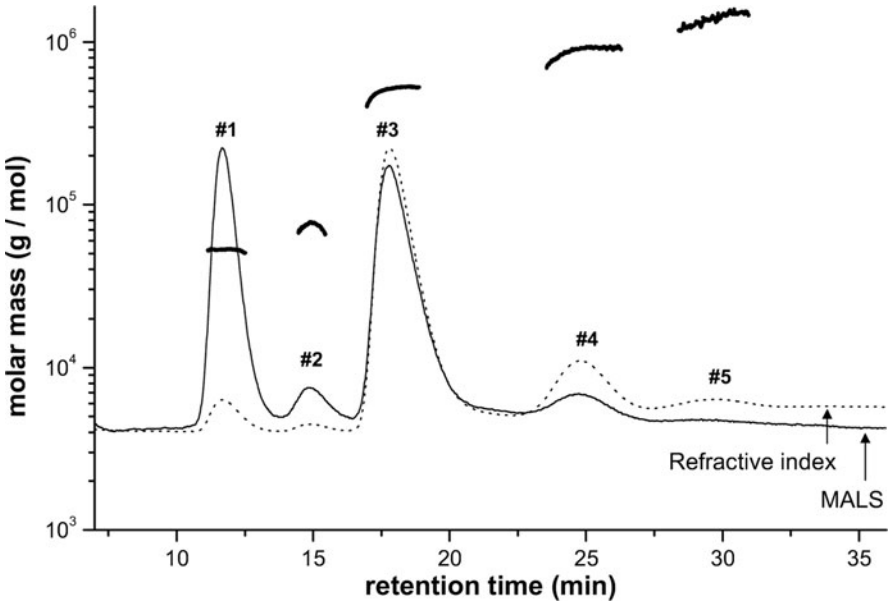

Fig. 3.2 HF5-MALS of BSA and ferritin. $F_{in} = 1.2$ mL/min; $F_{rad} = 0.85$ mL/min. Mobile phase: 10 mM ammonium acetate. *Thin, solid line:* refractive index signal; *dotted line:* MALS signal; *thick, solid line*: molar mass values determined from MALS detection. Peak #1, BSA monomer 66 KDa; peak #2, BSA dimer 132 KDa; peak #3, ferritin monomer 450 KDa; peak #4, ferritin dimer 900 KDa; peak #5, ferritin trimer 1,350 KDa

Very accurate measurements of the actual M_r value is the prime goal when identifying intact proteins and protein complexes. Electrospray ionization (ESI) is particularly suited for MS-based identification and structural characterization of intact proteins and protein complexes. By ESI/MS, accurate mass measures, and indications on the higher-order structure of proteins and non-covalent protein complexes can be obtained. Equipped with time-of-flight (TOF) mass analyzers, ESI/TOFMS provides characterization of intact proteins and protein complexes over a very wide molar mass range, since TOF analyzers are able to scan broad ranges of m/z values. In the case of complex protein samples (e.g. cell lysates), direct ESI/TOFMS shows, however, limited success, mainly because the spectral results are very complex to interpret. First, the spectra contain a very high number of signals due to the high number of ionized species. These species can be originated not only from the different proteins present in the sample but also from the sample contaminants. The presence of sample contaminants plays an important role in terms of sensitivity and accuracy of the ESI/TOFMS methods for intact proteins. Among such contaminants, non-volatile salts generally present in protein samples of either biological or synthetic origin give formation of adduct ions, reducing sensitivity and increasing complication in molar mass determination. This can be a particularly serious issue when proteins from cell lysates, or produced by biotechnological processes, are analyzed, due to the high concentration of salts

present in the growth media. Sample desalting methods are thus necessary. Second, the mechanism of competitive ionization, which is characterized by the suppression of molecular ion species of a given protein in the presence of other proteins in the mixture, also complicates spectral interpretation. Rapid and efficient separation methods able to purify the sample without affecting either the three-dimensional structure or the non-covalent chemistry can significantly enhance the power of ESI/TOFMS methods applied to intact proteins. The increase in analytical information can be achieved not only in terms of protein identification but also of stoichiometry and characterization of aggregation features of the protein complexes.

HF5 can be online coupled to ESI/TOFMS by connecting the detector outlet to the ion source via a splitting valve. During fractionation the proteins can maintain their native structure [14]. Possible correlation between the M_r values independently measured by ESI/TOFMS spectra and from HF5 retention time measurements (e.g. in Fig. 3.3a) can then produce significant information on the quaternary structure of the fractionated proteins. In Fig. 3.3 (adapted from ref. [14]) we report an example of HF5-ESI/TOF MS of horseradish peroxidase (HRP).

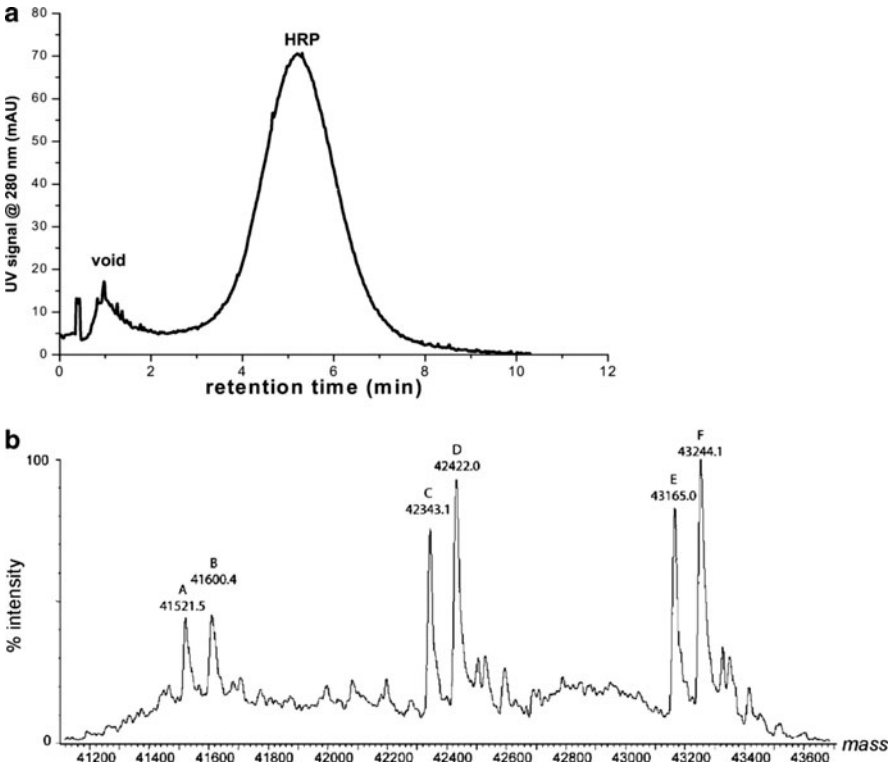

Fig. 3.3 HF5-ESI/TOF MS of HRP. $F_{in} = 0.70$ mL/min; $F_{rad} = 0.38$ mL/min. Mobile phase: 50 mM ammonium acetate, pH = 7.0. (**a**) UV/vis fractogram at 280 nm; (**b**) mass spectrum at the fractogram maximum ($t_r = 5.2$ min) (Adapted with permission from [14], © 2005, American Chemical Society)

HRP is an extracellular heme enzyme consisting of 308 amino acids and a single protoporphyrin IX prosthetic group, two calcium ions, four disulfide bridges, and three N-glycosylation sites [23–25]. When RP HPLC-ESI/TOFMS of HRP was performed, three species had been found whose masses corresponded to the binding of, respectively, one, two and three $(GlucNAc)_2$-$(Man)_3$ structures to the HRP polypeptide chain. This oligosaccharide structure, that constitutes the common core of all the glycosidic anchors present in N-glycosylated proteins, has nominal $M_r = 894$. In fact, the molar mass of each of the three glycosylated species found in Fig. 3.3b increased about 615 Da with respect to the values that had been observed in RP HPLC-ESI/TOFMS. The mass spectrum in Fig. 3.3b also shows that the glycosylated species were present as doublets, while RP HPLC-ESI/TOFMS had given no mass signal for doublets corresponding to these species. Since the nominal molar mass of the heme prosthetic group is $M_r = 615.23$, and the difference in mass between the peaks of each doublet is about 80 Da, which is the mass of $2Ca^{2+}$, these findings supported two important indications. First, the elution through HF5 did not alter the non-covalent bond between the polypeptide chain and the prosthetic group, as it had done during elution through RP HPLC. Second, comparing the relative intensity of the two peaks of each doublet, it was proven that most of the HRP molecules retained, through HF5, the calcium ions that were non-covalently bound to the enzyme. It was also worth noting that there was a total absence of species corresponding to the binding of one, rather than two, calcium ions. This confirmed the strong interdependence of the two calcium-binding sites, and it suggested that the observed species had not been generated by unspecific absorption of metal ions from the sample solution. This was an indirect proof that the protein sample solution was actually desalted through HF5.

3.3.1.3 HF5 & CL

Spectrophotometric UV/Vis absorption detection is generally characterized by relatively low sensitivity and specificity. CL detection can reduce the limit of detection and enhance sensitivity and specificity with respect to UV/Vis absorption detection, being the analytical signal generated without a light source because of a specific chemical reaction. CL emission is often catalyzed by an enzyme [26]. Various, reliable CL systems for the ultrasensitive detection of enzymes such as HRP, alkaline phosphatase (AP), and β-galactosidase have been developed [27, 28]. The CL intensity results are proportional to the enzyme activity when the amount of CL substrate exceeds the enzyme mass. This makes CL suitable to quantitative analysis.

HF5 coupled with an enzymatic CL assay specifically designed for ultra-sensitive evaluation of the activity of the functional protein urate oxidase (uricase) was employed to characterize, under native conditions, the activity of different uricase oligomers possibly present in solution [15]. Uricase in native form is a homotetramer, the M_r of which is about 132,000. X-ray analysis shows that the tetramer is composed of two dimers, which form a tunnel-shaped protein. Uricase was fractionated through HF5, and the sample fractions were then analyzed to evaluate the enzymatic activity of their components. The CL assay relied on detection of the

hydrogen peroxide produced by the enzymatic reaction through the CL oxidation of bis(2,4,6-trichlorophenyl)oxalate (TCPO) in the presence of the fluorescent energy acceptor dipyridamole. A key feature of this assay is its extremely high sensitivity (the limit of detection is of the order of 0.01 ng of uricase), which makes it suitable for the enzymatic activity measurement of even trace components of the uricase fractions obtained by HF5. In Fig. 3.4a,b are respectively shown the fractogram and the CL signals measured for the fractions of a reagent-grade, uricase sample.

The CL signal exhibits its maximum value in correspondence of the retention time of the enzyme tetramer. At the retention time corresponding to the M_r value of the enzyme dimer, a second CL signal maximum appears, which confirms that also the uricase dimer was present in solution, and that it was active. Because of the non-denaturing conditions of HF5, its use with CL enzyme activity assay then allowed relating the supramolecular structure of the enzyme with its enzymatic activity.

3.3.2 *Cells*

Cell sorting is an outstanding topic in many fields, from diagnostics and biotechnology, to stem cell-assisted therapy and transplants. Few flow-assisted separation

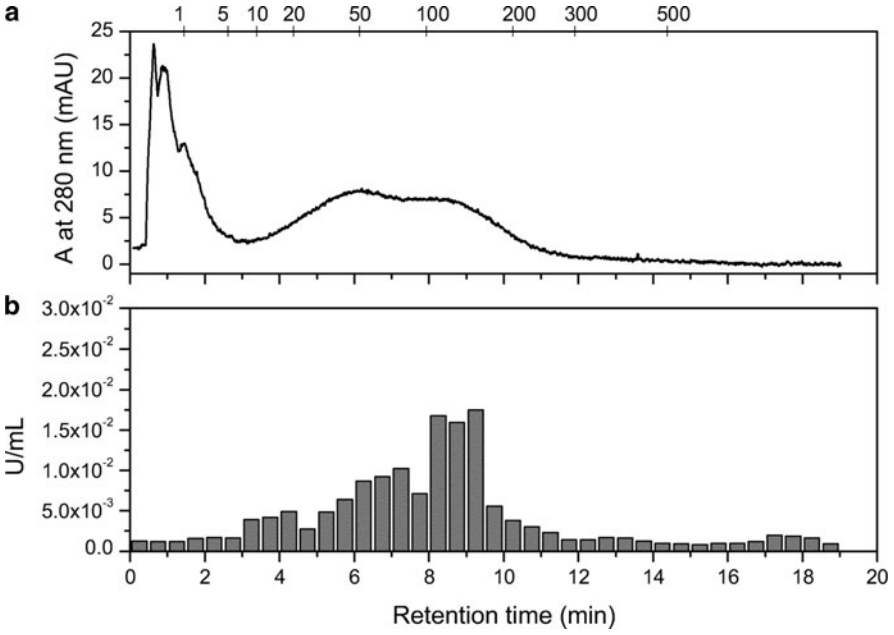

Fig. 3.4 HF5 of a reagent-grade uricase. $F_{in} = 0.70$ mL/min; $F_{rad} = 0.40$ mL/min. Mobile phase: 50 mM ammonium acetate, pH = 7.0. (**a**) UV/vis fractogram at 280 nm. (**b**) Enzymatic activity of the collected fractions determined by the CL assay (Adapted with permission from [15], © 2006, American Chemical Society)

methods are available for the sorting of whole cells. Since the early 1980s, the possibility to develop FFF-based cell sorting was established by Caldwell et al. in a pioneering work where they demonstrated the possibility to separate different types of cells of different characteristics [29]. It was then due to the extensive work of Cardot et al. [30] that the development of biocompatible FFF instrumentation for living cell separation [31] became available, as well as the procedures to sterilize separators, and to collect viable and reusable purified cells [32, 33]. Bacterial cell sorting is also of great interest. The very first examples of HF5 sorting of bacteria have been reported for different serotypes of deactivated *Vibrio cholerae* (*V. cholerae*) used for whole-cell vaccines [12]. Subsequently, other bacteria (*Escherichia coli; E.coli*) and different types of cells (human red blood cells, winemaking yeast from *Saccharomyces cerevisiae*) were fractionated with superior size-based selectivity, and reduced analysis time with respect to flat-channel Hyp FlFFF [34]. The intrinsic features of HF5 have indicated for Hyp HF5 interesting perspectives in terms of cell sorting, firstly because of the low cost and short analysis time. Secondly, compared to most techniques for cell sorting, HF5 can avoid sample carry-over and sterility issues, because of the potentially disposable use of the channels.

In Hyp HF5 cells are fractionated according to differences in their physical features. Such differences cannot however make cells be identified based on retention time differences. Powerful characterization methods must be coupled to HF5, as cell quantification is not easily possible from conversion of the signal intensity if UV/Vis detection is employed. This is because signal intensity does not depend on light absorptivity but rather on low-angle light scattering of the fractionated cells.

3.3.2.1 HF5 & MALDI/TOF MS

Mass spectrometry has proven to be powerful tool for the rapid identification and characterization of bacterial cells [35]. Fenselau and co-workers have pioneered development and application of matrix-assisted laser desorption/ionization (MALDI) TOF MS for the characterization of intact bacteria [36]. The most common approaches so far employed to identify unknowns by MALDI/TOF MS analysis of intact bacteria are based on the similarity between the spectra of the unknown bacteria and those in MALDI/TOF MS libraries of reference bacterial species [37]. Nonetheless, for these methods to be valid, a high degree of reproducibility is required. This is a particularly critical aspect in the identification of bacteria mixtures with high differences in the relative percentage of the different strains, because the resulting spectra are highly complicated. MALDI/TOF MS of bacteria mixtures is not only complicated by the high number of ion signals in the spectra, but also by the fact that MALDI is a competitive ionization process, and the spectra of bacteria mixtures can be quite different from the linear combination of characteristic signals obtained for each individual bacterial species. Sample preparation methods able to enrich the sample in one bacterial species can potentially reduce the analytical complexity and difficulties in interpreting spectra obtained for bacteria mixtures.

The first example of FlFFF as pre-MALDI/TOF MS of whole bacterial cells employed a commercial, macro-column FlFFF channel [38]. That work threw light on three issues that could limit the effective use of FlFFF for MALDI/TOF MS of whole bacteria. Firstly, possible run-to-run sample carry-over due to incomplete sample recovery from FlFFF could affect spectra reproducibility and, thus, reduce fingerprinting capabilities of MALDI/TOF MS. Secondly, the relatively high sample dilution reached after the FlFFF step could result in cell concentrations that are below the detection limits for MALDI/TOF MS. A concentration step before MS would be necessary, and this would increase method complexity, analysis time, and risk of sample losses and/or further decrease of sensitivity. Thirdly, the time required by the FlFFF step could also affect the intrinsic rapidity of MALDI/TOF MS analysis. HF5 shows itself able to overcome these limitations. When applied to MALDI/TOF MS of whole bacteria, identification capabilities have been found to significantly improve [39]. Representative results obtained from applying HF5 to MALDI/TOF MS are shown in Fig. 3.5a–c. In Fig. 3.5a it is reported an example of a fractogram obtained for a 1:1 mixture of lyophilized *E. coli* and *Bacillus subtilis* (*B. subtilis*) mixture. A complete separation between the two species was achieved. As representatively shown in Fig. 3.5b,c, two completely different spectra were obtained from the fractions collected in correspondence to bands **A** and **B** (shaded fractions **1** and **2**, respectively), with the spectral features found for each individual bacterial species that was found in each spectrum. None of the most characteristic *E. coli* ion signals was found in spectra obtained from bands of type **A**, and none of the most characteristic *B. subtilis* ion signals was found in spectra from bands of type **B**. The number of characteristic signals of each species found in the spectra from each band also increased with respect to the number of characteristic signals found in the spectra of the unfractionated mixture. It is also worth noting that in the representative spectrum in Fig. 3.5c, the *E. coli* ion signal likely assigned to the protein #P02429 is recovered, while it was lost in the spectra of the unfractionated mixture.

3.3.2.2 HF5-UV/Vis Turbidity DAD

With dispersed analytes separated by flow-assisted separation techniques, UV/Vis spectrophotometric detectors are generally employed as turbidimeters, more exactly as low-angle, light scattering detectors [40]. In order to directly convert the analytical signal for quantitative analysis, the extinction properties of the analyte fractionated in dispersion must be known. A method has been proposed to experimentally obtain – by single-run, flow-assisted separation methods with UV/Vis diode-array detectors – the mass-size (or number-size) distribution function of the fractionated, dispersed analytes if a retention-to-size relationship for sizing is either theoretically or empirically available for the chosen separation technique, as in the case of HF5 [41]. The method needs neither standards nor to rely on a method to predict the optical properties of the analytes, and it therefore makes use of a separation method like HF5 to have the required retention-to-size relationship

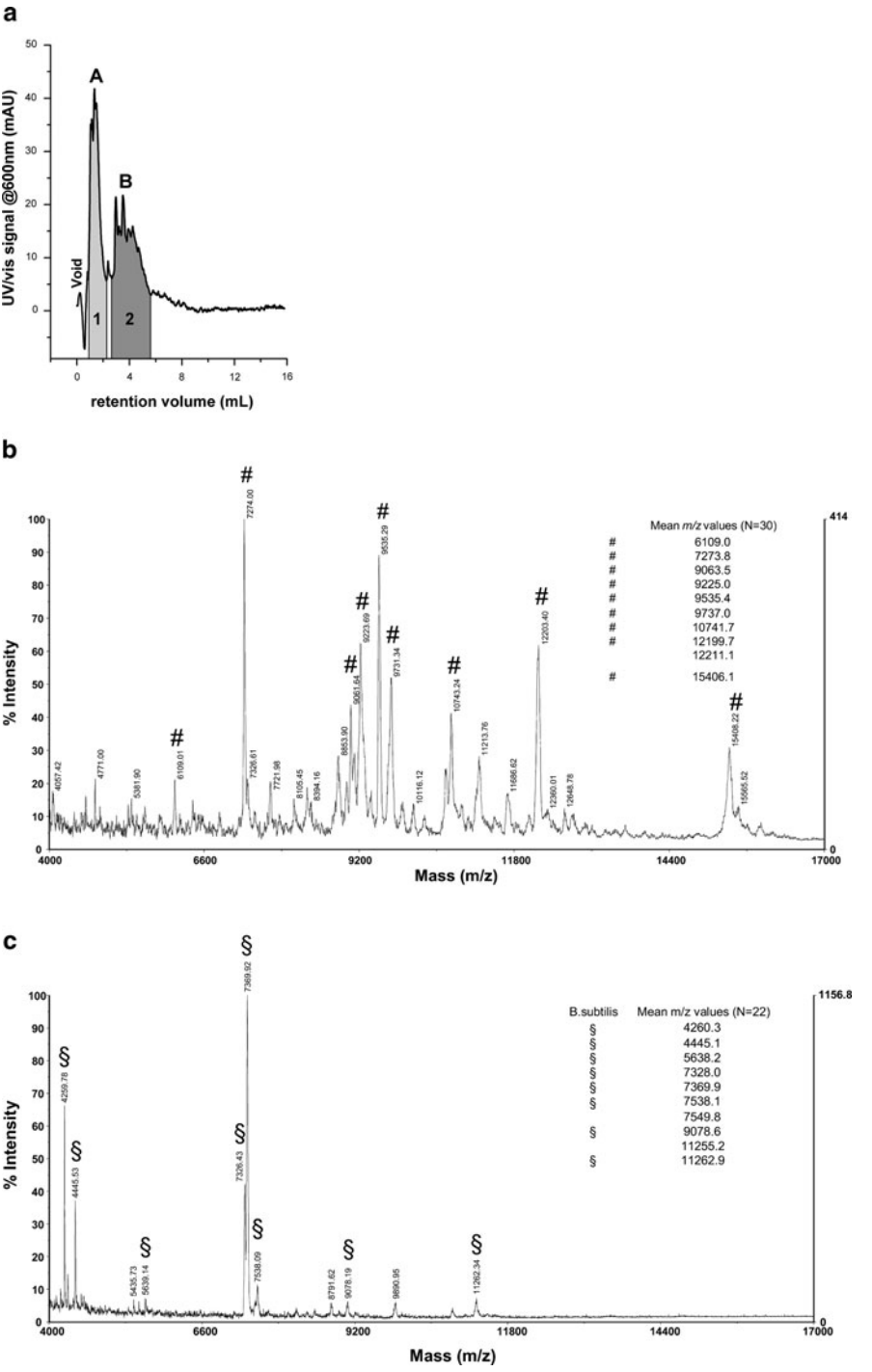

Fig. 3.5 (**a**) Fractogram of a 1:1 mixture of lyophilized *E. coli* and *B. subtilis* cells. $F_{in} = 4.0$ mL/min; $F_{rad} = 0.8$ mL/min. Mobile phase: 1 mM ammonium cholate, pH = 9.2. Band A: *B. subtilis*; band B: *E. coli*. Fraction collection times: fraction 1 (*B. subtilis*) from 20 to 40 s; fraction 2 (*E. coli*) from

for quantifying the fractionated analytes and obtain their particle size-amount distribution (PSAD) from a single fractionation run. The method is based on the fundamental property of the extinction efficiency to be a function of the ratio between the diameter of dispersed, spherical particles and the incident wavelength when the particle refractive index is constant [42]. It then requires the use of a UV/Vis diode-array detector (UV/Vis DAD) to on-real-time record turbidity as a function of the incident wavelength. It must be noted that the assumption of a constant particle refractive index is respected only if absorption is independent of the incident wavelength. The method must thus be applied only within the wavelength ranges in which the analytes do not show specific absorption.

In Fig. 3.6 are reported the mass-size (f, dashed line), and the number-size (f_n, full line) distribution obtained by applying the method to a HF5-UV/Vis DAD fractogram of human red blood cells (HRBCs). Only data collected in the region where HRBCs do not show specific absorption were processed ($\lambda_{min} = 450$ nm; $\lambda_{max} = 800$ nm).

Morphology and size distribution of HRBCs are known to depend on medium osmolarity [43, 44]. It is known that in 170 mOsm media at pH 7.4 (e.g. phosphate

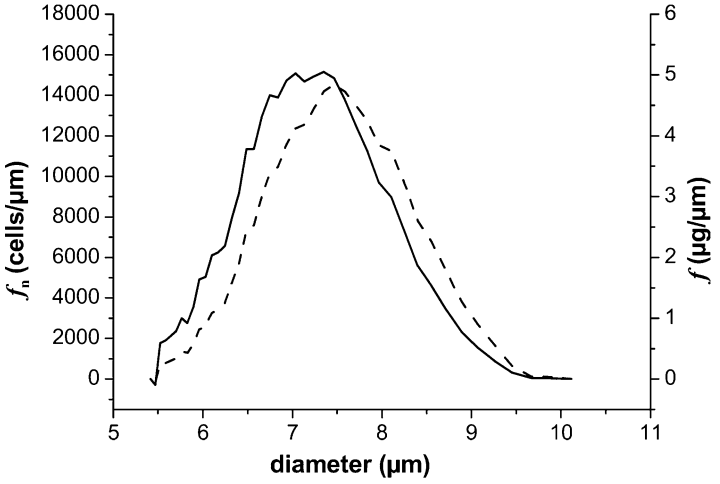

Fig. 3.6 HF5-UV/Vis DAD of spherical HRBCs. Injected HRBCs were 7.0 10^4, the channel flow rate at the HF inlet was 3.00 mL/min, and the radial flow rate was 0.30 mL/min (Adapted with permission from [41], © 2003, American Chemical Society)

Fig. 3.5 (continued) 50 to 100 s. (**b**) MALDI/TOF m/z spectrum of the collected fraction 1; §: Most characteristic *B. subtilis* peaks recovered. (**c**) MALDI/TOF m/z spectrum of the collected fraction 2; #: Most characteristic *E. coli* peaks recovered (Adapted with permission from [39], © 2004, American Chemical Society)

buffered saline, PBS, 85 mM) the HRBC is perfectly spherical, its hydrodynamic diameter corresponding to 1.24 AGV1/3, where AGV is the average HRBC volume. Previous HF5 experiments on spherical HRBCs had shown good agreement between the HRBC size obtained from the AGV measured by uncorrelated methods of clinical analysis and the size determined from HF5 retention time [34]. For the experiment in Fig. 3.6, to have spherical HRBCs the suspending medium and the mobile phase were PBS 170 mOsm. Because of the independence of HF5 retention on particle density, this made the necessary conversion from retention to spherical HRBC size possible by calibration with micrometer-sized, PS spheres, as described in the literature [34]. If the mean value of the number-average size distribution (f_n) reported in Fig. 3.6 (full line) is compared to the mean value given by the reference method employed for sizing the HRBCs sample, reasonably good agreement is found: 7.2 μm vs. 6.6 μm, respectively. It must be recalled that differences as high as 10% in size are quite often obtained by independent, uncorrelated methods for particle size analysis [45].

3.4 Outlook

HF5 is able to overcome some intrinsic issues of standard flat-type FlFFF methodologies, which are related to possible run-to-run sample carry-over due to incomplete sample recovery caused by sample interaction with the channel, to significant sample dilution, and to sterility needs. Therefore, coupling HF5 shows effective to improve performance of even powerful characterization/identification methods for macromolecules (proteins) and micronsized particles (whole cells). The development of coupled methods shows particularly promising to make HF5 soon enter a mature, third-generation phase. Quite a few technical developments such as channel cartridge engineering, and system operation automation such as flow pattern commutation and flow programming have been most recently accomplished to make HF5 technology evolve from a prototype to a pre-competitive phase and, finally, to a commercialized technology. Its recent commercialization will make HF5 technology find most widespread application that we reckon this technology should deserve.

References

1. Lee HL, Reis JFG, Dohner J, Lightfoot EN (1974) Single-phase chromatography: solute retardation by ultrafiltration and electrophoresis. AIChE J 20:776–784
2. Jonsson JA, Carlshaf A (1989) Flow field-flow fractionation in hollow cylindrical fibers. Anal Chem 61:11–18
3. Lee WJ, Min BR, Moon MH (1999) Improvement in particle separation by hollow fiber flow field-flow fractionation and the potential use in obtaining particle site distribution. Anal Chem 71:3446–3452

4. Wijnhoven J, Koorn JP, Poppe H, Kok WT (1995) Hollow-fiber flow field-flow fractionation of polystyrene sulfonates. J Chromatogr A 699:119–129
5. van Bruijnsvoort M, Kok WT, Tijssen R (2001) Hollow-fiber flow field-flow fractionation of synthetic polymers in organic solvents. Anal Chem 73:4736–4742
6. Caldwell KD, Brimhall SL, Gao Y, Giddings JC (1988) Sample overloading effects in polymer characterization by field-flow fractionation. J Appl Polym Sci 36:703–719
7. Kang D, Moon MH (2005) Hollow fiber flow field-flow fractionation of proteins using a microbore channel. Anal Chem 77:4207–4212
8. Giddings JC (1983) Hyperlayer field-flow fractionation. Sep Sci Technol 18:765–773
9. Moon MH, Lee KH, Min BR (1999) Effect of temperature on particle separation in hollow fiber flow field-flow fractionation. J Microcol Sep 11:676–681
10. Min BR, Kim SJ, Ahn KH, Moon MH (2002) Hyperlayer separation in hollow fiber flow field-flow fractionation: effect of membrane materials on resolution and selectivity. J Chromatogr A 950:175–182
11. Wahlund KG, Zattoni A (2002) Size separation of supermicrometer particles in asymmetrical flow field-flow fractionation. Flow conditions for rapid elution. Anal Chem 74:5621–5628
12. Reschiglian P, Roda B, Zattoni A et al (2002) High performance, disposable hollow fiber flow field-flow fractionation for bacteria and cells. First application to deactivated *Vibrio cholerae*. J Sep Sci 25:490–498
13. Park I, Paeng K-J, Kang D, Moon MH (2005) Performance of hollow-fiber flow field-flow fractionation in protein separation. J Sep Sci 28:2043–2049
14. Reschiglian P, Zattoni A, Roda B et al (2005) On-line hollow-fiber flow field-flow fractionation-electrospray ionization/time-of-flight mass spectrometry of intact proteins. Anal Chem 77:47–56
15. Roda A, Parisi D, Guardigli M et al (2006) Combined approach to the analysis of recombinant protein drugs using hollow-fiber flow field-flow fractionation, mass spectrometry, and chemiluminescence detection. Anal Chem 78:1085–1092
16. van Bruijnsvoort M, Tijssen R, Kok WT (2001) Assessment of the diffusional behavior of polystyrene sulfonates in the dilute regime by hollow-fiber flow field-flow fractionation. J Polym Sci B 39:1756–1765
17. Zhu RH, Frankema W, Huo YL, Kok WT (2005) Studying protein aggregation by programmed flow field-flow fractionation using ceramic hollow fibers. Anal Chem 77:4581–4586
18. Roda B, Cioffi N, Ditaranto N et al (2005) Biocompatible channels for field-flow fractionation of biological samples: correlation between surface composition and operating performance. Anal Bioanal Chem 381:639–646
19. Shin SJ, Chung HJ, Min BR et al (2003) Improvement of separation of polystyrene particles with PAN membranes in hollow fiber flow field-flow fractionation. Bull Kor Chem Soc 24:1333–1338
20. Kim HJ, Oh S, Moon MH (2006) Hollow-fiber flow/hyperlayer field-f low fractionation for the size characterization of airborne particle fractions obtained by SPLITT fractionation. J Sep Sci 29:423–428
21. Wijnhoven J, Koorn JP, Poppe H, Kok WT (1996) Influence of injected mass and ionic strength on retention of water-soluble polymers and proteins in hollow-fibre flow field-flow fractionation. J Chromatogr A 732:307–315
22. Rambaldi DC, Zattoni A, Casolari S et al (2007) An analytical method for size and shape characterization of blood lipoproteins. Clin Chem 53:2026–2029
23. Morishima I, Kurono M, Shiro Y (1986) Presence of endogenous calcium-ion in horseradish-peroxidase - elucidation of metal-binding site by substitutions of divalent and lanthanide ions for calcium and use of metal-induced NMR (H-1 and Cd-113) resonances. J Biol Chem 261:9391–9399
24. Dunford HB (1986) Horseradish peroxidase: structure and kinetic properties. In: Everse JE, Everse KE, Grisham MB (eds) Peroxidases in chemistry and biology. CRC Press, Boca Raton

25. Yang BY, Gray JSS, Montgomery R (1996) The glycans of horseradish peroxidase. Carbohydr Res 287:203–212
26. Campbell AK (1998) Chemiluminescence. Principles and applications in biology and medicine. Ellis Horwood, Chichester
27. Roda A, Pasini P, Guardigli M et al (2000) Bio- and chemiluminescence in bioanalysis. Fresen J Anal Chem 366:752–759
28. Roda A, Pasini P, Musiani M et al (1996) Chemiluminescent low-light imaging of biospecific reactions on macro- and microsamples using a videocamera-based luminograph. Anal Chem 68:1073–1080
29. Caldwell KD, Cheng ZQ, Hradecky P, Giddings JC (1984) Separation of human and animal-cells by steric field-flow fractionation. Cell Biophys 6:233–251
30. Lucas A, Lepage F, Cardot PJP (2000) Cell separations. In: Schimpf ME, Caldwell K, Giddings JC (eds) Field-flow fractionation handbook. Wiley, New York
31. Metreau JM, Gallet S, Cardot PJP et al (1997) Sedimentation field-flow fractionation of cellular species. Anal Biochem 251:178–186
32. Rasouli S, Assidjo E, Chianea T, Cardot PJP (2001) Experimental design methodology applied to the study of channel dimensions on the elution of red blood cells in gravitational field-flow fractionation. J Chromatogr B 754:11–21
33. Battu S, Roux A, Delebasee S et al (2001) Sedimentation field-flow fractionation device cleaning, decontamination and sterilization procedures for cellular analysis. J Chromatogr B 751:131–141
34. Reschiglian P, Zattoni A, Roda B et al (2003) Hyperlayer hollow-fiber flow field-flow fractionation of cells. J Chromatogr A 985:519–529
35. Anhalt JP, Fenselau C (1975) Identification of bacteria using mass spectrometry. Anal Chem 47:219–225
36. Fenselau C, Demirev PA (2001) Characterization of intact microorganisms by MALDI mass spectrometry. Mass Spectrom Rev 20:157–171
37. Jarman KH, Cebula ST, Saenz AJ et al (2000) An algorithm for automated bacterial identification using matrix-assisted laser desorption/ionization mass spectrometry. Anal Chem 72:1217–1223
38. Lee H, Williams SKR, Wahl KL, Valentine NB (2003) Analysis of whole bacterial cells by flow field-flow fractionation and matrix-assisted laser desorption/ionization time-of-flight mass spectrometry. Anal Chem 75:2746–2752
39. Reschiglian P, Zattoni A, Cinque L et al (2004) Hollow-fiber flow field-flow fractionation for whole bacteria analysis by matrix-assisted laser desorption/ionization time-of-flight mass spectrometry. Anal Chem 76:2103–2111
40. Reschiglian P, Zattoni A, Torsi G, Melucci D (2001) Quantitative analysis by UV-Vis detection in flow-assisted separation techniques for dispersed samples. Rev Anal Chem 20:239–269
41. Zattoni A, Piccolomini EL, Torsi G, Reschiglian P (2003) Turbidimetric detection method in flow-assisted separation of dispersed samples. Anal Chem 75:6469–6477
42. van de Hulst HC (1981) Light scattering by small particles. Dover Publications, New York
43. Weinstein RS (1974) In: Surgenor DN (ed) The red blood cell. Academic, New York
44. Assidjo NE, Chianea T, Clarot I et al (1999) Osmolarity effects on red blood cell elution in sedimentation field-flow fractionation. J Chromatogr Sci 37:229–236
45. Barth HG (1984) Modern methods of particle size analysis. Wiley, New York

Chapter 4
Two-Dimensional Separation for Proteomic Analysis

Myeong Hee Moon, Ki Hun Kim, and Dukjin Kang

Abstract This chapter describes the development of the two-dimensional separation methods using flow field-flow fractionation (F4) and isoelectric focusing for proteomics utility. The methods described here are the rapid, non-gel-based, on-line, two-dimensional separation methods in which proteins are separated by isoelectric focusing (IEF) in the first dimension according to differences in isoelectric point (pI) followed by size based separation using F4 (either hollow fiber F4 or multilane asymmetrical F4 channels) in an orthogonal direction. In this chapter, the capillary IEF-HF5 and IEF-AF4 methods are described with the demonstration of system performances using protein standards. Also described are the applications to human urinary proteome samples in which proteome fractions are collected and tryptic digested for the proteomic analysis using nanoflow liquid chromatography-tandem mass spectrometry (nLC-ESI-MS-MS).

Keywords 2D protein separation • Non gel based protein separation • Isoelectic focusing • Flow FFF • IEF-AF4 • Proteomics

4.1 Introduction

Flow field-flow fractionation (F4) is an elution based separation method that adopts either a rectangular channel system [1–4] or a cylindrical hollow fiber membrane module (hollow fiber flow field-flow fractionation or HF5) [5–7]. Recently, when F4 methods are combined with an off-line combination of nanoflow liquid

M.H. Moon (✉) • K.H. Kim
Department of Chemistry, Yonsei University, Seoul, South Korea
e-mail: mhmoon@yonsei.ac.kr

D. Kang
Center for Bioanalysis, Division of Metrology for Quality of Life, Korea Research Institute of Standards and Science, Daejeon, South Korea

S.K.R. Williams and K.D. Caldwell (eds.), *Field-Flow Fractionation in Biopolymer Analysis*, DOI 10.1007/978-3-7091-0154-4_4,

chromatography-electrospray ionization-tandem mass spectrometry (nLC-ESI-MS-MS), it has shown the capability as a prefractionation device for proteomics research by the size based fractionation of biological macromolecules followed by the shotgun identification of proteins/peptides. Proteomics applications of F4 with nLC-ESI-MS-MS have been made with the size fractionation of mitochondria [8] or exosomes [9, 10] by F4, with a semi-preparative separation/isolation of membrane debris [11] from cell lysates for the characterization of membrane proteins, and with a selective isolation of N-linked glycosylated proteins [12] using lectin affinity.

F4 can be integrated into a powerful alternative method for proteomics research as a multi-dimensional protein separation device when it is on-line hyphenated with isoelectric focusing (IEF) in an orthogonal dimension. Proteomics often requires a combination of comprehensive analytical methods such as high performance separation methods, mass spectrometry (MS), and bioinformatics. Since the proteome itself is so complicated that currently available, sophisticated, and high resolution MS can not analyze the proteome mixture all at once, a proper fractionation or isolation of target proteins is required prior to MS analysis. Multidimensional protein separation has been attempted by a number of approaches. The most common multidimensional separation method is the two-dimensional polyacrylamide gel electrophoresis (2D-PAGE) in which separation of proteins is carried out by the differences of isoelectric points (pI) with IEF as the first dimension in an immobilized ampholyte strip and then followed by MW separation with gel electrophoresis as the second dimension in a perpendicular direction. [13–16]. Since it is simple in operation and provides a high resolution separation that can accommodate more than 1,000 proteins spots from complicated proteome mixtures, it is widely being utilized in biological and clinical laboratories. Due to the orthogonal combination of the two different separation principles, peak capacity of each separation technique can be multiplied to yield a high resolution separation method among currently available separation methods [16]. However, 2D-PAGE exhibits some difficulties in handling low abundance proteins, retrieving intact proteins from gel matrix, automation and the inevitable denaturation of proteins due to the use of sodium dodecyl sulfate (SDS). Other 2D separation methods for proteins are based on capillary IEF (CIEF) on-line hyphenated with reversed phase [14, 17, 18] or size exclusion [19] chromatography and hyphenated with zone based [20] or gel based [21] capillary electrophoresis. Most of these methods are based on the use of organic solvent or surfactants which induce protein denaturation or dissociation of protein subunits. Moreover, the use of packing media or gels as the second dimension may cause sample loss or deformation and ampholyte solutions utilized for IEF must be removed by a separate means prior to the subsequent analysis using an MS based method.

As an alternative to the gel-based or packing-based method, F4 can be utilized as a second dimension separation method to IEF. Protein bands can be fractionated by size either by hyphenation of CIEF with hollow fiber flow field-flow fractionation (CIEF-HF5) [22] or by IEF coupled to multilane asymmetrical F4 (IEF-AF4) [23, 24]. Ampholyte solution used for IEF can be simultaneously removed during F4

separation so that a separate step to remove ampholyte such as microdialysis is not needed. Proteins retain their three dimensional conformation since aqueous buffer solution is utilized for F4 separation so that intact proteins can be retrieved for secondary analysis. Moreover, the entire operation can be reduced to less than an hour while conventional 2D-PAGE often requires more than 36 h. In this chapter, 2D separation methods based on F4 will be discussed with proteomic applications.

4.2 A Capillary Type of 2D Intact Protein Separation: CIEF-HF5

4.2.1 Configuration of CIEF-HF5

Two-dimensional intact protein separation can be accomplished by assembling CIEF with HF5 in a serial connection via a 6-port sample injection valve as shown in Fig. 4.1. For CIEF, a 9.5-cm long, 310-μm i.d. Teflon tubing is utilized and the Teflon tubing is ended with two micro-tee's at both ends for the connection of another micro-tee to provide electrical connection with anolyte (20 mM NaOH)

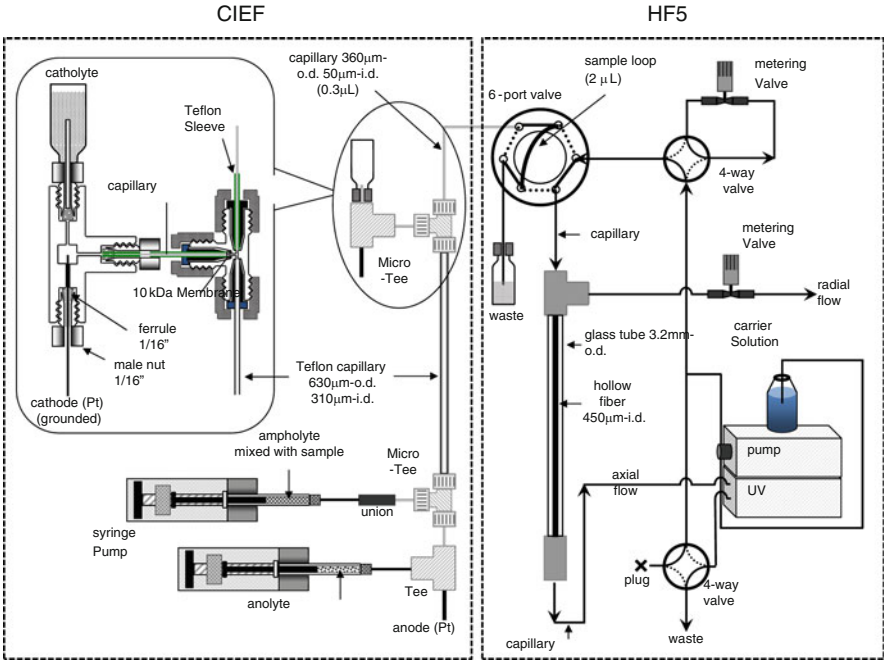

Fig. 4.1 Schematic of the on-line integration of CIEF with HF5. For details, see the Experimental section (Reprinted with permission from [22], © 2006, American Chemical Society)

for anode, and catholyte (20 mM H_3PO_4) for cathode. For the cathodic side, inset of Fig. 4.1 illustrates how the catholyte reservoir is placed in an upright position in order to absorb possible bubbles generated from the electrode surface while a small piece of membrane is placed at the micro-tee connection port so that proteins should not be attracted toward the electrode side. A general assembly of HF5 is explained in literature [5, 25]. However, HF5 in this case utilizes a microbore hollow fiber. The HF5 module is constructed by inserting a microbore polysulfone HF having 450-μm i.d. into a 3.2-mm o.d. and 1.6-mm i.d. glass tube and both ends of the HF are connected with silica capillary tubing (200-μm i.d./360-μm o.d.) by means of a union at one end and a Derlin tee at the other end without the use of glue. A precise description can be found from literature [6].

For the operation of CIEF-HF5 [22], proteome sample mixed with ampholyte solution (less than 10 μL) is first injected via syringe pump into the Teflon capillary and then CIEF separation is carried out with the application of an electrical field at 500 V/cm for 20 min. After CIEF is completed, a small portion (1 ~ 2 μL) of fractionated protein bands is transferred to the 6-port injection valve depending on the desired pI interval to be analyzed by pushing anolyte solution to the CIEF tube using a syringe pump. Once a small volume fraction of protein bands is loaded onto the injection valve, the valve is turned so that sample can be delivered to the HF5 module with flow from an HPLC pump. During sample loading, pump flow is set to divide into two parts from the two 4-way valves so that focusing/relaxation of sample components can be accomplished by delivering two counter-directing flows from both ends of the HF to the 1/10 position of the fiber length. The focusing/relaxation period (which includes sample loading) is ~1 min in a typical protein separation using microbore HF. Carrier liquid for HF5 is 10 mM NH_4HCO_3 solution prepared from ultra pure water. After the focusing/relaxation, all flows are diverted to the HF5 inlet only so that size fractionation of proteins can be accomplished. While the HF5 separation process is on-going, protein bands of the next pI interval are sequentially transferred to the sample loop for the next HF5 run and simultaneously the rest of the protein bands remaining in CIEF tube are kept under electrical field.

4.2.2 CIEF-HF5 for Protein Separation

The performance of CIEF-HF5 is tested with protein standard mixtures (1: horse myoglobin (16.9 kDa, pI 7.2), 2: trypsinogen (24 kDa, pI 9.3), 3: carbonic anhydrase (29 kDa, pI 5.85) 4: BSA (66 kDa, pI 4.8), 5. YADH (yeast alcohol dehydrogenase, 150 kDa, pI 6.23)) and the HF5 fractograms obtained with or without CIEF are shown in Fig. 4.2a. When the HF5 separation is carried out alone without CIEF separation, proteins 1–3 are not resolved at all (top fractogram in Fig. 4.2a) since their MW values are close to each other. When CIEF is performed prior to HF5 separation, proteins of different pIs elute at different HF5 times. For the present mixtures, four different fractions (pH intervals of 3–5, 5–6,

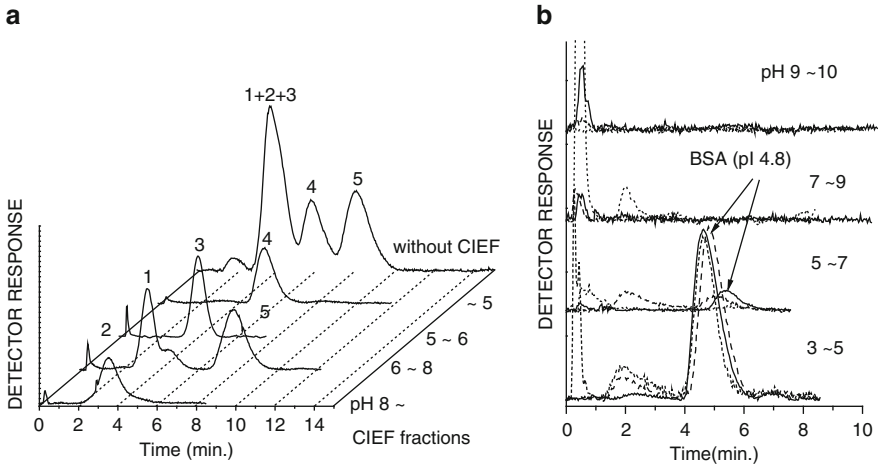

Fig. 4.2 (**a**) The HF5 fractograms of various proteins without CIEF and after CIEF; 1: horse myoglobin (16.9 kDa, pI 7.2), 2: trypsinogen (24 kDa, pI 9.3), 3: carbonic anhydrase (29 kDa, pI 5.85) 4: BSA (66 kDa, pI 4.8), 5. YADH (yeast alcohol dehydrogenase, 150 kDa, pI 6.23). Flow rates were 0.6 mL/min for the inlet flow and 60 μL/min for the outlet flow. (**b**) The reproducibility of the CIEF-HF5 separation of BSA (Reprinted with permission from [22], © 2006, American Chemical Society)

6–8, and 8–10) are sequentially separated by HF5. The pH interval of the first CIEF fraction loaded to HF5 is pH 8–10 (~2 μL) in which trypsinogen (peak 2, pI 9.3) elutes within 6 min. For the HF5 run of the CIEF fraction having pH 6–8, myoglobin and YADH are successfully resolved by their sizes along with the presumable dimer peaks of myoglobin at the rear shoulder of peak 1. Figure 4.2a shows that CIEF-HF5 not only separates proteins according to pI (peaks 1–3 eluted at different runs) but also by size. In addition, peak 5 which is from YADH appears at a sufficiently long retention time which supports the notion of maintained protein conformation while a 2D-PAGE experiment of the same mixture shows dissociated subunit spots at a MW marker position between 36.5 KDa and 55 KDa (see ref. 22). Reproducibility of the CIEF-HF5 system is evaluated with three repeat injections of 300 ng BSA. Data in Fig. 4.2b, show that of the relative standard deviation in retention time is within 3.0% and the sample recovery is 88. 4 ± 0.1% (compared to the peak area measured from an HF5 run for BSA without CIEF).

4.2.3 CIEF-HF5 for Human Urinary Proteome

CIEF-HF5 is applied to the fractionation of a human urinary proteome sample. In this study, a urine sample is first filtered using a membrane filter of 30 kDa MWCO and only the protein fraction larger than 30 kDa is utilized. Figure 4.3a shows the HF5 fractograms obtained for the CIEF fractions of six sequential pH intervals

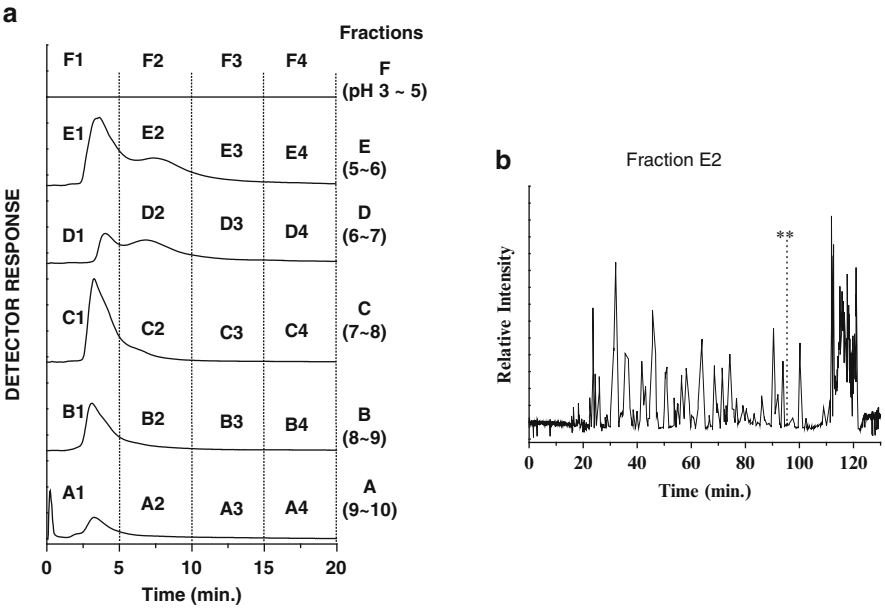

Fig. 4.3 (**a**) The CIEF-HF5 fractionation of a human urinary proteome sample. The HF5 fractograms for the six CIEF fractions of the urine proteins (~40 μg). (**b**) Base peak chromatograms (BPC's) of the four CIEF-HF5 fraction E2 by nanoflow LC-MS-MS after the tryptic digestion of each protein fraction (Reprinted with permission from [22], © 2006, American Chemical Society)

(marked in the right axis of Fig. 4.3a), injected from 40 μg of the proteome sample. The elution profile of each pH fraction shows differences in protein distribution except for fraction F which presents an artifact from the electroosmotic flow of proteins to a nearby fraction (toward the high pH region). The entire run for Fig. 4.3a takes less than 3 h while 2D-PAGE requires at least 36 h. Protein fractions are collected during CIEF-HF5 run for 5-min intervals and each collected fraction is digested with trypsin to produce peptide mixtures for shotgun identification of proteins/peptides. Figure 4.3b shows the base peak chromatogram of the digested peptide mixture from the fraction E2 during nLC-ESI-MS-MS run. The numerous peaks shown in Fig. 4.3b represent the elution of peptide mixtures generated from the digestion of the fraction E2 and they are analyzed by data dependent collision induced dissociation for fragment ion MS spectra. The precursor scan MS spectra obtained for the peak at 95.4 min (marked as ** in Figure 4.3b) contains a peptide ion m/z 987.06 (+2: doubly protonated). Its CID spectra results in the identification of a monocyte differentiation antigen CD14 with a peptide sequence of R.AFPALTSLDLSDNPGLGER.G, of which protein is reported as biomarkers for an inflamed pilonidal abscess in the literature [26], from database search. Peptide peaks from all fractions are analyzed to obtain protein identifications by shotgun analysis using nLC-ESI-MS-MS. For the nLC-ESI-MS-MS analysis, a pulled tip

capillary LC column (75 μm i.d., 360 μm o.d., 15 cm L, 5 μm 100 Å Magic C_{18AQ}) without a separate emitter is prepared in our laboratory. A detailed method to assemble a nanoflow LC setup is explained in literature [27, 28]. For nLC separation, a binary RP gradient elution (mobile phase composition of (A) 3% CH_3CN in water and (B) 95% CH_3CN in water, both containing 0.1% HCOOH) is utilized. For ESI-MS-MS, a spray voltage of 2.5 kV in the positive mode of ionization is employed. Data analysis of the collected raw MS-MS spectra is performed with the Mascot Search program using both Swiss-Prot and NCBI human data bases and only peptides yielding larger than a minimum Mascot score of 30 are accepted as an extensive homology for data screening.

From the nLC-ESI-MS-MS analysis of all fractions collected, a total of 114 proteins are identified and the entire list can be found from literature [22].

4.3 A Flat Bed Type of 2D Intact Protein Separation: IEF-AF4

While the CIEF-HF5 system provides non-gel based 2D intact protein separation with several features such as isolation/collection of intact proteins in a certain pI and d_s (hydrodynamic diameter) and online removal of carrier ampholyte solution, the maximum injection amount of proteome sample is limited (~40 μg) due to the use of narrow bore tubes (Teflon tube for CIEF and microbore hollow fiber for HF5). In addition, while one pI fraction of proteins is loaded into HF5 for size separation, the other pI fractions should be left in the CIEF tube until HF5 separation of the previous fraction is completed. Though the entire separation time in CIEF-HF5 is significantly reduced by a factor of 10 from that of 2D-PAGE, stagnation of fractionated proteins in CIEF tubing under the electrical field causes a shift in the position of protein bands from the influence of electroosmotic flow as well as unnecessary delay in time. For the high throughput and high speed separation, the new multilane channel system is designed by adopting the conventional rectangular design of an FFF channel with an array of multiple asymmetrical flow field-flow fractionation (AF4) channels [23].

4.3.1 System Configuration of IEF-AF4

IEF-AF4 multilane channel system consists of six miniaturized AF4 channels that are aligned in parallel as shown in Fig. 4.4a and the beginning area of the six channels are opened together in order to provide an IEF segment [23]. Thus, IEF is carried out in a direction normal to the AF4 channel axis. At both ends of the IEF segment, anolyte (0.010 M phosphoric acid) and catholyte (0.020 M NaOH) reservoirs are connected by capillary tube with each electrode immersed inside. The multilane channel has six parallel trapezoidal design (11.0 cm tip-to-tip, 1.0–0.3 cm in breadths, 300-μm-thick) with the IEF sector (between 1.0 and

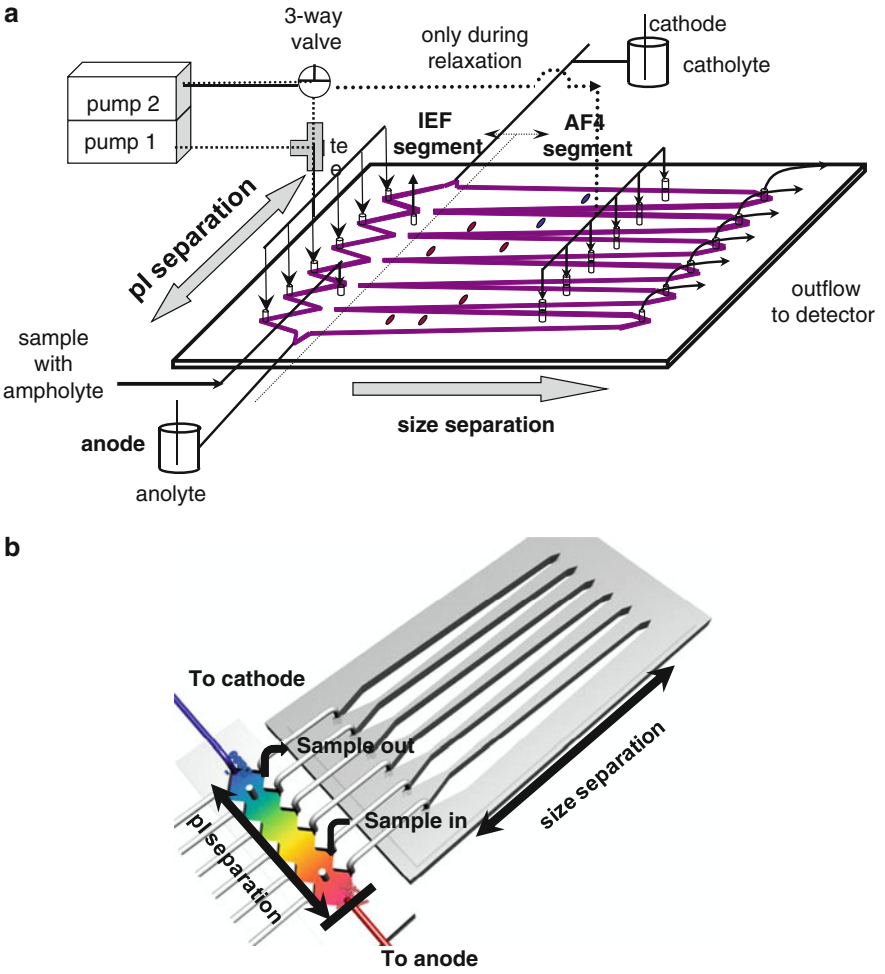

Fig. 4.4 (**a**) Schematics of multilane FlFFF channel structure for IEF-AF4 (Reprinted with permission [23], © American Chemical Society, 2009), (**b**) modification of IEF-AF4 channel by isolation of the IEF sector with a separate IEF channel (Reprinted with permission from [24], © 2009, American Chemical Society)

1.5 cm from each channel inlet) open together. Therefore, the length of the AF4 channel itself is 9.5 cm from the beginning of the channel divider to the end of each channel. Below the channel spacer in Fig. 4.4a, a PLCGC (MWCO, 20 kDa) from Millipore Corp. (Danvers, MA) is layered above the ceramic frit having 5 μm pores. When sample is loaded with ampholyte solution for IEF using a syringe pump, all inlets and outlets of IEF-AF4 channel and the crossflow outlet in Fig. 4.4a are closed except for the outlet of the IEF segment so that proteins with ampholyte mixtures are placed between the two ports. Before the sample loading, the interface between each electrolyte reservoir and the IEF segment needs to be filled with

electrolyte solutions. Otherwise, ampholyte solution can be pulled out of the IEF segment toward each electrode when the electric field is applied, causing a loss of proteins having extreme pIs close to the limiting end of the pI interval of an electrolyte. After sample loading to the IEF segment, 1–3 kV is applied for 5 min to carry out IEF separation. When the IEF process is completed, protein bands fractionated by pI differences in the IEF segment are immediately transferred to the beginning of each AF4 channel, and then each protein fraction undergoes the focusing/relaxation procedure to establish equilibrium states of proteins before separation. During focusing/relaxation period, flows from both pumps are delivered to channel to focus at the vicinity of the beginning of each AF4 channel for 100 s. Once focusing/relaxation is finished, only fluid from pump flow 1 is delivered to the six inlets of the AF4 channel at flow rates required for separation.

The IEF segment can be isolated from the multilane channel system as shown in Fig. 4.4b. Isolation of the IEF segment into a separate IEF channel can be made similarly to an FFF channel by using a Teflon spacer cut in a saw-tooth shape (6.0 cm long, 0.5 cm wide, and 0.030 cm thick) as shown in Fig. 4.4b and the IEF channel is connected with AF4 multilane channels with narrow bore PEEK tubing [24]. This design gives an additional advantage, as it bypasses possible sample clogging at the channel membrane surface during IEF when IEF is embedded as shown in Fig. 4.4a.

4.3.2 Evaluation of IEF-AF4 Multilane Channel System

For the IEF-AF4 channel system, the effects of ampholyte concentration and electrical voltage on the performance of IEF are initially evaluated using BSA. When the concentration of ampholyte solution (Fluka Ampholyte High-Resolution pH 3–10) is varied from 0.5% to 2%, 1% ampholyte provides efficient separation of BSA eluted at the right channel lane under 3 kV for 5 min for IEF in Fig. 4.5a. When the ampholyte concentration is 0.5%, BSA is found to elute from channel 1 (data not shown), which means the pH gradient is not properly built up in the IEF segment. Since the pI value of BSA is 4.8, it is expected to elute from the channel 2 (ideal ΔpH of channel 2 is 4.17 ~ 5.33 assumed from the linear gradient).

The effect of electrical voltage on IEF is tested with carbonic anhydrase (CA, pI 5.8) mixed with 1.0% ampholyte by applying different voltages. At 1.0 kV, IEF of CA is not completed during a time interval of 100 s because CA molecules elute from all three channel lanes. However, when the voltage is increased to 3.0 kV, CA appears to elute exclusively from the channel lane 3 (ideal ΔpH = 5.34 ~ 6.50) with a sharp peak in Fig. 4.5b.

4.3.3 IEF-AF4 for Protein Separation

Evaluation of the modified IEF-AF4 system is carried out by the separation of seven protein standard mixtures. Figure 4.6a shows the AF4 fractograms obtained at each AF4 channel lane after IEF using 1.0% ampholyte solution having a narrower pH

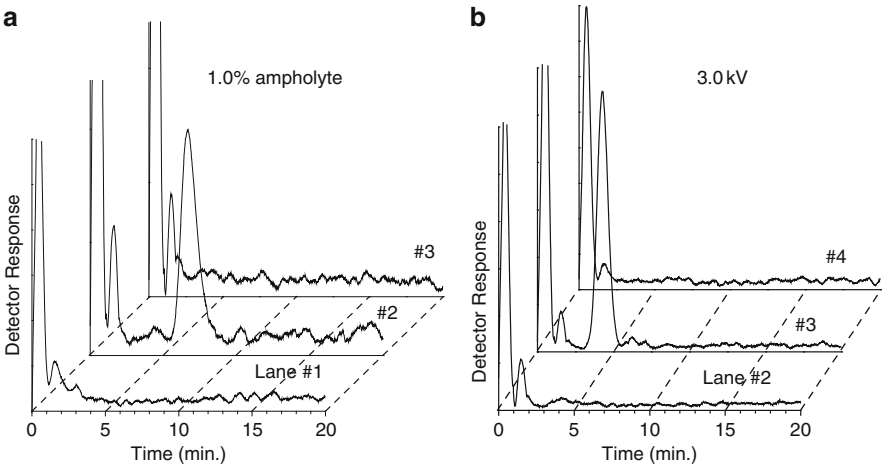

Fig. 4.5 (**a**) IEF-AF4 separation of BSA (pI = 4.8, 66 kDa, injection amount = 1.0 μg) at 1.0% ampholyte at 3 kV and (**b**) effect of IEF voltage on IEF-AF4 separation of carbonic anhydrase (pI = 5.8, 29 kDa, injection amount = 1.0 μg). Ideal pH range of each FFF channel is 3.00–4.16, 4.17–5.33, and 5.34–6.50 for lane 1, 2, and 3, respectively. The flow rates for AF4 separation at each channel lane are $\dot{V}_{in}/\dot{V}_{out}$ = 1.0/0.25 in mL/min (focusing/relaxation period for AF4 = 100 s) (Reprinted with permission from [23], © 2009, American Chemical Society)

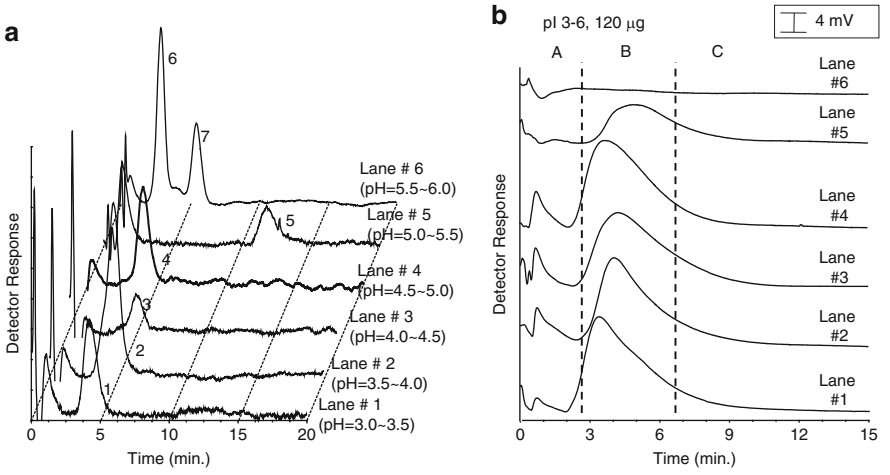

Fig. 4.6 (**a**) IEF-AF4 fractograms of protein mixtures: peak no. 1: fetuin (48 kDa, pI = 3.3), 2: amyloglucosidase (48 kDa, pI = 3.6), 3: glucose oxidase (66 kDa, pI = 4.2), 4: BSA (66 kDa, pI = 4.8), 5: apoferritin (444 kDa, pI = 5.4), 6: carbonic anhydrase (29 kDa, pI = 5.8), and 7: alcohol dehydrogenase (150 kDa, pI = 5.9). Flow rate conditions for AF4 are V_{in}/V_{out} = 0.84/0.24 in mL/min for each AF4 channel. (**b**) IEF-AF4 separation of human urinary proteome using ampholyte solutions with pH = 3.0–6.0 under the same experimental conditions used in Fig. 4.6a. Protein fractions (three for each AF4 run) are collected for shotgun proteomic analysis (Reprinted with permission from [24], © 2009, American Chemical Society)

range (3.0 ~ 6.0) under 2 kV for 500 s. In this case, expected ΔpH of each AF4 channel is 0.5 unit. In Fig. 4.6a, proteins elute at each AF4 channel of which ΔpH includes the pI value of the protein standard as peak 1: fetuin (48 kDa, pI = 3.3), 2: amyloglucosidase (48 kDa, pI = 3.6), 3: glucose oxidase (66 kDa, pI = 4.2), and 4: BSA (66 kDa, pI = 4.8), 5: apoferritin (444 kDa, pI 5.4), 6: CA (29 kDa, pI 5.8), 7: ADH (150 kDa, pI 5.9). It is noted that carbonic anhydrase (peak # 6, 29 kDa, pI = 5.8) and alcohol dehydrogenase (#7, 150 kDa, pI = 5.9), eluted at lane 6 show a clear separation according to MW. It also indicates that AF4 successfully provides the size separation of proteins during elution and that IEF-AF4 resolves larger molar mass proteins (>100 kDa) successfully, as shown in peaks 5 and 7, while 2D-PAGE shows limited capability in resolving larger proteins. Injection amount for each protein standard is 10 μg (total 70 μg), representing the increase of throughput compared to the capillary type of 2D separation. It also demonstrates that an ampholyte solution of a narrower pH interval can be utilized for a finer separation of proteins having small differences in pI values.

The IEF-AF4 channel system modified with an isolated IEF sector is employed for the 2D fractionation of a human urinary proteome sample from a healthy donor. IEF is carried out by using two carrier ampholyte solutions: pH = 3.0–6.0 and pH 3.0–10.0 in order to compare the performances of protein identification. Figure 4.6b shows the AF4 fractograms obtained from an injection of 120 μg of the urinary proteome sample with an ampholyte having pH = 3.0–6.0. IEF operation and AF4 separation are carried out at the same run conditions utilized for Fig. 4.6a. For the nLC-ESI-MS-MS analysis, fractions are collected at the time interval marked by the broken lines in Fig. 4.6b and five IEF-AF4 runs are made for the accumulation of each fraction. A similar run is made for the sample using an ampholyte of pH 3.0–10.0. The collected fractions are digested by proteomics grade trypsin and the resulting peptide mixture sample of each fraction is analyzed by nLC-ESI-MS-MS.

It can be expected that using an ampholyte solution of a narrow pH interval offers a finer separation of proteins during IEF, which eventually reduces the ionization suppression effect from high abundant peptides. This can be explained with the following MS spectra obtained for the similar time frame for fractions from the two IEF-AF4 runs. The two MS spectra shown in Fig. 4.7 are the precursor MS scans of peptide mixtures from (a) the fraction 4C (representing the AF4 fraction C of the channel lane 4 with the expected pH interval of 4.5–5.0 in Fig. 4.6b) employed with pH 3.0–6.0 at 48.3 min of nLC and (b) the fraction 2C (pH 4.2–5.3) employed with pH 3.0–10.0 ampholyte at 44.2 min (nLC). Proteins contained in the fraction 4C are expected to exist in the fraction 2C since the pH interval of the fraction 2C is broader than that of the fraction 4C. The difference in retention times originate from the use of different capillary columns. However, the selection of the retention time frame shown in Fig. 4.7 is based on the monitoring of the same peptide ions simultaneously found from both runs: peptide ions of m/z 716.6 and 1106.5 in Fig. 4.7a match with those of m/z 716.6 and 1107.3 in Fig. 4.7b. However, due to the influence of high abundant co-eluting ions, their CID experiments show differences in the identification of proteins. For the case of both ions of m/z 1106.5 and 1107.3, they are identified from the CID spectra as

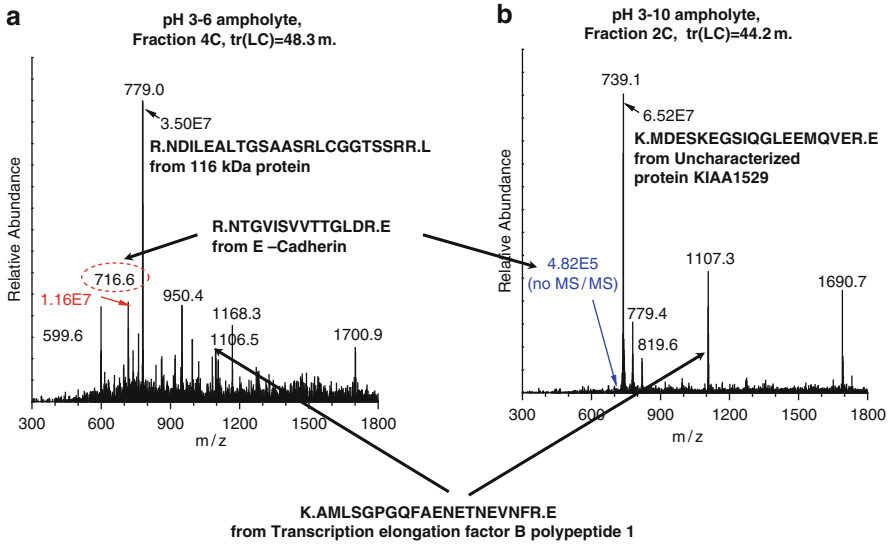

Fig. 4.7 Precursor scan MS spectra of digested AF4 fractions collected by changing ampholyte solutions (**a**. pH = 3.0–6.0 and **b**. pH = 3.0–10.0). (**a**) Fraction 4C represents the AF4 fraction C of the channel lane 4 and (**b**) fraction 2C for the fraction C of the lane 2. The retention time of each spectrum represents the time slice of the corresponding precursor MS scan during nLC-ESI-MS-MS (Reprinted with permission from [24], © 2009, American Chemical Society)

K.AMLSGPGQFAENEVNFR.E from transcription elongation factor B polypeptide 1 (pI = 4.78). However, while the precursor ion of m/z 716.6 at Fig. 4.7a is identified as R.NTGVISVVTTGLDR.E from E-cadherin (pI = 4.58), the same precursor ion is not successfully identified from CID due to the weak intensity (4.8×10^5) of the peptide ion peak in the precursor scan of Fig. 4.7b. This is caused by ionization suppression from three other abundant peptide ions (m/z 739.1, 1107.3, and 1690.7) exhibiting relatively high intensities ($> \sim 2 \times 10^7$ in intensity).

Protein numbers identified from nLC-ESI-MS-MS using the human data base yield a total of 245 urinary proteins for both experiments carried out with two different ampholyte solutions: 164 proteins from the experiment with pH 3–10 ampholyte and 190 proteins from pH 3–6 ampholyte solution as shown in Fig. 4.8. For both experiments, 107 proteins are commonly found. Though the number of proteins identified from these experiments is not as great as the literature value (~1,580) accumulated so far [28–32], 110 unique species among the total 245 proteins found in our study have not been reported elsewhere. Moreover, 42 proteins (including 28 unique species) are found to be above 100 kDa which demonstrates the efficiency of AF4 separation in recovering larger molecular species (>100 kDa). The entire protein lists can be found from literature [24]. Since urine is the most convenient source of clinical sample without an invasive procedure, urinary proteome analysis can offer biomarker development in the

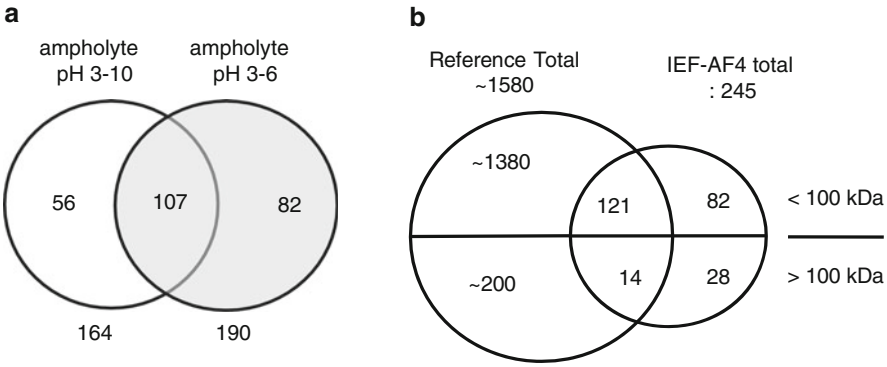

Fig. 4.8 The number of urinary proteins identified from IEF-AF4 separation followed by nLC-ESI-MS-MS analysis of collected fractions after digestion; (**a**) protein numbers from different ampholyte solutions are compared and (**b**) from references according to MW values (Reprinted with permission from [24], © 2009, American Chemical Society)

inherited diseases. In the case of known targets, selective fractionation of target proteins by IEF-AF4 can be a good analytical tool to monitor disease biomarkers and for clinical or genetic treatments. In our experiment using the narrow pH ampholyte solution, identified proteins such as oncostatin-M specific receptor subunit beta precursor, alpha-galactosidase A precursor, cathepsin D precursor, and cublin precursor are known to trigger diseases such as primary localized cutaneous amyloidosis [33], Fabry disease [34], human neurodegenerative disorder [35], and megaloblastic anemia [36], respectively, when they are deficient or mutated pathogenically. The developed channel can provide a finer separation of protein pI intervals when more AF4 channels are implemented simultaneously. This will provide a flexibility to handle post-translationally modified proteins as an alternative speedway for therapeutic and clinical utilities.

Acknowledgments This work was supported by a Korea National Research Foundation Grant (NRF-2010-0014046).

References

1. Giddings JC (1993) Field-flow fractionation: analysis of macromolecular, colloidal, and particulate materials. Science 260:1456–1465
2. Ratanathanawongs-Williams SK (2000) Flow field-flow fractionation. In: Schimpf ME, Caldwell KD, Giddings JC (eds) Field-flow fractionation handbook. Wiley-Interscience, New York
3. Wahlund KG, Giddings JC (1987) Properties of an asymmetrical flow field-flow fractionation channel having one permeable wall. Anal Chem 59:1332–1339
4. Moon MH, Kwon HS, Park I (1997) Stopless flow injection in asymmetrical flow field-flow fractionation using a frit inlet. Anal Chem 69:1436–1440

5. Jönsson JA, Carlshaf A (1989) Flow field-flow fractionation in hollow cylindrical fibers. Anal Chem 61:11–18
6. Lee WJ, Min BR, Moon MH (1999) Improvement in particle separation by hollow fiber flow field-flow fractionation and the potential use in obtaining particle size distribution. Anal Chem 71:3446–3452
7. Bruijnsvoort MV, Kok WT, Tijssen R (2001) Hollow-fiber flow field-flow fractionation of synthetic polymers in organic solvents. Anal Chem 73:4736–4742
8. Kang D, Oh S, Reschiglian P, Moon MH (2008) Separation of mitochondria by flow field-flow fractionation for proteomic analysis. Analyst 133:505–515
9. Oh S, Kang D, Ahn SM, Simpson RJ, Lee BH, Moon MH (2007) Miniaturized asymmetrical flow field-flow fractionation: application to biological vesicles. J Sep Sci 30:1082–1087
10. Kang D, Oh S, Ahn SM, Lee BH, Moon MH (2008) Proteomic analysis of exosomes from human neural stem cells by flow field-flow fractionation and nanoflow liquid chromatography – tandem mass spectrometry. J Proteome Res 7:3475–3480
11. Kang D, Yoo JS, Kim MO, Moon MH (2009) A soft preparative method for membrane proteome analysis using frit inlet asymmetrical flow field-flow fractionation: application in a prostatic cancer cell line. J Proteome Res 8:982–991
12. Kang D, Ji E, Moon MH, Yoo JS (2010) Lectin based enrichment method for glycoproteomics using hollow fiber flow field-flow fractionation: application to streptococcus pyogenes. J Proteome Res. (in Press)
13. Righetti PG, Castagna A, Herbert B (2001) Peer reviewed: prefractionation techniques in proteome analysis. A new approach identifies more low-abundance proteins. Anal Chem 73:320A–326A
14. Zhou F, Johnston MV (2004) Protein characterization by on-line capillary isoelectric focusing, reversed-phase liquid chromatography, and mass spectrometry. Anal Chem 76:2734–2740
15. Klose J, Kobalz U (1995) Two-dimensional electrophoresis of proteins: an updated protocol and implications for a functional analysis of the genome. Electrophoresis 16:1034–1059
16. Giddings JC (1991) Unified separation science. John, New York, pp 126–128
17. Chen J, Lee CS, Shen Y, Smith RD, Baehrecke EH (2002) Integration of capillary isoelectric focusing with capillary reversed-phase liquid chromatography for two-dimensional proteomics separation. Electrophoresis 23:3143–3148
18. Chen J, Balgley BM, DeVoe DL, Lee CS (2003) Capillary isoelectric focusing-based multidimensional concentration/separation platform for proteome analysis. Anal Chem 75:3145–3152
19. Tragas C, Pawliszyn J (2000) On-line coupling of high performance gel filtration chromatography with imaged capillary isoelectric focusing using a membrane interface. Electrophoresis 21:227–237
20. Yang C, Zhang L, Liu H, Zhang W, Zhang Y (2003) Two-dimensional capillary electrophoresis involving capillary isoelectric focusing and capillary zone electrophoresis. J Chromatogr A 1018:97–103
21. Yang C, Liu H, Yang Q, Zhang L, Zhang W, Zhang Y (2003) On-line hyphenation of capillary isoelectric focusing and capillary gel electrophoresis by a dialysis interface. Anal Chem 75:215–218
22. Kang D, Moon MH (2006) Development of non-gel-based two-dimensional separation of intact proteins by an on-line hyphenation of capillary isoelectric focusing and hollow fiber flow field-flow fractionation. Anal Chem 78:5789–5798
23. Kim KH, Moon MH (2009) Development of a multilane channel system for nongel-based two-dimensional protein separations using isoelectric focusing and asymmetrical flow field-flow fractionation. Anal Chem 81:1715–1721
24. Kim KH, Moon MH (2009) High speed two-dimensional protein separation without gel by isoelectric focusing-asymmetrical flow field-flow fractionation:application to urinary proteome. J Proteome Res 8:4272–4278
25. Reschiglian P, Zattoni A, Cinque L, Roda B, Piaz FD, Roda A, Moon MH, Min BR (2004) Hollow-fiber flow field-flow fractionation for whole bacteria analysis by matrix-assisted laser desorption/ionization time-of-flight mass spectrometry. Anal Chem 76:2103–2111

26. Pang JX, Gianni N, Dongre AR, Hefta SA, Opiteck GJ (2002) Biomarker discovery in urine by proteomics. J Proteome Res 1:161–169
27. Kang D, Nam H, Kim YS, Moon MH (2005) Dual-purpose sample trap for on-line strong cation-exchange chromatography/reversed-phase liquid chromatography/tandem mass spectrometry for shotgun proteomics application to the human jurkat T-cell proteome. J Chromatogr A 1070:193–200
28. Castagna A, Cecconi D, Sennels L, Rappsilber J, Guerrier L, Fortis F, Boschetti E, Lomas L, Righetti PG (2005) Exploring the hidden human urinary proteome via ligand library beads. J Proteome Res 4:1917–1930
29. Coon JJ, Zürbig P, Dakna M, Dominiczak AF, Decramer S, Fliser D, Frommberger M, Golovko I, Good DM, Herget-Rosenthal S, Jankowski J, Julian BA, Kellmann M, Kolch W, Massy Z, Novak J, Rossing K, Schanstra JP, Schiffer E, Theodorescu D, Vanholder R, Weissinger EM, Mischak H, Schmitt-Kopplin P (2008) CE-MS analysis of the human urinary proteome for biomarker discovery and disease diagnostics. Proteomics 2:964–973
30. Spahr CS, Davis MT, McGinley MD, Robinson JH, Bures EJ, Beierle J, Mort J, Courchesne PL, Chen K, Wahl RC, Yu W, Luethy R, Patterson SD (2001) Towards defining the urinary proteome using liquid chromatography-tandem mass spectrometry. I. Profiling an unfractionated tryptic digest. Proteomics 1:93–107
31. Pieper R, Gatlin CL, McGrath AM, Makusky AJ, Mondal M, Seonarain M, Field E, Schatz CR, Estock MA, Ahmed N, Anderson NG, Steiner S (2004) Characterization of the human urinary proteome: a method for high-resolution display of urinary proteins on two-dimensional electrophoresis gels with a yield of nearly 1400 distinct protein spots. Proteomics 4:1159–1174
32. Adachi J, Kumar C, Zhang Y, Olsen JV, Mann M (2006) The human urinary proteome contains more than 1500 proteins, including a large proportion of membrane proteins. Genome Biol 7:R80
33. Arita K, South AP, Hans-Filho G, Sakuma TH, Lai-Cheong J, Clements S, Odashiro M, Odashiro DN, Hans-Neto G, Hans NR, Holder MV, Bhogal BS, Hartshorne ST, Akiyama M, Shimizu H, McGrath JA (2008) Oncostatin M receptor-beta mutations underlie familial primary localized cutaneous amyloidosis. Am J Hum Genet 82:73–80
34. Lai LW, Whitehair O, Wu MJ, O'Meara M, Lien YH (2003) Analysis of splice-site mutations of the alpha-galactosidase A gene in Fabry disease. Clin Genet 63:476–482
35. Steinfeld R, Reinhardt K, Schreiber K, Hillebrand M, Kraetzner R, Bruck W, Saftig P, Gartner J (2006) Cathepsin D deficiency is associated with a human neurodegenerative disorder. Am J Hum Genet 78:988–998
36. Aminoff M, Carter JE, Chadwick RB, Johnson C, Grasbeck R, Abdelaal MA, Broch H, Jenner LB, Verroust PJ, Moestrup SK, de la Chapelle A, Krahe R (1999) Mutations in CUBN, encoding the intrinsic factor-vitamin B12 receptor, cubilin, cause hereditary megaloblastic anaemia 1. Nat Genet 21:309–313

Chapter 5
Field-Flow Fractionation in Therapeutic Protein Development

Joey Pollastrini, Linda O. Narhi, Yijia Jiang, and Shawn Cao

Abstract The development lifecycle for pharmaceutical proteins begins with target identification and demonstration of the biological relevance of a particular protein or protein property, continues to identification of which lead product candidate and cell line to advance, then proceeds through process and formulation development and characterization, clinical trials and commercialization. The launch of a product represents the beginning of a different kind of product support, which includes lot release, exploration of different delivery devices, comparability, and support for investigations. The past several decades have seen demonstration and documentation of the utility of asymmetrical flow field-flow fractionation (AF4) in biotechnology applicable to each of these protein drug development phases, but as yet, with limited industrial or routine implementation. This chapter seeks to provide a survey of such applications and potential opportunities for inspiration and exploitation of the distinct characteristics of AF4 throughout the long, winding and multifaceted drug development process.

Keywords AF4 • Aggregation • Biotechnology • FFF • Monoclonal antibodies • Particle • Protein therapeutic

5.1 Introduction

The development lifecycle for pharmaceutical proteins begins with target identification and demonstration of the biological relevance of a particular protein property or protein, continues to identification of which lead product candidate and cell line

J. Pollastrini • L.O. Narhi • Y. Jiang
Process and Product Development, Amgen Inc, Thousand Oaks, CA, USA

S. Cao (✉)
M/S 30E-1-C, Amgen Inc. One Amgen Center Dr, Thousand Oaks, CA, USA
e-mail: scao@amgen.com

S.K.R. Williams and K.D. Caldwell (eds.), *Field-Flow Fractionation in Biopolymer Analysis*, DOI 10.1007/978-3-7091-0154-4_5,

to use, and then proceeds through process and formulation development and characterization, clinical trials and commercialization. The launch of a product represents the beginning of a different kind of product support, which includes lot release, exploration of different delivery devices, indications, comparability, and support for investigations. Asymmetric flow field-flow fractionation (FFF) holds promise as an analytical tool that can be applied through all of these development stages.

During the identification of potential biological targets that might be efficacious in mitigating a given disease, one of the important properties that must be analyzed is the affinity between ligand and receptors, antibodies and antigens, etc. FFF can be a potent tool for determining the solution affinity of different molecules, and also the ratio in which the individual components exist in the final complex. This can be a higher throughput tool than cell based binding assays, and avoids the immobilizing step necessary for plasmon resonance techniques.

Once a target has been identified, the next stage is often to choose the final candidate to advance to the next stage of development, and the clonal cell line to use to ensure consistent yield and product quality. FFF can be used to assess the amount of monomer and aggregate present in the cell culture media prior to purification. This information can be used during clone selection to pick the clone that will produce the optimal amount of monomer right from the beginning of the process. The ability to do this without any purification steps prior to analysis ensures that the results are not affected by separation conditions, and affords higher efficiency. This information will contribute to selection of the final commercial cell line that optimizes yield and product quality.

For selection of the product candidate itself, in addition to biological activity, the ideal molecule will need to be stable to process and storage conditions. This includes low pH for viral clearance if it is a mammalian cell line derived molecule, refolding conditions if it is an *E. coli* derived protein in the form of inclusion bodies, and storage in solution at 4–8°C for 2 years, often at protein concentrations above 100 mg/ml. Screening for this type of stability usually involves stressing the material, and then assessing the integrity of the remaining protein. Controlling and minimizing protein degradation, including protein aggregation, is very important. FFF can be used for obtaining the size distribution profile of the material following different types of stresses, and determining the amount of both clips (smaller species) and larger self-associated aggregates. FFF has the ability to span a much larger size range than size exclusion chromatography (SEC), with the added advantage that there is no filtering out and removal of the micron sized aggregates by the chromatography column. Being able to measure protein aggregates between 0.5 and 10 μm in size is especially important, due to elevated concerns around the potential immunogenicity of protein aggregates of this size. FFF also has the potential to determine the affinity of the protein for association into different aggregated species. Coupling FFF to mass spectrometry (MS) can yield information on the chemical modification of these aggregates as well. Information on changes in conformation, especially unfolding or an increase in the hydrodynamic radius, can also be determined from FFF. Thus there is the potential to use FFF to follow effects of solution conditions on the conformation of the monomer and oligomeric species of the product candidates as well.

During scale up and process and formulation stability studies, FFF can be used to determine the size distribution of samples after each process step and follow formulation stability experiments during accelerated studies. There is the potential for FFF to be run on line, as a Process Analytical Technology (PAT) assay that can be used to ensure process consistency, and also to trigger pooling events so that the material with the same product quality can be obtained from lot to lot, without worrying about small differences in the elution profile from run to run. Application of FFF to assess the quality of product in the conditioned media, as it is used for clone selection, can ensure that the starting material for downstream purification is comparable, or better, as the process is optimized, with the amount of protein aggregate minimized.

During formulation development, the stability of a protein is assessed against different buffer compositions, pH, storage temperature and time etc. Many samples can be generated which need to be analyzed for determination of the optimal formulation conditions. If a high throughput FFF method can be developed this would be useful, by decreasing the amount of time and material necessary to screen protein self-association under different conditions, and to determine what solution conditions minimize aggregation, modification, clipping, and degradation, and increase stability. This method could be applied during both real time and accelerated stability studies as part of the formulation development.

Different devices can be used to deliver protein therapeutics, and the effect of storage and delivery in these devices on the quality of the protein therapeutic is another area where FFF can be used. Analysis of the sub-μm and μm species present in drug product from pre-filled syringes (PFS) can be confounded by the presence of silicone oil droplets, which cannot be differentiated from protein particles by many techniques. FFF coupled with various detection mechanisms has the potential to be able to identify not only the size of the species, but to determine if they are silicone oil, protein, or a complex of both. For the emerging use of nano-particles as a delivery device, FFF is one of the few techniques that can differentiate between empty nano-particles, protein, and the protein-nano-particle complexes.

During preclinical studies, FFF can be used to analyze animal samples for the type of species that form during in vivo circulation. When coupled with western blot analyses of isolated fractions it can be used to monitor any immune complexes, or other heterogeneous complexes that form, and to determine if the drug product is involved in this reaction. It can also be used to determine the oligomeric state of the majority of the biotherapeutic following different routes of administration.

Once the candidate and process have been locked, the emphasis switches from developing and optimizing conditions to maintaining process control. FFF can be used as part of the comparability protocol, to ensure that the individual lots have the same size distribution profile, and protein conformation. As mentioned above, it can also be used to determine which fractions should be pooled and which should be discarded to maintain product quality by way of process analytical technologies (PAT) during downstream purification.

An important aspect of preclinical and clinical development is the monitoring of sample stability, stored both under accelerated and recommended conditions. This

is another potential area for the application of FFF, to monitor both the size distribution and the species generated, and to identify storage conditions that cannot be used for a particular drug product.

As additional disease indications are developed for a therapeutic product, FFF can be used as one of the tools to ensure that changes in device, concentration and formulation do not increase the amount of degradants. Again, coupling with MS would allow identification of any chemical modification that might have occurred, and the ratios of the different species formed, in addition to the determination of their size.

FFF can also be used to support commercial product investigations, for example those involving lots rejected for containing particles. Determining the aggregate size distribution of the suspected product, or coupling FFF with western blot and similar analyses, and determining if the aggregated species are product related, is vital information for these types of investigations. Assessing the nature of the product in vivo using drug isolated from sera obtained from animals, or from healthy human volunteers, to probe the self-association behavior, and determine which species are in equilibrium as soon as the drug is administered is another potential application of FFF. If the analysis can be done directly on sera (using western blot analysis of individual FFF fractions, or labeling specific to the product) this would address a gap in our current analytical ability.

For many of these applications the sensitivity of detection methods coupled to FFF, especially for species greater than 100 nm, will need to improve, so that the presence of a small number of particles can be detected and quantified. Coupling FFF with different novel detection systems beyond multi-angle light scattering (MALS), labeling systems, and MS, is an area for development that would allow FFF to dramatically expand our ability to analyze the presence of different self-associated protein species throughout the product lifecycle.

5.2 Discussion

FFF applications in different phases of protein therapeutic development are discussed in detail below. In addition to proof-of-concept studies, attention has been paid to identifying current analytical gaps and needs, and if and why FFF can be used to fill those gaps. In places where such potentials have not been realized, underlying causes such as instrumental limitations have been discussed and possible solutions proposed.

5.2.1 Discovery Research

FFF has been applied to a variety of bioanalyses relevant to the discovery phase of protein therapeutic development. One emerging application with significant potential is in the area of proteomics, especially functional proteomics. The starting point for protein therapeutic development is disease molecular etiology and the

identification of potentially gain-of-function inducing protein engineering opportunities, often referred to as drug target identification [1]. Disease molecular etiology and drug target identification involve the discovery and understanding of cellular activity pathways. Proteomics is key to this process because it enables the identification of the complex array of proteins and their chemical state, such as phosphorylation, present in a given system at a given time such as cells, serum, etc.

Conventionally, two technical challenges have limited the information available from mass spectrometric proteomic analysis (1) harsh sample introduction causing the destruction of native conformation and properties such as binding (2) despite the staggering power of MS in shotgun sequencing and protein identification in complex samples, sample complexity still poses challenges in terms of data processing and extractable information. The development of soft sample introduction and ionization approaches such as electrospray ionization (ESI) and matrix-assisted laser desorption/ionization (MALDI) has gone a long way to overcome the first challenge. Coupling of FFF with MS makes a further stride towards resolving both of these issues. With regard to the first challenge, FFF as a separation technique is exceptional in its ability to separate without denaturing the analytes. The preservation of very weak protein binding interactions that would not survive typical pre-analysis sample preparation techniques such as chromatography or gel-based separations, has been demonstrated [2]. This quality complements the soft-ionization techniques for MS introduction. In regard to the second challenge, sample simplification, separation by size is a powerful approach, lifting much of the burden off of the mass spectrometer and ensuing data analysis to interpret the overwhelmingly complex ion spectra [35].

In cases where sample simplification by size alone is insufficient, the process can be further enhanced by so-called 2D methods as shown in Fig. 5.1 [4]. FFF

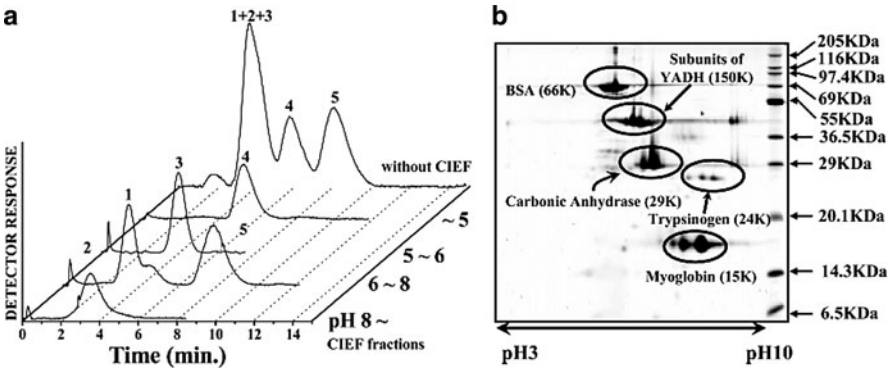

Fig. 5.1 (**a**) μHF5 fractograms without CIEF and after CIEF: (*1*) horse myoglobin (16.9 kDa, pI 7.2), (*2*) trypsinogen (24 kDa, pI 9.3), (*3*) carbonic anhydrase (29 kDa, pI 5.85), (*4*) BSA (66 kDa, pI 4.8), and (*5*) YADH (yeast alcohol dehydrogenase, 150 kDa, pI 6.23). Flow rates: inlet flow = 0.6 mL/min; outlet flow = 60 μL/min. After CIEF, protein bands at four consecutive pH intervals (pH 3–5, 5–6, 6–8, and 8–10) were injected into μHF5. Flow rates: outlet flow = 60 μL/min; radial flow = 540 μL/min. (**b**) 2D PAGE for five proteins: YADH appears as dissociated subunits (Reprinted with permission from [3], © 2006, American Chemical Society)

separates the sample by the different sizes of the analytes present. In this light, FFF has been coupled with a wide array of complimentary techniques for a second dimension of separation, notably non-gel based and non-denaturing techniques. One of the most impressive of these has been the coupling of FFF with the exquisite charge based separation achieved by capillary isoelectric focusing (cIEF) [3]. Placing the FFF as the second dimension in the 2D separation series provided the additional benefit of online removal of the ampholyte. In multiple reports, significantly more proteins were identified in samples after pre-analysis and separation with FFF or FFF-cIEF, demonstrating the power of such combinations for proteomics research at the drug discovery stage [3, 5].

Another property of FFF that makes it amenable to coupling with MS is the fact that it is fundamentally a tangential flow filtration apparatus, thus the injected sample is quickly and thoroughly diafiltered into the running buffer. Complementary to this diafiltering quality of FFF is its broad carrier fluid compatibility, permitting the use of MS compatible volatile and non-denaturing solvents such as ammonium acetate, enabling online desalting simultaneous with analyte separation [6]. FFF is also compatible with low flow rates, which provides a boost to the MS detection sensitivity.

An intense area of current disease study is blood lipoproteins and their correlation with coronary artery disease (CAD). Multiple studies have been reported showing the effectiveness of serum lipoprotein analysis by FFF, particularly coupled with enhancing detection techniques such as Sudan Black dye for specific lipid detection and MALS for particle size distributions [7–11]. Relative amounts of the HDL, LDL and VLDL can be readily measured with FFF, as shown in Fig. 5.2, more rapidly and conveniently than with existing methods such as analytical ultracentrifugation (AUC) and permit the important benefit of fraction collection for further analyses.

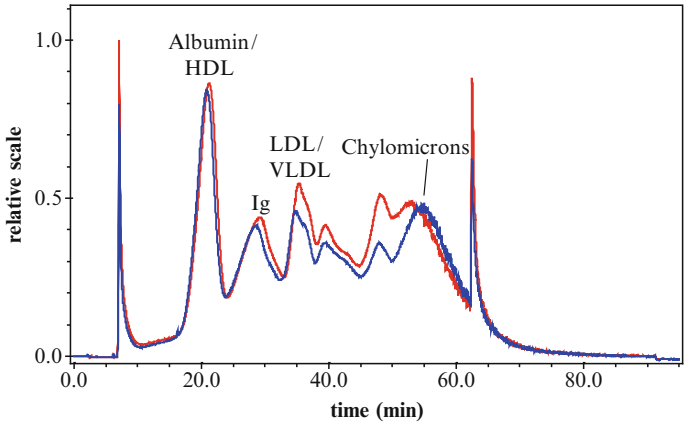

Fig. 5.2 FFF separation of two different whole blood serum samples (*red* and *blue*) showing the separation of high abundance proteins (HAP) albumin and immunoglobulin as well as lipoproteins HDL, LDL, VLDL and Chylomicrons

5.2.2 Process and Analytical Development

The transition from protein drug discovery to development has received significant attention lately. Increasingly, the physicochemical stability of drug candidates is being extensively evaluated and screened to select molecules likely to survive intact the stresses of the manufacturing, shipment and storage processes, prior to substantial investment in drug programs. Recently FFF has been applied at this stage to screen the aggregation state of drug candidates across a wide pH range [12]. The mobile phase flexibility of FFF permitted use of the screening buffers across this pH range as carrier solution, thus testing the desired state of the samples. Minimal or no method development was required for the analyses in the different carrier solutions.

Once a stable lead drug molecule candidate is identified, the next phase in therapeutic protein development is translating the novel molecule into a drug product. Much of this work consists of developing and demonstrating a robust process capable of consistently producing quality product. Protein production begins with transfected microbial and mammalian cell culture fermentation. Before this is started, the cell lines to be used need to be optimized, selecting for performance, especially high protein product titer. Cell line and process optimization are highly complex endeavors with multitude interacting parameters to be tested including cell media and metabolites. FFF can be applied at this stage, as it has been shown to effectively separate tRNA and ribosomal subunits in a single run on unprepared cell lysate [13]. Such measurements can be used to compare yields and other cell line characteristics. The selected cell line will generally be used for production for the lifetime of this product, and thus it is worth investing resources in the development and optimization of this cell line, including application of protoeomics and metabolomics in order to obtain as much protein per unit cell as possible. As in the research discovery phase, this is an opportunity for pre-analytical application of FFF [14].

For *E. coli* fermentation processes, the protein is most often produced in inclusion bodies, which contain the enriched protein product in an insoluble form that needs to be solubilized and refolded into a native functional therapeutic. Inclusion bodies range in size from approximately 400–1,200 nm in diameter, a range of characteristic strength for FFF. The size and mass distributions of the inclusion bodies can be indicative of cell productivity and protein quality. FFF-MALS has been used to analyze the size and mass distributions of inclusion bodies produced in *E. coli* under varying conditions of temperature and induction time [15]. The analysis showed distinct differences in the physical properties of the inclusion bodies correlating to the different cell growing conditions. This application of FFF can be used to optimize the protein expression system chosen for commercial production. Improvement in cell productivity can contribute significantly to the commercial viability of a protein therapeutic.

In a report from the Joint Center for Structural Genomics Group, under the umbrella of the Protein Structure Initiative, FFF-LS was incorporated into the high-throughput protein expression/purification workstream. Specifically, the FFF system was implemented as a part of the protein refolding process. Protein refolding is

a largely empirical process where a large number of refolding conditions, such as pH, denaturant and other additives, are screened for optimum protein refolding [16]. However, evaluating the array of conditions can be challenging due to limitations of commonly used techniques such as turbidity and activity assays. FFF-LS was used to evaluate the presence of small, monodisperse oligomers as a measure of proper protein refolding and recovery. The wide dynamic range of FFF separation, and its lack of solid column matrices which avoids clogging issues (an area of particular concern in a high-throughput setting), were cited as strengths of the technique leveraged in this application. Additionally, ease of use, speed, flexibility to mobile phase conditions and inhomogeneous samples, as well as the ability to collect fractions for offline analysis, were considered valuable for monitoring protein therapeutic product quality during the refolding process.

A similar application [17, 36] has been the high throughput analysis of aggregate present in lysed cell culture samples for the purpose of cell line selection. In this case, impure cell culture lysate was analyzed; the protein monomer and aggregate signals were high enough to still be observed above the signal from the complex impurities of the crude sample. The FFF run conditions were optimized to permit high-throughput analysis in under 10 min including inter-sample wash steps. The application of FFF for this purpose was an alternative to an SEC approach that incorporated prior sample purification with protein A resin. The primary drawbacks of FFF in this case were low monomer-aggregate resolution, and interference from impurities with some samples.

During protein therapeutic development, process analytical technology (PAT) is of high value for process and product development and control. Such technologies are those which are amenable to the demanding throughput and ruggedness of the process environment, sometimes referred to as online or near real-time type of analyses. The authors are aware of recent unpublished efforts to implement FFF as a PAT in the commercial environment similar to that of the DiDonato group [16], again attempting to leverage the openness of the separation channel to avoid purifying sample preparation steps as well as mobile phase limitations. Process refolding conditions often contain significant levels of glycerol, which can result in high back pressure on column matrices due to its high viscosity. This is less likely to be an issue with FFF because the semipermeable membrane employed can be obtained at increased porosities to facilitate analysis of high viscosity solutions if this results in elevated pressure. One commonly cited strength of FFF has been its ability to perform fast separations on the scale of 3–10 min. This is in contrast to slower conventional SEC runtimes [18]. It is worth noting here that recent developments in chromatography such as Ultra-High Pressure Chromatography (UPLC) and monolithic columns are facilitating SEC runtimes on very short timescales, such as 2 min. This may be particularly relevant in another recent unpublished attempt at PAT implementation of FFF of which the authors are aware. In this case FFF was being explored for near-real time aggregate analysis at a later stage of processing where protein is in a more purified state. Two primary potential advantages of FFF were being explored here (1) the potential higher speed of FFF separation and (2) the potential for FFF to observe larger aggregates. The UPLC-SEC methods eliminate the potential throughput advantage with FFF, while

the possibility of observing larger aggregates remains a distinguishing advantage. However, at this more purified stage in the process, obtaining the sensitivity necessary to detect the small amount of these larger aggregates present is very challenging. Although, since the primary goal of PAT is to ensure product quality, if the requisite detection sensitivity can be obtained, FFF will be a suitable technique for this purpose.

5.3 Aggregation

One of the most promising and anticipated applications of FFF has been protein aggregate analysis. (Protein aggregation is not limited to the context of product stability. Various disease states are linked with in vivo protein aggregation such as Alzheimer's disease and prion pathogens. FFF has shown to be effective in the study of prion aggregates [19], however this section deals with aggregation as a matter of product purity.) Almost two decades ago elegant reports demonstrated the proficiency of FFF in separating protein aggregates from the monomeric form and from each other, particularly the aggregates present in several monoclonal antibody preparations [18]. Some proof-of-concept experiments even showed superior performance by FFF compared to SEC in resolution, resolvable analyte size range, and analysis duration. Protein aggregation is one of the most significant challenges the industry faces during protein therapeutic process, formulation, stability and product development [20, 21]. One of the molecular attributes that distinguishes traditional small molecule pharmaceutics and protein biopharmaceutics is the difference in shelf life stability. While the former are not prone to degradation and are relatively easily stabilized for long shelf life, the latter, due to their complex chemical composition and structure, are prone to multiple pathways of degradation, one common outcome of which is protein aggregation. Aggregated proteins could possibly affect the safety and efficacy of the drug product, as they are potentially immunogenic, and can also have either decreased or increased activity relative to the monomeric protein. The analysis and characterization of protein aggregates can be applied during all stages of product development. In addition to monitoring and comparing relative aggregate formation of product candidates, and cell culture conditions, FFF can also be used to optimize the design space during protein process development. In this application the developmental protein is tested at the various steps of purification for signs of degradation, informing the design of the production process as well as formulation conditions.

There have been several reports analyzing the suitability of FFF for these types of studies for therapeutic monoclonal antibody (mAb) drug candidates [22–24]. The results from these studies reveal several conclusions about the application of FFF to aggregate analysis as demonstrated in Fig. 5.3. One, despite the prospect for the gentle separation conditions of FFF to more fully preserve weakly associated aggregates, the results from FFF generally match those of SEC, therefore it remains as one of the orthogonal techniques to verify the performance of SEC. Second, the ability of FFF to analyze across a size range covering orders of magnitude is often

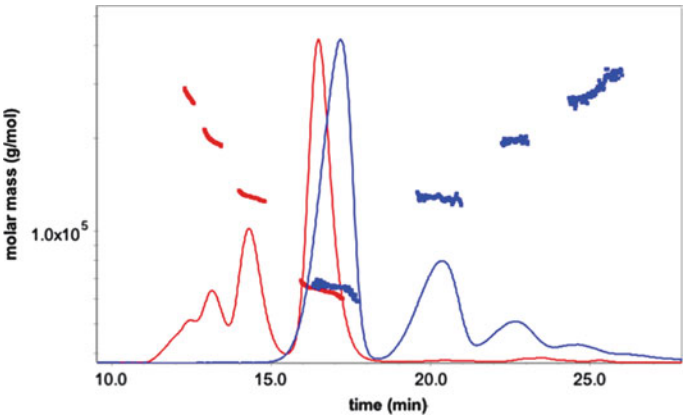

Fig. 5.3 Overlay of chromatogram and fractogram of peptibody aggregates separated on SEC (*red*) and FFF (*blue*), respectively. FFF Fractogram shows the wide protein aggregate size range available to separation by FFF in the rare case that such broad species are present. There is arguably no advantage to using FFF for typical aggregation analysis when the protein solution is relatively pure and homogeneous, containing only trace amounts of stable small oligomers

limited by the sample load limitations and detection sensitivity [24]. There is usually a small amount of larger sized aggregates present in actual process samples, which decreases to trace levels as the purity of the therapeutic increases, so combined with limited load capacity this poses a formidable obstacle.

However, in cases where substantial aggregation is present, for example samples from accelerated stress and kinetic studies, FFF can have a distinct advantage over SEC. Subjecting the sample to conditions that are on the edge of normal parameters can allow one to determine what condition can be tolerated, defining the design space of the process step. The utility of this method for aggregate characterization was well demonstrated in a study on the mechanism of protein aggregation. The aggregate eluting as a single peak at or near the void volume was initially interpreted as being relatively homogeneous with respect to size. The elution time, which becomes unreliable near the void volume, indicated a specific aggregate size of approximately 1 MDa or about 8 monomer units as a kinetically favored endpoint [25]. Ensuing FFF-MALS analysis, however, showed the peak eluting near the void volume by SEC to be a wide distribution of size species spanning a mass range corresponding to complexes of 7 to upwards of 70 monomer units shown in Fig. 5.4.

A 2004 report cited separating and detecting silicon oil droplets, protein monomer, and large aggregates in a single run [26]. There are reports of exploiting the ultrafiltration aspect of FFF to enrich specific analyte in the sample prior to the elution step [8, 27]. In a recent report from a bioanalytical contract company, FFF was successfully used for the formulation screening and the assessment of the effects of different stresses upon aggregation propensity. The data obtained by FFF was demonstrated to both correlate well with orthogonal techniques used for supra-micron particle measurement and to reveal aggregates that were masked by SEC due to their large size [28].

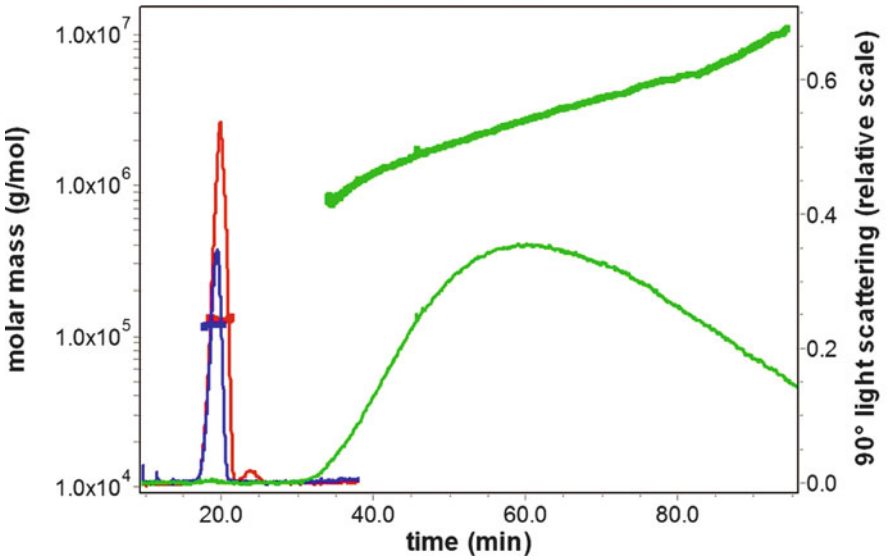

Fig. 5.4 Fractogram (*right axes*) of antibody unstressed control sample (*red*) and stressed antibody fractions collected post SEC, monomer fraction (*blue*) and aggregate fraction (*green*). Dots (*left axes*) are molar mass calculations based on light scattering

In summary, FFF is not yet widely applied for aggregate analysis in developing protein therapeutics, in spite of its strengths relative to the ubiquitous SEC technology. The availability of a system sensitive enough to reach down to pico-, femtomolar or even single particle and single molecule detection in solution would enhance the information available during product and process development. While examples do exist of FFF being applied in this context, they tend to be on well controlled, proof-of-principle systems. It's worth noting that one of the prime anticipated advantages of FFF has been the flexibility of compatible carrier fluid composition. This results in the ability to analyze potential therapeutic proteins in their native formulation buffers rather than having to manipulate them into a buffer that is designed to prevent analyte interaction with a column matrix, as is the case with SEC. This would be advantageous because there is always the possibility that the state of the aggregate can change when introduced into different buffer environments. This is desirable from a product characterization and control perspective. However, upon testing a series of developmental mAbs with FFF using a range of common formulation buffers, severe tailing of the elution profile was observed. As indicated in previous studies, it was concluded that carrier fluid composition played a significant role in preventing electrostatic interactions between the analyte and the accumulation wall [29, 30]. Upon investigation it was found that an ionic strength of approximately 400 mM was required to abrogate strong protein – membrane interactions. However, such ionic strength is not found in typical robust mAb formulations. Theoretically, a broad range of membrane surfaces can be used at the FFF accumulation wall to reduce or eliminate the

interactions; in practice however, such membranes have not proven effective. Of the three membrane types readily available; regenerated cellulose, cellulose acetate, and polyethersulfone, the latter two have not shown significant improvement in reducing interaction with protein or robustness compared to the regenerated cellulose membrane. Work continues to find a way around such interactions, but to date this has posed a significant limitation to the promise of FFF as a technique to monitor aggregation under native formulation conditions with low ionic strength.

5.4 Clinical Immunology

An FFF application reported by the authors that falls under the clinical realm of protein therapeutic development [31] is the analysis of anti-drug antibody (ADA) complexes in serum. An ADA response in the presence of high concentrations of human monoclonal antibody therapeutic can result in Type III hypersensitivity reactions and adverse reactions such as complement activation and circulating immune complex (CIC) deposition into various tissues. A novel combination of techniques was devised as a universal method applying FFF and immunoassay with electrochemiluminescent (ECL) detection to separate and detect immune complexes in serum after administration of a human monoclonal antibody therapeutic. A critical aspect of this method is the ability to not only detect the presence of ADA, but to elucidate the size of agglutinated CIC in serum. Leveraging the characteristic strengths of the technique, FFF was employed for separation of the ADA complexes directly from the serum. The entire separation is rapid and non-destructive without a stationary phase that may interact, degrade, or alter the sample. Multiple detection modes were applied to the eluate: UV absorbance, sensitive to protein presence and concentration; MALS, sensitive to protein molecular mass and concentration; and immunoassay with ECL detection specific for primate IgG-human IgG immune complexes. Fractions were collected across the separation profile and analyzed using an immunoassay specific for primate IgG-human IgG immune complexes. An antibody specific for human IgG was biotinylated and coated onto a streptavidin Meso Scale Development (MSD) plate. The FFF fractions were added to the plate followed by an antibody specific for primate IgG which had been conjugated with an ECL label. Light was measured in an MSD instrument and converted to ECL units. The method was effective in elucidating the presence of ADA CIC as well as providing a measure of their physical size. An analogous method coupling FFF with other techniques for protein-small molecule drug complex detection in serum has been reported as shown in Fig. 5.5 [9]. Reports on related applications are also available [32, 33].

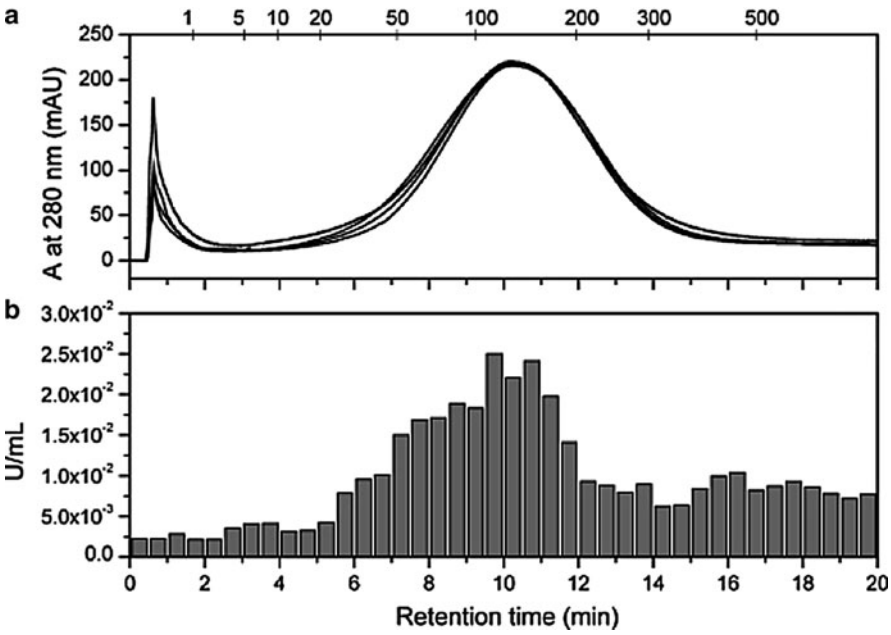

Fig. 5.5 HF FlFFF of Rasburicase. (**a**) UV/visible fractogram at 280 nm; four repeated runs. (**b**) Enzymatic activity of the collected fractions determined by the CL assay (Reprinted with permission from [32], © 2006, American Chemical Society)

5.5 Other Applications

Another recent unpublished potential application of FFF lies in its nature as a derivative tangential flow filtration (TFF) apparatus. A major obstacle that has developed in protein therapeutic development is the difficulty of analyzing samples directly in the high protein concentrations required to achieve effective pharmacodynamics and pharmacokinetics. Formulated protein concentrations of 1–200 mg/mL are regularly sought to meet the high mg/kg dosing regimens with reasonable introduction volumes, typically around 1 mL. Such high protein concentrations pose specific challenges to the therapeutic protein development process including manufacturing, stability and delivery. One key point of stress in the manufacturing process results from the significantly elevated viscosities of these formulations. After purification through a variety of chromatographic steps and filters, one of the final steps in the manufacturing process is accomplished via TFF, in which the purified protein pool must be exchanged into its final formulation solution and adjusted to the proper protein concentration. There are limits to the pressure that can be tolerated with the large scale equipment used for this step. In the process of concentrating the protein on these units, the rise in viscosity causes a backpressure which often exceeds the operating limit. FFF could conceivably be used to model and characterize this step. Applying FFF as an analytical scale TFF with online detection, a series of monoclonal antibodies (mAbs) were injected into the

FFF channel at equivalent high load amounts and analyzed at high and low crossflows. The high crossflow rate resulted in effective overloading of the FFF channel manifesting as a distorted elution peak profile, while the low crossflow rate resulted in a normally eluting peak. The different mAbs exhibited overlapping, symmetric peak profiles at the low crossflow; while at the higher, overload inducing crossflow, the elution profiles differed. Work by Arfvidsson [34] has shown that the overloading phenomena in FFF are linked to viscosity, therefore the varying mAb elution profiles are suspected as being due to protein self-interactions and viscosity at high concentrations. This hypothesis was supported by direct viscometry measurements of the samples which corresponded with the observations by FFF. The experiments were repeated using a variety of solutions including formulation solutions as FFF carrier fluids, and the results were found to be formulation dependent, opening up another possible application of screening formulations and TFF behavior by FFF with online detection.

Trace amounts of host cell proteins in the final drug product constitute a critical quality attribute. Typical analysis involves ELISA's, 2D gel electrophoresis and MS analysis. As described earlier, online non-gel-based 2D separation with online desalting may have the potential to offer increased sensitivity for host cell impurities at various stages of the process.

5.6 Conclusion

In this chapter we have discussed a broad range of potential applications of FFF to the protein therapeutic discovery and development process. Many of these applications have been proven in concept, yet have not been widely adapted in practice. For example, FFF has exciting promise as a tool to provide information even more rich than that obtained from SEC for characterizing protein aggregates in commercial therapeutic protein development. However, that promise has run into several fairly serious impediments; (1) unexpectedly high membrane interactions placing commensurate restrictions on carrier fluid composition; (2) low separation efficiency in the size range of many proteins and their low order oligomers relative to SEC; and (3) severe load limitations (low tens of micrograms) manifesting in weak signal to noise ratios.

Nonetheless, there are strengths of FFF that make it amenable to these types of applications. The technologies for FFF, SEC, and AUC are all evolving along with the number and applications to protein therapeutics, and it will be interesting to see where we are with these technologies in a few years. Currently SEC is the work-horse, and AUC is often used as the orthogonal method to SEC, with FFF applied as a niche technique. Due to its technical complexity and labor-intensive nature, AUC's applicability is rather limited; and with improved performance such as detection sensitivity and resolution, FFF has the potential to replace AUC as the default orthogonal sizing method, particularly in cases where high throughput is required.

One area in which FFF can potentially make a significant impact is the analysis of particles such as the fractionation and quantification of sub-visible and sub-micron particles. With the right detection mechanism, FFF has the potential to quantify the amount of particles present in samples in a high throughput, automated manner while requiring little sample amount. This will find ample applications in protein product and process development. Another such area is the analysis of protein aggregate using formulation buffer as the FFF carrier fluid, providing significant benefit in permitting the sample to be maintained in a desired environment during analysis.

References

1. Kennedy T (1998) Pharmaceutical project management. M. Dekker, New York
2. Pollastrini J, Dillon TM, Bondarenko P, Chou RY-T (2011) Field-flow fractionation for assessing FcRn and Fcg receptor binding to monoclonal antibodies in solution. Anal Biochem 414(1):88–98
3. Kang D, Moon MH (2006) Development of non-gel-based two-dimensional separation of intact proteins by an on-line hyphenation of capillary isoelectric focusing and hollow fiber flow field-flow fractionation. Anal Chem 78(16):5789–5798
4. Giddings JC (1990) Two-dimensional field-flow fractionation. J Chromatogr A 504:247–258
5. Kim KH, Moon MH (2009) Development of a multilane channel system for nongel-based two-dimensional protein separations using isoelectric focusing and asymmetrical flow field-flow fractionation. Anal Chem 81(4):1715–1721
6. Reschiglian P et al (2004) On-line hollow-fiber flow field-flow fractionation-electrospray ionization/time-of-flight mass spectrometry of intact proteins. Anal Chem 77(1):47–56
7. Li P, Hansen M, Giddings JC (1997) Separation of lipoproteins from human plasma by flow field-flow fractionation. J Liq Chromatogr Relat Technol 20(16):2777–2802
8. Li P, Giddings JC (1996) Isolation and measurement of colloids in human plasma by membrane-selective flow field-flow fractionation: Lipoproteins and pharmaceutical colloids. J Pharm Sci 85(8):895–898
9. Madörin M et al (1997) Analysis of drug/plasma protein interactions by means of asymmetrical flow field-flow fractionation. Pharm Res 14(12):1706–1712
10. Park I et al (2002) Separation and selective detection of lipoprotein particles of patients with coronary artery disease by frit-inlet asymmetrical flow field-flow fractionation. J Chromatogr B 780(2):415–422
11. Yohannes G et al (2006) Miniaturization of asymmetrical flow field-flow fractionation and application to studies on lipoprotein aggregation and fusion. Anal Biochem 354(2):255–265
12. Cynthia H, Li LN, Wen J, Dimitrova M, Wen Z-Q, Li J, Pollastrini J, Nguyen X, Jiang Y (2011) The effect of pH, temperature and salt on the stability of E. coli expressed IgG1 Fc. manuscript in preparation
13. Arfvidsson C, Wahlund K-G (2003) Time-minimized determination of ribosome and tRNA levels in bacterial cells using flow field-flow fractionation. Anal Biochem 313(1):76–85
14. Reschiglian P et al (2004) Hollow-fiber flow field-flow fractionation for whole bacteria analysis by matrix-assisted laser desorption/ionization time-of-flight mass spectrometry. Anal Chem 76(7):2103–2111
15. Luo J et al (2006) Size characterization of green fluorescent protein inclusion bodies in E. coli using asymmetrical flow field-flow fractionation-multi-angle light scattering. J Chromatogr A 1120(1–2):158–164

16. DiDonato M et al (2004) A scaleable and integrated crystallization pipeline applied to mining the Thermotoga maritim proteome. J Struct Funct Genomics 5(1):133–146
17. Pollastrini J, Hai P, Cao S (2008) Protein aggregation analysis using field-flow fractionation with multi-angle light scattering (FFF-MALS). In: ACS division of biochemical technology national meeting 2008
18. Litzen A et al (1993) Separation and quantitation of monoclonal antibody aggregates by asymmetrical flow field-flow fractionation and comparison to gel permeation chromatography. Anal Biochem 212(2):469–480
19. Silveira JR et al (2006) Fractionation of prion protein aggregates by asymmetrical flow field [hyphen (true graphic)]flow fractionation. In: Colowick SP, Kaplan NO, Abelson JN, Simon MI, Inglese J (eds) Methods in enzymology. Academic, San Diego, pp 21–33
20. Mahler H-C et al (2010) Protein aggregation and particle formation: effects of formulation, interfaces, and drug product manufacturing operations. In: Aggregation of therapeutic proteins. Wiley, Hoboken, pp 301–331
21. Singh SK et al (2010) An industry perspective on the monitoring of subvisible particles as a quality attribute for protein therapeutics. J Pharm Sci 99:3302–3321, Wiley Subscription Services, Inc., A Wiley Company
22. Liu J, Andya J, Shire S (2006) A critical review of analytical ultracentrifugation and field-flow fractionation methods for measuring protein aggregation. AAPS J 8(3):E580–E589
23. Gabrielson JP et al (2007) Quantitation of aggregate levels in a recombinant humanized monoclonal antibody formulation by size-exclusion chromatography, asymmetrical flow field-flow fractionation, and sedimentation velocity. J Pharm Sci 96:268–279, Wiley Subscription Services, Inc., A Wiley Company
24. Cao P, Pollastrini J, Jiang Y (2009) Separation and characterization of protein aggregates and particles by field-flow fractionation. Curr Pharm Biotechnol 10:382–390
25. Wiltzius JJW, Ball NR, Wen J, Dillon TM, Xiao G, Pollastrini JM, Bondarenko PV (2011) Differential mechanisms of immunoglobulin aggregation. manuscript in preparation
26. Fraunhofer W, Winter G (2004) The use of asymmetrical flow field-flow fractionation in pharmaceutics and biopharmaceutics. Eur J Pharm Biopharm 58(2):369–383
27. Lee H, Williams SKR, Giddings JC (1998) Particle size analysis of dilute environmental colloids by flow field-flow fractionation using an opposed flow sample concentration technique. Anal Chem 70(13):2495–2503
28. Davis J (2010) AF4 for protein formulation evaluation and analysis of large proteins. In: International light scattering colloquium FFF-MALS focus meeting, 2010. 4.
29. Wijnhoven JEGJ et al (1996) Influence of injected mass and ionic strength on retention of water-soluble polymers and proteins in hollow-fibre flow field-flow fractionation. J Chromatogr A 732(2):307–315
30. Benincasa M-A, Fratte CD (2004) Influence of ionic strength, sample size, and flow conditions on the retention behavior of pullulan in flow field-flow fractionation. J Chromatogr A 1046 (1–2):175–184
31. Miller MJ, Pollastrini J, Cao S, Mytych D, Chirmule N, Swanson S, Moxness M (2010) Separation and detection of immune complexes that form after administration of a human monoclonal antibody therapeutic to non-human primates. In: AAPS national biotechnology conference
32. Roda A et al (2006) Combined approach to the analysis of recombinant protein drugs using hollow-fiber flow field-flow fractionation, mass spectrometry, and chemiluminescence detection. Anal Chem 78(4):1085–1092
33. Reschiglian P et al (2003) Flow field-flow fractionation with chemiluminescence detection for flow-assisted, multianalyte assays in heterogeneous phase. J Sep Sci 26(15–16):1417–1421
34. Arfvidsson C, Wahlund K-G (2003) Mass overloading in the flow field-flow fractionation channel studied by the behaviour of the ultra-large wheat protein glutenin. J Chromatogr A 1011(1–2):99–109
35. Zattoni A et al (2008) Hollow-fiber flow field-flow fractionation of whole blood serum. J Chromatogr A 1183(1–2):135–142
36. Westland K, Joseph P, Hai P (2009) Field-flow fractionation as a high-throughput technology to quantify aggregates in cell culture samples. In: Society for biological engineering 2nd international conference on accelerating biopharmaceutical development

Chapter 6
Assessing and Improving Asymmetric Flow Field-Flow Fractionation of Therapeutic Proteins

Jun Liu, Qing Zhu, Steven J. Shire, and Barthélemy Demeule

Keywords Analytical ultracentrifugation • Field-flow fractionation • Monoclonal antibodies • Protein aggregates • Size exclusion chromatography

6.1 Introduction

Field-flow fractionation (FFF) refers to a family of flow-based separation techniques that have been widely utilized to separate and analyze cells [1], macromolecules [2] and particles [3, 4]. The method was originally invented by J.C. Giddings in 1966 as a separation tool for macromolecules [5], and later has been found useful for analyzing large particles that are beyond the normal separation range of chromatographic and electrophoretic methods [4]. Unlike conventional separation methods, FFF separates macromolecules inside a buffer-filled open channel without any column matrix. Separation of macromolecules or particles in FFF is achieved by applying an externally generated field that is perpendicular to a laminar channel flow. The external orthogonal field can be gravitational, centrifugal, magnetic, electrical, temperature or flow-based according to the physical properties of macromolecules, such as size, shape and apparent charge [5].

Flow field-flow fractionation methods have provided useful alternatives for protein aggregate characterization [6, 7]. The method covers a wide range of molecular sizes from 0.001 to 50 μm in size [5]. There are no matrices involved that may influence the separation. The methods can be applied to proteins under a broad range of buffer conditions, even in the formulation buffers of biopharmaceuticals. This would be extremely valuable to understand protein aggregation that is susceptible to ionic strength, pH, buffer and excipient conditions. Flow FFF has a

J. Liu (✉) • Q. Zhu • S.J. Shire • B. Demeule
Late Stage Pharmaceutical Development, MS 56-1A, Genentech, Inc, South San Francisco, CA, USA
e-mail: jliu@gene.com

S.K.R. Williams and K.D. Caldwell (eds.), *Field-Flow Fractionation in Biopolymer Analysis*, DOI 10.1007/978-3-7091-0154-4_6,

solid theoretical basis, and when used with suitable detectors, has a potential to provide an accurate estimation about quantity, size and shape of multiple protein aggregate species without the use of molecular weight standards [5]. Like typical chromatography methods, flow FFF can also be interfaced with ultraviolet (UV), refractive index (RI) and light scattering (LS) detectors for further protein characterization. The UV and RI detectors are mainly used to measure the concentration of proteins, and an on-line LS detector can be used for protein characterization and determination of the molecular weight for each species.

Among all the flow FFF configurations, asymmetrical flow FFF (AF4) is the most commonly used for therapeutic proteins. As discussed in other chapters, separation by AF4 is achieved by applying a cross flow that is perpendicular to a laminar flow in a channel. The cross flow drives macromolecules toward an accumulation wall and differences in diffusion coefficients create a concentration distribution in the laminar flow, resulting in different elution times. This method has been used for separation of proteins and their aggregates [8]. For most protein molecules, the size of aggregates is well below ~1 μm and therefore separation depends mainly on the diffusion coefficient of the protein species. This is also known as normal mode FFF operation. In this elution mode, the retention time is related by a well-defined equation to the applied field and the translational diffusion of the proteins [8]. The diffusion coefficient of different proteins, fragments and aggregates can then be determined and molecular weight can be calculated assuming spherical structures for all components.

In contrast, for protein particles that are larger than ~1 μm in size, the diffusion effect that drives the molecule towards the center of the channel is essentially negligible compared to the cross flow effect that moves the molecule towards the membrane [5]. The larger particles driven by the vertical field will form equilibrium layers whose thicknesses are determined by the size of the particles. The larger the particle, the further its center of mass is from the wall and the earlier the elution. This is also known as the steric-hyperlayer mode [8].

Overall AF4 has several advantages over the traditional symmetrical flow FFF system. It has a simpler construction of the fractionation channel with only one permeable wall covered by a semi-permeable membrane on the bottom of channel. The upper wall usually consists of a transparent plastic block, allowing visual monitoring of samples and membranes, and also the presence of air bubbles during the experiment. In addition the channel has a trapezoidal shape, which is used to compensate for the loss of flow along the channel. This results in reduced dilution and much improved relaxation and focusing properties that may potentially improve the separation [9].

Despite these advantages, the precision and accuracy of AF4 for detecting protein aggregates and fragments are not well established for many protein molecules and very often extensive development activities are required to optimize the method. In this chapter, we have reviewed the use of AF4 technologies for quantitative characterization of several well-characterized protein molecules and their mixtures. Considerations for experimental conditions and data analyses are also proposed to improve quantification of protein aggregates.

6.2 Advantages and Challenges

Size exclusion chromatography (SEC) has been the workhorse of the pharmaceutical industry for determining size distribution of protein therapeutics. However, AF4 has several advantages over SEC. Unlike conventional SEC, the AF4 method does not use a stationary phase. Thus, all separations occur in a single aqueous phase eliminating potential problems, such as changes in retention time and loss of aggregates, caused by column fouling and matrix-protein interactions. Although membrane-protein interactions may compromise separation and recovery in an AF4 channel, particularly at high cross flows, these problems can be partially mitigated by selecting low adsorption membranes or by lowering the cross-flow rate.

The AF4 method has a broad dynamic range and is one of the few methods that is capable of separating proteins over the entire colloidal size range (1–1,000 nm) with a reasonable resolution [5]. The method can resolve protein fragments, soluble aggregates and protein particles. In particular, it has been successfully used for analyzing larger aggregates or particles that are filtered by an SEC column matrix or sediment instantaneously under a centrifugal field [10]. However, AF4 also has several limitations. The separation of protein and aggregates is based on hydrodynamic properties, such as the diffusion coefficient, rather than the molecular mass. Therefore an on-line light scattering detector is often connected to the AF4 system to determine the molar mass of each species. The AF4 system is also not suitable for the analysis of high concentration protein solutions, since the concentrated protein may form a viscous layer during the focusing and relaxation step and this would significantly compromise the resolution [11]. For better resolution, small amounts of samples are often loaded into the channel. This will create significant dilution of the protein during the elution process and is therefore not suitable to study aggregates that dissociate rapidly at lower concentrations.

6.3 Selection of Channel Components

The structure and geometry of the AF4 channel, where samples are separated, are critical for instrument performance and determination of separation speed, resolution, accuracy and sample capacity. The channel typically has a dimension of 10–50 cm in length and 50–500 um in thickness, which is controlled by a plastic spacer. The actual thickness of the channel compartment is usually less than that of the spacer because of the compressibility/swelling of the membrane [12]. A trapezoidal design of the spacer is often used for AF4 in order to help maintain a reasonable channel flow velocity. The thickness of the spacer is a critical parameter that will have direct impact on the shape of the parabolic profile of the laminar flow, and therefore impact the separation and retention time. In general, a thin spacer will provide a steeper gradient of laminar flow and less dilution (channel flowrate is constant), which may lead to a better and faster separation. However, the minimum

allowable thickness usually is determined by the compressibility/swelling of the membrane under a specific running condition. For a given sample, reducing the channel thickness (while maintaining the same channel flowrate) must be accompanied by an increase in cross flow to maintain the separation resolution, and this increased cross flow can lead to very high system pressure that may go beyond the system limit. In addition, using a thin channel may increase the perturbations arising from surface imperfections that may reduce the overall resolution [9].

The semi-permeable membrane is another key component of the AF4 channel. Ideally the membrane should be completely flat and permeable to the mobile phase but not the protein samples. The membrane should also be compatible with the carrier and protein without significant adsorption of proteins. The typical membranes used for proteins include regenerated cellulose, poly(ether)sulfone, polycarbonate, and polyamide [8]. These membranes have been shown to provide adequate separation for many protein molecules under normal conditions [8]. However, the interactions of these membranes with proteins can vary significantly from protein to protein and from mobile phase to mobile phase. To study these effects, three well characterized proteins, protein I (a full length monoclonal antibody), protein II (a single-armed monoclonal antibody), and protein III (a Fab fragment from a monoclonal antibody) with approximate molecular weights of 150, 100 and 50 kDa respectively were selected. These protein molecules were mixed at a near equal weight ratio and then analyzed by AF4. Although a model system containing well defined protein aggregates would be more relevant for our study, unfortunately there is no easy way to prepare these protein aggregates and ensure their stability. Instead, we have selected a model system with well characterized protein monomers which have sizes and diffusion coefficients in the typical range of many protein aggregates. This model system should be useful to provide relevant information about resolution, precision and accuracy of the AF4 method. As shown in Fig. 6.1, although a separation between each individual molecule in 10 mM Na/K phosphate, 140 mM Na/K Cl at pH 7.2 was achieved at a cross flow of 3.0 mL/min and a channel flow of 0.4 mL/min using a poly(ether)sulfone (PES) membrane, the peak area and retention time for each individual molecule were not consistent with repeated injections. For clarity, results are shown for only the first, third, and fifth injections. Both proteins I and II showed an increase of elution time and peak areas, while protein III showed an increase of elution time and a reduction in peak area with repeated injections. These results suggest that there are significant protein membrane interactions under the conditions of the experiment. The increase of peak area for protein I and II over repeated injections suggests that the adsorption of these proteins on the membrane is quite strong and these adsorbed proteins cannot be easily removed during the washing step. As a result, the binding of the membrane with these proteins appears to be saturated over time. On the other hand, the decrease of the peak area for protein III over repeated injections suggests that there is an increase of protein III adsorption on the membrane over time. It is not clear what causes this phenomenon. One possible explanation is that the adsorption of protein III to the membrane may be enhanced by an increase of the binding of other

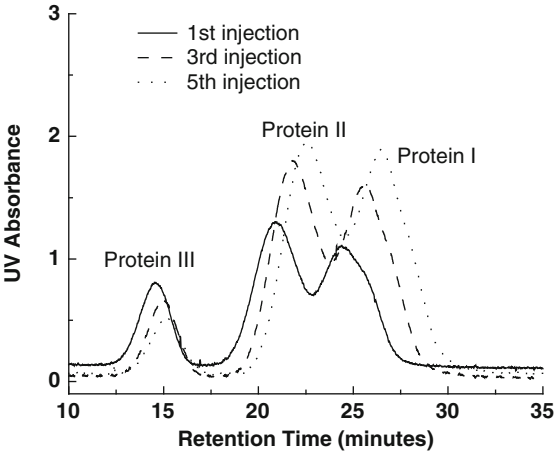

Fig. 6.1 Separation of a mixed protein sample by AF4 at a cross flow of 3.0 mL/min and a channel flow of 0.4 mL/min using a poly(ether)sulfone membrane on an AF2000 instrument from Postnova Analytics (Landsberg/Lech, Germany). The samples were injected repeatedly into the channel and data collected after each injection. The mobile phase contains 10 mM Na/K phosphate, 140 mM Na/K Cl at pH 7.2. The peaks were monitored using an on-line UV detection system at a wavelength of 280 nm

proteins. The results presented in Fig. 6.1 demonstrate the importance of minimizing protein-membrane interactions for consistent results.

The interaction between protein and membrane can be minimized by several different approaches. One of the more successful approaches is to replace the components of the mobile phase with molecules that can prevent protein-membrane interactions. As shown in Fig. 6.2, the reproducibility of the retention times and peak areas for protein I and protein II have been largely improved by replacing phosphate buffer with 0.2 M arginine acetate at pH 7.2. Results from four of the seven injections are shown. Although the reproducibility of the retention time for protein III was improved significantly, the increase of the peak area with repeated injections indicates that protein III has a strong adsorption on the membrane under these conditions, resulting in an eventual saturation of binding sites on the membrane.

Another approach to decrease the potential protein adsorption is to select a different membrane. As shown in Figs. 6.3 and 6.4, the replacement of the PES membrane with either regenerated cellulose or amphiphilic regenerated cellulose membranes has largely improved the reproducibility of retention time and peak areas for all molecules that were tested. Although there is slightly more peak broadening observed for protein I, this does not appear to interfere with the final results. Our studies also showed that, when the right membrane was selected, the impact of different elution buffers on the separation and quantification was minimized. The results were comparable whether we used the buffers containing arginine or phosphate. These data demonstrate the importance of selecting the right type of membrane in order to achieve more consistent and reliable results.

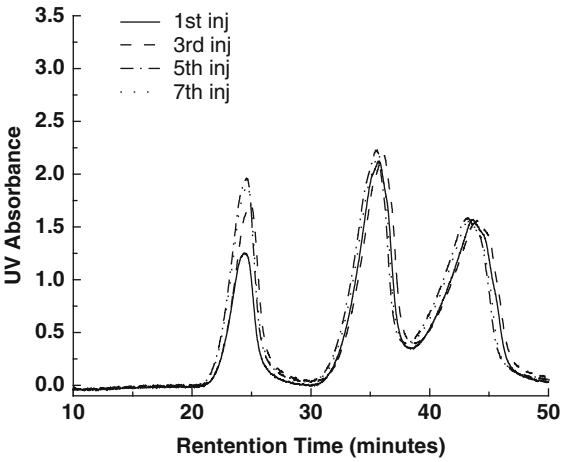

Fig. 6.2 Separation of a mixed protein sample by AF4 at a cross flow of 3.5 mL/min and a channel flow of 0.25 mL/min using a poly (ether)sulfone membrane on an AF2000 instrument. The mobile phase contains 0.2 M arginine acetate at pH 7.2. The peaks were monitored using an on-line UV detection system at a wavelength of 280 nm

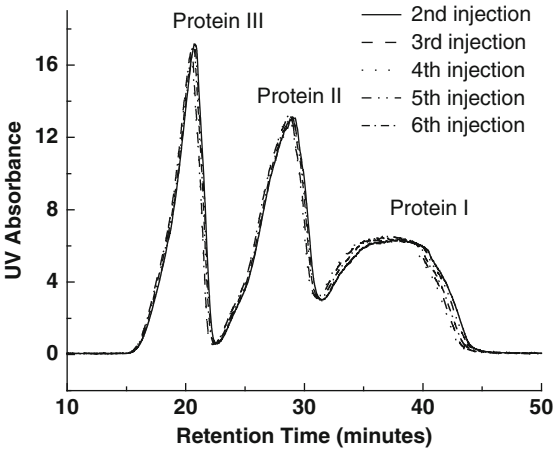

Fig. 6.3 Separation of a mixed protein sample using a regenerated cellulose AMPH amphiphilic membrane on an AF2000. The mobile phase contains 180 mM NaCl, 20 mM Na_2HPO_4, pH7.0. Flowrates and detection same as for Fig. 6.2

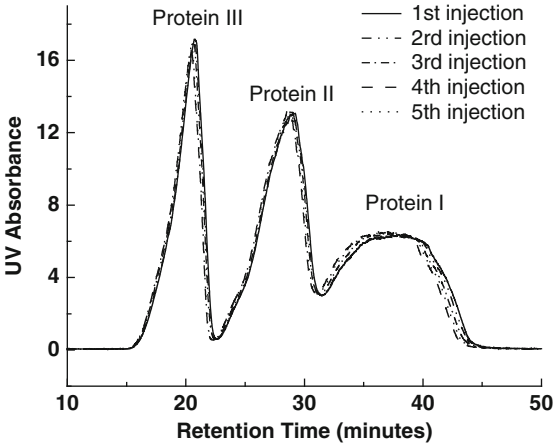

Fig. 6.4 Separation of mixed protein samples using a regenerated cellulose membrane on an AF2000. The mobile phase contains 180 mM NaCl, 20 mM Na_2HPO4, pH7.0. Flowrates and detection same as for Fig. 6.2

6.4 Selection of Operation Parameters

The typical AF4 experiment includes sample injection, relaxation/focusing, separation and detection. The selection and control of flow rates during these different stages are essential for optimal results. The strength of the cross-flow, which can be easily adjusted according to the size of the protein and aggregates, is a critical factor for AF4 performance. In addition, a cross flow gradient can also be programmed for optimal separation. In the normal mode operation, an increase in the cross flow increases resolution, but also results in an increase in the separation time, sample dilution, back pressure and non-specific adsorption. An excessively high cross flow is usually not recommended since it may also lead to significant sample loss due to the increased interaction with the membrane. For large particle separation, a lower cross flow is preferred since it minimizes the loss of protein due to non-specific adsorption onto the membrane. The channel flow rate is another important experimental parameter for AF4 performance whereby a decrease in the channel flow rate may improve resolution, but will result in longer separation times and increase of sample dilution.

A multivariate design of experiment study was conducted to further evaluate the impact of changing cross flow, channel flow, focus time, focus flow and injected mass on peak resolution and recovery. Our data (not shown) are consistent with previous observations [13] showing that the cross flow and channel flow are the two most important parameters that have significant impact on the overall resolution and recovery. The increase of the cross flow and decrease of the channel flow lead to an increase of resolution and a decrease of recovery. The other parameters appeared to have minimal impact on the resolution and recovery within the ranges that we have tested (data not shown).

Traditionally flow FFF systems operate only at ambient temperature. With the recent introduction of a temperature control apparatus with a temperature range from 5 to 80°C, it is now possible to analyze proteins by a flow FFF system at temperatures significantly different from ambient temperature. The increase in operating temperature can significantly increase the diffusion coefficients, and potentially can reduce the separation time and enhance the resolution [14]. In addition, the temperature-controlled flow FFF system may potentially be used to separate the intermediates of thermally unfolded proteins and help to better understand the protein unfolding process.

6.5 Precision and Accuracy

One of the most important applications of AF4 technology to biopharmaceuticals is the characterization of protein aggregates. Previous studies showed that AF4 can resolve protein fragments and aggregates [6, 7]. In addition, this method has been

found useful to detect large protein particles in combination with a light scattering detector [8].

The precision and accuracy of an analytical method are critical factors that should be carefully evaluated during the method development, qualification and validation. The precision and accuracy of AF4 can be influenced by many factors, including instrumentation, mobile phase, membrane, and running conditions, such as flow rates, focusing time and channel temperature. These parameters should be optimized to achieve the best results.

Quantitative analyses on precision and accuracy of an AF4 method have been assessed in a number of papers [6, 15, 16] for polymers and macromolecules. The result from a reproducibility study of AF4 measurements using two monoclonal antibodies showed reasonable repeatability with a standard deviation at ~2.3% to ~3.5% [15]. In a similar study, we have used the three well characterized therapeutic proteins as described previously (proteins I, II and III) to evaluate the intra-day precision and accuracy of the AF4 method. An optimized FFF procedure with an isocratic elution mode was successfully developed to separate these protein species in a mobile phase containing 180 mM NaCl, 20 mM Na_2HPO_4, pH 7.0. In this method, the cross flow was set at 3 mL/min and the channel flow was at 0.5 mL/min. As shown in Fig. 6.5, all three proteins with different molecular weight were well resolved by this method.

The precision of these measurements was determined by analyzing data from five repeat injections. As shown in Table 6.1, the standard deviation for experimentally determined % species from five repeat injections is only about 0.1%, which is comparable to the typical standard deviation from the size exclusion

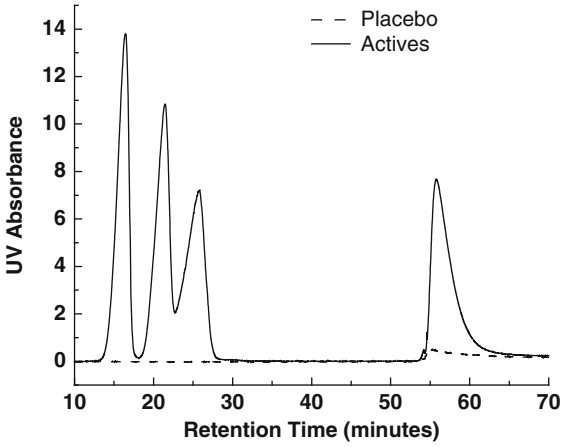

Fig. 6.5 Separation of a mixed protein sample at near equal weight ratios for Proteins I, II and III (as defined in the text) by AF4 at a cross flow of 3 mL/min and a channel flow of 0.5 mL/min using a regenerated cellulose AMPH amphiphilic membrane on an AF2000 instrument. The mobile phase is 180 mM NaCl, 20 mM Na_2HPO_4, pH 7.0. The peaks were monitored using an on-line UV detection system at a wavelength of 280 nm. The cross flow was turned off at ~52 min

Table 6.1 Analysis of a protein mixture by AF4

Samples	MW (kDa)	% Species (actual)	% Species (experimental) n = 5, mean ± σ	Accuracy[a] (%)	Retention time (min) n = 5,mean ± σ
Protein I	150	32.99	31.97 ± 0.13	−1.02	27.17 ± 0.19
Protein II	100	33.88	35.53 ± 0.08	+1.65	22.28 ± 0.10
Protein III	50	33.13	32.50 ± 0.05	−0.63	17.11 ± 0.09

[a]Accuracy was determined by subtracting the experimental values from actual values

chromatography method. In addition, the retention time between different repeated injections is also quite consistent, with a standard deviation less than 0.2 min (Table 6.1). Overall, these results demonstrate excellent intra-day precision of AF4 to separate and quantitate proteins in this size range (50–150 kDa). It should be noted that our intra-day precision is based on the results from a single user using the same membrane on the same day. It is likely that the true precision of this method may be lower if the data were generated by multiple users using multiple membranes on different days. These parameters should be carefully evaluated if the method needs to be fully validated.

The accuracy of this method was assessed by comparing the actual value (determined from a preparation at a near equal weight ratio of Proteins I, II and III) to the experimentally determined value. As shown in Table 6.1, the deviation from the actual percentage of each protein is less than 1.7%. This is comparable with many of the chromatographic and other orthogonal methods for size determination. The level of protein II showed the largest deviation, which is probably due to the lack of baseline resolution between protein I and protein II.

Besides the individual protein peaks, an additional peak was also observed at the end of each run after the cross flow was stopped (see Fig. 6.5). This peak corresponds to a significant portion of the total area. Although the retention time of this peak would indicate the presence of larger particles, data from light scattering and other orthogonal methods suggest that this peak is mostly composed of monomeric proteins (data not shown). This peak has been observed not only for the mixed protein samples, but also for each individual protein sample (data not shown). The size of the peak increases with an increase of the cross flow rate. A cross flow gradient can reduce the peak size, but cannot completely eliminate it. These observations suggest that this peak may be due to the non-specific adsorption of protein monomer to the membrane. In our case, this non-specific adsorption does not appear to interfere with the quantification of the percentage of individual protein species as shown in Table 6.1. However, for samples without prior knowledge of the size distribution, additional characterization studies are warranted. A comparison of results from different cross flows should provide a quick assessment of the potential impact of non-specific adsorption on the quantification. The other approaches to be considered are to compare the result from AF4 with those from other orthogonal methods or to collect this adsorption peak and re-inject it into the AF4 channel or SEC column. If the results from different orthogonal methods or from the purified peak are consistent with those from original samples, this would strongly indicate that the non-specific adsorption does not interfere with the quantification.

6.6 Comparison with Other Methods

In addition to the AF4 method, size exclusion chromatography (SEC) and analytical ultracentrifugation (AUC) are two of the most commonly used methods to determine the size distribution of therapeutic proteins [14]. In particular, SEC is the method of choice and has been fully validated for product release and stability testing in the Quality Control system of most biopharmaceuticals. AUC has been an important orthogonal method to support SEC development, qualification and validation [17].

To compare the precision and accuracy of these methods, the mixed protein sample that was used for AF4 evaluation was also analyzed by SEC and AUC sedimentation velocity. SEC experiments were conducted in 0.2 M potassium phosphate, 0.25 M potassium chloride, pH 6.2 using a TSK G3000SWXL column. The eluted peaks were detected by an on-line UV detector at a wavelength of 280 nm. As shown in Fig. 6.6, three individual proteins were well resolved by SEC. The precision from five repeat injections is extremely high with a standard deviation $<$ ~0.05% (Table 6.2). The percentage of each individual protein obtained by SEC analysis also matches the actual values quite well, with the largest deviation $<$0.5%. This is better than the results from AF4 analysis. These data demonstrate

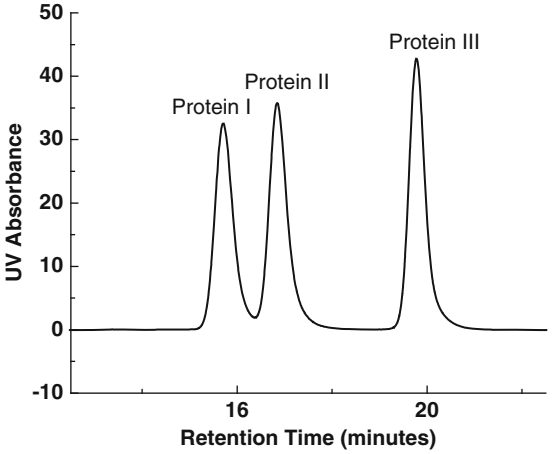

Fig. 6.6 Separation of a mixed protein sample by size exclusion chromatography at a flow rate of 0.5 mL/min using a TSK G3000SWXL column (7.8 × 300 mm) on an HP 1100 HPLC (Agilent). The mobile phase contains 0.2 M potassium phosphate, 0.25 M potassium chloride, pH 6.2. The peaks were monitored at a wavelength of 280 nm

Table 6.2 Analysis of a protein mixture by SEC

Samples	MW (kDa)	% Species (actual)	% Species (experimental) n = 5, mean ± σ	Accuracy[a] (%)	Retention time (min) n = 5,mean ± σ
Protein I	150	32.99	32.80 ± 0.03	−0.19	15.17 ± 0.01
Protein II	100	33.88	34.31 ± 0.05	+0.43	16.72 ± 0.01
Protein III	50	33.13	32.87 ± 0.04	−0.26	19.44 ± 0.00

[a]Accuracy was determined by subtracting the experimental values from actual values

Table 6.3 Analysis of a protein mixture by sedimentation velocity using a c(s) analysis

Samples	MW (kDa)	% Species (actual)	% Species (experimental) n = 6, mean ± σ	Accuracy[a] (%)
Protein I	150	32.99	36.5 ± 0.01	3.5
Protein II	100	33.88	33.6 ± 0.00	−0.3
Protein III	50	33.13	30.0 ± 0.00	−3.1

The c(s) fitting yielded an average frictional ratio of 1.38
[a]Accuracy was determined by subtracting the experimental values from actual values

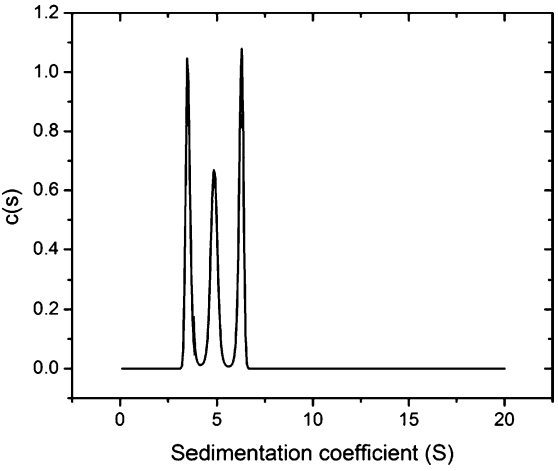

Fig. 6.7 Separation of a mixed protein sample by sedimentation velocity at 40,000 rpm and 20°C using ProteomeLab XLI analytical ultracentrifuge. Samples were diluted in 10 mM Na/K phosphate, 140 mM Na/K Cl at pH 7.2. The sedimentation was monitored at 280 nm. Data were analyzed using sedfit v12.1 b

that SEC is a very precise, accurate and robust method to determine the size distribution of proteins.

In a similar study the mixed protein sample was analyzed by sedimentation velocity, which is one of the most commonly used AUC methods to study the size distribution of proteins (Table 6.3). The sedimentation velocity experiments were conducted at 40,000 rpm and 20°C using a ProteomeLab XLI analytical ultracentrifuge (Beckman Coulter, Palo Alto). As shown in Fig. 6.7, the three protein species were well resolved by the sedimentation velocity method. The resolution from AUC is among the best in comparison with AF4 and SEC methods. The precision of the measurement from six repeat determinations is also very good, with a standard deviation of <0.01%. However, the results from a c(s) analysis with continuous distribution appear to be significantly different from the actual value. The largest deviation was observed at ~3.5% for protein III. Similar deviations were also observed previously from a mixed sample containing both full length antibody and Fab fragment [6]. This deviation has been attributed to significant differences between the frictional ratios of antibody and Fab fragment. Further analysis using a three discrete non-interacting species model (Table 6.4) leads to improved accuracy.

Table 6.4 Analysis of protein mixture by sedimentation velocity study using a model describing three discrete noninteracting species

Samples	MW (kDa)	f/f0[b] (fitted)	% Species (actual)	% Species (experimental) n = 6, mean ± σ	Accuracy[a] (%)
Protein I	150	1.56	32.99	31.1 ± 0.00	−1.9
Protein II	100	1.49	33.88	33.0 ± 0.00	−0.9
Protein III	50	1.30	33.13	35.9 ± 0.00	2.8

[a]Accuracy was determined by subtracting the experimental values from actual values
[b]The frictional ratio f/f_0 is obtained by fitting the data with a predefined molecular weight for each species

6.7 Conclusions

Field-flow fractionation is a useful orthogonal method to determine the size distribution of protein aggregates and fragments. With appropriate procedures and careful optimization, this method can provide useful quantitative information about the size and amounts of protein aggregates and particles. The nature and quality of the membrane is of particular importance for method optimization. Since AF4 is based on a different separation mechanism than the SEC method, with proper optimization AF4 may be used as an additional orthogonal technique to assess protein pharmaceutical quality. Overall this information is essential to maintain product quality and help to better understand the potential impact of aggregates on the safety and quality of protein pharmaceuticals.

References

1. Bernard A, Paulet B, Colin V, Cardot PJP (1995) Red blood cell separations by gravitational field-flow fractionation:instrumentation and applications. Trends Anal Chem 14:266–273
2. Qureshi RN, Kok WT (2010) Application of flow field-flow fractionation for the characterization of macromolecules of biological interest: a review. Anal Bioanal Chem 399:1401–1411, Epub 2010 Oct 1420
3. Colfen H, Antonietti M (2000) Field-flow fractionation techniques for polymer and colloid analysis. In: Advances in polymer science. Springer, Berlin/Heidelberg
4. Williams SKR, Runyon JR, Ashames AA (2010) Field-flow fractionation: addressing the nano challenge. Anal Chem 83:634–642
5. Giddings JC (2000) The field-flow fractionation family:underlying principles. In: Schimpf ME, Caldwell K, Giddings JC (eds) Field-flow fractionation handbook. Wiley, New York
6. Liu J, Andya JD, Shire SJ (2006) A critical review of analytical ultracentrifugation and field-flow fractionation methods for measuring protein aggregation. AAPS J 8:E580–E589
7. Rambaldi DC, Reschiglian P, Zattoni A (2010) Flow field-flow fractionation: recent trends in protein analysis. Anal Bioanal Chem 399:1439–1447
8. Fraunhofer W, Winter G (2004) The use of asymmetrical flow field-flow fractionation in pharmaceutics and biopharmaceutics. Eur J Pharm Biopharm 58:369–383
9. Wahlund KG (2000) Asymmetrical flow field-flow fractionation. In: Schimpf ME, Caldwell K, Giddings JC (eds) Field-flow fractionation handbook. Wiley, New York

10. Schauer T (2004) Symmetrical and asymmetrical flow field-flow fractionation for particle size determination. Part Part Syst Char 12:284–288
11. Caldwell KD, Brimhall SL, Gao Y (1988) Sample overloading effects in polymer characterization by field-flow fractionation. J Appl Polym Sci 36:703–719
12. Williams SKR (2000) Flow field-flow fractionation. In: Schimpf ME, Caldwell K, Giddings JC (eds) Field-flow fractionation handbook. Wiley, New York
13. Schimpf ME (2000) Optimization. In: Schimpf ME, Caldwell K, Giddings JC (eds) Field-flow fractionation handbook. Wiley, New York
14. Liu J, Demeule B, Shire SJ (2010) Separation based analytical methods for measuring protein aggregation. In: Mahler HC, Jiskoot W (eds) Analysis of aggregates and particles in protein pharmaceuticals. Wiley, New York
15. Litzen A, Walter JK, Krischollek H, Wahlund KG (1993) Separation and quantitation of monoclonal antibody aggregates by asymmetrical flow field-flow fractionation and comparison to gel permeation chromatography. Anal Biochem 212:469–480
16. Li JM, Caldwell KD (1991) Improved accuracy in the determination of field-flow fractionation elution volumes. J Chromatogr 555:260–266
17. Philo JS (2009) A critical review of methods for size characterization of non-particulate protein aggregates. Curr Pharm Biotechnol 10:359–372

Chapter 7
Studies of Loose Protein Aggregates by Flow Field-Flow Fractionation (FFF) Coupled to Multi-Angle Laser Light Scattering (MALLS)

Caroline Palais, Martinus Capelle, and Tudor Arvinte

Abstract Flow FFF was used to study the aggregation properties of an antibody, two different proteins and a protein-polysaccharide conjugate (PPC). Two FFF methods were applied, the standard FFF method with separation (with focus flow and with cross flow) and FFF without separation (without focus flow and without cross flow). The FFF method without separation was found to be less destructive on the aggregates. By comparing the two FFF methods, loose aggregates could be detected for the antibody and the two different proteins. These loose aggregates reversed to mainly monomers during standard FFF analyses. The presence of these aggregates was confirmed by complementary spectroscopic and microscopic techniques. In the case of the PPC, focus flow and cross flow induced the formation of bigger and smaller aggregates. These results document the importance of using different methods to characterize the complexity of protein aggregation.

Keywords Antibody aggregation • Effects of cross flow • Effects of focus flow • Flow field-flow fractionation • Freeze-thaw cycles • Loose aggregates • Protein aggregation • Protein-polysaccharide conjugate • Stability studies

7.1 Introduction

Development of biopharmaceuticals is often confronted with various types of protein aggregation phenomena. A complex battery of analytical methods- including less destructive methods for loose aggregates- is needed to detect and characterize these protein structures.

C. Palais • M. Capelle • T. Arvinte (✉)
Therapeomic Inc, Basel, Switzerland
e-mail: caroline.palais@therapeomic.com; martinus.capelle@therapeomic.com; tudor.arvinte@therapeomic.com

S.K.R. Williams and K.D. Caldwell (eds.), *Field-Flow Fractionation in Biopolymer Analysis*, DOI 10.1007/978-3-7091-0154-4_7,

Compared to size-exclusion chromatography, the flow field-flow fractionation (FFF) technique applies less stresses on protein samples during separation. However, protein aggregation state may also be disturbed or induced by FFF during the concentration of the sample by focusing or during the fractionation when a perpendicular flow field is applied. Minimal sample disturbance can be achieved by using FFF without focus flow (V_F) and without cross flow (V_X); the sample is only eluting with the main flow (V_M). Under these conditions, we were able to obtain information on the presence of loose antibody aggregates in Herceptin [1]. Depending on the formulation, the eluted antibody was either monomeric or in an aggregated state [1].

In this chapter, we will present four protein case studies where loose aggregates were investigated by standard FFF methods [2] and by the FFF method without focus flow and cross flow.

7.2 Instrumentation

All FFF measurements were performed using a Wyatt Eclipse Separation System (Dernbach, Germany), coupled with an Agilent UV detector (Waldbronn, Germany) monitored at 280 nm, and a Wyatt MALLS instrument (Dernbach, Germany). The separation channel consisted of a porous frit covered with a Mycrodin Nadir (Wiesbaden, Germany) regenerated cellulose ultrafiltration membrane with a molecular weight cut-off of 10 KDa and a 350 µm spacer. For each sample, the carrier fluid had the same composition as the protein formulation buffer. Data analyses were performed using the Wyatt software, Astra. The results are presented as molar mass or rms radius (dots; left Y-axis; logarithmic scale) versus time graphs with the UV signals at 280 nm (solid lines; right Y-axis; relative scale).

The UV-Vis absorbance measurements were recorded in a quartz cuvette at 25°C with a GBC Cintra 40 spectrophotometer (Melbourne, Australia) with a double beam and two monochromators. The 90° light-scatter measurements were performed with a Spex FluoroMax spectrofluorometer (Stanmore, UK) at 25°C.

The protein samples stained with Nile Red (Invitrogen) were observed on a Zeiss Axiovert 200 microscope (Göttingen, Germany) equipped with a mercury discharge lamp. The images were acquired with a QImaging cooled Retiga 1300C color CCD camera (Burnaby, Canada).

7.3 Therapeutic Antibody, About 150 KDa

A therapeutic antibody in liquid formulation was stored for 1 year at –80°C, 2–8°C, 25°C and 40°C. The samples were analyzed with an optimized FFF method (V_M = 1.0 ml/min, V_X = 1.5 ml/min, V_F = 1.0 ml/min), Fig. 7.1a. No significant

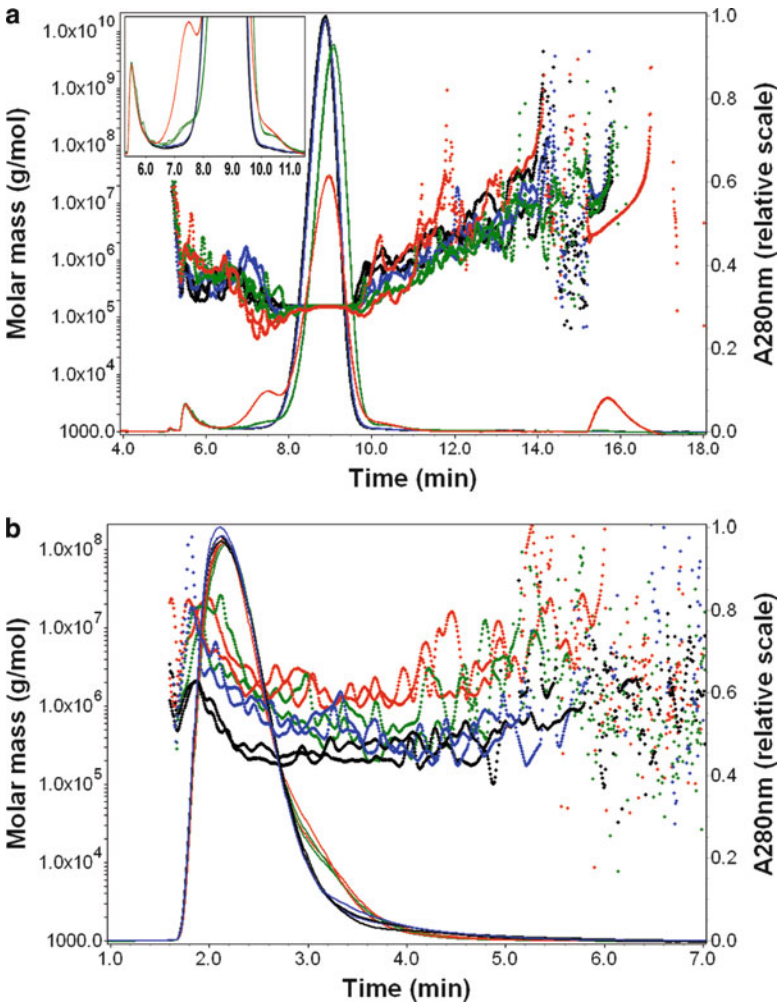

Fig. 7.1 Molar mass (*dots*) versus time graphs with the UV signals at 280 nm (*solid lines*) of the antibody stored at different temperatures (*black*, –80°C; *blue*, 2°–8°C; *green*, 25°C; *red*, 40°C). (**a**) FFF method with separation (V_M = 1.0 ml/min, V_X = 1.5 ml/min, V_F = 1.0 ml/min). The insert is a magnified view of the chromatograms between 5 and 12 min. (**b**) FFF method without separation (V_M = 1.0 ml/min, no focus flow, no cross flow). For each method, each sample was injected twice. The FFF running buffer was the same as the protein formulation buffer

differences could be observed between the samples stored at –80°C and at 2–8°C for 1 year. They contained about 95% of monomer. The chromatograms of the antibody solutions stored at 25°C and 40°C presented two additional peaks, one between 7 and 8 min, and one between 10 and 11 min, insert in Fig. 7.1a. For the sample stored at 40°C, a peak eluted during the cleaning phase (no cross flow), between 15 and 17 min. The samples stored for 12 months at 25°C and at 40°C

contained 93% and 80% of monomer, respectively. These FFF results show that in solution the antibody degraded and aggregated after storage at 25°C and 40°C. There were no differences observed in the stability of the therapeutic antibody for the solutions stored at –80°C or 2–8°C for 1 year.

Chromatograms of the antibody solutions analyzed by the FFF method without separation (V_M = 1.0 ml/min, no focus flow, no cross flow) consisted of one peak, Fig. 7.1b. The peaks of the samples stored at 25°C and 40°C showed a tailing between 3 and 4 min. For the sample stored at –80°C, the main peak corresponded to particles with a molecular weight between 200 and 2,000 KDa. Higher molecular weight complexes were observed in all the other samples, including the solution stored at 2–8°C. Thus, the FFF method without separation was able to detect differences between the –80°C and the 2–8°C samples, Fig. 7.1b. These differences were not detected by the FFF method with separation, Fig. 7.1a.

These results show that the antibody formed loose aggregates when stored for 1 year at 2–8°C, aggregates that are reversed to monomers during the standard FFF analysis. The presence of aggregates in the antibody samples stored at 25°C and 40°C was observed by both FFF methods. The FFF method with separation detected antibody fragments, small amount of presumably dimers and, for the sample stored 1 year at 40°C, large aggregates during the cleaning phase. The ultrasonic resonator technology (TF instruments, Heidelberg, Germany), UV-Vis spectroscopy, 90° light-scatter measurements in cuvette (data not shown), together with the FFF results showed that the –80°C sample contained the smallest amount of protein aggregates.

7.4 Protein X, 60 KDa

The effect of successive freeze-thaw cycles (freezing at –24°C and thawing in a thermostated bath at 25°C) on the protein X (MW ~ 60 KDa) was studied by FFF with and without separation. The protein solution was analyzed at start and after each freeze-thaw cycle.

With the FFF method with separation (V_M = 0.5 ml/min, V_X = 3.0 ml/min, V_F = 1.0 ml/min), small differences in the chromatograms were observed before and after freeze-thawing, Fig. 7.2a. After the third freeze-thaw cycle, the retention time of the main peak increased of about 0.3 min and the peak intensity slightly decreased. However, the molecular weights of the main peak (monomer) and of the eluted aggregates were the same after each freeze-thaw cycle. Thus, based on the FFF method with separation, one will conclude that protein X survives the freeze-thawing process without the formation of aggregates; the observed increase of the retention time may be due to changes in the protein conformation.

Analysis of the protein X samples with the FFF method without separation (V_M = 0.5 ml/min, no focus flow, no cross flow) showed that each freeze-thaw cycle induced aggregation of protein X; the molar mass of the detected particles increased after each freeze-thaw cycle, Fig. 7.2b. After three freeze-thaw cycles,

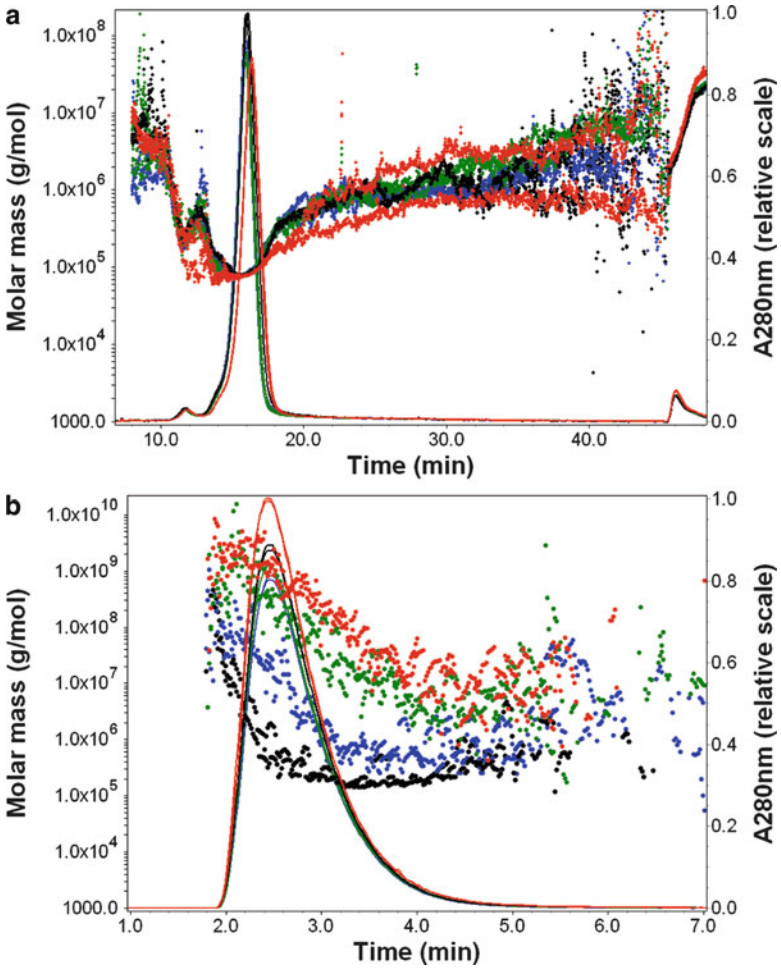

Fig. 7.2 Molar mass (*dots*) versus time graphs with the UV signals at 280 nm (*solid lines*) of the protein X at time 0 (*black*), after one freeze-thaw cycle (*blue*), after the second freeze-thaw cycle (*green*), and after the third freeze-thaw cycle (*red*). (**a**) FFF method with separation ($V_M = 0.5$ ml/min, $V_X = 3.0$ ml/min, $V_F = 1.0$ ml/min). (**b**) FFF method without separation ($V_M = 0.5$ ml/min, no focus flow, no cross flow). For each method, each sample was injected twice. The FFF running buffer was the same as the protein formulation buffer

large aggregates formed with a molecular weight between 10^3 KDa and 10^6 KDa. The presence of such large aggregates after freeze-thawing was confirmed by UV-Vis absorbance, 90° light-scattering and fluorescence microscopy, Fig. 7.3. After one freeze-thaw cycle a small increase in the UV-Vis background spectrum of protein X was observed around 250 nm showing the formation of small aggregates (mainly Rayleigh scatter), Fig. 7.3a. After the third freeze-thawing cycle, there was a strong increase of the background absorbance between 320 and 450 nm,

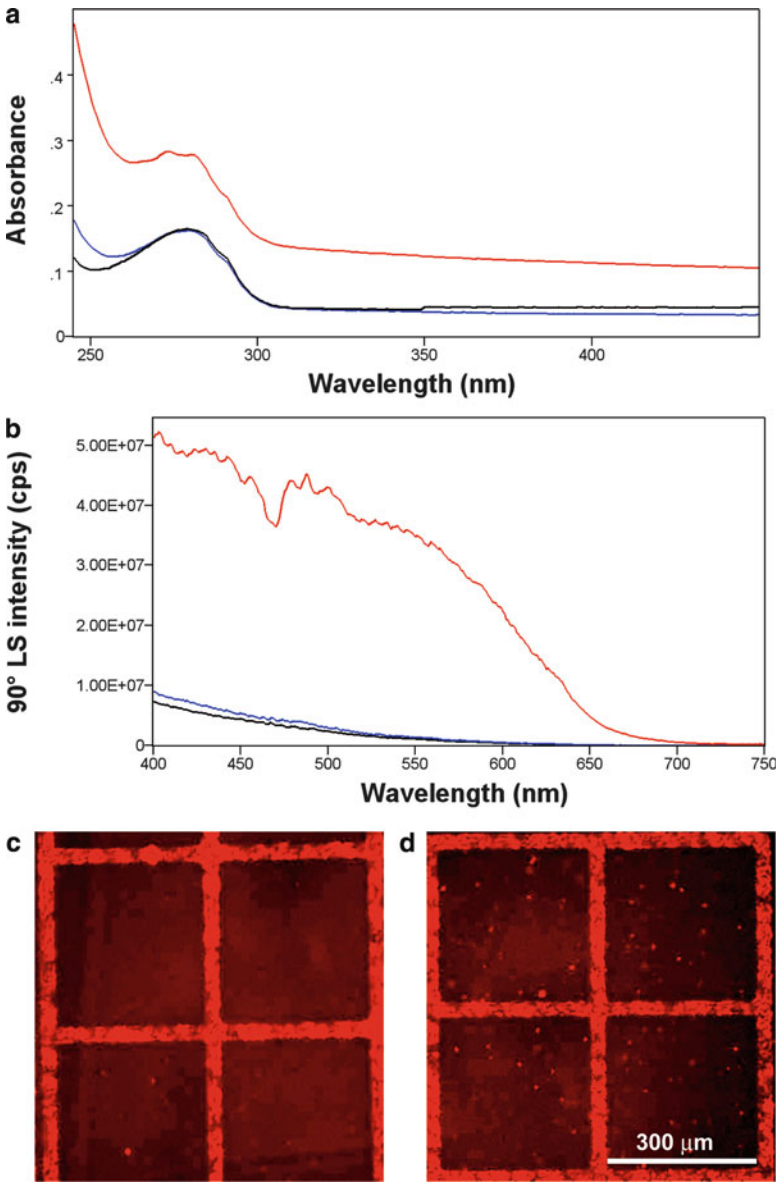

Fig. 7.3 Effect of successive freeze-thaw cycles on protein X. The sample was characterized by UV-Vis absorbance (**a**) and 90° light-scattering (**b**) at time 0 (*black*), after one freeze-thaw cycle (*blue*), and after the third freeze-thaw cycle (*red*). Protein X was also observed by Nile Red fluorescence microscopy at time 0 (**c**) and after three freeze-thaw cycles (**d**)

which indicates the formation of large aggregates (Thompson and Mie scatter). 90° light-scatter measurements of the protein X samples showed a small increase in scatter after the first freeze-thaw cycle and a strong increase after the third freeze-

thawing, Fig. 7.3b. Nile Red fluorescence microscopy [3] showed few particles before freeze-thawing, Fig. 7.3c (13 ± 5 particles in 0.9 µl), and a strong increase in the number of aggregates after three freeze-thaw cycles, Fig. 7.3d (490 ± 100 particles in 0.9 µl).

The UV-Vis spectroscopy, 90° light-scattering and Nile red microscopy data together with the FFF results show that freeze-thawing induced aggregation of protein X. These aggregates are loose since a mild FFF separation cannot detect their presence, Fig. 7.2a.

7.5 Protein-Polysaccharide Conjugate, 5,000–10,000 KDa

Effects of cross flow and focus flow on a heterogeneous protein-polysaccharide conjugate (PPC) were studied in more details. The heterogeneous PPC had about 30% polysaccharide content and a molecular weight varying between 5,000 and 10,000 KDa.

In a first step, PPC was characterized by FFF with separation (V_M = 1.0 ml/min, V_X = 0.5 ml/min, V_F = 1.0 ml/min); the rms radius versus time graph shows a broad size distribution, radii between 20 and 600 nm, Fig. 7.4a. FFF without separation (V_M = 0.2 ml/min, no focus flow, no cross flow) showed the presence of relatively uniform particles with radii between 70 and 90 nm, Fig. 7.4b (black plots). With the latter method, using main flows of 0.5, 1 and 2 ml/min did not change the size of the detected particles (data not shown). All the areas under the curve were the same for the two FFF methods, showing that PPC did not bind to the membrane during focusing or separation.

However, the focus flow had a strong effect on the size distribution of PPC. Increasing the focusing flow (V_F of 0.2, 0.5 and 1.0 ml/min) induced the formation of both smaller and larger PPC aggregates, radii between 50 and 600 nm. Interestingly, we could not detect the 20 nm aggregates which were observed in Fig 7.4a. The smallest detected particles had radii between 45 and 60 nm, Fig. 7.4b. The FFF standard method with focus flow and with cross flow induced a further reduction in the size of the protein aggregates (20 nm radius), the large particles of 600 nm remaining present, Fig. 7.4a.

7.6 Protein Y, About 33 KDa

Differences in the aggregation state of protein Y (MW ~ 33 KDa) in two manufacturing batches were investigated using the two FFF methods, Fig. 7.5. The FFF method with separation (V_M = 0.5 ml/min, V_X = 1.0 ml/min, V_F = 1.0 ml/min) showed that the batches have similar molecular weight distributions, Fig. 7.5a. However, the UV chromatograms were different, Fig. 7.5a.

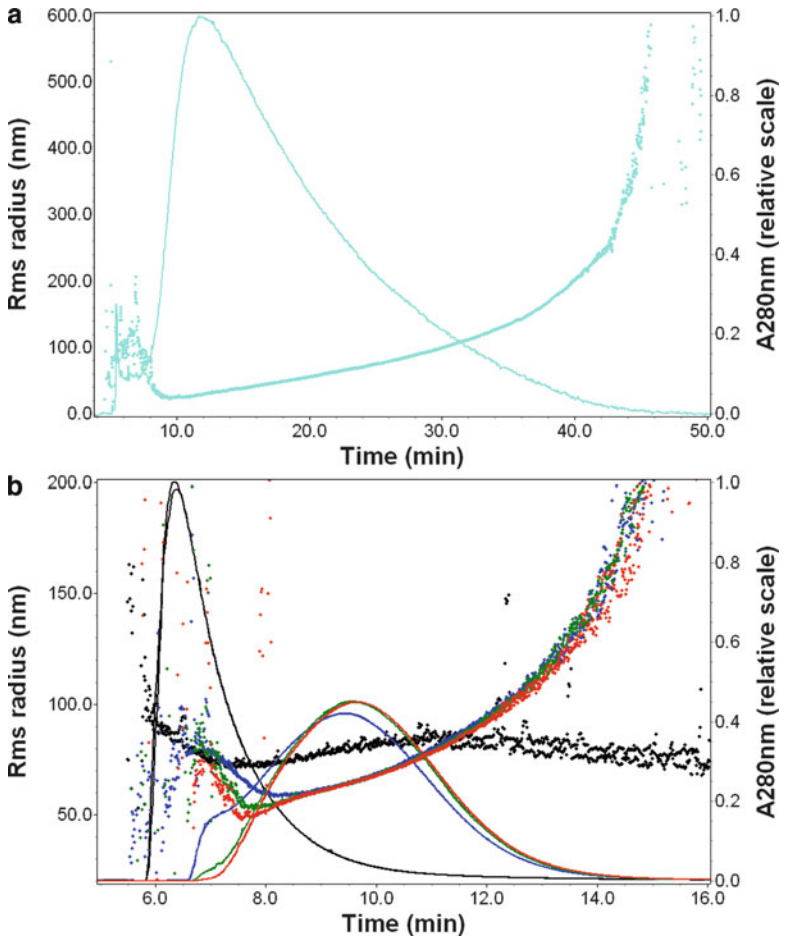

Fig. 7.4 Rms radius (*dots*) versus time graphs with the UV signals at 280 nm (*solid lines*) of the protein-polysaccharide conjugate (PPC). (**a**) FFF method with separation ($V_M = 1.0$ ml/min, $V_X = 0.5$ ml/min, $V_F = 1.0$ ml/min). (**b**) FFF method without separation; effect of the focus flow on the rms radius (*black*, $V_F = 0$ ml/min; *blue*, $V_F = 0.2$ ml/min; *green*, $V_F = 0.5$ ml/min; *red*, $V_F = 1.0$ ml/min), with $V_M = 0.2$ ml/min and no cross flow. For each method, each sample was injected twice. The FFF running buffer was the same as the protein formulation buffer

The main population of the two samples corresponds to the particles detected in the width of the main peak at the half-peak height. For batch 1, the main peak contained monomers and aggregates up to about 100 KDa, between 7 and 12 min. For the second batch, aggregates with larger molar mass, 100–500 KDa, were detected between 11 and 15 min.

The FFF chromatograms ($V_M = 1.0$ ml/min, no focus flow, no cross flow; Fig. 7.5b), UV-VIS spectroscopy, 90° light-scatter measurements in cuvette and Nile Red microscopy showed the presence of much larger aggregates in batch

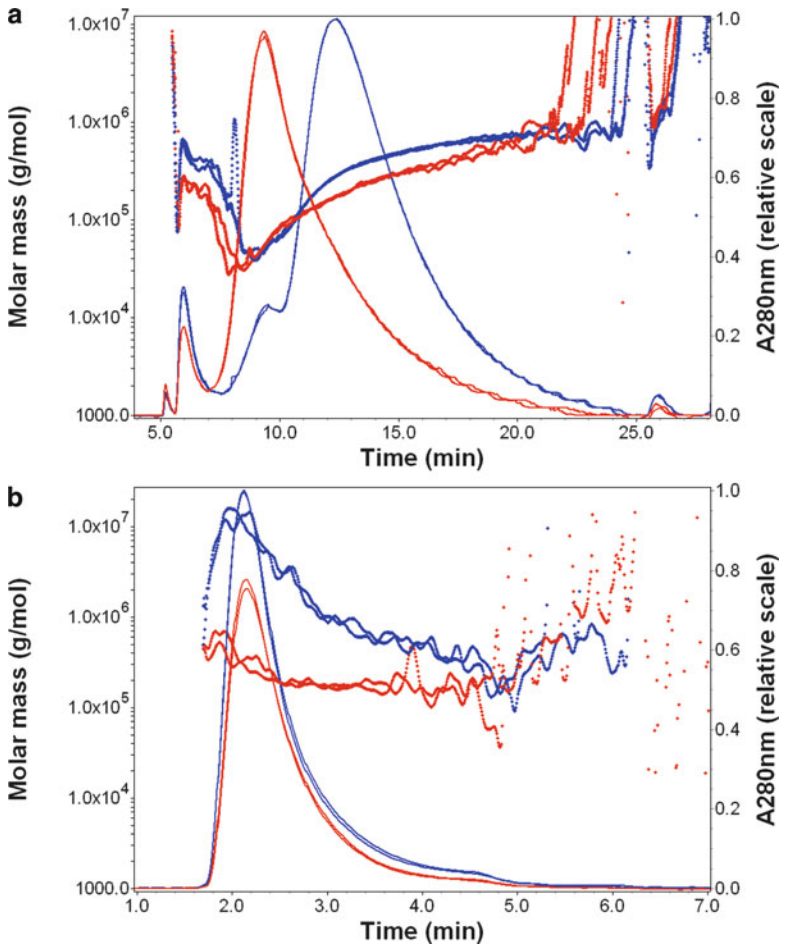

Fig. 7.5 Molar mass (*dots*) versus time graphs with the UV signals at 280 nm (*solid lines*) of two batches (*red*, batch 1; *blue*, batch 2) of protein Y. (**a**) FFF method with separation ($V_M = 0.5$ ml/min, $V_X = 1.0$ ml/min, $V_F = 1.0$ ml/min). (**b**) FFF method without separation ($V_M = 1.0$ ml/min, no focus flow, no cross flow). For each method, each sample was injected twice. The FFF running buffer was the same as the protein formulation buffer

2 (data not shown). For batch 1 the mass distribution was between 200 and 700 KDa whereas for batch 2 the maximum detected mass was 2×10^4 KDa.

The two FFF methods provided complementary information. The FFF results with focus flow and cross flow show that both batches contained aggregates of similar molar mass, but in different proportions, Fig. 7.5a. The protein in both batches has a tendency to form loose aggregates; this process is more pronounced in batch 2.

References

1. Demeule B, Palais C, Machaidze G, Gurny R, Arvinte R (2009) New methods allowing the detection of protein aggregates: a case study on trastuzumab. MAbs 1(2):142–150
2. Arakawa T, Philo JS, Ejima D, Sato H, Tsumoto K (2007) Aggregation analysis of therapeutic proteins, part 3; principles and optimization of field-flow fractionation (FFF). BioProcess Int 5(10):52–70
3. Demeule B, Gurny R, Arvinte T (2007) Detection and characterization of protein aggregates by fluorescence microscopy. Int J Pharm 329(1–2):37–45

Chapter 8
Field-Flow Fractionation for Assessing Biomolecular Interactions in Solution

Robert Y. -T. Chou, Joey Pollastrini, Thomas M. Dillon, Pavel V. Bondarenko, Lei-Ting T. Tam, Jill Miller, Michael Moxness, and Shawn Cao

Abstract Many biological systems are primarily governed by protein-protein interactions. It is important to develop sensitive analytical techniques to identify and characterize these bimolecular interactions in order to understand their fundamental roles in biological processes and in disease. In this book chapter, we summarize three case studies that applied asymmetrical flow field-flow fractionation (AF4) to access the protein-protein interactions of therapeutic proteins with their counterparts. These new applications of AF4 provide a unique and innovative tool that extends the bioanalytical capability to study protein complexes beyond micro-molar affinity.

Keywords AF4 • Aggregation • FcRn • Fcγ Receptor • FFF • Human serum albumin • Monoclonal antibodies • Particle • Protein interaction

8.1 Introduction

Many biological systems are primarily governed by protein-protein interactions, such as signal transduction, transcriptional regulation, activation of the immune system, and protein recycling by Fc receptors (Fcγ/FcRn). It is important to

R.Y.-T. Chou (✉)
Department of Formulation & Analytical Resources, Amgen Inc, Thousand Oaks, CA, USA

Amgen Inc, Thousand Oaks, CA, USA
e-mail: ychou@amgen.com

J. Pollastrini • T.M. Dillon • P.V. Bondarenko • S. Cao
Department of Formulation & Analytical Resources, Amgen Inc, Thousand Oaks, CA, USA

L.-T.T. Tam
Department of Protein Science, Amgen Inc, Thousand Oaks, CA, USA

J. Miller • M. Moxness
Department of Clinical Immunology, Amgen Inc, Thousand Oaks, CA, USA

S.K.R. Williams and K.D. Caldwell (eds.), *Field-Flow Fractionation in Biopolymer Analysis*, DOI 10.1007/978-3-7091-0154-4_8,

develop sensitive analytical techniques to identify and characterize these bimolecular interactions in order to understand their fundamental roles in biological processes and in disease. A variety of methods have been utilized in recent years to study protein-protein interactions both in vivo and in vitro [1, 2]. The yeast two-hybrid system, protein fragment complementation, and resonance energy transfer are the major techniques for identification of protein-protein interactions in vivo, while immunoprecipitation, pull-down assays and protein microarrays provide in vitro evidence for these interactions [1]. For characterizing the interactions of purified proteins in vitro, several biophysical and biochemical analytical tools have been used to obtain the binding kinetics, the stoichiometric ratio, the oligomeric state and even the conformations of the interaction sites [2]. The techniques include surface plasmon resonance (SPR), mass spectrometry (MS), nuclear magnetic resonance (NMR) spectroscopy, isothermal titration calorimetry (ITC), analytical ultracentrifugation (AUC), liquid chromatography (LC) and others. There are a few major challenges for the current techniques, especially to indentify and characterize "weak" protein-protein interactions ($K_d > \mu M$), as well as to study complex protein interactions that have more than two protein components.

In the biopharmaceutical industry, therapeutic monoclonal antibodies (mAbs) comprise the majority of recombinant proteins currently in clinical development, because of their high specificity and strong binding to a selected antigen, predictable properties and long life in circulation. However, the major therapeutic immunoglobulin gamma (IgG) mAbs also interact weakly by their conserved regions with several Fcγ receptors expressed on leukocytes, complement and neonatal Fc receptor (FcRn) expressed on many cells[3, 4]. These interactions are weak with K_d values in the μM range and also involve multiple protein components (Fig. 8.1). Size-exclusion chromatography (SEC), a technique commonly used for strong antibody-antigen interactions, has been less successful while characterizing weak protein-protein interactions due to the secondary interactions of protein with the column media and on-column dilution effects. Unlike SEC, asymmetrical flow

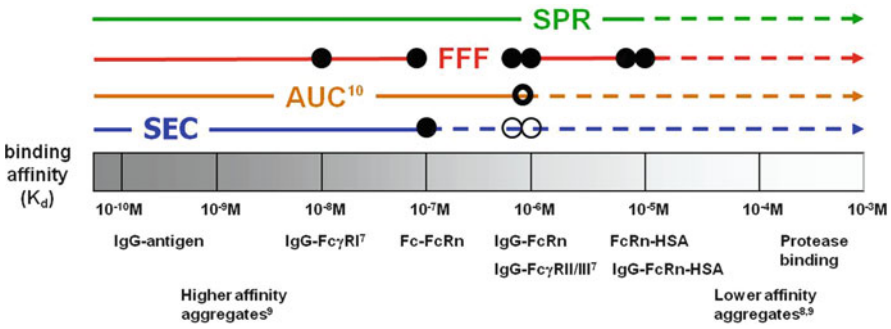

Fig. 8.1 Comparison of enhanced resolution of AF4 in detecting weak binding with other methods [7–11]. (● represents the experiments where the binding was detected in this report and [11]; ◎- was detected by AUC [10]; ○- was not detected in [11])

field-flow fractionation (AF4), the most commonly used form of the field-flow fractionation (FFF) technique, is a matrix-free system that utilizes a flow-assisted fractionation method whereby the analytes are separated along a ribbon-like channel by differences in their diffusion coefficients [5]. AF4 has been considered an orthogonal method to other separation techniques, such as SEC and AUC [5]. The ability of AF4 to separate analytes in a wide size range (from nanometers to microns) [6] is gaining attention due to an increasing demand for studying aggregation and particles in protein therapeutics. Recently AF4 has been exploited in the studies of protein-protein interactions of therapeutic proteins that involve multiple binding events.

In this book chapter, we summarize three case studies that applied AF4 to access the protein-protein interactions of therapeutic proteins with their counter parts. These new applications of AF4 provide a unique and innovative tool that extends the bioanalytical capability to study protein complexes beyond micro-molar affinity (Fig. 8.1).

8.2 Case Studies

8.2.1 Experimental

Unless otherwise specified, AF4 experiments in all case studies were performed using an Agilent LC system (degasser, autosampler and pump) connected to a Wyatt Eclipse 3 Separation System. Detection included an Agilent UV detector (wavelengths 215 and 280 nm collected), Wyatt HELEOS on line multi-angle light scattering (MALS) detector, and a Wyatt rEX differential refractive index (RI) detector. The separations were performed using a 10 kDa molecular weight cutoff regenerated cellulose membrane in the 25 cm channel with a 490 μm spacer thickness, 21.5 mm breadth. The tests were carried out at ambient temperature using Dulbecco's phosphate-buffered saline (DPBS) as the carrier fluid (3.2 mM Na_2HPO_4, 0.5 mM KH_2PO_4, 1.3 mM KCl, 135 mM NaCl). Astra (Wyatt) and ChemStation (Agilent) software were used to process all signals.

8.2.2 Case Study 1: FcRn:IgG Binding

8.2.2.1 Introduction

The neonatal Fc receptor (FcRn) salvages the two most abundant soluble proteins in serum, IgG and human serum albumin (HSA), from the lysosomal degradation pathway, resulting in reduced clearance and extended half-lives [12, 13]. HSA

maintains the oncotic pressure of the circulatory system and functions as a carrier protein for steroids, fatty acids, thyroid hormones, and drugs. IgG is composed of two unique structural properties, two variable antigen-binding (Fab) regions and the constant (Fc) region, which represent its specificity for the target antigen, and unique effector functions [14], respectively. IgG, comprising 75% of serum immunoglobulins in humans, provides the majority of antibody-based immunity against invading pathogens. IgG also interacts with the FcγR family (FcγRI, FcγRII, FcγRIII and FcγRIV) to mediate effector responses, including antibody-dependent cell-mediated cytotoxicity (ADCC), inflammation, cell activation and antibody production [15, 16]. Therefore, recombinant IgG antibody therapeutics hold the promise of being one of the major treatments for various diseases. Studying the protein-protein interactions between FcRn and IgG, as well as HSA have become major interests in the biopharmaceutical industry.

FcRn interacts with both IgG and HSA in a pH-dependent manner, in which FcRn-binding occurs in the endosome at acidic pH (pH $<$ 6.5), and IgG/HSA are released at the neutral cell surface (pH ~ 7.4) [17]. Although this pH-dependence is due to the presence of conserved histidine residues, the protein-protein interactions of IgG and FcRn are distinct from that of HSA and FcRn [12, 18]. FcRn interacts with IgG at the CH2–CH3 domain interface, mediated by electrostatic interactions involving histidine residues H310, H433, H435 and H436 [19]. These interactions serve as the basis for the currently proposed mechanism of intracellular IgG trafficking and recycling. Both hydrophobic and electrostatic interactions between H166 of FcRn and HSA domain III have been proposed as the mechanism for the FcRn:HSA interactions [12, 18, 20].

SPR, ITC, X-ray crystal structures and many other analytical/biophysical techniques have been developed and used to characterize the FcRn and IgG interactions [21–23], and interactions between FcRn and HSA [12, 18]. However, the relatively weak interaction ($K_d > \mu M$) between FcRn and IgG and between FcRn and HSA have presented difficulty in studying these interactions. Recently, AF4 has been applied to study the weak protein-protein interactions between IgG and FcRn, and also to assess the physiologically relevant multi-component IgG:FcRn:HSA complexes in solution [11]. These new applications demonstrate that AF4 is a unique and innovative bioanalytical tool in studying weak protein-protein interactions ($K_d > \mu M$) in complex protein systems. The following case study discusses the findings of these applications.

8.2.2.2 Method

The recombinant IgGs were expressed in Chinese Hamster Ovary (CHO) cells and purified using conventional manufacturing process steps. Recombinant, soluble human FcRn was expressed in CHO cells and purified using nickel-NTA chromatography by the Amgen Protein Science department. Native Albumin (Human) was purchased from CSL Behring LLC (Kankakee, IL). The samples were prepared at approximately 0.3–1 mg/mL in PBS and injections were made

in the range of 10 uL to target 6–20 ug loads. The tests were carried out at various pHs (5.2, 5.8, 6.1, 6.3, 6.5, 6.6, 7.4 and 8.1). The run parameters used for all samples included a focus flow of 2 mL/min for 2 min duration and the elution conditions consisted of channel flow at 1.0 mL/min throughout, and a constant crossflow of 2.3 mL/min.

8.2.2.3 Results and Discussion

pH-Dependent FcRn:IgG Binding Observed by AF4

AF4 was used to assess the interactions between FcRn and IgG at different pH values (from pH 7.4 to 5.2). Equal amounts (0.07 μmol) of FcRn and IgG were mixed and injected onto AF4 system. At pH 7.4, both peak areas and retention times of free FcRn and IgG2 were equal to the controls (data not shown), indicating that no binding between FcRn and IgG2 occurred. At mildly acidic conditions (Fig. 8.2), binding was observed and binding affinity was seen to increase with decreasing pH, based on the observation of changes in retention times of IgG:FcRn complex and the amount of free FcRn. The ability to monitor the pH-dependent binding event of IgG to FcRn by AF4, which was also observed previously by other groups using other analytical methods [24–27], suggested that AF4 was capable of characterizing weak protein-protein interactions with K_d in the μM range.

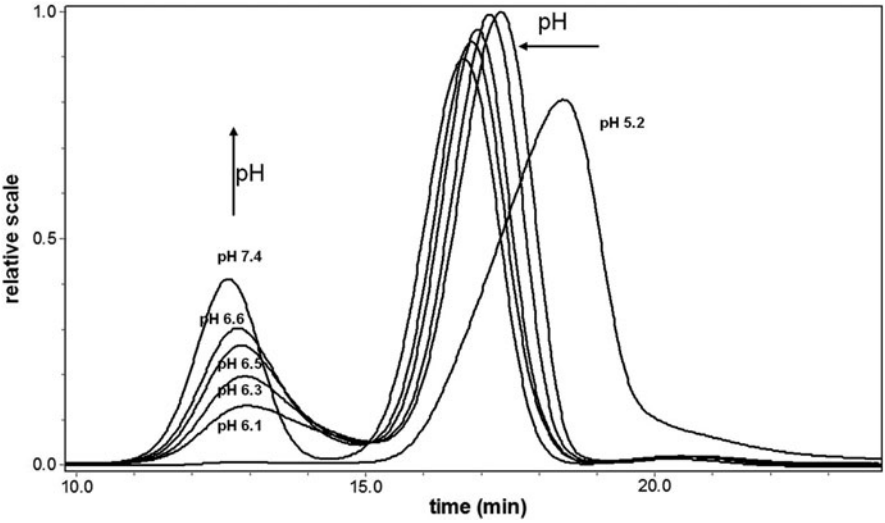

Fig. 8.2 AF4 analyses of IgG2:FcRn complexes at different pHs. The IgG:FcRn complex was mixed at a 1 to 1 molar ratio prior to injection (0.07 μmol)

AF4 Analyses of Interactions Among HSA, FcRn and IgG

FcRn has been reported to bind both HSA and IgG independently and in the same pH-dependent manner [18, 28]. To characterize the interactions of the three components FcRn:HSA:IgG, mixtures at different ratios of FcRn (0.14 μmol), HSA (0.14 μmol), and/or IgG (0.070 μmol) were prepared and analyzed by AF4 (Fig. 8.3) [11]. As expected, no complex was formed when HSA and IgG were incubated without FcRn (Fig. 8.3(4)) [11]. When HSA and FcRn were incubated together, an HSA:FcRn complex was resolved (Fig. 8.3(5)) [11]. Although a significant amount of free FcRn was still present, this was thought to be the result of weak μM binding (Fig. 8.3(5)) [11]. Due to overlapping peaks between FcRn (44.7 kDa) and HSA (66.7 kDa), a quantitative assessment of peak areas was not feasible. However, future adjustments could be made to the instrument settings to achieve optimized separation resolution between FcRn and HSA. The purpose of this experiment was to qualitatively characterize the binding of FcRn, HSA, and IgG (147 kDa) at the same time. Therefore, the AF4 method was optimized for the separation of the higher molecular weight complexes. Since both HSA:FcRn and FcRn:IgG interactions fall into the weak binding category ($K_d > \mu M$), it has been shown that the observed complex peak contains both unbound individual components and bound complex under an equilibrium state determined by K_d; for that reason, the peak of complexes is relatively broader than the peak of each individual component. Breadth of the complex peak also owes to the combined 1:1 and 2:1 stoichiometries being unresolved under a single peak. Based on the internal reference standards (FcRn 44.7 kDa, HSA 66.7 kDa, FcRn:HSA 111 kDa, HSA dimer 133 kDa, IgG 147 kDa, 2FcRn:IgG 236 kDa and IgG dimer 294 kDa), the elution time of the predominant species was consistent ($r = 0.989$) with the mass of HSA:FcRn:IgG:FcRn complex (303 kDa), with the next few possible

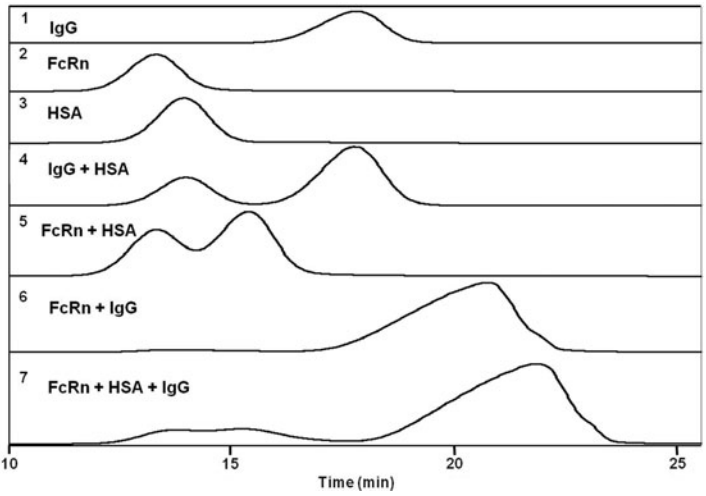

Fig. 8.3 AF4 analyses of interactions among HSA (0.14 μmol), FcRn (0.14 μmol) and IgG (0.07 μmol). (1) IgG, (2) FcRn, (3) HSA, (4) HSA + IgG, (5) FcRn + HSA, (6) FcRn + IgG, and (7) FcRn + HSA + IgG (This figure was adapted from [11])

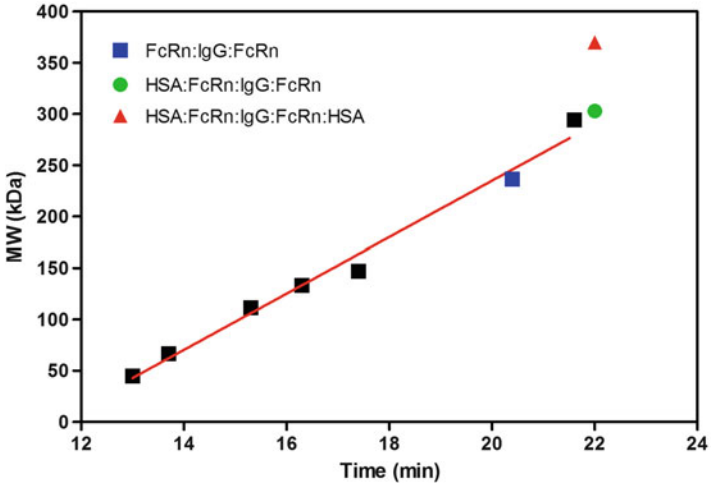

Fig. 8.4 Internal size reference standard curve for AF4 analyses of interactions among HSA, FcRn and IgG (This figure was modified from [11])

complexes being HSA:FcRn:IgG:FcRn:HSA (370 kDa), HSA:FcRn:IgG (258 kDa) and FcRn:IgG:FcRn (236 kDa) (Figs. 8.3 and 8.4) [11]. The observation of predominant species HSA:FcRn:IgG:FcRn was unexpected, but was not surprising, although it has not been reported yet in published studies. SPR and immunoblotting experiments have shown that both IgG and HSA bind non-cooperatively to distinct sites on FcRn [18], which may imply that HSA:FcRn:IgG:FcRn:HSA should be the predominant species. However, under similar weak protein-protein interactions ($K_d \sim \mu M$) [15] and our experimental condition (molar ratios HSA:FcRn:IgG = 2:2:1), the extra available binding site of IgG to FcRn may be one possible reason to explain why HSA:FcRn:IgG:FcRn is the predominant species at the equilibrium state in solution. The qualitative results described here could not address the influence of each ligand but suggested that the binding of IgG to FcRn was slightly stronger than the binding of HSA to FcRn, based on the relative amounts of unbound FcRn in Fig. 8.3(5, 6) [11]. Unlike SPR and other techniques, utilizing AF4 to study weak protein-protein interactions has the advantage that interactions were observed in solution state without having to immobilize proteins to a matrix. Improving the resolution of AF4 for studying proteins with similar molecular weights will be the direction for further development.

8.2.3 Case Study 2: FGF21:FGFR Binding

8.2.3.1 Introduction

Fibroblast growth factor 21 (FGF21) is a potent hormone involved in regulating blood glucose and triglyceride levels [29–31] and can be a very attractive

therapeutic protein to treat diabetes. In order to develop FGF21 for therapeutic uses, it is important to understand its mode of action. It has been shown that FGF21 alone cannot activate its receptor (FGFR); it requires a cofactor βKlotho for FGFR signaling [32]. However, the nature of interaction between FGF21, FGFR and βKlotho is not completely understood. It has been suggested that FGF21, βKlotho and FGFR may form a ternary complex in a highly coordinated manner [33]. Thus far, the existence of such a complex has not been observed by any analytical means. The following case study demonstrates the application of FFF to study the formation of such a complex in solution.

8.2.3.2 Method

Recombinant engineered forms of FGF21, βKlotho and FGFR were cloned, expressed, purified, and analyzed on SEC and AF4. The sample injection amount was about 10 μg each. AF4 separation conditions included a detector flow of 1.0 mL/min, a focus-flow at 1.5 mL/min for 3 min, a constant cross-flow at 1.5 mL/min for 30 min then ramping to 0 mL/min for 10 min, and an inject flow of 0.2 mL/min.

8.2.3.3 Results and Discussion

Figure 8.5 shows the overlaid UV traces of SEC chromatograms and AF4 fractograms of the recombinant engineered forms of FGF21, βKlotho, FGFR and their mixture. A peak corresponding to a high molecular weight complex in mixture (d) was observed by AF4, but was not quite clear by SEC. The light scattering signals of the mixture (d) from both SEC and AF4 were further analyzed as shown in Fig. 8.6. The results confirmed that the high molecular weight complex observed by AF4 is indeed a ternary complex of FGF21, β-Klotho, and FGFR1c. As suggested earlier, the interactions between FGF21, FGFR and β-Klotho are very weak. Apparently, the ternary complex formed in their mixture readily dissociated on SEC while still remained intact on AF4. These results demonstrated that AF4 can be applied to study the formation of FGF21-βKlotho-FGFR complex, as well as other weak protein-protein interactions in solution, particularly those involving multiple components.

8.2.4 Case Study 3: Immune Complex

8.2.4.1 Introduction

Anti-drug antibody (ADA) responses against human mAb therapeutics can result in formation of circulating immune complexes (CIC). These complexes consist of human IgG (drug) non-covalently complexed with IgM or IgG (antibody), which can result in type 3 hypersensitivity reactions such as complement activation and CIC

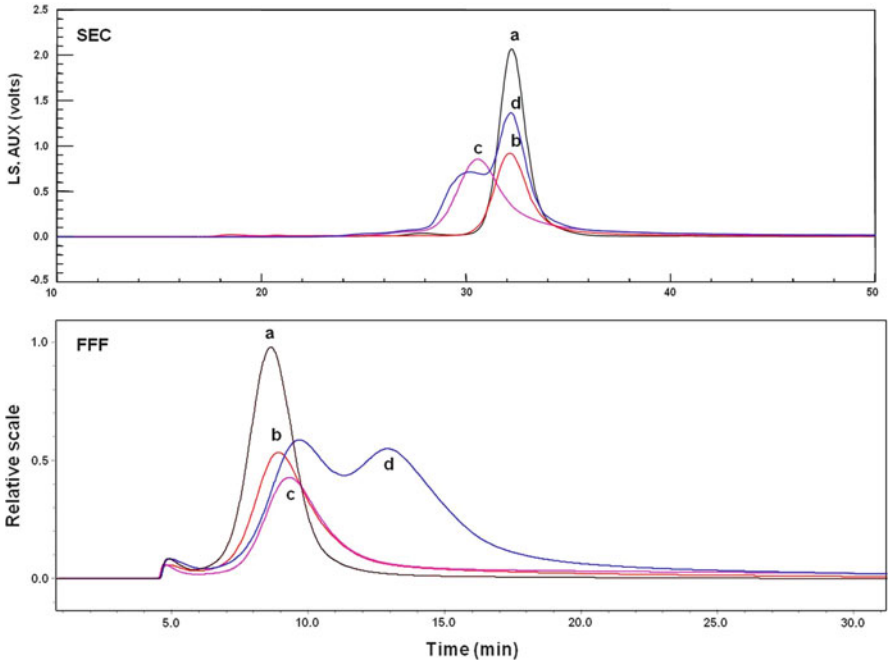

Fig. 8.5 Overlaid UV traces of recombinant engineered forms of FGF21 (a), βKlotho (b), FGFR (c) and their mixture (d)

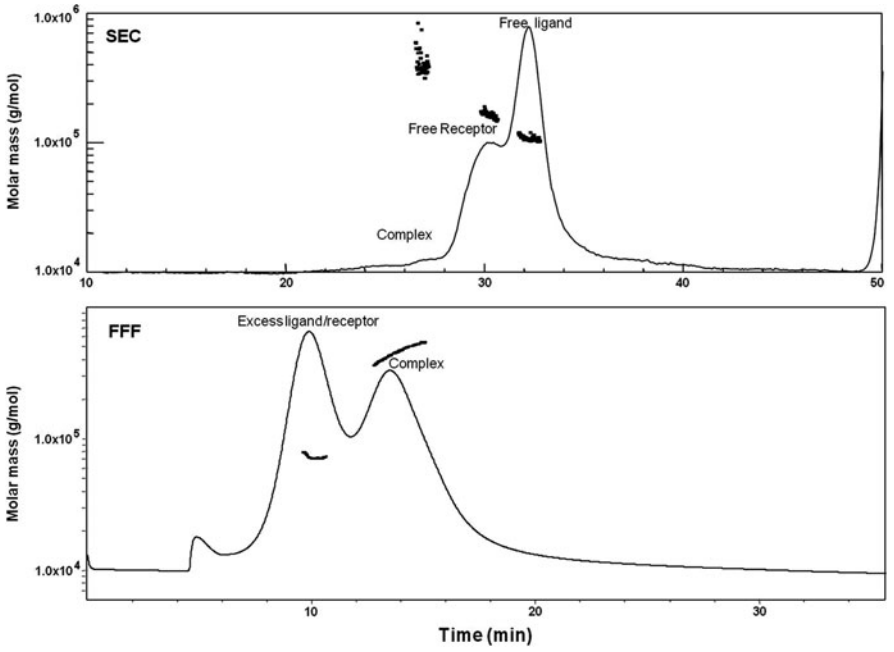

Fig. 8.6 SEC-MALS and AF4-MALS analyses of mixture (d) shown in Fig. 8.5

deposition into various tissues. The size of CIC can range from the nanometer to micrometer range. SEC is effective at separating smaller CIC from monomeric IgG; however, larger CIC may be lost or disrupted on the column bed. FFF has been applied to blood plasma and serum to study the distribution of lipoproteins which range in size from approximately 5–600 nm in diameter [34–36]. The retention profile of patient's lipoproteins samples was clearly distinguishable between healthy and those exhibiting coronary heart disease. FFF was effectively applied to quickly separate plasma proteins and to characterize drug/plasma protein interactions [37]. In the following case study, an AF4 method was developed to separate serum components and to investigate the potential presence and size of ADA CIC. FFF was chosen because it does not utilize filters or chromatography media, which can cause artifactual removal of large aggregates and disruption of non-covalent bonds in a sample.

8.2.4.2 Method

Serum was diluted threefold with DPBS containing a fluorescently labeled anti-human IgG Fab fragment (Fab-488) (Molecular Probes, Inc., Eugene, OR). The sample injection volume was 6 uL. Separation conditions included a detector flow rate of 1.0 mL/min, a cross-flow rate starting at 2 mL/min ramping to 0.0 mL/min over 30 min, and an injection flow rate of 0.2 mL/min. In addition to UV, LS and RI, fluorescence detection (FLD), obtained with a fluorescence detector (Agilent) set to absorbance at 495 nm and emission at 519 nm, was used to specifically detect Fab-488-labeled serum human immunoglobulins.

8.2.4.3 Results and Discussion

Albumin, immunoglobulin, and lipoproteins were identified as major peaks in both the MALS and UV profiles [35]. UV 280 and LS 90 traces of the AF4 separated profiles demonstrated that the Fab-488 probe did not alter the elution profile (Fig. 8.7). The FLD profile of normal serum showed two response peaks, a free Fab-488 peak and a second peak eluting in a region of the profile consistent with the elution time and size of serum IgG (Fig. 8.8). Samples containing CIC demonstrated a shoulder on the serum IgG peak indicating larger molecular size (Fig. 8.9).

The method was successfully implemented for separating the individual components of the serum samples and specifically detecting human IgG using the Fab-488 as a label. MALS detection allowed for the detection and molecular weight analysis of human IgG as well as immune complexes comprised of ADA and human monoclonal therapeutic in different animal models. This assay has been applied to detect and measure the molecular weight of uncomplexed and complexed human IgG in preclinical and clinical studies to better understand the role of immune complexes and related pathology findings.

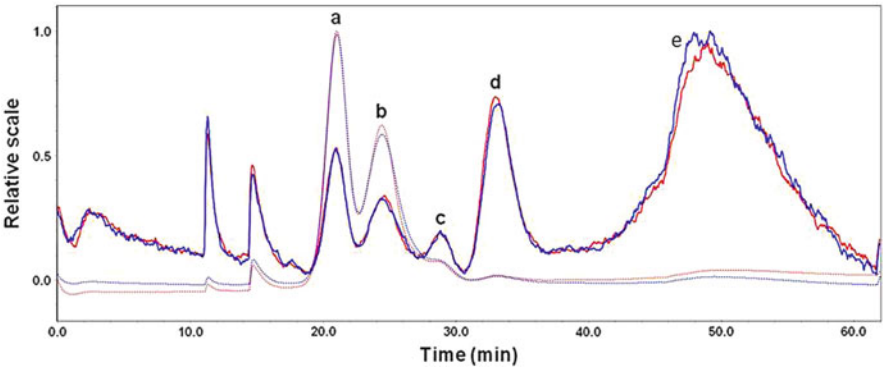

Fig. 8.7 AF4 separation with MALS (*solid lines*) and UV 280 nm (*dotted lines*) detection profile overlay of 5 uL PNHS diluted with 10 uL 1X DPBS (*red trace*) or 10 uL Fab-488 (*blue trace*), 6 uL injection of each. serum albumin (+HDL) (a), IgG (b), LDL (c), VLDL (d), chylomicrons (e)

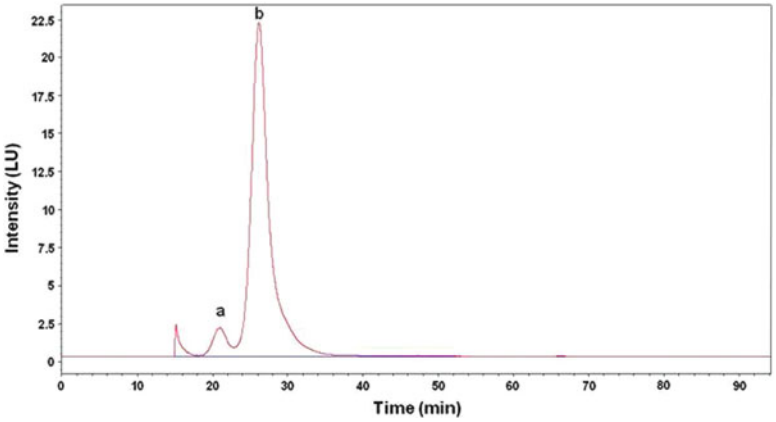

Fig. 8.8 AF4 separation with FLD profile overlay of 5 uL PNHS diluted with 10 uL 1X DPBS (*blue trace*) and 10 uL Fab-488 (*red trace*), 6 uL injection of each. (a) free Fab-488 (b) IgG + Fab-488

8.3 Conclusions

Weak protein-protein interactions play an important role in biological systems. Characterizing and understanding these weak interactions is essential in developing effective protein therapeutics. Currently there exists an analytical gap in our ability to analyze these weak protein-protein interactions. Due to its gentle and matrix free separation mechanism, FFF has the potential to fractionate complexes bound by weak interactions, therefore offering an opportunity to characterize such weak interactions with this technique. However, it must be pointed out that up to this

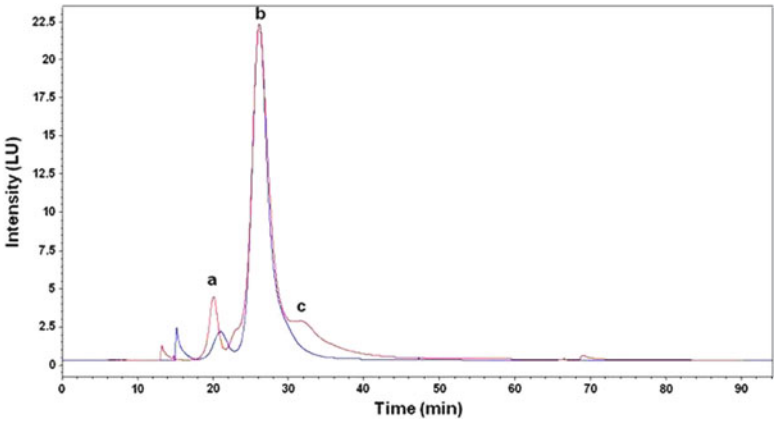

Fig. 8.9 AF4 separation with FLD (Ex 495 nm/Em 519 nm) profile overlay of 5 uL PNHS diluted with 10 uL Fab-488, 6 uL injection (*blue trace*) and 1:1 hu IgG + gt anti-hu IgG (H + L) (2.5 uL) + Fab-488 (10 uL), 6 uL injection (*red trace*). Free Fab-488 (a), hu IgG and/or gt anti-IgG + Fab-488 (b), hu IgG + anti-hu IgG + Fab-488 complex (c)

point only qualitative results have been obtained in the form of complex preservation, and sometimes stoichiometry estimation based on species elution time and analysis of collected fractions under denaturing conditions. Precise and detailed calculations of association rate constants, k_a, dissociation rate constants, k_d, and affinity K_d are complicated by the variations of protein concentrations in the FFF channel. The technique will also benefit from better resolution of the separation of species with close molecular weight values. We hope that these limitations of FFF will be addressed in the future.

References

1. Piehler J (2005) New methodologies for measuring protein interactions in vivo and in vitro. Curr Opin Struct Biol 15(1):4–14
2. Charbonnier S, Gallego O, Gavin A-C (2008) The social network of a cell: recent advances in interactome mapping. Biotechnol Annu Rev 14:1–28
3. Jefferis R, Lund J (2002) Interaction sites on human IgG-Fc for FcgammaR: current models. Immunol Lett 82:57–65
4. Hulett MD, Hogarth PM (1994) Molecular basis of Fc receptor function. Adv Immunol 57:1–127
5. Cao S, Pollastrini J, Jiang Y (2009) Separation and characterization of protein aggregates and particles by field-flow fractionation. Curr Pharm Biotechnol 10:382–390
6. Giddings JC (1993) Field-flow fractionation: analysis of macromolecular, colloidal, and particulate materials. Science 260:123–125
7. Cohen-Solal JFG et al (2004) Fcγ receptors. Immunol Lett 92:199–205
8. Murphy RM et al (2006) Self-association of therapeutic proteins. In: Misbehaving proteins. Springer, New York, pp 313–333

9. Philo JS (1999) Overview of the quantitation of protein intercations. In: Current protocols in protein science. Wiley, New York, pp 20.1.1–20.1.13
10. Schuck P et al (1999) Sedimentation equilibrium analysis of recombinant mouse FcRn with murine IgG1. Mol Immunol 36:1117–1125
11. Pollastrini J, Dillon TM, Bondarenko P, Chou RY-T (2011) Field-flow fractionation for assessing neonatal Fc receptor and Fcγ receptor binding to monoclonal antibodies in solution. Anal Biochem 414:88–98
12. Anderson CL et al (2006) Perspective – FcRn transports albumin: relevance to immunology and medicine. Trends Immunol 27(7):343–348
13. Lencer WI, Blumberg RS (2005) A passionate kiss, then run: exocytosis and recycling of IgG by FcRn. Trends Cell Biol 15(1):5–9
14. Salfeld JG (2007) Isotype selection in antibody engineering. Nat Biotechnol 25 (12):1369–1372
15. Nimmerjahn F, Ravetch JV (2008) Fc[gamma] receptors as regulators of immune responses. Nat Rev Immunol 8(1):34–47
16. Raghavan M, Bjorkman PJ (1996) Fc receptors and their interactions with immunoglobulins. Annu Rev Cell Dev Biol 12(1):181–220
17. Roopenian DC, Akilesh S (2007) FcRn: the neonatal Fc receptor comes of age. Nat Rev Immunol 7(9):715–725
18. Chaudhury C et al (2006) Albumin binding to FcRn: distinct from the FcRn-IgG interaction. Biochemistry 45(15):4983–4990
19. Vaughn DE, Bjorkman PJ (1997) High-affinity binding of the neonatal Fc receptor to its IgG ligand requires receptor immobilization. Biochemistry 36:9374
20. Andersen JT, Dee Qian J, Sandlie I (2006) The conserved histidine 166 residue of the human neonatal Fc receptor heavy chain is critical for the pH-dependent binding to albumin. Eur J Immunol 36(11):3044–3051
21. Firan M et al (2001) The MHC class I-related receptor, FcRn, plays an essential role in the maternofetal transfer of {gamma}-globulin in humans. Int Immunol 13(8):993–1002
22. West AP, Bjorkman PJ (2000) Crystal structure and immunoglobulin G binding properties of the human major histocompatibility complex-related Fc receptor. Biochemistry 39 (32):9698–9708
23. Martin WL, Bjorkman PJ (1999) Characterization of the 2:1 complex between the class I MHC-related Fc receptor and its Fc ligand in solution. Biochemistry 38:12639
24. Raghavan M et al (1995) Analysis of the pH dependence of the neonatal Fc receptor/ immunoglobulin G interaction using antibody and receptor variants. Biochemistry 34 (45):14649–14657
25. Rodewald R (1976) pH-dependent binding of immunoglobulins to intestinal cells of the neonatal rat. J Cell Biol 71(2):666–669
26. Popov S et al (1996) The stoichiometry and affinity of the interaction of murine Fc fragments with the MHC class I-related receptor, FcRn. Mol Immunol 33(6):521–530
27. Junghans RP, Anderson CL (1996) The protection receptor for IgG catabolism is the beta2-microglobulin-containing neonatal intestinal transport receptor. Proc Natl Acad Sci USA 93 (11):5512–5516
28. Chaudhury C et al (2003) The major histocompatibility complex-related Fc receptor for IgG (FcRn) binds albumin and prolongs its lifespan. J Exp Med 197:315
29. Kharitonenkov A, Shiyanova TL, Koester A, Ford AM, Micanovic R, Galbreath EJ, Sandusky GE, Hammond LJ, Moyers JS, Owens RA, Gromada J, Brozinick JT, Hawkins ED, Wroblewski VJ, Li DS, Mehrbod F, Jaskunas SR, Shanafelt AB (2005) FGF-21 as a novel metabolic regulator. J Clin Invest 115:1627–1635
30. Xu J, Stanislaus S, Chinookoswong N, Lau YY, Hager T, Patel J, Ge H, Weiszmann J, Lu SC, Graham M, Busby J, Hecht R, Li YS, Li Y, Lindberg RA, Veniant MM (2009) Acute glucose-lowering and insulin-sensitizing action of FGF21 in insulin resistant mouse models—association with liver and adipose tissue effects. Am J Physiol 297:E1105–E1114

31. Kharitonenkov A, Wroblewski VJ, Koester A, Chen YF, Clutinger CK, Tigno XT, Hansen BC, Shanafelt AB, Etgen GJ (2007) The metabolic state of diabetic monkeys is regulated by fibroblast growth factor-21. Endocrinology 148:774–781
32. Kharitonenkov A, Dunbar JD, Bina HA, Bright S, Moyers JS, Zhang C, Ding L, Micanovic R, Mehrbod SF, Knierman MD, Hale JE, Coskun T, Shanafelt A (2008) FGF-21/FGF-21 receptor interaction and activation is determined by beta Klotho. J Cell Physiol 215:1–7
33. Yie J, Hecht R, Patet J, Stevens J, Wang W, Hawkins N, Steavenson S, Smith S, Winters D, Fisher S, Cai L, Belouski E, Ching C, Michaels M, Li Y, Lindberg R, Wang M, Veniant M, Xu J (2009) FGF21 N- and C-termini play different roles in receptor interaction and activation. FEBS Lett 583:19–24
34. Park I et al (2002) Separation and selective detection of lipoprotein particles of patients with coronary artery disease by frit-inlet asymmetrical flow field-flow fractionation. J Chromatogr B 780(2):415–422
35. Rambaldi DC et al (2007) An analytical method for size and shape characterization of blood lipoproteins. Clin Chem 53(11):2026–2029
36. Park I et al (2005) Performance of hollow-fiber flow field-flow fractionation in protein separation. J Sep Sci 28(16):2043–2049
37. Madörin M et al (1997) Analysis of drug/plasma protein interactions by means of asymmetrical flow field-flow fractionation. Pharm Res 14(12):1706–1712

Chapter 9
Flow Field-Flow Fractionation: Analysis of Biomolecules and Their Complexes

Samantha Schachermeyer and Wenwan Zhong

Abstract This chapter is an overview on flow field-flow fractionation (FlFFF) and its use for investigations of biomolecules and their complexes. Separation theory will be discussed and compared to other separation methods. Example studies will be described applying FlFFF for the analysis of a wide range of biological subjects including proteins, ribosomes, viruses, and bacteria. In addition, the utilization of FlFFF as a biological clean-up tool and as a method for investigating biomolecules-metal interactions will be explored.

Keywords Bacteria • Biomolecule-metal complex • Biomolecules • Clean-up • Flow field-flow fractionation • Organelles • Protein analysis • Theory • Viruses

9.1 Introduction and Theory

FlFFF differs from other FFF techniques in that the separation force is provided by a secondary carrier-flow introduced into the system perpendicular to the channel-flow. In FlFFF, the channel walls are permeable, which allow such a cross-flow to enter and escape. The channel flow forms a parabolic profile due to the viscosity of the carrier solution. The flow rate approaches zero near the channel walls and reaches the maximum at the center of the channel [1]. Analytes positioned further into the channel experience a greater flow velocity than those towards the wall and are eluted faster. The cross-flow pushes analytes towards the opposing wall, while the analytes attempt to diffuse back to the center of the channel. The balance of these two determines the analyte's location within the parabolic flow profile. Analytes with larger diffusion coefficients can travel furthest into the channel and be eluted first. Smaller molecules have greater diffusion coefficients leading to an

S. Schachermeyer • W. Zhong (✉)
Department of Chemistry, University of California, Riverside, USA
e-mail: wenwan.zhong@ucr.edu

S.K.R. Williams and K.D. Caldwell (eds.), *Field-Flow Fractionation in Biopolymer Analysis*, DOI 10.1007/978-3-7091-0154-4_9,

elution order of small to large, and this elution mode is called the normal mode. The diffusion plays a lesser role for analytes larger than 1 μm. Instead, the mass center of such large analytes already locates at a distance no closer than one radius from the wall. Consequently, the larger analytes position closer to the center of the channel, and are eluted earlier than the smaller ones, the so-called "steric" mode. Additionally, a high channel-flow rate can be employed to separate large particles. It is believed that a hydrodynamic force could be created from the high-speed channel-flow to lift the molecules approximately twice the diameters' width away from the wall. This phenomenon is termed the hyperlayer mode. In the normal mode, the retention time t_r can be estimated for analytes with known hydration sizes; or the hydrodynamic radius of a particle can be calculated from t_r, using Eq. 9.1,

$$t_r = \frac{\pi \eta w^2 d V_c}{2kTV} \tag{9.1}$$

in which V_c is the cross flow rate, w the channel thickness, d the particle hydration diameter, η the carrier viscosity, T the temperature, k the Boltzmann constant, and V the axial flow rate.

FlFFF can be operated with either symmetrical or asymmetrical channels. In the symmetrical channel, there are two permeable walls. The axial- and cross-flows are operated separately by two pumps. The cross-flow passes through the top wall into the channel and leaves via the opposite wall. On the contrary, asymmetrical FlFFF (AsFlFFF) only contains one permeable wall and requires only one pump (Fig. 9.1). The cross-flow is generated by the loss of liquid through the membrane and is controlled by a valve that indicates the total volume passage. As the carrier fluid moves down the channel, it continuously leaves via the membrane. The decrease of

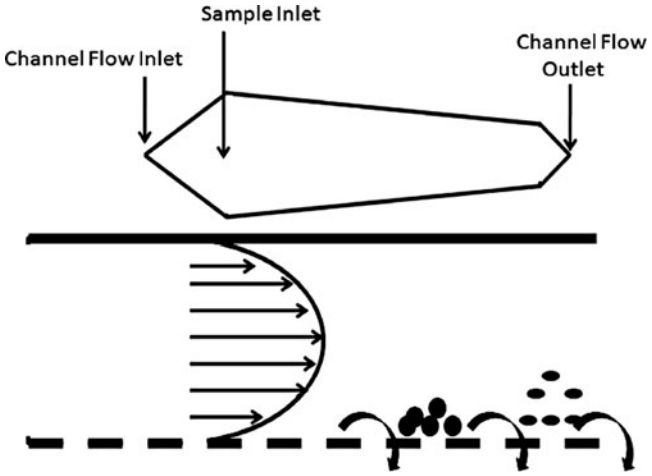

Fig. 9.1 AsFlFFF channel structure and parabolic flow profile

total volume in turn reduces the channel pressure. To compensate for the loss of liquid and to maintain the pressure, the channel is designed to decrease in width. This not only allows for controlling the pressure, but also has the added benefit of concentrating the analytes relative to symmetrical FlFFF. For this reason AsFlFFF has found greater use in research over the symmetrical apparatus.

Unlike other separation apparatuses, such as HPLC, FlFFF lacks the packing material that can be harsh on biological molecules. FLFFF can be used in a wide variety of solution conditions such as pH, temperature, and high salt concentration, which is advantageous in comparison with another open-channel liquid-based separation technique, capillary electrophoresis (CE). This feature allows selecting the optimal buffer conditions to maintain the integrity of analytes like protein complexes and biological particles. It is necessary to mention, however, that care needs to be taken in choosing such conditions as to minimize interactions between the membrane wall and analytes. Any interaction between the two may affect the retention of the analytes, skew the size information, and increase sample adsorption on the membrane. The most common membrane material used with biological samples is regenerated cellulose (RC) as it offers good resistance to adsorption of proteins.

The biggest advantage of FlFFF is the wide size range of its analytes. The minimum size is determined by the molecular weight cut-off (MWCO) of the membrane. The upper size limit can be estimated by 20% of the channel height. Analytes as small as 1 kDa and as large as 100 μm in diameter have been separated using FlFFF [2]. In the case of size exclusion chromatography (SEC), the upper size limit is only 50 nm. The main limitation of FlFFF is the inability to separate analytes of very similar sizes. As shown by Fraunhofer and Winter, full resolution of human serum albumin (HSA) dimer (133 kDa) and immunoglobulin (Ig) G (147 kDa) could not be achieved even under optimized conditions [3]. Analytes should have at least 20% difference in diameter to be resolved by FlFFF.

9.2 Protein Analysis

FlFFF has found great use in the study of proteins, because its large analyte size range is well compatible with the wide size distribution of proteins. The size of proteins can range from a few kDa to a few hundred kDa; and they can be found as monomers, dimers, or larger aggregates. Early use of FlFFF in the food industry studied the large proteins found in wheat [4, 5] and dairy products [6]. Aggregation of recombinant proteins can be of interest to biotechnology processes. For example, inclusion bodies (IB) can form due to the over-expression of foreign genes in prokaryotes. The location, size, and molar mass of IBs are important for the downstream processing of the recombinant proteins. AsFlFFF has been applied to analyze the size distributions of the green fluorescent protein (GFP) IBs in *Escherichia coli* (*E. coli*) [7]. By monitoring the hydrodynamic radius of IBs formed under different culture conditions, IBs production was optimized, and the

cell culture and disruption conditions for *E. coli* were identified. Coupled with a multiangle light scattering detector (MALS), the size of IBs was found to range from 400 to 1,000 nm, and the shape was near spherical.

Proteins can aggregate after undergoing destabilization. Unfolding of protein due to environmental stress such as heat, high levels of salt, and pH variations can result in intermolecular bonding and thus protein aggregation. FlFFF has been used to monitor the thermal aggregation for bovine serum albumin (BSA) when temperature changed from room temperature to 80°C (Fig. 9.2) [8]. BSA was shown to have remained stable up to 60°C with only the monomers and dimers being observed, which agreed with the BSA denaturing temperature of 63.4°C previously measured by calorimetry [9]. Above the denaturing temperature larger aggregates began to appear as the proteins began to unfold and reveal potential bonding sites. In addition to the incubation temperature, effects from other factors such as BSA concentration, incubation time, and salt concentration have been studied. It was found that heat alone could not induce aggregation. Without the presence of NaCl, minimal protein aggregation existed even at high temperatures due to the electrostatic repulsion between protein molecules.

Although small molecules cannot be individually analyzed by FlFFF, their interactions with proteins can be monitored. Drug-protein analysis is a particularly important area of study for pharmaceutical industries, because protein binding can affect the adsorption, distribution, metabolism, and elimination (ADME) properties of a drug [10]. To analyze the drug distribution in a complex sample, such as blood plasma, can be challenging, and FlFFF may provide effective solutions.

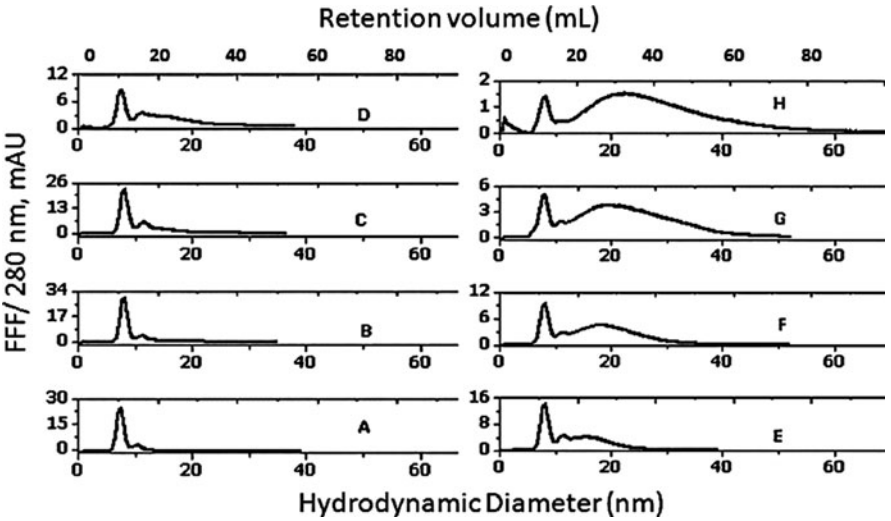

Fig. 9.2 BSA (1.0 mg·mL^{-1}) particle size after 1 h incubation at different temperatures. Outlet flow: cross-flow (0.50:2.52 mL·min^{-1}). (**a**) room temperature, (**b**) 50°C, (**c**) 60°C, (**d**) 63°C, (**e**) 65°C, (**f**) 70°C, (**g**) 75°C, and (**h**) 80°C [8] (Reprinted from [8], © 2010, with permission from Elsevier)

By applying AsFlFFF, Leuenberger et al. were able to separate human plasma in under 10 min into four major protein fractions, including human serum albumin (HSA), high density lipoprotein (HDL), α_2-macroglobulin, and low density lipoprotein (LDL) [11]. The distribution of the lipophilic drug N-benzoyl-staurosporine (NBS) within the human plasma was then analyzed by fluorescence microscopy. In their study, it was found that the membrane material and carrier fluid significantly influenced the recovery of drug and proteins and needed to be carefully examined. NBS was completely adsorbed onto the RC membrane with PBS as the carrier fluid, while the recovery of the FITC-labeled serum albumin was 70%. Addition of a nonionic surfactant, Tween 80, could increase the drug recovery to almost 97% even with the RC membrane; or a hydrophobic ALPHA membrane was discovered to prevent the NBS adsorption without the addition of surfactant. However, due to the possibility of the surfactant interacting with the lipoprotein structure and skewing drug-binding data, the study was conducted using the ALPHA membrane and the phosphate buffer without the addition of Tween 80, decreasing the drug recovery to 70%. NBS was found only in the HSA fraction of the human plasma, showing the feasibility of AsFlFFF in studying drug/protein binding under near native conditions.

9.3 Ribosomes and Mitochondria

Intracellular organelles such as mitochondria and ribosomes are important cellular machineries, the functions of which are not fully understood. It is very challenging to extract specific organelles with high purity for functional analysis or gene/protein expression study. Ultracentrifugation could be used, but it requires long centrifugation times of up to several hours and laborious experimental handling, both resulting in residual artifacts [12]. FlFFF could be a superior technique to the centrifugation-based methods in that it is able to fractionate organelles by size, while well preserving the organelle structure and significantly cleaning it up with its open separation channel and continuous liquid flows.

FlFFF methods have been developed to analyze ribosomes that are responsible for intracellular protein synthesis by translating RNA to genes. Active ribosomes (70 S) are composed of two subunits, the small subunit (30 S) and the large subunit (50 S). One important development in this area was to use AsFlFFF to study the ribosomes and ribosomal subunits in *E. coli* under different protein production and expression conditions [13]. The 30 S, 50 S, and the whole ribosome were fully separated with calculated hydrodynamic radiuses of 17, 20, and 24 nm. In addition to the ribosome peaks, a tRNA and a protein fraction were identified with the elution time equivalent to that of the 5-nm and 10-nm particles, respectively. Samples were taken from *E. coli* cell cultures at lag, logarithmic (log), stationary, and declining phases; and it was revealed that the number of ribosomes per cell differed depending on the growth phase with the exception of the stationary and log phases. The measured ribosome amounts corresponded well with *E. coli's* growth

activity, with the stationary and log phases having the highest amount of ribosomes and the declining phase consisting of the lowest. In addition to normal cell culture conditions, cells treated with antibiotics were examined to determine the effect of antibiotics on ribosomal composition, which should indicate the state of protein synthesis. The antibiotic chosen for this study was chloroamphenicol, which targets the 70 S ribosome to inhibit peptide bond formation. After the addition of chloroamphenicol, the number of the 30 S and 50 S ribosomal subunits increased while the 70 S ribosomes decreased, solid proof of the termination of protein synthesis. Further optimization of cell harvest, lysis, and separation conditions has reduced the entire analysis time from almost 2 h to 16 min, providing a fast method for investigating ribosome levels [14].

Mitochondria play vital roles in cellular functions, such as energy production and apoptosis, and irregularities have been linked to several neurodegenerative diseases like Huntington's and Alzheimer's disease [15]. Analyzing protein expression within mitochondria at various disease stages or under different environmental stimulus may help to reveal the fundamentals of disease development, which could be achieved by first isolating mitochondria from intact cells using AsFlFFF. In one representative study performed by the Moon research group, mitochondria was isolated from rat liver and analyzed using nLC-ESI-MS-MS to identify 130 proteins, among which 105 were uniquely mitochondrial [16]. In addition, the MS result indicated that the protein contents increased proportionately with the size of mitochondria.

9.4 Virus and Virus-Like Particles (VLPs)

Virus and virus-like particles are large protein complexes that can exceed a couple 100 nm in diameter. They are imperative to the pharmaceutical industry as vaccines and as gene delivering agents. Therefore, it is important to have a well-defined and high-throughput method to monitor batch-to-batch consistency. Early work with FlFFF and viruses brought concerns on membrane adsorption and on the possibility of changing the aggregation state by the "adsorption effect" [17]. "Adsorption effect" means that particles retained on the membrane become reversibly adsorbed. A delay in retention time is then observed. Giddings' early work using FlFFF to calculate the diffusivity of a variety of viruses exemplified this problem. The greatest error in calculation of diffusion coefficients was seen at high cross-flow rates in which the viruses were forced to interact more closely with the membrane. The pressing by cross-flow exacerbated the adsorption or trapping of the particles. This suggests that lower cross-flow rates are desirable as to minimize analyte-analyte and analyte-membrane interactions. Middelberg et al. has also shown that by optimizing the cross-flow rates, analyte adsorption could be minimized [18]. However, low cross-flow rates result in poor resolution for nanometer-sized subjects. Another potential solution would be to discard the membrane completely and use the frit as the accumulation wall [19]. Although this method has been

shown to work with some degree of success, it also requires stringent optimization of the separation conditions to minimize wall-particle interactions.

AsFlFFF coupled with MALS has been proved to be powerful in virus analysis with less occurrence of adsorption. In the development of vaccines, the quality of produced virions within chick embryos is essential. They could be a heterogeneous mixture of infectious and non-infectious particles. In a study carried out by Wei et al., the virus subpopulations were analyzed and characterized with AsFlFFF-MALS [20]. The virus content measured by AsFlFFF-MALS was compared with the gold virus counting standards, transmission electron microscopy (TEM) and polymerase chain reaction (PCR), and little difference was found. This study well demonstrated that AsFlFFF was effective in rapidly analyzing size distributions and quantifying particle count, and has great potential for monitoring the virus quality in vaccine production.

9.5 Bacteria

It is of great interest to bioremediation, biodefense, and biotechnology to quantify bacteria in complex matrices, such as food, soil, and blood. The biggest challenge is the separation of bacteria from other particulate matter and the differentiation of live and dead bacteria. The dead bacteria can dissemble and release endotoxins to the environment, acting on disease-causing mechanisms different than the live bacteria [21]. Flow cytometry can be an effective approach in separating and quantifying bacteria [22], but is restricted from analyzing smaller bacteria due to its lower size limit of 200 nm. FlFFF, sedimentation FFF (SdFFF), and electrical FFF (ElFFF) were found to be able to separate four different bacterial strains within 15 min [23]. In addition, the live bacterial particles were resolved from the dead ones with earlier elution times.

Whole-cell bacterial vaccines rely on characteristic surface features of the deactivated bacteria. The surface features of bacteria can affect the pathology of bacteria and, thus, their usefulness in vaccines. Gravitational FFF (GrFFF) and AsFlFFF have been applied to separate *E. coli* based on the presence of fimbriae on the bacterial membrane [24]. AsFlFFF was able to achieve baseline separation of bacteria belonging to the same strain, but with surface characteristic difference.

Due to the fast reproduction rate of bacteria and the health hazards they pose, there are pressing needs for early identification of even trace levels of bacterial contamination in the food industry to prevent food-borne diseases in consumers. Conventional culturing methods require several days. Utilizing FlFFF to fractionate the whole bacterial cells and analyzing the cells using matrix-assisted laser desorption/ionization time-of-flight mass spectrometry (MALDI-TOF/MS) [25], the entire bacterial analysis was accomplished within 1 h, a promising high-throughput method. Some optimization was necessary in order to successfully combine the two instruments, as some of the standard FlFFF conditions were not compatible with MS. For instance, the commonly used ionic surfactant FL-70 carrier solution

could generate background in MS and probably reduce the efficiency of MALDI. To prevent this, a non-ionic surfactant, such as Triton-X100, can be used to replace FL-70.

9.6 Biological Clean-up Tool

Another application of FlFFF is the use as a clean-up tool. By utilizing the cross-flow as a washing force, nonspecific bindings can be removed while preserving the specific interaction. The problem that often occurs during a standard vortex and centrifugation wash is the co-precipitation of the non-specific, background molecules that generate artifacts in down-stream analysis. Since FlFFF can withstand a wide range of solution conditions (salt concentrations, pH, and buffer compositions), it is a favorable tool for cleaning up immune-complexes. In a feasibility study carried out by our group, the Protein A-conjugated microparticles were incubated with its interactive proteins in the crude yeast cell lysate, and then washed using either the standard centrifugation or magnetic pull-down methods, or with FlFFF [26]. The collected particles were analyzed on a SDS-PAGE gel and the results showed similar antibody bands proving that the specific protein A- immunoglobulin G (IgG) bond was preserved throughout the FlFFF process. However, the FlFFF had significantly reduced nonspecific bands when compared with the standard methods (Fig. 9.3a).

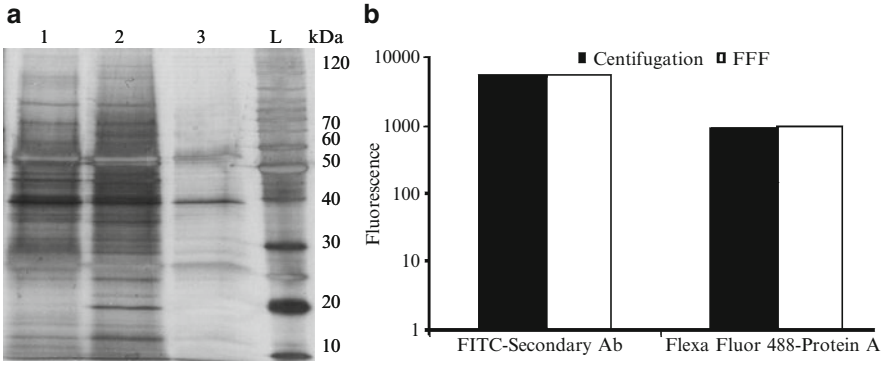

Fig. 9.3 (**a**) SDS-PAGE of proteins extracted through three different procedures. Lane 1, proteins extracted by regular magnetic particle with the magnetic pull-down procedure; lane 2, proteins extracted by the modified polystyrene microspheres with the magnetic pull-down procedure; lane 3, proteins extracted by the modified polystyrene microspheres with the MAPcP procedure; lane L, protein molecular weight marker [26] (Reprinted with permission from [26], © 2008, American Chemical Society). (**b**) Flow cytometry fluorescence data showing preserved binding between Protein A and the secondary antibody for both centrifugation and FlFFF wash [27] (Reprinted with permission from [27], © 2008, American Chemical Society)

The clean background can help to enhance the signal-to-noise ratio in immunoassays. Thus, our group has explored the feasibility of coupling FlFFF with flow cytometry to create a two dimensional suspension array system for multiplexed protein detection [26]. The IgG-conjugated microparticles were incubated with the FITC-labeled protein A or the secondary antibody, separated by FlFFF, and detected in the flow cytometer. Comparable fluorescence levels to those obtained with centrifugation-based washes were detected on both particles, proving the possibility of using FlFFF to remove background interference in the bead-based immunoassays (Fig. 9.3b).

9.7 Biomolecule-Metal Complexation Analysis

Inductively coupled plasma (ICP) is a powerful tool in metal analysis, but the high nebulizer flow-rates can complicate the interface design if used as an on-line detector. Both HPLC and FlFFF's flow-rates are compatible with ICP nebulization, however, because of its low sheer force that effectively maintains any weak but specific interaction, FlFFF is more attractive in coupling to ICP for simultaneous elemental and size distribution analysis of biological samples. Many proteins carry out their functions through complexation with metals. By utilizing on-line ICP-MS detection, it is possible to study these complexations. Barnes and Siripinyanond applied FlFFF-ICP-MS to analyze several different proteins ranging from 6 to 669 kDa and their associated metals as a feasibility study [28]. Several protein standards were analyzed and both Zn and to a lesser extent, Cu, were found in the metalloenzymes, carbonic anhydrase and alcohol dehydrogenase. In addition, the authors examined Cu and Zn distribution in bovine ceruloplasmin. Here, the free Cu and Zn eluted early followed by the first main peak of the ceruloplasmin in which only Cu was bound and the final peak contained both metal ions. This preliminary study showed the feasibility of using FlFFF-ICP-MS to study metal distribution in biological samples.

FlFFF-ICP-MS has also been applied in the study of environmental remediation. How bacteria participate in the transport of contaminates is of particular interest. FlFFF-ICP-MS was used to study the uptake of uranium in *Shewanella oneidensis* strain MR-1 [29]. Utilizing hyperlayer mode the cells were separated from exopolymers in the cell suspension. When comparing the adsorption behavior of a fixed uranium concentration over a range of pH 5–9, the optimum adsorption pH was found to be pH 5, which was in agreement with literature values (Fig. 9.4). At the maximum adsorption pH of 5, the complexation occurred between the negative carboxyls present on the cells surface and the cationic UO_2^{2+}. As the pH increased, the portion of positively charged uranium species was reduced due to the reaction of uranium with hydroxides and carbonates, inhibiting their interactions with cell surfaces. For the first time, the presence of a uranium binding exopolymer was detected by the ICP. By combining ICP with FlFFF, metal associating biomolecules that have minimal UV absorption can be studied.

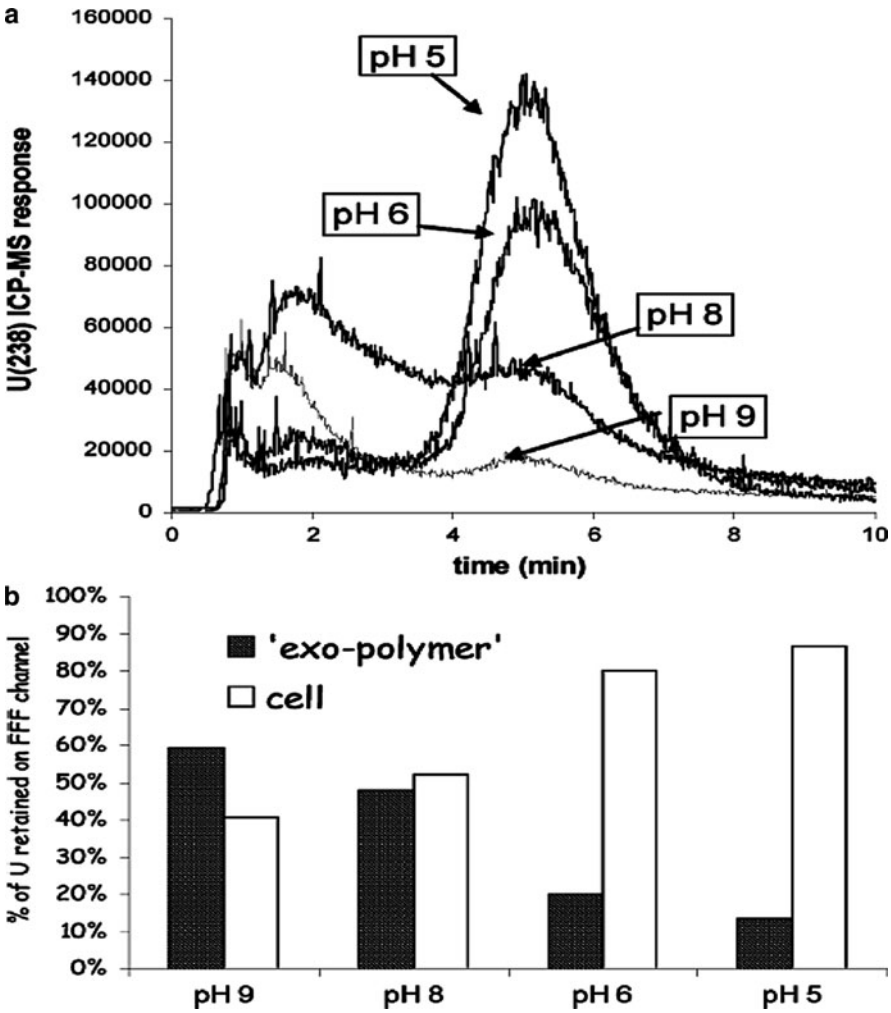

Fig. 9.4 (**a**) Decreasing cellular uranium sorption as pH increases (**b**) Percentage of uranium bound to the exo-polymer relative to the cell as a function of pH [29] (Reprinted with permission from [29], © 2005, American Chemical Society)

9.8 Conclusion

FlFFF has great potential in biological research. With a large separation size range of 1 nm to 100 um, it is compatible with a variety of biomolecules from proteins to cells. The high tolerance to salt, buffer compositions, pH, and temperature allows the researcher to explore and understand how biomolecules react to different environmental conditions. In addition, coupled with ICP-MS on-line, metal-molecule interactions can be studied and quantified. Finally, the cross-flow can be taken

advantage of as a washing force and be used as a biological clean-up tool which, in combination with the size separation ability, can be exploited in detection assays for the removal of background materials in complex matrices providing a potential method to increase the signal-to-noise level of the assay and thus the limit of detection. More understanding of the membrane-analyte interactions, minimizing such interactions, and increasing sample loading would widen the application of FlFFF in the bio-related fields.

References

1. Giddings JC, Yang FJ, Myers MN (1976) Flow-field-flow fractionation: a versatile new separation method. Science 193:1244–1245
2. Ratanathanawongs SK, Giddings JC (1993) Chapter 2: Particle-size analysis using flow field-flow fractionation. In: Provder T (ed) Chromatography of polymers. American Chemical Society, Washington, DC, pp 13–29
3. Fraunhofer W, Winter G (2004) The use of asymmetrical flow field-flow fractionation in pharmaceutics and biopharmaceutics. Eur J Pharm Biopharm 58:369–383
4. Stevenson SG, You S, Izydorczyk MS, Preston KR (2003) Characterization of polymeric wheat proteins by flow field-flow fractionation/MALLS. J Liq Chromatogr Relat Technol 26:2771–2781
5. Stevenson SG, Preston KR (1996) Flow field-flow fractionation of wheat proteins. J Cereal Sci 23:121–131
6. Jussila MA, Yohannes G, Riekkola ML (1997) Flow field-flow fractionation in the study of dairy products. J Microcolumn Sep 9:601–609
7. Luo J, Leeman M, Ballagi A, Elfwing A, Su Z, Janson J-C, Wahlund K-GSize (2006) characterization of green fluorescent protein inclusion bodies in E. coli using asymmetrical flow field-flow fractionation-multi-angle light scattering. J Chromatogr A 1120:158–164
8. Yohannes G, Wiedmer SK, Elomaa M, Jussila M, Aseyev V, Riekkola M-L (2010) Thermal aggregation of bovine serum albumin studied by asymmetrical flow field-flow fractionation. Anal Chim Acta 675:191–198
9. Boye JI, Alli I, Ismail AA (1996) Interactions involved in the gelation of bovine serum albumin. J Agric Food Chem 44:996–1004
10. Kratochwil NA, Huber W, Müller F, Kansy M, Gerber PR (2002) Predicting plasma protein binding of drugs: a new approach. Biochem Pharmacol 64:1355–1374
11. Madörin M, van Hoogevest P, Hilfiker R, Langwost B, Kresbach GM, Ehrat M, Leuenberger H (1997) Analysis of drug/plasma protein interactions by neans of asymmetrical flow field-flow fractionation. Pharm Res 14:1706–1712
12. Liu J, Andya J, Shire S (2006) A critical review of analytical ultracentrifugation and field-flow fractionation methods for measuring protein aggregation. AAPS J 8:E580–E589
13. Alasonati E, Slaveykova VI, Gallard H, Croué J-P, Benedetti MF (2010) Characterization of the colloidal organic matter from the Amazonian basin by asymmetrical flow field-flow fractionation and size exclusion chromatography. Water Res 44:223–231
14. Arfvidsson C, Wahlund K-G (2003) Time-minimized determination of ribosome and tRNA levels in bacterial cells using flow field-flow fractionation. Anal Biochem 313:76–85
15. Scheffler E (2001) Mitochondron 1:3–31
16. Kang D, Oh S, Reschiglian P, Moon MH (2008) Separation of mitochondria by flow field-flow fractionation for proteomic analysis. Analyst 133:505–515
17. Giddings JC, Yang FJ, Myers MN (1977) Flow field-flow fractionation: new method for separating, purifying, and characterizing the diffusivity of viruses. J Virol 21:131–138

18. Chuan YP, Fan YY, Lua L, Middelberg AP (2008) Quantitative analysis of virus-like particle size and distribution by field-flow fractionation. Biotechnol Bioeng 99:1425–1433
19. Reschiglian P, Melucci D, Zattoni A, Malló L, Hansen M, Kummerow A, Miller M (2000) Working without accumulation membrane in flow field-flow fractionationa. Anal Chem 72:5945–5954
20. Wei Z, McEvoy M, Razinkov V, Polozova A, Li E, Casas-Finet J, Tous GI, Balu P, Pan AA, Mehta H et al (2007) Biophysical characterization of influenza virus subpopulations using field-flow fractionation and multiangle light scattering: correlation of particle counts, size distribution and infectivity. J Virol Methods 144:122–132
21. Shenep JL, Mogan KA (1984) Kinetics of endotoxin release during antibiotic therapy for experimental gram-negative bacterial sepsis. J Infect Dis 150:380–388
22. Nebe-von-Caron G, Stephens PJ, Hewitt CJ, Powell JR, Badley RA (2000) Analysis of bacterial function by multi-colour fluorescence flow cytometry and single cell sorting. J Microbiol Methods 42:97–114
23. Saenton S, Lee H, Gao Y-S, Ranville JF, Williams SKR (2000) Evaluation of different field-flow fractionation techniques for separating bacteria. Sep Sci Technol 35:1761–1775
24. Reschiglian P, Zattoni A, Roda B, Casolari S, Moon MH, Lee J, Jung J, Rodmalm K, Cenacchi G (2002) Bacteria sorting by field-flow fractionation. Application to whole-cell Escherichia coli vaccine strains. Anal Chem 74:4895–4904
25. Lee H, Williams SKR, Wahl KL, Valentine NB (2003) Analysis of whole bacterial cells by flow field-flow fractionation and matrix-assisted laser desorption/ionization time-of-flight mass spectrometry. Anal Chem 75:2746–2752
26. Li J, Ge J, Yin Y, Zhong W (2008) Multiplexed affinity-based protein complex purification. Anal Chem 80:7068–7074
27. Li J, Zhong W (2008) A two-dimensional suspension array system by coupling field-flow fractionation to flow cytometry. J Chromatogr A 1183:143–149
28. Siripinyanond A, Barnes RM (1999) Flow field-flow fractionation-inductively coupled plasma mass spectrometry and metal speciation in proteins: a feasibility study. J Anal Atomic Spectrom 14:1527–1531
29. Jackson BP, Ranville JF, Neal AL (2005) Application of flow field-flow fractionation-ICPMS for the study of uranium binding in bacterial cell suspensions. Anal Chem 77:1393–1397

Chapter 10
Analysis of Prions by Field-Flow Fractionation

Kelly A Barton, Valerie L Sim, Andrew G Hughson, and Byron Caughey

Abstract Prion diseases, like many protein misfolding diseases, are characterized by the formation of abnormal protein aggregates that can range in size from oligomers to large amyloid fibrils and plaques. An important issue is the extent to which various abnormal prion protein multimers contribute to prion disease transmission and neuropathogenesis. In order to understand the etiology of these diseases and to design effective diagnoses, prophylaxes, and therapies, the relationship of prion protein aggregate size and structure to infectivity and neurotoxicity must be considered. A variety of approaches have been taken to fractionate and characterize abnormal prion protein particles. One method that has been effectively employed is flow field-flow fractionation (FlFFF), which separates particles on the basis of diffusion coefficient. Advantages of FlFFF include fractionation across wide dynamic range of particle sizes and the ease of making in-line connections to a variety of detectors (i.e., light scattering, refractive index and UV) that can rapidly evaluate particle size, shape, and concentration. Here we review the application of FlFFF to the characterization of prions.

Keywords Amyloid fibrils • Asymmetrical flow FFF • Effects of sonication • Particle size • Prion aggregates • Prion protein • Size-infectivity relationship • Spongiform encephalopathies • Template-directed polymerization

K.A. Barton (✉) • A.G. Hughson • B. Caughey
Rocky Mountain Laboratories, National Institute of Allergy and Infectious Diseases, National Institutes of Health, Hamilton, MT, USA
e-mail: bartonk@niaid.nih.gov

V.L. Sim
Centre for Prions and Protein Folding Diseases, University of Alberta, Edmonton, AB, Canada

S.K.R. Williams and K.D. Caldwell (eds.), *Field-Flow Fractionation in Biopolymer Analysis*, DOI 10.1007/978-3-7091-0154-4_10,

10.1 Introduction

Transmissible spongiform encephalopathies (TSEs) or prion diseases are infectious neurodegenerative diseases characterized by aggregation of the host's prion protein (PrP) and spongiform degeneration of the brain [1]. These diseases, which include Creutzfeldt-Jakob disease in humans, bovine spongiform encephalopathy (mad cow disease), scrapie in sheep, and chronic wasting disease in cervids, can have inherited, sporadic, or infectious origins. Inherited prion diseases are linked to specific host PrP mutations, which can in turn result in the accumulation of infectious prion aggregates. The exact components and structure of the infectious agent are not fully established, but recent studies have shown that at least modest levels of infectivity can be propagated in vitro using purified PrP alone [2–5], or, more effectively, with the addition of brain homogenates [6, 7] or cofactors such as RNA and lipids [8, 9].

The normal cellular prion protein (PrP^C) is a glycosylphosphatidylinositol (GPI)-linked glycoprotein [10, 11] enriched in detergent resistant membranes. PrP^C has a long, flexible N-terminal tail and a globular C-terminal domain comprised of three alpha helices and a short two-stranded antiparallel β-sheet [12, 13]. Within the N-terminal tail is a set of five repeats of an eight amino acid sequence believed to be important in metal and ligand binding (for reviews, see [14, 15])

During disease pathogenesis, the soluble and protease sensitive PrP^C molecule undergoes a conformational shift from a largely alpha helical structure to one characterized by a large proportion of β-sheet [16–18]. The converted PrP molecule, (PrP^{res} or PrP^{Sc}), tends to be less soluble and more protease resistant than PrP^C [19]. These different properties are due in part to the oligomerization that accompanies the conformational change [20–24] (for recent review, see [1]). Under a variety of in vitro conditions, purified PrP^{res} can induce the conversion of PrP^C to new PrP^{res} [8, 25–31] which can in turn be infectious [2, 6–8]. Although the mechanistic details of the conversion reaction remain to be determined, considerable evidence is consistent with an autocatalytic seeded polymerization or template-directed mechanism [20, 24, 25, 32, 33]. In such mechanisms, interactions between PrP^C and an existing PrP^{res} oligomer catalyze or stabilize the conversion of the former to the latter as it is recruited into a growing PrP^{res} multimer, as has been observed in in vitro reactions (e.g., [21, 23, 28]).

In infected cells, the conversion of membrane anchored PrP^C occurs on the cell surface or in endocytic vesicles that are internalized from the cell surface [34–36]. The GPI-anchored PrP^C may interact with PrP^{res} aggregates that are also anchored to the membrane, leading most commonly to amorphous accumulations on cell surfaces or in intracellular vesicles (for review, see [1]). Alternatively, and most notably with human Gerstmann-Sträussler-Scheinker syndrome or scrapie-infected transgenic mice expressing only PrP^C that lacks the GPI anchor [37], the PrP molecules can escape from cells and accumulate in extra-cellular amyloid fibrils and plaques (Fig. 10.1a). Some purified PrP^{res} samples have paracrystalline

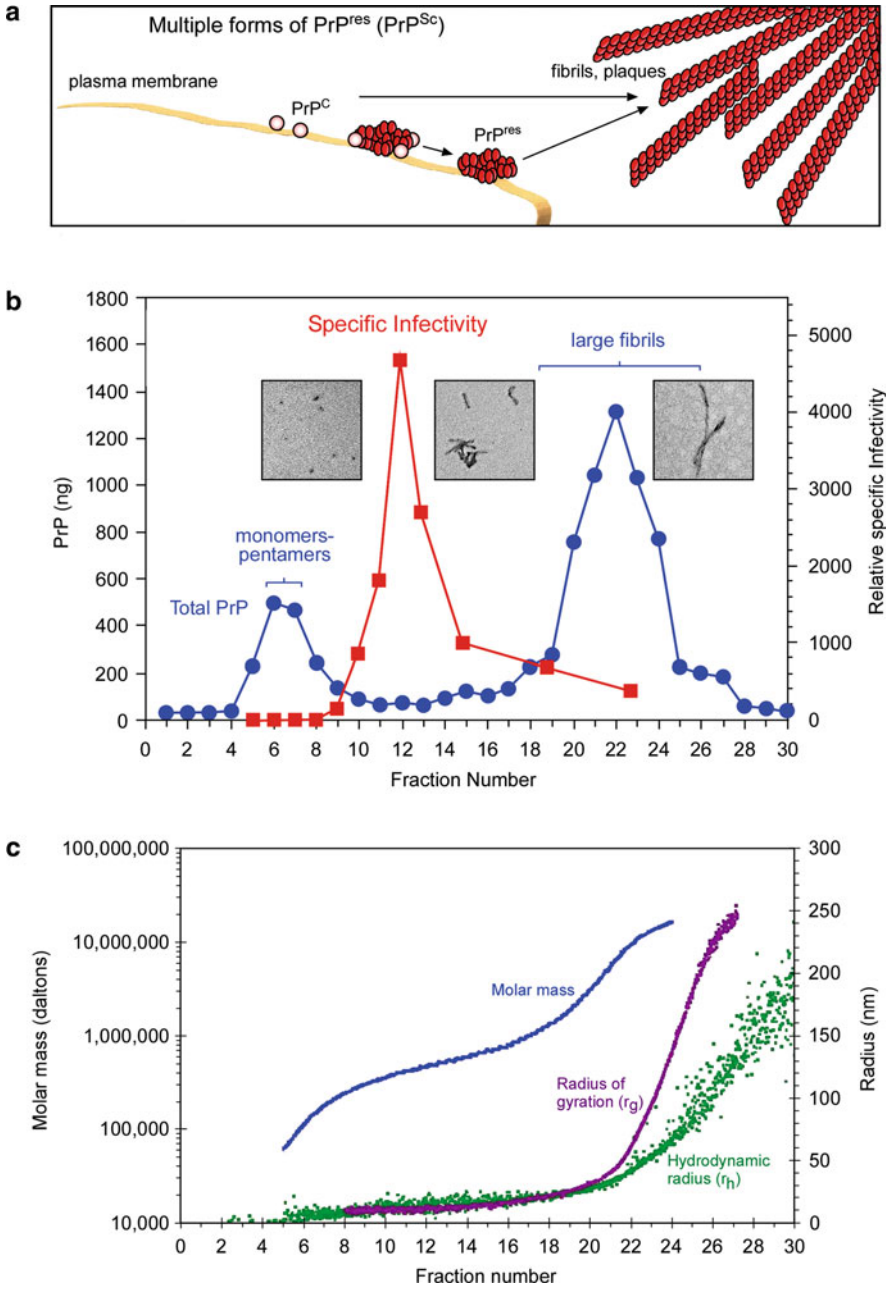

Fig. 10.1 Analysis of PrP size ranges. (**a**) GPI-anchored PrP^C is usually present on the cell surface as a monomer. PrP^C can be converted to PrP^{res} upon interaction with PrP^{res} aggregates on the cell surface, endosomes, or in extracellular fibril deposits or amyloid plaques. (**b**) Quantification of PrP (per fraction) by dot immunoblotting with anti-PrP antibody (*blue circles*), calculated specific infectivity (*red squares*), and transmission electron microscopy images of PrP^{res} oligomers

two-dimensional arrays [38] of what appear to be ring-like trimers [39], potentially the basic unit of prion amyloid fibrils.

Understanding the relationship between PrP^{res} particle size, infectivity, converting activity, and toxicity is important in identifying effective prevention and treatment strategies [1, 40]. The reported sizes of infective prion particles have ranged greatly from 20 kDa [41] to ~1 MDa with the former corresponding in mass to a single PrP molecule. However, the association of infectivity with PrP monomers has not been readily confirmed.

Studies on several neurodegenerative protein misfolding diseases have implied that small abnormal protein oligomers might be much more neurotoxic than larger amyloid fibrils of the same protein or peptide [40, 42]. In a variety of prion diseases, little or no accumulation of amyloid fibrils or plaques of PrP^{res} is apparent (for review, see [1]), despite the fact that the diseases are fatal and transmissible. Such observations have led to suggestions that, rather than being problematic, the formation of large amyloid fibrils might be protective by sequestering more harmful oligomers into a relatively inert state [40, 42]. However, this is clearly not always true in the case of prion diseases because scrapie infections in the anchorless PrP transgenic mice lead to accumulations of PrP^{res} mainly in amyloid plaques which, in turn, cause fatal transmissible neurodegenerative disease [37]. Interestingly, the clinical and neuropathological manifestations of scrapie in these mice differ substantially from those of classical scrapie, and instead resemble a cerebral amyloid angiopathy [43]. On the other hand, inoculation of human Gerstmann-Straussler-Scheinker infectivity into transgenic mice expressing a mutant GPI-anchored PrP^{C} can cause PrP amyloid accumulation without spongiform encephalopathy or clinical deficits [44]. Clearly, much remains to be learned about the roles, or lack thereof, of various types of abnormal PrP aggregates in the transmission and neuropathogenesis of various prion diseases.

Many techniques have been used to separate prion protein aggregates on the basis of size. Some techniques are limited by small fractionation ranges which would be unable to cover the wide assortment of prion protein aggregate sizes. Size exclusion chromatography, polyacrylamide gel electrophoresis, and filtration depend on sieving effects involving contact between aggregates and some form of stationary matrix. As prion aggregates are inherently sticky, they may interact with solid matrices and yield artifactual results.

Field-flow fractionation (FFF) techniques provide alternative methods for size-based separation of macromolecular complexes with a wide range of particle dimensions (see other chapters in this volume). FFF separates sample components on the basis of diffusion coefficients, not chemistry or sieving, by loading them into a thin open channel and applying an external force to move the sample

Fig. 10.1 (continued) in early, middle and late fractions. (**c**) Analysis of in-line light scattering results with ASTRA software to determine values for molar mass (*blue*), radius of gyration (*purple*) and hydrodynamic radius (*green*) (Adapted by permission from Macmillan Publishers Ltd: *Nature* [46], © 2005)

components perpendicular to the main flow of the mobile phase. The applied force causes the particles to move towards the accumulation wall while this effect is directly counteracted by diffusion. Smaller particles, with their higher diffusion coefficients, will naturally migrate more rapidly away from the accumulation wall and into the main stream of the mobile phase, resulting in faster elution. The more rapid elution of smaller particles, which is the opposite of what occurs in size exclusion chromatography, can be a distinct advantage when attempting to characterize the smallest particles with a given activity because there is less likelihood that large active particles will contaminate small-particle fractions due to artifactual interactions with the matrix.

Sklaviadis, Manuelidis and colleagues pioneered the use of sedimentation field-flow fractionation (SdFFF) to analyze prion particles isolated with sarkosyl disaggregation and density gradient fractionation [45]. Sedimentation FFF generates an external centrifugal force perpendicular to mobile phase flow by rotating the separation channel in a centrifuge rotor basket. Their analyses indicated a molecular mass of ~15 MDa and a radius of ~30 nm for the infectious particles, which they proposed to be protein-nucleic acid complexes.

More recently, Silveira and colleagues characterized much smaller infectious particles in analyses of the sizes of infectious prion particles, and their relative specific infectivities, using an alternative method called flow field-flow fractionation (FlFFF) [46, 47]. As described in more detail in Chap. 1, FlFFF differs from SdFFF in that the external force is applied with a fluid stream crossflow. Here we review the use of FlFFF for the characterization of prions.

10.2 Flow Field-Flow Fractionation of PrP^{res}

PrP^{res} is typically purified from infected hamster brains through a series of centrifugations and washes. In the Silveira et al. studies [46], particles ranging from PrP monomers to long amyloid fibrils were generated from large detergent insoluble aggregates by treating purified PrP^{res} samples with 1% sodium *n*-undecyl sulfate, sonication, freeze/thaw, and heating. The partially disaggregated samples were passed through a 0.2 μm filter to remove large particles or contaminants. Asymmetrical FlFFF on an Eclipse F instrument (Wyatt) was used to resolve and separate the various sizes of PrP containing particles. The trapezoidal channel was 26.5 cm in length, 350 μm in height and a maximum of 21 mm in width at the inlet port. A polyethersulphone membrane with a 10 kDa molecular weight cut-off (MWCO) was chosen for the accumulation wall due to its compatibility with the mobile phase and low sample loss. Samples of PrP were loaded in five repeated injections with each injection followed by a 3-min focus. After the last injection/focus cycle, an additional 12 min focus concentrated the protein in a thin band prior to elution. Focusing times were kept to a minimum to decrease the chances of reorganization or re-aggregation of PrP particles upon concentration. The small percentage of SUS in the mobile phase (20 mM Tris, pH 7.0, with 0.1% SUS)

reduced sample aggregation, reorganization, and binding to solid surfaces but was kept below the critical micelle concentration to prevent interference with light scattering measurements. Programmable elution modulated the crossflow linearly from 3 to 0 mL/min over 20 min followed by an additional 10 min elution without any crossflow.

Elution of PrP was monitored with in-line static light scattering (Dawn EOS), refractive index (Optilab DSP) and dynamic light scattering (QELS) while 1 mL fractions were collected. Unlike the homogeneous peak observed in the SdFFF experiments, two main peaks or populations of PrP were evident: one within fractions 5–8 that had low light scattering and the other within fractions 19–27 that had high scattering (Fig. 10.1b). The first peak corresponded to PrP monomers and small oligomers and the latter peak contained much larger PrP fibrils as seen in EM images (Fig. 10.1b inset). Using ASTRA software, the data from all the detectors was compiled to calculate a weight average molar mass (M_w), average radius of gyration (r_g), and hydrodynamic radius (r_h). The wide range of separation in a single FlFFF run was evident from the analysis; a 30-fold range (5–150 nm) of hydrodynamic radii accompanied masses ranging from 70 kDa to 10 MDa (Fig. 10.1c). With this large range of fractionated sizes there was reduced resolution, most notably at the extremes. Small oligomers co-eluted with the monomers and the large fibrils eluted in a bolus at the end of the crossflow. With these crossflow and elution parameters, the greatest resolution was found in the particles sized 10–30 nm or fractions 10–16. For these experiments, this was the range of interest, but it should be said that resolution can be predictably improved within specific size ranges with adjustments of the cross-flow gradient relative to the main flow.

10.3 Infectivity Measurements of Fractionated PrP^{res}

To assess the infectivity associated with the various particle sizes of PrP^{res}, the collected fractions were diluted into normal hamster brain homogenate and inoculated intercerebrally into hamsters. The incubation times of the disease, which are inversely related to infectivity levels, shortened beginning at fraction 9 and reached a minimum at fraction 12. Levels of infectivity for each fraction were estimated based on the comparisons of incubation times to those obtained from scrapie brain homogenate standards. A $>$ 600 fold increase in infectivity correlated to the 28-day shortening of the incubation period seen between fractions 7 and 12. The small amount of infectivity seen before fraction 7 was most likely due to the leading edge of the infective particles. Although infectivity was sustained throughout the elution of larger fibrils, fractions 18–25 had a much higher quantity of protein. These results demonstrated a major discordance between PrP concentration, particle size, and infectivity.

To more accurately describe infectivity in terms of the PrP^{res} components, a ‘specific infectivity’ value was calculated by dividing each fractions’ infectivity

values by their total PrP content determined by semi-quantitative immunoblotting. This analysis showed a sharp peak at fraction 12, indicating the presence of the most active infective particles per unit PrP (Fig. 10.1a – red squares). Light scattering analysis indicated that these particles had 12–14 nm radii and weighed several hundred kDa. The compact nature of the particle can be estimated using a ratio of the radius of gyration to the hydrodynamic radius (ρ value). Higher ρ values are typical for extended structures but the ρ value of ~0.9 for the fraction 12 particles indicated a fairly compact, spherical or ellipsoid structure.

The average mass and radius assigned to the particles represented not only the mass of the infectious particles but also any bound detergent molecules or other as yet unidentified constituents. A set of protein standards run in the presence or absence of detergent showed that the presence of detergent could increase the molecular weight and hydrodynamic radius by as much as 73% and 60%, respectively. Therefore the most infectious PrP particles (named J-particles, after their discoverer), when devoid of detergent, would likely have had molecular mass values between 300 and 600 kDa and be 17–27 nM in diameter. Assuming the infectious particles were only PrP molecules with average molecular weights of 21.5 kDa, each infectious particle would contain 14–28 PrP molecules. This suggested that although large amyloid bundles of PrP^{res} are extremely stable and able to transmit the disease, the most infectious particles per unit protein are smaller oligomeric species.

The most infectious J-particles identified by Silveira and colleagues [46] were considerably smaller than the 60 nm, 15 MDa particles characterized by Sklaviadis, Manuelidis and colleagues using SdFFF [45]. We presume that the differences in these findings can be largely attributable to sample preparation, which, in the Silveira study, intentionally included strong partial disaggregating conditions to enhance the chances of generating a continuum of PrP particle sizes including not only large amyloid fibrils, but also the smallest infectious particles and non-infectious monomers and oligomers.

10.4 Perspectives

In FlFFF experiments, elution can be monitored with a myriad of detectors, including RI and QELS. Most recently, we have tried to use absorbance detection to more accurately quantify the protein in individual fractions to refine the size of the most infectious particle. Interestingly, the absorbance profile does not align fully with the profile of PrP concentrations (Fig. 10.2). These results revealed some hazards in using UV absorbance detection. Although proteins absorb at 280 nm, other contaminants or mobile phase constituents may add to the overall absorbance due to chromophores or light scattering. The mobile phase absorbance can be subtracted by running a blank without protein. Contaminants or substances that co-purify with the protein aggregate sample (i.e., nucleic acids or lipids) may remain bound to the prions or be freed during the disaggregation procedure and

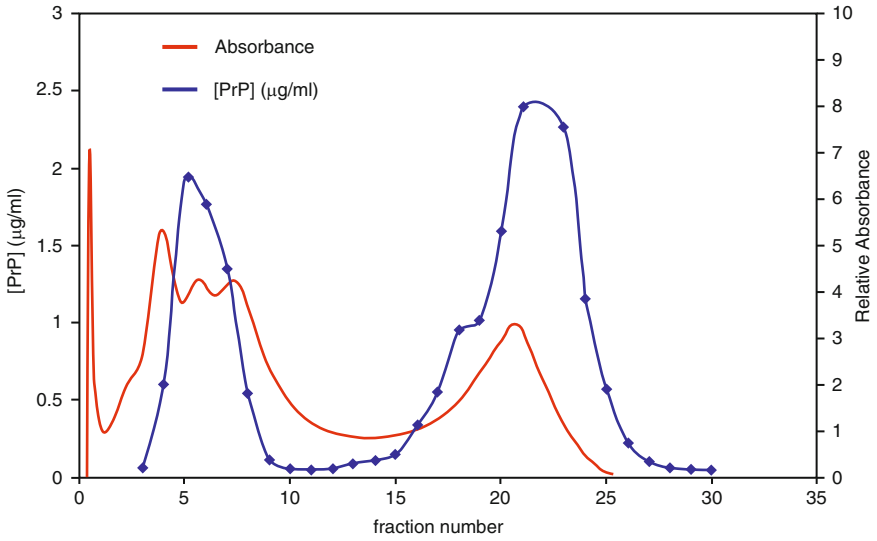

Fig. 10.2 Relationship between absorbance detection and quantity of PrP. Quantification of PrP by semi-quantitative Western blot compared with the raw in-line A_{280} data

fractionated by size along with protein during the elution. Moreover the molar extinction coefficients of proteins can vary between their monomeric and highly packed aggregated forms [48], complicating UV absorbance based estimations of the protein concentration.

Another limitation of FlFFF relative to some other size-based fractionation methods such as sedimentation velocity centrifugation is the small amount of sample that can be loaded, focused, and effectively fractionated. With our instrumentation, we have been limited to <100 μg PrP^{res} when largely purified. This has been particularly problematic because our goal has been to produce and analyze the most active particles, but only small amounts were produced from the disaggregation protocol. We have found that the characteristic saddle shape of the elution profile can be altered with different sonication times and powers. However, these treatments have tended to change the ratio of small oligomers ($\leq$4 PrP molecules) to larger aggregates or fibrils, rather than the proportion of intermediate-sized particles. If another disaggregation protocol was found to produce more intermediate sized particles, less total protein could be loaded. In more recent attempts to fractionate more complex tissue extracts, we have rapidly overloaded the capacity of our FlFFF instrument. Thus, if fractionation of a larger amount of starting materials is required, alternative methodologies or modifications of the FlFFF instrumentation will likely be required.

Nonetheless, FlFFF has been successfully used to separate prion protein aggregates. Moreover, the general technique should be widely applicable to other protein aggregates or macromolecular structures. The sizes and compositions of channel and membrane can be chosen to optimize fractionation of samples of

different types, volumes, and properties. Also, as noted above, changes in the beginning and ending crossflow rates as well as the slope of the gradient elution can enhance resolution of smaller or larger particle size ranges. For example, Rambaldi and colleagues used FlFFF to follow the aggregation process of $A\beta_{1-42}$ that is a crucial event in the pathogenesis of Alzheimer's disease [49]. Using FlFFF, they were able to separate not only the small, soluble oligomers of a 4 kDa peptide but also the less soluble, larger aggregates. Further applications of FlFFF to the analysis of different types of prions and other peptide and protein aggregates may provide valuable insights into their physiological and/or pathological functions.

Acknowledgements This work was supported by the Intramural Research Program of the National Institute of Allergy and Infectious Diseases. We thank Gary Hettrick for his assistance with figure preparation.

References

1. Caughey B, Baron GS, Chesebro B, Jeffrey M (2009) Getting a grip on prions: oligomers, amyloids, anchors and pathological membrane interactions. Annu Rev Biochem 78:177–204
2. Kim JI, Cali I, Surewicz K, Kong Q, Raymond GJ et al (2010) Mammalian prions generated from bacterially expressed prion protein in the absence of any mammalian cofactors. J Biol Chem 285(19):14083–14087
3. Legname G, Baskakov IV, Nguyen HO, Riesner D, Cohen FE et al (2004) Synthetic mammalian prions. Science 305:673–676
4. Colby DW, Wain R, Baskakov IV, Legname G, Palmer CG et al (2010) Protease-sensitive synthetic prions. PLoS Pathog 6:e1000736
5. Makarava N, Kovacs GG, Bocharova O, Savtchenko R, Alexeeva I et al (2010) Recombinant prion protein induces a new transmissible prion disease in wild-type animals. Acta Neuropathol 119:177–187
6. Castilla J, Saa P, Hetz C, Soto C (2005) In vitro generation of infectious scrapie prions. Cell 121:195–206
7. Weber P, Giese A, Piening N, Mitteregger G, Thomzig A et al (2006) Cell-free formation of misfolded prion protein with authentic prion infectivity. Proc Natl Acad Sci USA 103:15818–15823
8. Deleault NR, Harris BT, Rees JR, Supattapone S (2007) Formation of native prions from minimal components in vitro. Proc Natl Acad Sci USA 104:9741–9746
9. Wang F, Wang X, Yuan CG, Ma J (2010) Generating a prion with bacterially expressed recombinant prion protein. Science 327:1132–1135
10. Stahl N, Borchelt DR, Hsiao K, Prusiner SB (1987) Scrapie prion protein contains a phosphatidylinositol glycolipid. Cell 51:229–240
11. Vey M, Pilkuhn S, Wille H, Nixon R, DeArmond SJ et al (1996) Subcellular colocalization of the cellular and scrapie prion proteins in caveolae-like membranous domains. Proc Natl Acad Sci USA 93:14945–14949
12. Riek R, Hornemann S, Wider G, Billeter M, Glockshuber R, Wuthrich K (1996) NMR structure of the mouse prion protein domain PrP(121-231). Nature 382:180–182
13. Riek R, Hornemann S, Wider G, Glockshuber R, Wuthrich K (1997) NMR characterization of the full-length recombinant murine prion protein, *m*PrP(23-231). FEBS Lett 413:282–288
14. Millhauser GL (2007) Copper and the prion protein: methods, structures, function, and disease. Annu Rev Phys Chem 58:299–320

15. Caughey B, Caughey WS, Kocisko DA, Lee KS, Silveira JR, Morrey JD (2006) Prions and transmissible spongiform encephalopathy (TSE) chemotherapeutics: a common mechanism for anti-TSE compounds? Acc Chem Res 39:646–653
16. Caughey BW, Dong A, Bhat KS, Ernst D, Hayes SF, Caughey WS (1991) Secondary structure analysis of the scrapie-associated protein PrP 27-30 in water by infrared spectroscopy. Biochemistry 30:7672–7680
17. Pan K-M, Baldwin M, Nguyen J, Gasset M, Serban A et al (1993) Conversion of alpha-helices into beta-sheets features in the formation of the scrapie prion protein. Proc Natl Acad Sci USA 90:10962–10966
18. Safar J, Roller PP, Gajdusek DC, Gibbs CJ Jr (1993) Conformational transitions, dissociation, and unfolding of scrapie amyloid (prion) protein. J Biol Chem 268:20276–20284
19. McKinley MP, Bolton DC, Prusiner SB (1983) A protease-resistant protein is a structural component of the scrapie prion. Cell 35:57–62
20. Jarrett JT, Lansbury PT Jr (1993) Seeding "One-Dimensional Crystallization" of Amyloid: a Pathogenic Mechanism in Alzheimer's Disease and Scrapie? Cell 73:1055–1058
21. Caughey B, Kocisko DA, Raymond GJ, Lansbury PT (1995) Aggregates of scrapie associated prion protein induce the cell-free conversion of protease-sensitive prion protein to the protease-resistant state. Chem Biol 2:807–817
22. Swietnicki W, Morillas M, Chen SG, Gambetti P, Surewicz WK (2000) Aggregation and fibrillization of the recombinant human prion protein huPrP 90-231. Biochemistry 39:424–431
23. Horiuchi M, Priola SA, Chabry J, Caughey B (2000) Interactions between heterologous forms of prion protein: binding, inhibition of conversion, and species barriers. Proc Natl Acad Sci USA 97:5836–5841
24. Gadjusek DC (1988) Transmissible and nontransmissible amyloidoses: autocatalytic post-translational conversion of host precursor proteins to beta-pleated configurations. J Neuroimmunol 20:95–110
25. Kocisko DA, Come JH, Priola SA, Chesebro B, Raymond GJ et al (1994) Cell-free formation of protease-resistant prion protein. Nature 370:471–474
26. Atarashi R, Moore RA, Sim VL, Hughson AG, Dorward DW et al (2007) Ultrasensitive detection of scrapie prion protein using seeded conversion of recombinant prion protein. Nat Methods 4:645–650
27. Baron GS, Wehrly K, Dorward DW, Chesebro B, Caughey B (2002) Conversion of raft associated prion protein to the protease-resistant state requires insertion of PrP-res (PrP(Sc)) into contiguous membranes. EMBO J 21:1031–1040
28. Horiuchi M, Chabry J, Caughey B (1999) Specific binding of normal prion protein to the scrapie form via a localized domain initiates its conversion to the protease- resistant state. EMBO J 18:3193–3203
29. Saborio GP, Permanne B, Soto C (2001) Sensitive detection of pathological prion protein by cyclic amplification of protein misfolding. Nature 411:810–813
30. Deleault NR, Lucassen RW, Supattapone S (2003) RNA molecules stimulate prion protein conversion. Nature 425:717–720
31. Deleault NR, Geoghegan JC, Nishina K, Kascsak R, Williamson RA, Supattapone S (2005) Protease-resistant prion protein amplification reconstituted with partially purified substrates and synthetic polyanions. J Biol Chem 280:26873–26879
32. Cohen FE, Pan KM, Huang Z, Baldwin M, Fletterick RJ, Prusiner SB (1994) Structural clues to prion replication. Science 264:530–531
33. Eigen M (1996) Prionics or the kinetic basis of prion diseases. Biophys Chem 63:A1–A18
34. Caughey B, Raymond GJ (1991) The scrapie-associated form of PrP is made from a cell surface precursor that is both protease- and phospholipase-sensitive. J Biol Chem 266:18217–18223
35. Caughey B, Raymond GJ, Ernst D, Race RE (1991) N-terminal truncation of the scrapie-associated form of PrP by lysosomal protease(s): implications regarding the site of conversion of PrP to the protease-resistant state. J Virol 65:6597–6603

36. Borchelt DR, Taraboulos A, Prusiner SB (1992) Evidence for synthesis of scrapie prion protein in the endocytic pathway. J Biol Chem 267:16188–16199
37. Chesebro B, Trifilo M, Race R, Meade-White K, Teng C et al (2005) Anchorless prion protein results in infectious amyloid disease without clinical scrapie. Science 308:1435–1439
38. Wille H, Michelitsch MD, Guenebaut V, Supattapone S, Serban A et al (2002) Structural studies of the scrapie prion protein by electron crystallography. Proc Natl Acad Sci USA 99:3563–3568
39. Govaerts C, Wille H, Prusiner SB, Cohen FE (2004) Evidence for assembly of prions with left-handed beta-helices into trimers. Proc Natl Acad Sci USA 101:8342–8347
40. Caughey B, Lansbury PT (2003) Protofibrils, pores, fibrils, and neurodegeneration: separating the responsible protein aggregates from the innocent bystanders. Annu Rev Neurosci 26:267–298
41. Safar J, Wang W, Padgett MP, Ceroni M, Piccardo P et al (1990) Molecular mass, biochemical composition, and physicochemical behavior of the infectious form of the scrapie precursor protein monomer. Proc Natl Acad Sci USA 87:6373–6377
42. Baron GS, Caughey B (2003) Effect of glycosylphosphatidylinositol anchor-dependent and –independent prion protein association with model raft membranes on conversion to the protease-resistant Isoform. J Biol Chem 278:14883–14892
43. Chesebro B, Race B, Meade-White K, LaCasse R, Race R et al (2010) Fatal transmissible amyloid encephalopathy: a new type of prion disease associated with lack of prion protein membrane anchoring. PLoS Pathog 6:e1000800
44. Piccardo P, Manson JC, King D, Ghetti B, Barron RM (2007) Accumulation of prion protein in the brain that is not associated with transmissible disease. Proc Natl Acad Sci USA 104:4712–4717
45. Sklaviadis T, Dreyer R, Manuelidis L (1992) Analysis of Creutzfeldt-Jakob disease infectious fractions by gel permeation chromatography and sedimentation field-flow fractionation. Virus Res 26:241–254
46. Silveira JR, Raymond GJ, Hughson AG, Race RE, Sim VL et al (2005) The most infectious prion protein particles. Nature 437:257–261
47. Silveira JR, Hughson AG, Caughey B (2006) Fractionation of prion protein aggregates by asymmetrical flow field-flow fractionation. Methods Enzymol 412:21–33
48. Pace CN, Vajdos F, Fee L, Grimsley G, Gray T (1995) How to measure and predict the molar absorption coefficient of a protein. Protein Sci 4:2411–2423
49. Rambaldi DC, Zattoni A, Reschiglian P, Colombo R, De LE (2009) In vitro amyloid Abeta(1-42) peptide aggregation monitoring by asymmetrical flow field-flow fractionation with multi-angle light scattering detection. Anal Bioanal Chem 394:2145–2149

Chapter 11
Multifunctionalized Particles for Biosensor Use

Karin D. Caldwell and Karin Fromell

Abstract *The mass sensitive sedimentation* subtechnique of FFF differs from the flow analogue in two principal ways: Firstly, resolution in sdFFF varies with analyte size to the third power – compared to the first power size dependence for the flow system. Secondly, conversion of sdFFF retention data into mass or size information for the analyte requires knowledge of its density, a quantity that has to be determined separately. Since no such input parameter is required to extract size information from flow FFF data, the sedimentation analogue has obtained a reputation for being less "universal" than its flow counterpart. The present article intends to demonstrate some of the advantages offered by the high mass sensitivity of the sdFFF technique, especially in the design and optimization of bioanalytical processes involving nanoparticles.

Keywords Controlled surface modification of nanoparticles • Lectins • Luminometry • Multiple attachment modes • Particle attachment to surfaces • Quantification of protein attachment • Reactivity of attached binders. • Sedimentation FFF • Ultra-mass sensitive balance

11.1 Introduction

In recent years biofunctionalized nanoparticles have attracted significant interest for use in various contexts, ranging from servicing as vehicles for drug delivery to being responsible for the capture and quantification of metabolites and clinical markers in the diagnosing of disease [1–5]. For many of these applications it is essential to know not only the particle size, but its load of drug or of capturing

K.D. Caldwell (✉) • K. Fromell
Department of Physical and Analytical Chemistry, Section of Surface Biotechnology, Uppsala University, Uppsala, Sweden
e-mail: karin.caldwell@biorg.uu.se

S.K.R. Williams and K.D. Caldwell (eds.), *Field-Flow Fractionation in Biopolymer Analysis*, DOI 10.1007/978-3-7091-0154-4_11,

moiety as well. For instance, particles intended for in vivo use will perform very differently depending on their size and load, as they will reach different target organs depending on their physical size. This means, for instance, that they may perform a site-specific delivery of a size-related amount of a drug with which they are loaded.

In designing an optimally performing particle-based diagnostic process it is frequently desirable to determine both the number of grafting sites implanted on a particle surface as well as the grafting efficiency, i.e., the number of sites that have the ability to become occupied with a particular ligand. Additional questions to be answered concern the grafting density and its effect on the ligand's biological activity, as well as the amounts of specific and nonspecific adsorption of the analyte to the particle. None of these questions are easy to answer without access to a sensitive analytical balance, such as a sdFFF instrument.

11.2 Theory of sdFFF

In the following we will briefly review the retention theory applicable to sdFFF and exemplify its use with the linking of polymers and proteins to the surfaces of primarily polymeric nanoparticles.

The general theory of FFF retention relates to the parabolic flow of carrier through a thin duct. This applies to all systems, regardless of which field is used to concentrate an injected sample into a thin sliver near one of the channel walls. With the ribbon-like channel geometry, common to FFF systems, the elution volume V_e explicitly relates to the reduced thickness of this sliver labeled "λ" in general FFF literature [6, 7]:

$$V^0/V_e = 6\lambda[\coth(1/2\lambda) - 2\lambda] \approx \left(6\lambda - 12\lambda^2\right) \tag{11.1}$$

In the case of sd FFF, the field G is gravitational (centrifugal). For most practical applications the separation channel is therefore coiled and positioned inside a centrifugal rotor basket.

The sample property which makes it susceptible to the field is the buoyant mass

$$M' = m\Delta\rho/\rho' \tag{11.2}$$

i.e., the mass m of the particle corrected for the mass of carrier displaced by the particle as it sediments towards the channel wall. If m is replaced by the product of volume and density, and the volume is expressed in terms of particle diameter d, M′ can be written in a form that clearly demonstrates the high (third order) size selectivity of the SdFFF technique

$$M' = \pi\Delta\rho \mathrm{d}^3/6 \tag{11.3}$$

In the above expressions Δρ stands for the difference in density between particle and carrier, while ρ' symbolizes the density of the particle. The reduced layer thickness λ in the SdFFF case is given by [7]

$$\lambda = \mathrm{kT}/\mathrm{GM'w} \tag{11.4}$$

From Eqs. 11.2 and 11.4 it is quite evident that an evaluation of SdFFF retention data requires input of density data for both particle and carrier. While this can appear somewhat cumbersome, it actually allows a composition analysis of even highly complex layered particle structures, such as those that are generated when polymeric particles are allowed to adsorb or bind complex mixtures of proteins and polymers.

For a composite sample, M′ in Eq. 11.4 can be replaced by M'_{comp} as the sum of the various mass-density pairs (i) that make up the sample, ranging from the core particle (i = 1) to its various adsorption/grafting layers (i = n).

$$M'_{comp} = \sum\nolimits_i m_i(\Delta\rho/\rho_i) \tag{11.5}$$

In this manner the sequential uptake of ligands to a binder-derivatized surface is conveniently performed and evaluated, as will be discussed below.

An early demonstration of FFF-based surface analysis of adsorption complexes involved the comparative adsorption of the two milk proteins β-lactoglobulin (BLG) and β-casein (BCN) to polystyrene (PS) latex particles of uniform size [8]. The conventional way of performing this type of comparison consisted of adding a known amount of particles to an aliquot of well quantified protein, and determining the uptake as the difference in aliquot protein concentration before and after exposure to the particles. Given that this approach is rather error prone it was decided to quantify the amounts adsorbed, both by SdFFF and also by amino acid analysis of the particle-protein complex. A clear advantage of the FFF approach is the constant washing that the coated particles undergo as they travel down the separation channel. In this way the analytical procedure itself removes all loosely adhering protein, leaving behind only that which might be actively involved in the subsequent function of the coated particle such as being the active part in an immunodiagnostic test. The agreement between the various analytical methods used in ref. [8] was quite comforting and encouraged further refinements of the SdFFF quantification technique [9–11].

11.3 Ligand Attachment to Polymeric Nanoparticles

Most polymeric latex particles are hydrophobic in nature, and their behavior as protein adsorbents is well illustrated by the numerous polystyrene standard particles that are commercially available in a wide variety of sizes. One issue of great interest

is the possibility to shield a surface from an unwanted uptake of protein. This type of problem is readily studied using nanoparticles exposed to different coatings, whose protective qualities are illustrated by their respective uptake of protein following the coating. In our laboratories we have frequently based the protection on an adsorbed layer of polymeric surfactants of the poloxamer type. These surfactants are block copolymers consisting of hydrophilic PEO-containing blocks that frame one or more hydrophobic PPO-containing blocks. In an aqueous environment the latter adsorb rapidly and tenaciously [12–14] to hydrophobic surfaces, providing them with a protein repellant shield of highly mobile PEO chains. Although the naked PS surface adsorbs significant amounts of protein, the adsorbed molecules are frequently more or less denatured by the adsorption, leading to a loss in biological activity, as seen in Fig. 11.1. The *sweet pea lectin* (LOA) in solution

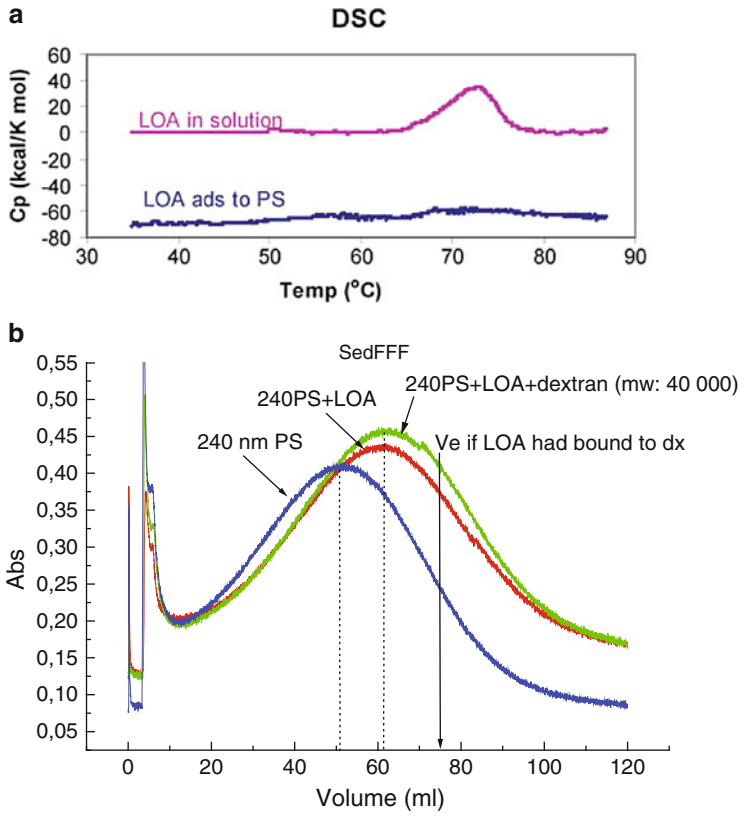

Fig. 11.1 *Studies of lectin from Lathyrus odoratus (LOA).* (**a**) Differential Scanning Calorimetric profiles of LOA in native condition (*solution*) and adsorbed to 240 nm PS latex with apparent loss of secondary structure; (**b**) sdFFF of 240 nm PS latex: bare (*bottom trace*), in adsorption complex with LOA (*middle trace*), in complex with LOA in presence of excess of dextran 5,000 (*top trace*). The lack of mass difference between the top and middle samples indicates adsorption-induced loss of LOA carbohydrate binding ability

has a strong affinity for the carbohydrate glucose. Following adsorption to PS latex particles, a SdFFF analysis of the LOA coated particles in the figure confirmed that the particles contained just under 1 mg/m^2 of protein. Yet, this carbohydrate-binding protein had totally lost its ability to bind the glucose polymer Dextran 500. A calorimetric look at the particle-protein complex further revealed that during the adsorption the protein had completely lost its original secondary structure. This and many similar examples clearly illustrate that the mere presence of a protein, be it a receptor or an enzyme, on a surface is not enough to ensure a reactive arrangement.

For this reason we have turned to the poloxamers, in particular to a product referred to as Pluronic F108, for surface protection. Given its efficiency and ease of handling this product has further inspired our efforts to introduce different reactive structures at the ends of the PEO chains. Thus modified, the Pluronic derivatives have offered a practical approach to ligand attachment while also providing protection against non-wanted adsorption. The end-groups are generally without effect on the surfactant's adsorption, and one can therefore readily mix differentially derivatized Pluronics with the underivatized compound, and recognize the stoichiometry of the solution mixture upon analysis of the surface composition following adsorption.

Figure 11.2 illustrates a bouquet of Pluronic F108 derivatives that are produced to couple certain specific ligands to the surface to which they are adsorbed. Examples of such ligands are pyridyl disulfide with its specific ablility to attach thiol-containing structures [15], NHS-derivatives with strong affinity towards heavy metal ions such as Ni or Co chelated to some structure intended for linking [16], or some oligonucleotide which will specifically bind its complementary nucleotide sequence if such is introduced into a molecule for the purpose of allowing its specific attachment [17].

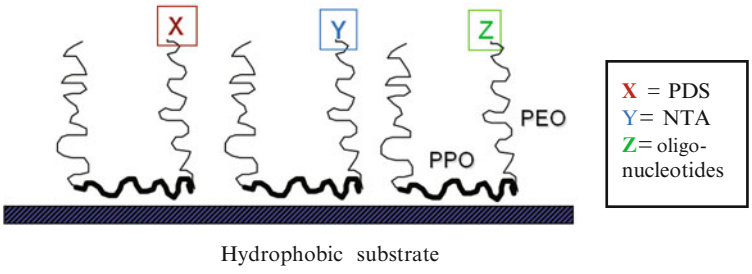

Fig. 11.2 *Schematic illustration of the polymeric surfactant Pluronic F108* with assorted reactive end groups introduced on the PEO for functionalizing the underlying surface

11.4 Analytical Instrumentation and Methods

The SdFFF instrument used in the characterizations described here is a precursor to the Model CF1000 from Postnova Analytics. The channel length and breadth are 94 cm and 2.0 cm, respectively, while the thickness, w, is 0.0254 cm. [7]. This channel is curved to fit inside a stainless steel rotor basket with a radius of 15.5 cm. The basket was spinning at rates controlled by the system's computer through use of a specially designed software package.

Densities were determined using a well thermostatted PAAR densitometer which enabled the determination of ρ for both carrier and analyte with six place accuracy. This was done in connection with each change in sample or carrier.

The pump rate and effluent volume were monitored by collecting the weight of the latter using a Mettler analytical balance, whose electronic output was fed directly to the system's control unit thus allowing a continuous monitoring of both field and flow.

The actual detection of sample protein was primarily done by luminometry, using a Berthold recording device. Alternatively, detection was based on the monitoring of fluorescence or UV absorbance, as indicated in each special case.

11.5 Examples of Applications

The ability to introduce and quantify multiple functionalities to a particle surface is extremely desirable, e.g., when optimizing surfaces for diagnostic use. Such surfaces normally contain some protein with high affinity for the analyte to be captured and quantified. The capturing moiety can for instance be a receptor analogue, if the tool is to be used in hormone analysis, or it may be an antibody or a specifically designed binder for analysis of plasma proteins with a marker function, indicating a clinical problem of some kind. Questions of importance in this context concern the ability of the analytical surface to reproducibly capture and report the concentration of the marker. The adsorption of inconsequential molecules must, as a rule, be kept to a minimum in order to provide maximum detection sensitivity. Another problem to be handled concerns the specific capture activity, i.e., the ability of each unit of analytical surface area, alternatively each capturing molecule, to execute its binding function. Here, the close-packing of binders is of importance, as is the possible steric hindrance presented by the attachment chemistry itself. Finally, storage stability is a matter of significant importance that also must be attended to. All of these questions require knowledge of the performance of specific protein types in their specific presentation.

Figure 11.3 exemplifies the SdFFF based analysis of a composite surface arrangement on a polystyrene latex particle, which is decorated to serve as a glycoprotein capturing agent. The particle has a diameter of 240 nm, a value verified by the sedimentation technique in the initial run of the sequence [18].

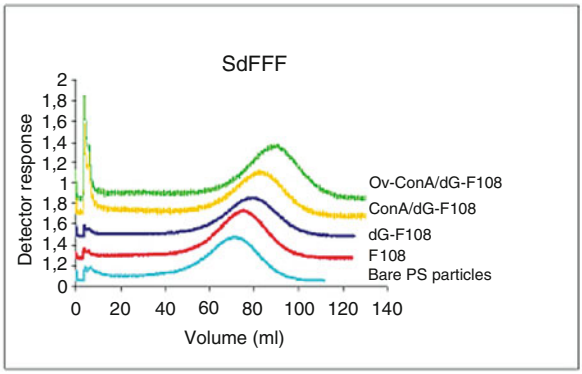

Bare PS: 239.4±1 nm	Surface conc (g/particle)	No of Molecules/ particle
F108-PDS	$3{,}5\times10^{-16}$	14400 ± 400
dG	$5{,}2\times10^{-17}$	6200 ± 1000
ConA	$1{,}2\times10^{-16}$	700 ± 55
Ovalbumin	$1{,}5\times10^{-16}$	2000 ± 125

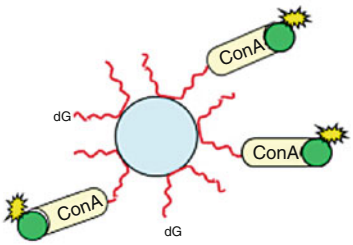

Fig. 11.3 *SdFFF analysis of a multilayered PS particle constructed for glycoprotein analysis via the lectin ConA*. Sequential analyses are used for layer-by-layer quantification of: (1) adsorbed Pluronic F108; (2) (F108 + dG); (3) (F108 + dG + ConA); and (4) the affinity trapped glycoprotein Ovalbumin. The SdFFF derived masses in each layer are given in the Table (Adapted from [18] with permission from Elsevier, © 2005)

The first step in configuring this surface consists of the adsorption of Pluronic F108 with its different PEO chain terminators, designed to link in the various functions that the particle is to acquire. Here, the FFF analysis reports that the particle surface has taken up 14 400 ± 400 Pluronic F108 molecules.

The next step in shaping this configuration is to attach an oligonucleotide, deoxyguanin (dG), to the surface-attached Pluronic. This is to enable the linking of the particle to a surface similarly coated with Pluronic F108, only this one containing the antagonist, deoxycytosin (dC). The two oligonucleotides hybridize, linking the particle to the surface in a firm attachment that can withstand washing at high shear [17]. In order to capture glycoproteins of interest, the carbohydrate-sensitive lectin Concanavalin A (ConA), is attached to the surface via an available thiol group that rapidly reacts with a pyridyldisulfide (PDS) group resident on a Pluronic F108. This coupling chemistry is not only efficient and robust, but has the added advantage of generating a strong chromophor, namely the pyridyl thioketone, as a reaction product when linking occurs [15].This compound has a unique

and strong UV-absorbance at 343 nm which allows quantification of the protein coupling by means of a route independent of the FFF assessment. A summary of the quantitations performed in conjunction with shaping the capturing entity is shown as an insert in Fig. 11.3.

Thus configured, the particles are ready for attachment to an analytical surface for capture and quantification of glycoproteins. The model analyte used in Fig. 11.4a, b is a fluorescently (Cy5) labeled Ovalbumin, known to contain at least one sugar moiety on its main peptide chain. Ovalbumin has a molecular weight of 45 kDa and is therefore large enough to potentially suffer steric hindrance in its binding to the capture agent, ConA, which is just over twice its size. It was therefore essential to investigate whether coupling could indeed take place. Remarkably, the SdFFF binding analysis showed that nearly 3 out of the 4 available binding sites on ConA were occupied by Ovalbumin. This is a good indication that

a

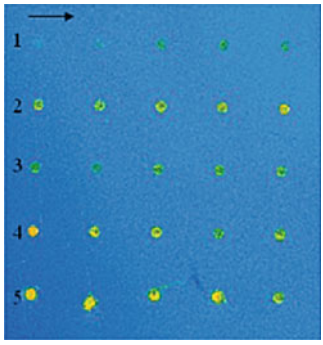

Row	*Sample*	*Intensity*
1	HSA	171 ± 108
2	Ovalbumin	1301 ± 540
3	Fetuin	714 ± 144
4	Thyroglobulin	1311 ± 468
5	Man-BSA	3765 ± 1157

b

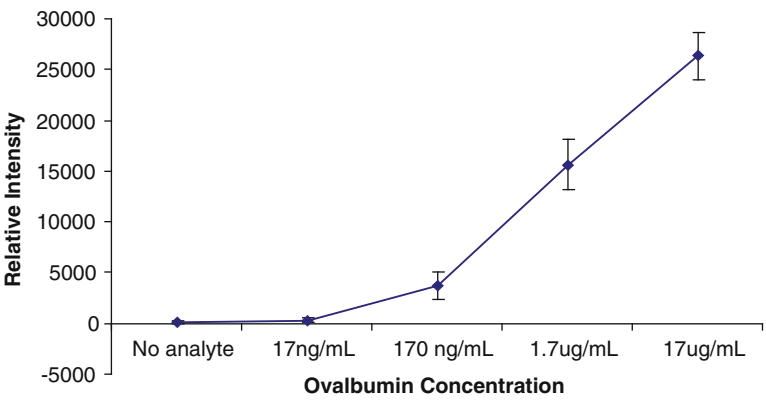

Fig. 11.4 *Thin-layer arrangement of the ConA particles from Fig. 11.3 for the analysis of glycoproteins*. (**a**) row 1 human serum albumin (unglycosylated), row 2 ovalbumin, row 3 fetuin, row 4, thyroglobulin, row 5 mannosylated bovine serum albumin; (**b**) Evaluation of the sensitivity of the ConA array. Measurements were based on fluorescence-labeled ovalbumin, analysed in ten replicates for each concentration

the particle itself causes no significant hindrance to binding, and furthermore, that the PEO-linker between Pluronic F108 and ConA causes minimal harm to the binding reaction.

Figure 11.4 compiles a number of fluorescence measurements on model particles of the type described in Fig. 11.3. Following suspension in buffer, these particles had been dispensed in 6.4 μL aliquots to a Polystyrene sheet coated with Pluronic F108-dC. The dispensing gave rise to spots of uniform size as shown in Fig. 11.4a, each spot containing approximately 10^6 particles. After 15 min of hybridization the sheet was washed extensively and solutions of Cy5-labeled Ovalbumin, or other similarly labeled proteins, were layered over rows of attached particles and incubated for 15 min followed by exhaustive washing. The analytical accuracy in this procedure is illustrated in Fig. 11.4b, where series of ten spots were exposed to one out of five concentrations of Cy5-Ovalbumin. The fluorescence intensity for each spot was measured and averaged for the ten spots in each series, as seen in Fig. 11.4b. The lack of signal between the spots is reassuring proof that the Pluronic F108-dC protects the surface from nonspecific protein adsorption.

11.6 Biosensor Applications Involving Nanoparticles

Diagnostic analyses of the type referred to as "Point-of-Care" tests are gaining ever more interest, as our population ages and will need health care that is rapidly and conveniently administered in private homes or at a nearby doctor's office. This implies that the analysis has to be performed on reasonably priced and easy-to-transport equipment, and executed by, at times, moderately inexperienced personnel. Such is particularly the case when it is left to the patient him- or herself to carry out the measurement and report the analytical result to the responsible physician. In the following we will outline two nanoparticle-based approaches, neither of which requires specialized high-technology clinical laboratories for execution.

In carrying out analytical work based on protein-coupled particles, it is especially important to pay attention to such practical details as efficiency of rinsing after sample contact, for the purpose of minimizing false background signals that are often caused by e.g., adhering reagents. The rinsing of nanoparticles without error-causing losses of the capture surface is a difficult proposition, since their small mass makes settling a slow process. This is true even under centrifugal fields such as those generated in ordinary table centrifuges, and collection of a "clean" population of analyte covered particles is typically both time-consuming and error prone. Alternately, filtration following washing is for the most part extremely wasteful in work with small particles, and results in large losses carrying with them significant analytical errors.

One way around this dilemma, recently explored in our laboratory [19], combines the practical advantages of working with large, massive and readily settling particles, with the capture sensitivity offered by the small protein decorated

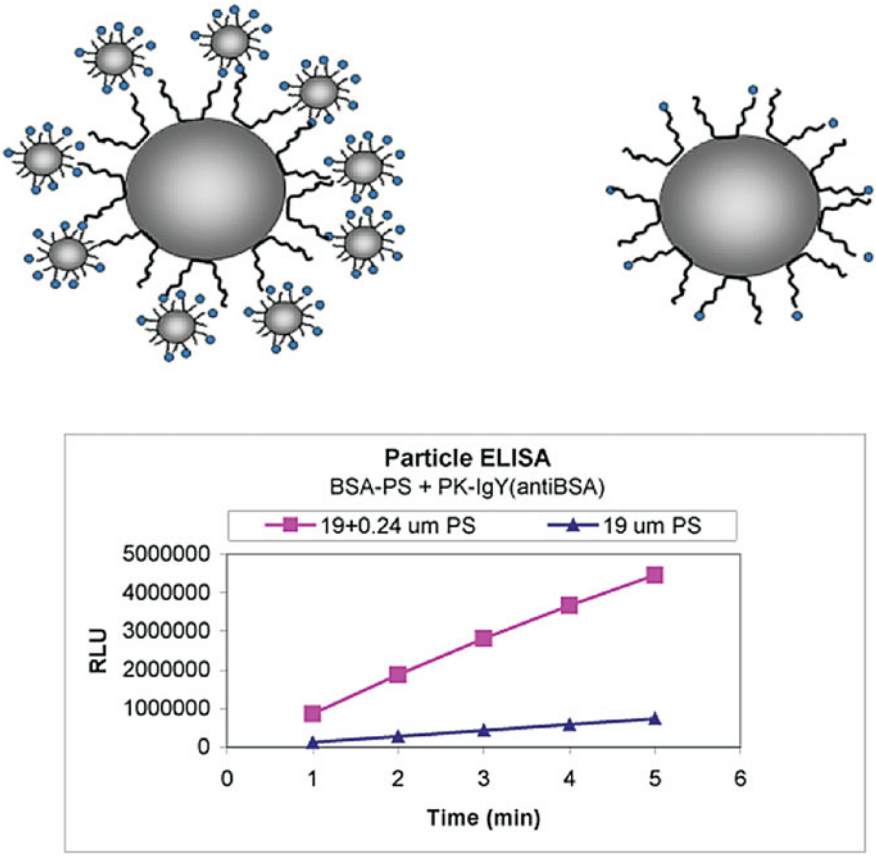

Fig. 11.5 *Method for surface expansion of large and easy-to-wash macroparticles*. Bovine serum albumin (BSA) was the analyte captured, either by direct adsorption to the 19 μm diameter PS particles, or to 240 nm PS particles, themselves attached to the 19 μm PS particles by means of an oligonucleotide coupling. The quantification was based on bioluminescence, generated by pyruvate kinase conjugated to an anti-BSA antibody

nanoparticles. The combination shown in Fig. 11.5 builds on the oligonucleotide coupling described above (see Fig. 11.2), only now the large particle serves the role of the flat surface to which the small particles are attached. Through this arrangement one gains both the rapid washing with minimal material losses that is offered by the macro-particles, and the high reactivity offered by the highly curved and readily accessed nano-particulate surfaces. Figure 11.5 illustrates a typical gain in signal that can be accomplished in this manner. The diagram illustrates a comparison between the bioluminescence intensity generated, on the one hand, by a given number of 19 μm PS particles (4.2×10^5 in this case) whose surfaces were decorated with Pluronic F108-linked BSA, and on the other hand with the same number of 19 μm PS particles (4.2×10^5), only now the surface decoration also included 0.24 μm PS particles equipped with the Pluronic-linked BSA as in the

companion case. The antigen binding was detected as the bioluminescence intensity generated by the anti-BSA linked kinase. In both cases the bioluminescence intensity is consequently proportional to the amount of BSA on the big particles, as it is generated by pyruvate kinase conjugated to anti-BSA. This construct readily binds to BSA on both large and small particles. After careful washing it is allowed to operate on its substrate which is contained in the suspension buffer together with luciferase/luciferin. The example shown in Fig. 11.5 clearly demonstrates the potential for gaining signal strength by working with hybrid particles, as suggested here.

11.7 Nanoparticles in Microfluidic Sensing

A biological system is characterized by a number of metabolic reactions that are "coupled" in the sense that the product of one enzymatically catalyzed reaction is shuttled to a neighboring enzyme where it will function as a reactant. A typical example of this behavior is demonstrated by the electron transport chain of mitochondrial reactions, where protons are oxidized to water through a series of 18

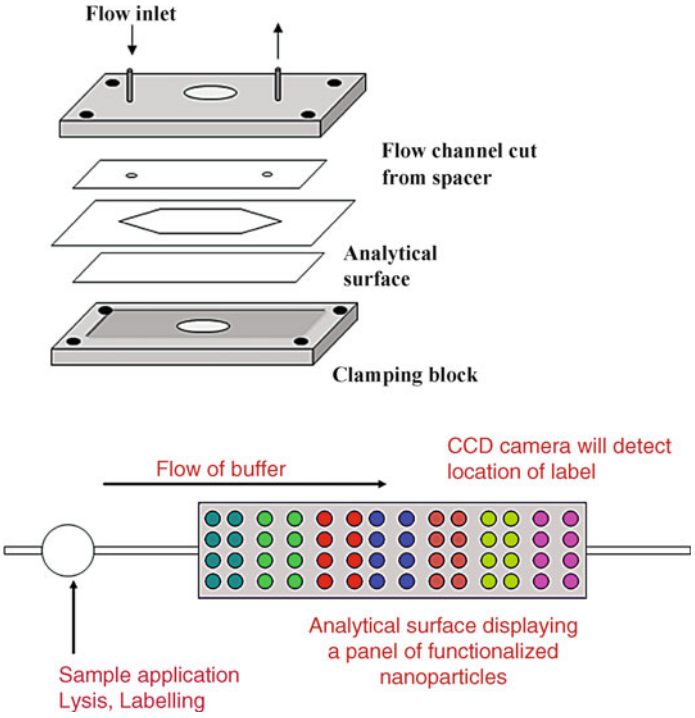

Fig. 11.6 *Schematic of the thin-layer biosensor design* (Adapted from [18] with permission from Elsevier, © 2005)

redox steps. In order for this sequence to have a chance to occur, the various enzymes engaged in the shuttle must be strategically positioned on the mitochondrial membrane surface with minuscule distances between producer and consumer. In order to maximize the productivity of coupled enzyme systems, like the ones in e.g., the Citric Acid Cycle, it is not enough to have the various catalysts free in solution in arrangements where intermolecular distances may be micron sized or more. Rather, one should strive for the Ångström-to-nm sized distances characteristic for living tissue and similar to those that can be obtained through controlled attachment to nanoparticles (It might be of interest in the present context to consider that the diameter of a more or less round liver mitochondrion is about 1 micron, i.e., four times the diameter of the PS latex particles frequently used in this study).

There are a great number of requirements put on a microfluidic device for sensing, as is illustrated in Fig. 11.6 [19]. Reaction chambers have to be minimized in number as well as in volume, reagents have to be stored on the device in a form that allows dispensing upon command, the analyte has to be transported into the reaction chamber in a reproducible fashion and there be able to bind the reading element in a manner that gives rise to a readable signal and, finally, the signal has to be read in triplicate, in parallel with similar maneuvers for calibrants. The entire arrangement has to have a shelf-life of at least a year.

In our study the first issue concerned the signal generation. A system was selected that was built around the enzyme pyruvate kinase, which would be made to bind to the analyte via an antibody or a specially designed peptide binder [20].

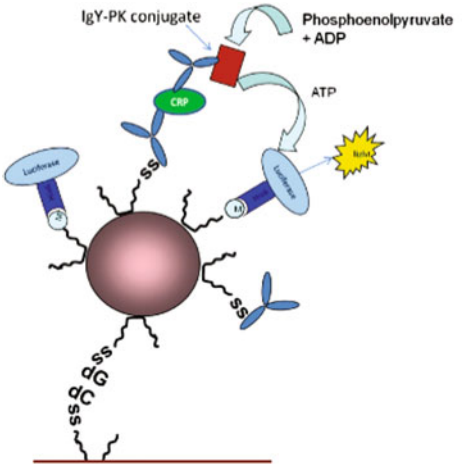

Surface conc. of:	*g / PS*	*Molecules / PS*	*mg / m2*
F108-PDS / NTA	$3.94 * 10^{-16}$	16250	2.18
dG	$8.48*10^{-18}$	1000	0.05
IgY	$4.32*10^{-17}$	145	0.24
Luciferase	$2.66*10^{-17}$	240	0.15

Fig. 11.7 *Light emitting sensor construct*. A PS core particle is decorated with Pluronic F108 to which are attached oligonucleotides for surface fixation, analyte capture molecule (e.g., antibody), and chelate-coupled luciferase for signal generation. The amounts of each, as determined by SdFFF, are given in the Table

The same capturing system was attached to 240 nm polystyrene particles, decorated in analogy with the particles in Fig. 11.3. The kinase was then immersed in a mixture of phosphoenol pyruvate and ADP, from which it produced ATP. Furthermore, the capturing particles also contained the enzyme luciferase, which produced sharp light pulses upon contact with ATP in the presence of luciferin. This substrate was packaged to surround the capturing particles, and the entire reaction sequence was optimized with the help of SdFFF, which kept a close tab on the number of capturing entities needed per particle in order to arrive at a readable signal. The idea was to let a sensitive mobile phone camera picture the luminescent surface and make possible a direct transmission of the image to a physician for simple distant diagnosis [19]. Regrettably, the design was never brought to market, but the small binder was attached to the capture particles in adequate numbers, so that these particles were found to contain on the average 240 luciferase molecules per particle. Given the number of particles per unit surface area that were observed in a preliminary study [18], the generated light intensity was considered to be easily detectable with a sensitive CCD device (Fig. 11.7).

11.8 Conclusion

Recent developments of diagnostic systems are to a large extent based on multifunctionalized nanoparticles, due to their small size and relative ease of handling [21–23]. Whenever a particle-based analytical system is being designed there is a general need to identify methods that allow quantification of the various functionalities that are built into the system. As shown in the present chapter, sedimentation FFF offers an unusually precise and accurate method for determining the mass of both the core particles as well as of their various designed shells, so that the designer can convince himself of the optimal nature of his design.

References

1. Calvert P (1999) Nanotube composites: a recipe for strength. Nature 399:210–211
2. Tenne R (2006) Inorganic nanotubes and fullerene-like nanoparticles. Nat Nanotechnol 1:103–111
3. Klein J (2007) Probing the interactions of proteins and nanoparticles. PNAS 104 (7):2029–2030
4. Gaumet M, Vargas A, Gurny R, Delie F (2008) Nanoparticles for drug delivery: the need for precision in reporting particle size parameters. Eur J Pharm Biopharm 69(1):1–9
5. Baptista P, Pereira E, Eaton P, Doria G, Miranda A, Gomes I, Quaresma P, Franco R (2008) Gold nanoparticles for the development of clinical diagnosis methods. Anal Bioanal Chem 391:943–950
6. Ratanathanawongs Williams SK, Runyon JR, Ashames AA (2011) Field-flow fractionation: addressing the nano challenge. Anal Chem 83(3):634–642

7. Schure MR, Schimpf ME, Schettler PD (2000) Retention – normal mode. In: Schimpf M, Caldwell K, Giddings JC (eds) Field-flow fractionation handbook. Wiley, New York, pp 31–48
8. Caldwell KD, Li J-M, Li J-T, Dalgleish D (1992) Adsorption behavior of milk proteins on polystyrene latex: a study based on sedimentation field-flow fractionation and dynamic light scattering. J Chromatogr 604:63–71
9. Li J-T, Caldwell KD (1991) Sedimentation field-flow fractionation in the determination of surface concentration of adsorbed materials. Langmuir 7:2034–2039
10. Beckett R, Ho J, Yang J, Giddings JC (1991) Measurement of mass and thickness of adsorbed films on colloidal particles by sedimentation field-flow fractionation. Langmuir 7:2040–2047
11. Langwost B, Caldwell KD (1992) Solid phase immune reactions as monitored by sedimentation field-flow fractionation. Chromatographia 34:317–324
12. Lee J, Martic PA, Tan JS (1989) Protein adsorption on pluronic copolymer-coated polystyrene particles. J Colloid Interface Sci 131:252–266
13. Lee JH, Kopecek J, Andrade JD (1989) Protein resistant surfaces prepared by PEO-containing block copolymer surfactants. J Biomed Mater Res 23(3):351–368
14. Jeon SI, Andrade JD (1992) The steric repulsion properties of polyethylene oxide. Bull Korean Chem Soc 13(3):245–248
15. Carlsson J, Drevin H, Axén R (1978) Protein thiolation and reversible protein-protein conjugation. N-Succinimidyl 3-(2-pyridyl dithio) propionate, a new heterobifunctional reagent. Biochem J 173(3):723–737
16. Ho C-H, Limberis L, Caldwell KD, Stewart RJ (1998) A metal-chelating pluronic for immobilization of histidin-tagged proteins at interfaces: immobilization of firefly luciferase on polystyrene beads. Langmuir 14:3889–3894
17. Andersson M, Elihn K, Fromell K, Caldwell KD (2004) Surface attachment of nanoparticles using oligonucleotides. Colloids Surf B Biointerfaces 34:165–171
18. Fromell K, Andersson M, Elihn K, Caldwell KD (2005) Nanoparticle decorated surfaces with potential use in glycosylation analysis. Colloids Surf B Biointerfaces 46:84–91
19. Fromell K (2007) Nanoscale reaction systems. Dissertation, nr. 350 from the Faculty of Science and Technology, Acta Universitatis Upsaliensis, p 11
20. Tegler LT, Nonglaton G, Buettner F, Caldwell K, Christopeit T, Danielson UH, Fromell K, Gossas T, Larsson A, Longati P, Norberg T, Rampanicker R, Rydberg J, Baltzer L (2011) Powerful protein binders from designed polypeptides and small organic molecules – a general concept for protein recognition. Angew Chemie – int'l ed 50(8):1823–1827
21. Borchars K, Weber A, Brunner H, Tovar GEM (2005) Microstructured layers of spherical biofunctional core-shell nanoparticles provide enlarged reactive surfaces for protein microarrays. Anal Bioanal Chem 383:738–746
22. Sanchez-Martin RM, Alexander L, Bradley M (2008) Multifunctionalized biocompatible microspheres for sensing. Ann N Y Acad Sci 1130:207–217
23. Graham D, Faulds K, Thompson D, McKenzie F, Stokes R, Dalton C, Stevenson R, Alexander J, Garside P, McFarlane E (2009) Functionalized nanoparticles for bioanalysis by SERRS. Biochem Soc Trans 37:697–701

Chapter 12
Starch and Other Polysaccharides

Lars Nilsson

Abstract Polysaccharides constitute one of the major groups of biological macromolecules and they include some of the most abundant macromolecules in nature. In this chapter instrumental considerations when analyzing polysaccharides with flow field-flow fractionation (flow FFF) are briefly discussed. Furthermore, an overview of characterized properties is given with special attention to multi angle light scattering. Included is an extensive review of literature on applications regarding flow FFF and polysaccharides.

Keywords Cellulose • Field-flow fractionation • Gums • Light scattering • Macromolecules • Polymers • Polysaccharides • Starch

12.1 Introduction

Polysaccharides constitute one of the major groups of biological macromolecules and they include some of the most abundant macromolecules in nature such as chitin, cellulose and amylopectin. A wide range of chemical structures can be found. The latter being dependant on the type of sugar monomer, glycosidic linkage and the presence of non-carbohydrate moieties in the macromolecule. Polysaccharides, naturally, play an important role in many biological systems as structuring, barrier and energy reserve molecules. Aside from the obvious nutritional importance of for instance starch and dietary fiber, polysaccharides are also important for many applications which can be found within the food, pharmaceutical, paper, coatings and other industries.

Polysaccharides are macromolecules that are inherently polydisperse which, together with their sometimes huge molar mass, can put great demands on the

L. Nilsson (✉)
Department of Food Technology, Engineering and Nutrition, Lund University, Lund, Sweden
e-mail: Lars.Nilsson@food.lth.se

S.K.R. Williams and K.D. Caldwell (eds.), *Field-Flow Fractionation in Biopolymer Analysis*, DOI 10.1007/978-3-7091-0154-4_12,

methods of characterization. Branching and self-association are other properties that further complicate the characterization work. Asymmetrical flow field-flow fractionation (AsFlFFF or AF4) is a powerful and highly suitable separation technique for the characterization of polysaccharides. The method's suitability for these applications is due to its large size range (approximately 2 to >800 nm), its mild separation conditions (i.e., low shear forces) and that filtering of samples is often not required prior to injection onto the separation channel. However, in order to obtain accurate and reliable information about molecular properties, as for instance molar mass (M), root-mean-square radius (r_{rms}) and conformation, it is a necessity to utilize adequate detection such as multi-angle light scattering (MALS). The suitability of AsFlFFF for the characterization of polysaccharides was demonstrated for dextran and hyaluronic acid by Wahlund et al. [1] Some early works showing the strength and possibilities of combining Flow FFF with MALS for polysaccharides were reported for symmetrical flow FFF [2, 3] and for AsFlFFF [2]. Due to the large size range that AsFlFFF is able to fractionate it is also possible to characterize samples containing super molecular aggregates. Naturally, the distinction between molecular species and aggregates can be very difficult if not impossible. However, it is possible that such distinctions can be made utilizing AsFlFFF-MALS as has been shown for aggregates of casein micelles.[3] The possibility to be able to do such distinctions would indeed be desirable for polysaccharides which are prone to aggregation in aqueous environments.

12.2 Instrumental Considerations When Analyzing Polysaccharides

12.2.1 Choice of Membrane

Several types of membrane material are commercially available. A suitable material for the analysis of polysaccharides is typically regenerated cellulose or other similar materials. If analysis under conditions utilizing, for instance, carrier liquids at high pH such materials are, however, unsuitable and membranes withstanding such harsh conditions must be selected. The potential adsorption of non-surface active polysaccharides at the membrane are sometimes discussed, especially in conjunction with poor mass recoveries from the separation channel [4]. This has, however, at present not been thoroughly investigated and such assumptions should be handled with care.

12.2.2 Validation of Separation Channel Performance

It is recommended that the performance of a newly assembled channel be verified before analysis of samples commences. This can typically be performed by

injecting a small amount of a water soluble dye, sufficiently hydrophilic to not adsorb strongly at the membrane surface. In the case of cellulose based membranes a suitable dye is bromophenol blue (BPB) in aqueous solution at pH 6.5 [5]. The dye should be injected during elution with a constant cross-flow and migrate along the center of the channel following a straight line. If deviations in the flow pattern are observed this can indicate a damaged membrane, flow obstructions, leaks etc. The focusing point in the channel can be checked by injecting the same dye during focusing; a colored macromolecule such as dextran blue can also be utilized. Finally, it is good to validate the performance of the system with a standard sample which may be a protein, a standard polysaccharide (such as pullulan or dextran) or a small colloidal particle.

12.2.3 Carrier Liquids

For neutral polysaccharides, in an aqueous environment, a carrier liquid consisting of dilute electrolyte (such as $NaNO_3$) with added NaN_3, to prevent microbial growth, is most of the time suitable. As for most applications pure water is not advisable to use as any electrostatic interaction acting during separation will become long range at such low ionic strength. This may, in turn, cause disturbances in the elution of sample components and poor reproducibility. The Debye length (κ^{-1}) [6] can be considered as the distance over which significant electrostatic interaction occurs and is given by

$$\kappa^{-1} = \sqrt{\frac{\varepsilon_r \varepsilon_0 k_B T}{2 N_A e^2 \cdot \frac{1}{2} \sum_{i=1}^{n} c_i z_i^2}} \tag{12.1}$$

where ε_r is the relative dielectric permittivity of the solvent, ε_0 is the dielectric permittivity of vacuum, k_B is the Boltzmann constant, T is the temperature, N_A is the Avogadro number, e is the elementary charge, c_i is the concentration (mol/m^3) of ion i and z_i is the valence of ion i. For comparison, κ^{-1} is about 3 nm in a 10 mM $NaNO_3$ solution (Fig. 12.1) which means that any weak electrostatic interaction present will be short ranged and, thus, is unlikely to influence the elution of sample components. For charged polysaccharides, higher ionic strengths in the carrier liquid may be necessary. It should be noted that this can, of course, influence the size and conformation of macromolecules [7]. An important consideration regarding ionic strengths of carrier liquids for the analysis of charged macromolecules is the dependence of the second virial coefficient, B_2, on the ionic strength, i.e., intermolecular interaction. In a study concerning diffusion of DNA (i.e., a polyelectrolyte), Ferrari et al. studied the influence of ionic strength on the diffusion coefficient, D [8]. The authors showed that B_2 decreased rather sharply with increasing ionic

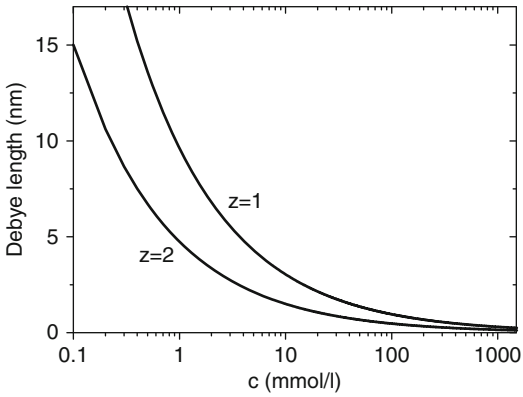

Fig. 12.1 The Debye length (κ^{-1}) versus salt concentration (c) for symmetric mono (z = 1) and divalent (z = 2) salts

strength indicative of less repulsion between molecules. Consequently, D had a strong dependence on DNA concentration at rather low ionic strength (at 10 mM NaCl, an increase in DNA concentration from about 12–17 mg/mL lead to a three fold increase in D). However, at an ionic strength above 0.05 M the obtained D values appeared stable. These are important factors to consider in the selection of carrier liquid ionic strength as one could expect differences in the apparent D for molecules of the same size. As there would be species of the same size with different apparent D, this would lead to increased peak-tailing because species with lower apparent D elute later. This phenomenon can be observed experimentally for anionic polysaccharides [9, 10] and can also contribute to tailing observed for cationic polysaccharides, although the latter can be further complicated by membrane-sample attraction.

12.2.4 Choice of Injected Amount and Flow Conditions

The amount injected onto the channel needs to be optimized in order to assure that overloading is eliminated or minimized and that sample components are eluted in normal mode. This is especially important if accurate data, such as diffusion coefficients, are to be obtained from the elution times. The optimization is straightforwardly performed by injecting various amounts of sample for which the retention time should be constant if elution occurs in normal mode. In Fig.12.2 examples of overloading in amylopectin fractionations are shown, illustrated by elution times which are dependent on injected amount and peak asymmetry.

Due to the high polydispersity of polysaccharides it is often beneficial to utilize programmed cross-flows (V_c) which decay in some suitable manner that optimizes selectivity over the entire size distribution. Common decays are linear and exponential but other decays such as stepwise decay and power programmed decay [12] are also utilized. The flow profiles for the above defined cross flows are shown in Fig.12.3. The employment of programmed fields for the separation of

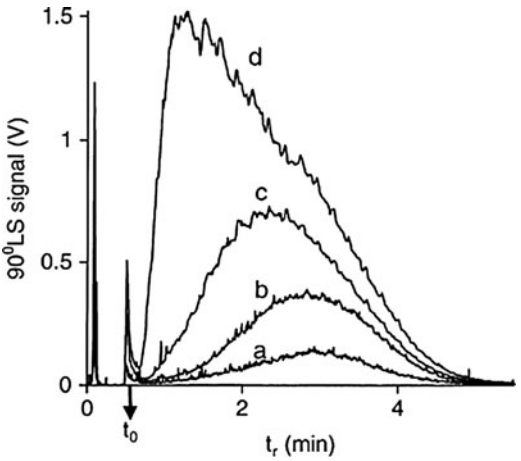

Fig. 12.2 Study of overloading in amylopectin analysis with AsFlFFF-MALS. Injected amounts: (a) 0.2 µg, (b) 0.5 µg, (c) 2 µg and (d) 5 µg (Reprinted from [11], © 2001, with permission from Elsevier)

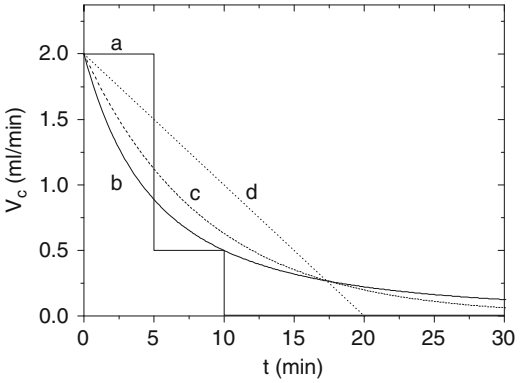

Fig. 12.3 Flow profiles for programmed cross flows expressed as cross flow (V_c) versus time (t). (a) step-wise decay, (b) power programmed decay, (c) exponential decay and (d) linear decay

macromolecules has been reported by several authors [13–15]. However, studies dealing with the basis for choosing a specific type of programmed cross-flow are scarce. Leeman et al. have investigated the suitability of different programmed cross-flows for the analysis of starch and cellulose derivatives utilizing pullulan standards [14]. The authors found that constant cross-flows did not result in satisfactory fractionation of the samples which was, however, accomplished using programmed cross-flows. By comparing different programmed cross-flows (i.e., linearly and exponentially decaying cross-flows) it was found that exponentially decaying cross-flows gave higher molar mass selectivity for high molar mass fractions. This was at the expense of only a minor decrease in selectivity for low molar mass fractions. Furthermore, no benefits were observed by having an initial constant cross-flow during elution, which then decayed. The authors observed rather large differences for late eluting pullulan estimated and observed retention times. The secondary relaxation effects are expected to be more pronounced for larger components [16, 17]. However, they should also be more pronounced for rapidly decaying cross flows, which was not observed. A possible explanation is

that the large components are forced so close to the accumulation wall at the beginning of elution that they are practically immobilized until the cross flow is decreased [13] which, together with the secondary relaxation effects, could explain the observations.

12.3 Preparation of Samples for Analysis

The aqueous dissolution of various polysaccharides can sometimes prove to be a demanding task. The difficulties encountered have different contributions as they suffer both from kinetic contributions and the fact that water is not necessarily a good solvent for the macromolecules. Many polysaccharides, such as starch, galactomannan gums and β-glucans, are well known as being difficult to dissolve. Dissolution procedures typically evolve around utilizing elevated temperatures, high pH, organic solvents (such as dimethylsulphoxide, DMSO), addition of salts (such as LiBr) etc. Table 12.1 shows an overview of methods, reported in the literature, for starch dissolution.

A problematic contribution to selecting a dissolution procedure is that there seems to be no or little comparison between different methods in the literature and, hence, a great demand for such studies to be undertaken exists. An important issue is, naturally, whether harsh conditions such as elevated temperatures and high pH will cause degradation. The dissolution process is schematically illustrated in Fig. 12.4. Thus, part of the difficulties stem from choosing conditions which result in dissolution but do not cause degradation. Another difficulty is the determination

Table 12.1 Examples of dissolution conditions for starches from the literature

Dissolution method (aqueous solutions)	Temperature (°C)	Time (min)	Note	Reference
Boiling	100	30	[a]	[18]
Microwave heating	143–211	0.6–1.5	[a]	[19]
	–	1.5		[20]
Autoclaving/pressure cooking	175	20–60		[21]
	–	30	[a]	[22]
	121	20	[a]	[4]
Jet cooking	110–140	–	[b]	[7]
Dissolution in non-aqueous solvents				
MSO	≈20–121	15–1440		[23]
	70	≈1000		[24]
	37–80	1–500		[25]
DMSO/LiBr	80	≥120		[26]
	90–120	60–480		[27]
N,N-dimethylacetamide/LiBr			[c]	[28]
1-butyl-3-methylimidazolium chloride	100	60		[29]

[a]Pre-treatment with DMSO at various conditions
[b]Cationically modified starch
[c]Step wise dissolution: 1. 150°C, 1 h; 2. 100°C, 1 h; 3. 50°C overnight

Fig. 12.4 Schematic illustration of a dissolution process of polysaccharides

of whether degradation has occurred as, for instance, a low degree of degradation of large macromolecules may be very difficult to detect.

12.4 Characterized Properties

12.4.1 Root-Mean-Square Radius and Molar Mass

The molecular properties obtained from analyses with AsFlFFF depend on the detectors utilized. Diffusion coefficient (D) and, hence, hydrodynamic radius (r_h) can be obtained directly from elution times from the channel but determination of molar mass requires the use of suitable detectors. Light scattering is one of the few methods with which direct molar masses can be obtained without calibration against molar mass standards or by assumptions regarding scaling between mass and size. Thus, it is a powerful tool for the characterization of samples fractionated by AsFlFFF. The most commonly used detectors are multi-angle light scattering (MALS) detectors which detect the scattered intensity at different angles in relation to the incoming light. A full treatise on light scattering is beyond the scope of this chapter and readers are referred to textbooks on the subject [30–32]. The obtained light scattering data is fitted to different models of which the Debye [33], Zimm [34, 35] and Berry [36] models are the most commonly utilized [37]. Basically, the models allow the determination of the rms radius (r_{rms}), also referred to as the radius of gyration (r_g), from the slope of a curve fitted to the angular dependence of the scattered light. Provided the refractive index increment with concentration (dn/dc) is known for the substance and a concentration detector is used, the molar mass can be determined from the intersection of the fitted curve. The selection of model is not necessarily straight forward. A comprehensive investigation regarding the suitability of the different models for different types of macromolecules has been performed by Andersson et al. [37]. In this work the authors showed that for relatively small scattering species ($r_{rms} < 50$ nm) the error in M is less than 1% regardless of which model is employed. However, for larger scattering objects the choice of method is more critical in order to obtain accurate results. It was also shown that higher order polynomial fitting gave more accurate fits but at the expense of robustness as they are more sensitive to errors in individual data points. As a general recommendation the authors suggested that for an unknown sample the utilization of low angle data, plotted with the Berry method, is preferable as good accuracy is obtained in both M and r_{rms} without using higher order polynomial fits.

12.4.2 Diffusion Coefficient and Hydrodynamic Radius

As separation in AsFlFFF occurs based on diffusion coefficient (D) of sample fractions, D can be determined from elution times. From D the hydrodynamic radius (r_h) can be obtained through the Stokes-Einstein equation [38]. The calculation of D from elution times becomes more complicated when utilizing programmed cross-flows, compared to constant cross-flows, as V_c is a function of both time and the position along the separation channel. Furthermore, the so-called secondary relaxation effects [39] may distort results as the field is continuously decaying causing sample components to migrate to new equilibrium distances from the accumulation wall. Hence, the concentration profile in the separation channel may lag behind the equilibrium distance if the field decays rapidly and/or diffusion of fractions is slow. For rectangular channels the calculation of D can be performed analytically [13]. However, for trapezoidal channels, which are common today, the equations for the calculation of D need to be solved numerically [40]. Recent findings have shown that good accuracy can be obtained by using the approach by Nilsson et al. [41] Errors are typically about a few percent but do increase rapidly when steeper time gradients in V_c are employed i.e. if accurate determination of D and r_h is desirable, steeply decaying functions for V_c should be avoided. This behavior is of a more general character for field-flow fractionation and has been observed in earlier studies [17, 42]. In-house made Matlab based software, for the calculation of r_h and other conformational properties, is available from the author upon request.

12.4.3 Conformation and Shape

Several macromolecular conformation measures can be obtained from AsFlFFF-MALS. A commonly used conformational measure is [43]

$$r_{rms} = kM^{\gamma} \tag{12.2}$$

and by plotting the logarithm of r_{rms} versus the logarithm of the molar mass, γ can be obtained as the slope of the plot. For a sphere $\gamma = 0.33$, for a rod γ is closer to 0.5 and for a random coil macromolecule $\gamma = 0.5 - 0.6$. The approach can be useful to distinguish between different conformations within the distribution obtained from the AsFlFFF. A drawback can sometimes be that if somewhat noisy data is processed γ will be rather sensitive to errors.

Another interesting conformational parameter is the ratio between r_{rms} and r_h. As discussed above, r_h can be readily obtained from AsFlFFF elution times. The ratio can give valuable information about conformation and shape of the macromolecules. For a solid, smooth sphere (i.e., r_h is identical to the geometrical radius) the ratio is equal to 0.775. Typical ratios for macromolecules are between

1 and 2 and ratios >2 generally indicate an anisotropy in the molecules i.e., more elongated conformations. Ratios <0.7 typically represents highly swollen macromolecules or "micro gels"[44]. In Table12.2 both theoretical and experimental values of r_{rms}/r_h from literature can been found. In a similar way as for γ, r_{rms}/r_h can be used to distinguish between different conformations present within the size distribution. Furthermore, r_{rms}/r_h has been proposed as a means of distinguishing between aggregates and non-aggregates in a population [3].

The apparent density over a size distribution can be obtained by calculating it from M and radii data, utilizing either r_{rms} or r_h as

$$\hat{\rho}_{rms,i} = \frac{M_i}{V(r_{\mathrm{rms}})_i} \cdot \alpha \quad or \quad \hat{\rho}_{h,i} = \frac{M_i}{V(r_{\mathrm{h}})_i} \tag{12.3}$$

Table 12.2 Calculated values for r_{rms}/r_h for different objects and experimental results from literature

Object	r_{rms}/r_h		Reference
Homogeneous sphere	0.775		
Rod			
Axial ratio = 25	2.1		[45]
Axial ratio = 100	2.8		[45]
Random coil, linear chain			
θ-conditions	1.50		[46]
Good solvent	1.78		[46]
Randomly branched polymer	1.73		[47]
Hyper branched polymer	1.23		[47]
Experimental results	r_{rms}/r_h	M range (10^6 g/mol)	Reference
Starch	1.0–1.8	0.07–100	[48]
Amylose	1.64–2.20	0.02–1.0	[49]
Amylopectin	1.02–1.29	78–270	[50]
Glycogen	0.4–1.5	1.9–35.9	[51]
Pullulan	1.1–1.5	0.15–0.9	[52]
	1.62–1.86	0.17–0.9[a]	[53]
Dextran	1.3–1.7	0.03–0.7	[52]
	1.00–1.27	0.013–2.66[a]	[54]
Non-ionic cellulose derivatives	1.71–2.64	0.23–5.0[a]	[55]
Xanthan Gum	2.17–2.95	1.37–2.94[a]	[56]
κ-Carrageenan (coil)	1.96	0.01–4	[57]
	1.65	0.31[a]	[58]
Alginate	1.1–2.5	0.06–1.0	[59]
Gum arabic	0.6–1.0	2–10	[60]
	1.0–3.0	0.15–30	[61]
Mesquite gum	1.7–3.0	1.5–5.0	[61]
Polyvinylacetate microgels	0.54–0.60	32–423	[44]

[a]Weight-average molar mass (M_w) or range of M_w

where M_i is the molar mass of fraction i, V_i is the volume of fraction i and α is given by Eq. 12.4 where r is the geometrical radius of a sphere.

$$\alpha = \frac{V_{\text{sphere}}(r_{\text{rms}})}{V_{\text{sphere}}(r)} = \frac{r_{\text{rms}}^3}{r^3} = \frac{\left(\sqrt{3/5}\cdot r\right)^3}{r^3} = \left(\frac{3}{5}\right)^{\frac{3}{2}} \tag{12.4}$$

Although being an apparent property it describes the distribution of mass in volume for the fractions and, thus, provides additional information about scaling in a macromolecular population. The apparent density also, indirectly, describes the apparent volume of the molecules. Thus, it may be considered to influence fundamental parameters such as the overlap concentration of macromolecules, i.e., the concentration where transition from dilute to semi-dilute solution occurs and solution viscosity starts to be strongly dependent on macromolecule concentration. Such a relationship has been shown for starch. [62] The apparent density is also linked to the branching density as highly branched macromolecules are expected to display a higher density than less branched molecules. Consequently, glycogen which is an $\alpha(1\text{-}>4)$ glucan with $\alpha(1\text{-}>6)$ linked branches and a degree of branching (DB) of 0.07–0.1 displays considerably higher apparent densities than amylopectin [51], which is also an $\alpha(1\text{-}>4)$ glucan with $\alpha(1\text{-}>6)$ linked branches although with lower DB (approximately 0.05) [63, 64].

Another useful way of processing light scattering data in order to obtain conformational data from the angular dependence of the scattered light is by the creation of a Kratky plot [65, 66], which requires high quality in the light scattering data [67]. The angular variation in the scattered light is described by the relationship

$$\frac{R_\theta}{Kc} = M_w \cdot P(u) \tag{12.5}$$

where R_θ is the excess Rayleigh ratio, K is an optical constant, M_w is the weight-average molar mass and $P(u)$ is the scattering function. The Kratky plot is created by plotting $u^2P(u)$ as a function of u defined as

$$u = q \cdot r_{rms} = \frac{4\pi n_0 \sin(\theta/2)}{\lambda_0} \cdot r_{rms} \tag{12.6}$$

where q is the scattering vector, n_0 is the refractive index of the solvent, θ is the scattering angle and λ_0 is the wavelength of the incident light. At low θ and for small objects $P(u) = 1\text{–}u^2/3$ while for larger objects $P(u)$ becomes increasingly dependent on structure and shape of the scattering macromolecule. The obtained experimental results plotted in this way are typically compared to theoretically calculated plots for differently shaped and structured macromolecules. In general, Kratky plots are useful for the characterization of macromolecules with $r_{\text{rms}} \geq 100$ nm and can for instance be a useful tool for detecting the presence of

branches in a molecular structure. [46] Kratky plots have been constructed from AsFlFFF-MALS data for the characterization of amylopectin [68], cationically modified amylopectin [7], as well as cellulose derivatives [69].

12.5 Starch, Starch Derivatives and Glycogen

AsFlFFF is one of a few separation methods that are well suited for the analysis of starches due to their high polydispersity and large size. Starch is a mixture of two macromolecules: amylopectin (branched) and amylose (largely unbranched). Amylopectin consists of α(1 → 4) linked glucose units and α(1 → 6) linked branches while amylose consists mainly of α(1 → 4) linked glucose units, but low amounts of α (1 → 6) branches can also be present [70]. The amylose/amylopectin composition of starch can vary widely but is commonly about 20–30% amylose. When discussing the separation and characterization of starches a distinction should be made between natural starches (sometimes referred to as "native starches") and those that have been modified chemically, enzymatically etc. The reason for the distinction is that separation and characterization of such substances can be considerably different compared to natural starches as modification often results in partial degradation. Studies on native starches were reported by van Bruijnswort et al. [11], utilizing AsFlFFF-MALS, Roger et al. [71] and You et al. [4], utilizing symmetrical FlFFF-MALS. These early studies displayed some of the difficulties that could be encountered with starch fractionation as for instance the sensitivity to overloading [11]. Roger et al. studied corn starch with varying amylose content and reported high recoveries (84–100%) using an initially constant crossflow which then decayed stepwise [71]. The authors found a fraction eluting close to the void peak (identified as amylose) and a late eluting, rather tailing, peak identified as amylopectin. No repeatability of the results was reported. The authors attempted to quantify the amount of amylose from an integrated RI-signal which was then compared to results obtained with iodine binding capacity (IBC). The values from the integrated RI-signal were higher than those from IBC and the deviation increased considerably when the amylose content increased. No size data could be obtained for the amylose peak as the MALS-signal was too weak. You et al. showed that efficient separation of barley starch amylose and amylopectin could not be achieved by applying constant cross-flows [4]. Hence, samples were analyzed using a cross flow profile with an initially higher cross flow which was then abruptly decreased to a low cross flow under which the remaining sample components were eluted. Rather low recoveries of about 70% were reported and attributed to extensive retention of amylopectin in the separation channel as recoveries decreased to about 50% when zero amylose barley starch was analyzed.

Rolland-Sabaté et al. performed an extensive study of amylopectins from various botanical sources utilizing AsFlFFF-MALS and linearly decaying cross flows [68]. The purpose of the study was to investigate branching and structure in

the various amylopectins which was performed with a comprehensive treatment of light scattering data. The authors found that it was impossible to discriminate between different amylopectins utilizing Kratky plots (discussed earlier in this chapter). Rather, fractal dimensions were determined from light scattering data which has the possible benefit that through such results obtain structural features free of M and r_{rms}. Shrinkage factors were determined for the amylopectins by comparing the rms radii for the branched (amylopectin) and corresponding linear macromolecule (amylose) enabling the acquisition of branching data. The authors observed peak distortions when the channel membrane supplier was changed which was attributed to sample adsorption at the membrane. Furthermore, the channel became more sensitive to overloading effects. This could indicate that the problem has contributions due to variations in channel thickness, w, illustrating the importance of adequate calibration of channel height [72] and validation of channel performance using standard proteins, polymers or particles. Rojas et al. have reported results for the characterization of waxy barley starch (6% amylose) [62]. The purpose of the study was the determination of influence of high-pressure homogenization on the molecular properties of the starch. Degradation was observed, the extent of which depended on the homogenization pressure. Drastic changes in conformation and apparent densities were observed. The apparent densities increased and the molecules appeared to have more spheroidal shapes (as represented by changes in r_{rms}/r_h) after homogenization. The results from the AsFlFFF-MALS analyses were compared to capillary viscometry and increases in apparent densities were reflected in increases in the overlap concentration, c*.

A number of different starch derivatives have been studied with AsFlFFF-MALS. These include hydroxypropyl and hydroxyethyl starch (HPS and HES) [73], octenyl succinic anhydride (OSA) starch [40, 74, 75], cationic starch [7, 76, 77] and carboxymethyl (CMS) [10]. The potential for rapid separation of starch derivatives was clearly shown by Wittgren et al. [73] The influence of high-pressure homogenization, a common process in the formation of emulsions, on the molecular properties of OSA starch (from waxy barley origin) has been reported. The authors found that homogenization caused a disruption of the macromolecules. Furthermore, dramatic effects on conformational properties, manifested by changes in apparent densities and r_{rms}/r_h, could be observed. The molar mass of the molecules decreased, apparent densities increased and r_{rms}/r_h decreased leading the authors to suggest a "hairy tennis ball" conformation as a result of high-pressure homogenization. The implications could be that the treatment may increase the surface activity of the material which would be beneficial as the substance is utilized as an emulsifier. The selective adsorption of ultra-high molar mass components from OSA starch, during emulsification, could also be quantified using AsFlFFF-MALS a task which would not have been feasible with other existing techniques [75]. Although bearing charges, the OSA starch should be considered a weak polyelectrolyte as the degree of substitution, for food applications, is low ($DS = 0.008 - 0.022$) [64]. However, for more densely charged starch derivatives fractionation can be expected to be more

demanding, especially if the charges are cationic in which case attractive interactions can be expected with, for instance, channel membranes. Lee et al. have analyzed cationically modified potato amylopectin (CPAP) [76]. In this study it was shown that peak tailing increases with increasing cross flow rate, indicating that it is desirable to keep cross flow rates as low as possible in order to minimize unfavorable attractive interaction between sample components and the channel membrane. However, a trade off may be involved as this may lead to loss in retention and, thus, resolution. Increasingly distorted peaks with increasing cross flow rates was also observed by Krentz et al. who studied highly substituted cationic starches (DS = 0.28 − 1.48) [77]. Modig et al. further investigated the influence of ionic strength and jet cooking temperature on the fractionation of CPAP and found that the recovery was 93–97% using carrier liquids with concentration $\geq$ 50 mM $NaNO_3$ while the recovery with 10 mM $NaNO_3$ was about 77% [7]. Lee et al., similarly, observed that peak tailing was substantially decreased when the salt concentration in the carrier liquid was increased to 50 mM $NaNO_3$ for the analysis of CMS [10] utilizing power programmed decaying cross flows [78]. The minimization of the unfavorable electrostatic interaction can be viewed in light of the Debye length [6] as shown in Fig. 12.1. The screening length dependence on salt concentration is quite weak above 50 mM of a salt with charge ratio 1:1. Hence, as shown by Modig et al. [7] and Lee et al. [10, 76], further minimization of unfavorable attraction is not necessarily obtained at higher concentrations. An approach may be to utilize ions with higher valence as the Debye-Hückel screening length depends strongly on ionic valence (Eq. 12.1).

Glycogen, the energy storage polysaccharide in animals, has a similar chemical structure to amylopectin however the branching density is higher: DB is approximately 0.07–0.1 as determined by ^{1}H-NMR. Fernandez et al. analyzed glycogen extracted from tissue from various animal sources with AsFlFFF-MALS [51]. The results showed that the average apparent densities were substantially higher (26–260 kg/m^3) than those found for barley amylopectin [62] (about 5 kg/ m^3). The glycogen samples also displayed a rather large difference in r_{rms}/r_h varying both between samples as well as over the respective size distribution. Values for r_{rms}/r_h stretched between those corresponding to branched polymers in good solvent to micro gels. In the study by Rolland-Sabaté et al. of amylopectins from various sources, discussed above, a commercially available glycogen was included as comparison to amylopectin [68].

12.6 Cellulose Derivatives

Cellulose is a linear chain of $\beta(1 \rightarrow 4)$ linked glucose units which is commonly chemically derivatized to yield a range of substances which are widely used in many applications. Comprehensive work with AsFlFFF has been performed on cellulose derivatives including hydroxypropylmethyl cellulose (HPMC) [2, 79],

hydroxypropyl cellulose (HPC) [14, 80], hydroxyethyl cellulose (HEC) [80], ethylhydroxyethyl cellulose (EHEC) [69, 81] and carboxymethyl cellulose (CMC) [82, 83]. Wittgren et al. illustrated the importance of optimizing experimental conditions, such as flow rates and injected amounts, in order to assure adequate analysis of modified celluloses [2]. Large injected amounts lead to underestimations of polydispersity and lower observed molar mass of a given sample which was attributed to a loss in size separation ability. The injected amounts also influenced the recovery which was >85% when the injected amount < 100 μg and decreased to <50% when the injected amount was 240 μg. Furthermore, high cross flow rates led to decreased recoveries. Andersson et al. detected an ultra-high molar mass (UHM) fraction in EHEC in separations performed utilizing constant cross flows (similarly to Wittgren et al. [2]) and emphasized the possibly beneficial effects of using decaying cross flow gradients [81]. The properties of the ultra-high molar mass component were further investigated in a later paper [69]. From Kratky plots and log r_{rms} versus log M plots it was shown that the UHM fraction had a denser structure and considerably different conformational properties than the lower molar mass material. These findings together suggest that the UHM fraction consists of supra molecular aggregates.

12.7 Dextran and Pullulan

Dextran is a branched bacterial glucan composed of α(1 → 6) linked glucose units with α(1 → 3) branches. Pullulan is a linear microbial glucan composed of α(1 → 6) linked maltotriose units. Since dextran and pullulan are available as standards they have been widely used to evaluate AsFlFFF performance and to investigate the effect of various parameters such as injected amount [1, 2, 84], temperature [52], flow conditions [2, 14], carrier liquid composition [83, 84] etc. on the fractionation. A number of studies on derivatives of pullulan have also been reported [85–88]. Williams et al. have reported on the biological and physical reactivity of dextran in sea water incubation, analyzed with symmetrical FlFFF [89]. Adolphi et al. performed extensive characterization of pullulan with symmetrical FlFFF-MALS determining molar masses and radii as well as the persistence length (i.e., chain stiffness), r_{rms}/r_h and apparent densities from average properties which were discussed in relation to the overlap concentration c* [53]. The results confirmed that pullulan behaved as a flexible coil in good solvent. Furthermore, the study is one of the earliest to show the strength of FlFFF-MALS for polysaccharide characterization.

12.8 β-glucans

β-glucans are a diverse group of polysaccharides composed of glucose units linked by β-glycosidic linkages. The position in the glucose unit at which the linkage occurs varies depending on the subtance. Sources of these types of polysaccharides

are commonly fungal, bacterial or from the bran of some cereals such as oats and barley. For cereal β-glucans (alternating blocks of β(1 → 3) and β(1 → 4) linked glucose units) the solubility varies greatly and dissolved molecules tend to readily aggregate into what has been described in the literature as "fringed micelles" [90]. Lambo-Fodje et al. investigated an exopolyssacharide (EPS) from *Pediococcus damnosus* 2.6 which is a linear β(1 → 3) β-glucan with β(1 → 2) linked side groups with AsFlFFF [91]. The authors investigated the influence of heating in the dissolution of the substances and found that heating did shift elution times to slightly shorter times. However, a corresponding shift in z-average r_{rms} and M_w was not observed and these parameters appeared to be unaffected. The authors attributed this to the relative error in the determination of M and r_{rms} which is higher than in the retention times resulting in that any changes in M_w and r_{rms} was within the experimental error. The results also showed the polysaccharide to have an elongated conformation in solution. In two studies by Ulmius et al. β-glucans from oat and barley were studied with AsFlFFF [92, 93]. The purpose of the investigations was to characterize the solution behavior depending on dissolution conditions and influence of common processing parameters i.e. heating, freezing etc. [92]. Furthermore, the purpose was to investigate the effect of simulated gastro-intestinal passage on the molecular properties and solution behavior [93]. β-glucans could be qualitatively identified in the elution profiles by fluorescence detection and labeling of sample components with calcoflour [94]. The labeling was performed in-line after the separation channel and the calcoflour was delivered using a separate piston pump. M and radii were obtained from separate runs utilizing MALS and RI detection. It is known in literature that common types of processing influences the molar mass and the solubility of β-glucans [95]; however, Ulmius et al. could, by utilizing AsFlFFF, show more comprehensive data regarding molecular and aggregate properties throughout the size distribution. The results show that complete dissolution of β-glucans could not be achieved even in 0.5 M NaOH which has been reported by other authors [96]. The aggregate structure found had similarities to the fringed micelle structure suggested earlier by Grimm et al., i.e., a structure consisting of a dense core with polymer coils emanating into the surrounding solution [90]. Passage through in vitro gastrointestinal passage showed that considerable disruption of aggregates occurred in the gastric conditions while extensive re-aggregation occurred when the environment was changed to intestinal conditions. Furthermore, re-aggregated structures displayed considerably different structural properties, i.e., considerably denser structures compared to the initial aggregates were observed. Such drastic changes in solution/colloidal properties and behavior are likely to have effects on the functional and nutritional aspects of β-glucans.

12.9 Gums and Pectin

Various types of gums are typically used as thickeners in different types of applications. Some gums posses surface active properties, i.e., gums that are exudates from various trees and shrubs. Gums have not been widely characterized

with FlFFF the exceptions being xanthan gum [58, 97], konjac glucomannans [83], gum Arabic [60, 61], mesquite gum [61] and pectin [98]. Xanthan gum is a microbial, anionic heteropolysaccharide composed of a repeating unit of a D-glucopyranosyl backbone with branches of mainly D-mannopyranosyl and D-glucopyranosyluronic acid. The substance is known for giving rise to highly pseudo-plastic flow properties already at low solution concentrations which is attributed to its ability to form double helices [99] with extended and rod-like conformation. The viscous properties are retained over a wide range of temperatures and pH. Pauck et al. have investigated xanthan gum with AsFlFFF in a comparative study with analytical ultra centrifugation [97]. The interpretation of the obtained results were that AsFlFFF gives the "wrong" diffusion coefficient for elongated and rod-like macromolecules. Unfortunately, however, the experiments reported in the paper are rather limited. For instance, no investigations on the influence of flow conditions and injected amounts are reported and the results can, thus, be regarded as rather inconclusive. Taking into consideration the rather extreme molecular structure and conformation and its very strong viscosity increasing properties, it is likely to be very sensitive for overloading as is the case for other highly viscosity increasing macromolecules [100]. The sensitivity to overloading for xanthan gum in AsFlFFF has been reported [58].

Gum arabic and mesquite gum have complex polysaccharide structures which are mainly of an arabinogalactan polymeric type. In the molecular structure, proteinaceous moieties, closely associated to the polysaccharide structure, are also present. The presence of these moieties gives rise to the surface activities of the substances and enables their utilization as emulsifiers. Gum arabic is known to contain two populations of which one is rich in protein and the other, major population, is rather poor in protein [101]. A comparison between size exclusion (SEC) chromatography and symmetrical FlFFF for the analysis of gum arabic has been performed by Picton et al. [60]. The authors reported that more extensive characterization could be obtained by FlFFF as the two populations had higher resolution than in SEC. The late eluting population (in the FlFFF analysis) had a non-gaussian appearance which the authors remedied by changing to a linearly decaying cross flow rather than a stepwise decrease. This illustrates the benefits of using continuously decaying programmed cross flows. By utilizing AsFlFFF with fluorescence detection on fluorescently labeled gum arabic and mesquite gum the distribution of proteinaceous matter over the size distribution was studied [61]. Contrary to gum arabic, mesquite gum was found to contain one population with an evenly distributed content of proteinaceous matter. In this study the conformational properties (as obtained from AsFlFFF-MALS) of the gums were related to their ability to stabilize emulsions. The gum arabic protein rich fraction which was selectively adsorbed displayed substantially better stabilizing properties against coalescence in the emulsions than mesquite gum. The higher conformational flexibility, of the protein rich population, as observed from the AsFlFFF-MALS results, was suggested as a possible explanation for the better stabilizing properties.

12.10 Marine Polysaccharides and Derivatives

The marine polysaccharides originate from different types of sea weeds (alginates and carrageenans) or from the exoskeletons of crustaceans (chitin). Chitin is, naturally, insoluble in water but can be transformed from a β-(1-4)-linked poly (N-acetylglucosamine) to a corresponding (1-4)-linked poly(N-glucosamine), containing randomly distributed residual acetyl glucosamine groups, by deacetylation. The resulting substance is known as chitosan and is water soluble at low pH. Due to its high charge density chitosan is notoriously difficult to characterize with separation techniques. Typically viscosity measurements at low pH are used as characterization which results in a rather rough estimate of its molecular properties [102]. A complication one could expect is extensive adsorption of chitosan at, for instance, the channel membrane. However, succesful analyses have been reported and it has been shown that, with utilization of a 0.1 M HAc/NaAc, pH 4.2 buffer as carrier liquid, recoveries in excess of 80% are obtained [102, 103]. In their work, Augsten et al. conclude that AsFlFFF-MALS is the ideal tool for chitosan characterization [102].

Alginate, or alginic acid, is a copolymer of β(1 → 4) linked D-mannuronate and α(1 → 4) linked L-guluronate. The monomers can appear in different sequences or blocks. Due to the polyelectrolyte character of alginates the difficulties encountered when analyzing these substances can be expected to be similar in character to those discussed above for charged polymers. Further complications may arise due to alginates' sometimes strong viscosity enhancing effects [104]. Alginates have been characterized with AsFlFFF [9, 59, 104] and so have alginates modified with poly(ε-caprolactone) [105]. Alasonati et al. studied alginate-heavy metal interactions and found interesting conformational changes in the presence of metal ions (Pb^{2+} and Cd^{2+}) [59]. In the absence of heavy metal ions, smaller molecules were found to be more elongated ($r_{rms}/r_h > 2$) which is what would be expected for a linear polysaccharide polyelectrolyte while the average r_{rms}/r_h was 1.7. Upon addition of metal ions M_w increased, indicating aggregate formation and the average r_{rms}/r_h increased to 2.0. This indicates that metal-alginate aggregates are more elongated than the individual molecules which may be explained by an "egg box" aggregation pattern. By utilizing inductively coupled plasma-mass spectrometry (ICP-MS) for detection the Pb and Cd concentration could be studied over the entire size distribution.

Carrageenan is a polysaccharide made up of galactose and 3,6-anhydrogalactose which can be both sulfated and non-sulfated. The monomers are linked by alternating β(1 → 4) and α(1 → 3) linkages and carrageenans exist in different classes with different solution behavior. The three main commercial classes are ι-, κ- and λ-carrageenan, of which κ-carrageenan has been analyzed with AsFlFFF. Wittgren et al. studied the salt induced coil-helix transition of κ-carrageenan. In 0.1 M NaCl κ-carrageenan behaves as a random coil while helical structures are formed in 0.1 M NaI [57]. Furthermore, CsI was added in order to trigger the formation of super helical rods which resulted in very large aggregates when ≥40% of the NaI was replaced by CsI. The authors found that the helices, i.e., in 0.1 M

NaI, had increased values for r_{rms} and M but the observed r_h (determined from retention times) decreased compared to the r_h of the random coil conformation. This led to an increase in r_{rms}/r_h from 1.9 (coil) to 4.0 (helix). Obviously the transition between random coil and helix is a change in conformation. However, 4.0 seems high, as it would correspond to a rod with axial ratio $> > 100$ (an axial ratio of 100 gives approximately $r_{rms}/r_h = 2.8$) [45]. The authors drew the conclusion that an error in the determination of r_h could be the reason and that insufficient data exist on the behavior of rod-like macromolecules in the separation channel. Viebke et al. has studied the temperature induced coil-helix transition of κ-carragenan which occurs when the temperature is decreased from 50°C to 25°C [58]. Interestingly, the authors found the same discrepancy between M and r_h. M_w more than doubled (309,000–675,000 g/mol) as a result of the helix formation while r_h decreased from 64 to 33 nm. The authors suggested that FlFFF theory has to be modified to be able to account for rod-like macromolecules. The authors also investigated xanthan gum which has a pronounced rod-like character but, unfortunately, no comparison was performed which could have shed further light on the observations.

12.11 Hyaluronan

Hyaluronan or hyaluronic acid is a linear polyelectrolyte composed of β(1 → 4) D-glucuronic acid and β(1 → 3) D-N acetylglucosamin units. Due to its semi-rigid character, viscoelastic solution properties and good biocompatibility hyaluronan is widely used in biomedical applications. Some studies concerning the analysis of hyaluronan with AsFlFFF have been reported [1, 83, 106–108]. Wahlund et al. fractionated fluorescein labeled hyaluronan and demonstrated the importance of carefully optimizing injected amounts in order to avoid overloading effects [1]. In a more recent study Maleki et al. have investigated the degradation of hyaluronan at $pH > 11$ and $pH < 4$ using AsFlFFF [107].

12.12 Concluding Remarks

There is an increasing amount of literature regarding polysaccharide analysis with AsFlFFF. The suitability of the method and its advantages should by now be firmly established and the purpose of the overview in this chapter has been to illustrate the benefits and large potential of AsFlFFF for polysaccharide characterization. It offers the possibility to obtain a number of molecular and conformational properties over a very wide size distribution under gentle conditions. As has been shown and discussed above the method is well suited for the investigation of functional properties over a large size distribution. Furthermore, due to its large size range, it offers the possibility to analyze both “free” polysaccharides in solution as well as aggregates thereof, which is perhaps one of the really strong benefits of the method.

References

1. Wahlund K-G, Litzen A (1989) J Chromatogr 476:413
2. Wittgren B, Wahlund K-G (1997) J Chromatogr A 760:205
3. Glantz M, Håkansson A, Lindmark-Månsson H, Paulsson M, Nilsson L (2010) Langmuir 26:12585
4. You S, Stevenson SG, Izydorczyk MS, Preston KR (2002) Cereal Chem 79:624
5. Wahlund K-G (2000) In: Schimpf ME, Caldwell K, Giddings JC (eds) Field-flow fractionation handbook. Wiley, New York, p 279
6. Debye P, Huckel E (1923) Physikalische Zeitschrift 24:185
7. Modig G, Nilsson P-O, Wahlund K-G (2006) Starch-Starke 58:55
8. Ferrari ME, Bloomfield VA (1992) Macromolecules 25:5266
9. Alasonati E, Benincasa MA, Slaveykova VI (2007) J Sep Sci 30:2332
10. Lee S, Kim ST, Pant BR, Kwen HD, Song HH, Lee SK, Nehete SV (2010) J Chromatogr A 1217:4623
11. van Bruijnsvoort M, Wahlund K-G, Nilsson G, Kok WT (2001) J Chromatogr A 925:171
12. Botana AM, Ratanathanawongs SK, Giddings JC (1995) J Microcolumn Sep 7:395
13. Kirkland JJ, Dilks CH Jr, Rementer SW, Yau WW (1992) J Chromatogr 593:339
14. Leeman M, Wahlund KG, Wittgren B (2006) J Chromatogr A 1134:236
15. Wahlund K-G, Winegarner HS, Caldwell KD, Giddings JC (1986) Anal Chem 58:573
16. Giddings JC (1986) Anal Chem 58:735
17. Hansen ME, Giddings JC, Schure MR, Beckett R (1988) Anal Chem 60:1434
18. Yoo SH, Jane JL (2002) Carbohydr Polym 49:307
19. Bello-Perez LA, Roger P, Baud B, Colonna P (1998) J Cereal Sci 27:267
20. Fishman ML, Hoagland PD (1994) Carbohydr Polym 23:175
21. Hanselmann R, Ehrat M, Widmer HM (1995) Starch-Starke 47:345
22. Bultosa G, Hamaker BR, BeMiller JN (2008) Starch-Starke 60:8
23. Han JA, Lim ST (2004) Carbohydr Polym 55:265
24. Nilsson GS, Bergquist K-E, Nilsson U, Gorton L (1996) Starch/Stärke 48:352
25. Dona A, Yuen CWW, Peate J, Gilbert RG, Castignolles P, Gaborieau M (2007) Carbohydr Res 342:2604
26. Hoang NL, Landolfi A, Kravchuk A, Girard E, Peate J, Hernandez JM, Gaborieau M, Kravchuk O, Gilbert RG, Guillaneuf Y, Castignolles P (2008) J Chromatogr A 1205:60
27. Zhong F, Yokoyama W, Wang Q, Shoemaker CF (2006) J Agric Food Chem 54:2320
28. Striegel AM, Timpa JD (1995) Carbohydr Res 267:271
29. Stevenson DG, Biswas A, Jane JL, Inglett GE (2007) Carbohydr Polym 67:21
30. Schärtl W (2007) Light scattering from polymer solutions and nanoparticle dispersions. Springer, Berlin
31. Kerker M (1969) The scattering of light and other electromagnetic radiation. Academic press, New York
32. van de Hulst HC (1981) Light scattering by small particles. Dover publications, New York
33. Debye P (1944) J Appl Phys 15:338
34. Zimm BH (1948) J Chem Phys 16:1093
35. Zimm BH (1948) J Chem Phys 16:1099
36. Berry GC (1966) J Chem Phys 44:4550
37. Andersson M, Wittgren B, Wahlund K-G (2003) Anal Chem 75:4279
38. Einstein A (1905) Ann Phys 17:549
39. Williams PS (2000) In: Schimpf ME, Caldwell K, Giddings JC (eds) Field-flow fractionation handbook. Wiley, New York, p 145
40. Nilsson L, Leeman M, Wahlund K-G, Bergenståhl B (2006) Biomacromolecules 7:2671
41. Magnusson E, Håkansson A, Janiak J, Bergenståhl B, Nilsson L Manuscript in preparation
42. Yau WW, Kirkland JJ (1984) Anal Chem 56:1461
43. Tanford C (1961) Physical chemistry of macromolecules. Wiley, New York

44. Schmidt M, Nerger D, Burchard W (1979) Polymer 20:582
45. Hansen S (2004) J Chem Phys 121:9111
46. Burchard W (1983) Adv Polym Sci 48:1
47. Burchard W (1999) Adv Polym Sci 143:113
48. Galinsky G, Burchard W (1995) Macromolecules 28:2363
49. Roger P, Colonna P (1992) Carbohydr Res 227:73
50. Roger P, Bello-Perez LA, Colonna P (1999) Polymer 40:6897
51. Fernandez C, Rojas CC, Nilsson L (2011) Int J Biol Macromol 49:458
52. Viebke C, Williams PA (2000) Anal Chem 72:3896
53. Adolphi U, Kulicke WM (1997) Polymer 38:1513
54. Ioan CE, Aberle T, Burchard W (2000) Macromolecules 33:5730
55. Nilsson S, Sundelöf L-O, Porsch B (1995) Carbohydr Polym 28:265
56. Coviello T, Kajiwara K, Burchard W, Dentini M, Crescenzi V (1986) Macromolecules 1986:2826
57. Wittgren B, Borgström J, Piculell L, Wahlund K-G (1998) Biopolymers 45:85
58. Viebke C, Williams PA (2000) Food Hydrocolloids 14:265
59. Alasonati E, Stolpe B, Benincasa MA, Hassellöv M, Slaveykova VI (2006) Environ Chem 3:192
60. Picton L, Bataille I, Muller G (2000) Carbohydr Polym 42:23
61. Alftrén J, Peñarrieta JM, Bergenståhl B, Nilsson L (2012) Food Hydrocolloids 26:54
62. Rojas CC, Wahlund K-G, Bergenståhl B, Nilsson L (2008) Biomacromolecules 9:1684
63. Nilsson L, Bergenståhl B (2006) Langmuir 22:8770
64. Nilsson L, Bergenståhl B (2007) J Agric Food Chem 55:1469
65. Kratky O, Porod G (1949) Recueil Des Travaux Chimiques Des Pays-Bas. J R Netherlands Chem Soc 68:1106
66. Burchard W, Vogel HJ (2000) Comput Theor Polym Sci 10:133
67. Kratochvil P (1987) Classical light scattering from polymer solutions. Elsevier Science Publishers, Amsterdam
68. Rolland-Sabate A, Colonna P, Mendez-Montealvo MG, Planchot V (2007) Biomacromolecules 8:2520
69. Andersson M, Wittgren B, Schagerlof H, Momcilovic D, Wahlund KG (2004) Biomacromolecules 5:97
70. Hizukuri S, Takeda Y, Yasuda M, Suzuki A (1981) Carbohydr Res 94:205
71. Roger P, Baud B, Colonna P (2001) J Chromatogr A 917:179
72. Litzen A (1993) Anal Chem 65:461
73. Wittgren B, Wahlund K-G, Andersson M, Arfvidsson C (2002) Int J Polym Anal Charact 7:19
74. Modig G, Nilsson L, Bergenståhl B, Wahlund K-G (2006) Food Hydrocolloids 20:1087
75. Nilsson L, Leeman M, Wahlund K-G, Bergenståhl B (2007) Langmuir 23:2346
76. Lee S, Nilsson P-O, Nilsson GS, Wahlund K-G (2003) J Chromatogr A 1011:111
77. Krentz DO, Lohmann C, Schwarz S, Bratskaya S, Liebert T, Laube J, Heinze T, Kulicke WM (2006) Starch-Starke 58:161
78. Moon MH, Williams PS, Kang DJ, Hwang I (2002) J Chromatogr A 955:263
79. Wittgren B, Wahlund K-G (2000) Carbohydr Polym 43:63
80. Kulicke WM, Clasen C, Lohman C (2005) Macromol Symp 223:151
81. Andersson M, Wittgren B, Wahlund K-G (2001) Anal Chem 73:4852
82. Clasen C, Kulicke WM (2001) Prog Polym Sci 26:1839
83. Benincasa MA, Cartoni G, Delle Fratte C (2002) J Chromatogr A 967:219
84. Benincasa MA, Delle Fratte C (2004) J Chromatogr A 1046:175
85. Duval C, Le Cerf D, Picton L, Muller G (2001) J Chromatogr B 753:115
86. Legros M, Dulong V, Picton L, Le Cerf D (2008) Polym J 40:1132
87. Simon S, Dugast JY, Le Cerf D, Picton L, Muller G (2003) Polymer 44:7917
88. Souguir Z, Roudesli S, Picton L, Le Cerf D, About-Jaudet E (2007) Eur Pol J 43:4940

89. Williams SKR, Keil RG (1997) J Liq Chromatogr Relat Technol 20:2815
90. Grimm A, Kruger E, Burchard W (1995) Carbohydr Polym 27:205
91. Lambo-Fodje AM, Leeman M, Wahlund K-G, Nyman M, Oste R, Larsson H (2007) Carbohydr Polym 68:577
92. Ulmius M, Önning G, Nilsson L (2012) Food Hydrocolloids 26:175
93. Ulmius M, Adapa S, Önning G, Nilsson L (2012) Food Chem 130:536
94. Jorgensen KG (1988) Carlsberg Res Commun 53:277
95. Brennan CS, Cleary LJ (2005) J Cereal Sci 42:1
96. Li W, Wang Q, Cui SW, Huang X, Kakuda Y (2006) Food Hydrocolloids 20:361
97. Pauck T, Colfen H (1998) Anal Chem 70:3886
98. Thielking H, Kulicke WM (1998) J Microcolumn Sep 10:51
99. Sato T, Norisuye T, Fujita H (1984) Polym J 16:341
100. Leeman M, Islam MT, Haseltine WG (2007) J Chromatogr A 1172:194
101. Vandevelde MC, Fenyo JC (1985) Carbohydr Polym 5:251
102. Augsten C, Mader K (2008) Int J Pharm 351:23
103. Mao S, Augsten C, Mader K, Kissel T (2007) J Pharm Biomed Anal 45:736
104. Storz H, Muller KJ, Ehrhart F, Gomez I, Shirley SG, Gessner P, Zimmermann G, Weyand E, Sukhorukov VL, Forst T, Weber MM, Zimmermann H, Kulicke WM, Zimmermann U (2009) Carbohydr Res 344:985
105. Colinet I, Dulong V, Hamaide T, Le Cerf D, Picton L (2009) Carbohydr Polym 75:454
106. Maleki A, Kjoniksen AL, Nystrom B (2007) Polymer Bulletin 59:217
107. Maleki A, Kjoniksen AL, Nystrom B (2008) Macromol Symp 274:131
108. Takahashi R, Al-Assaf S, Williams PA, Kubota K, Okamoto A, Nishinari K (2003) Biomacromolecules 4:404

Chapter 13
The Use of Field-Flow Fractionation for the Analysis of Drug and Gene Delivery Systems

Alexandre Moquin and Françoise M. Winnik

Abstract An increasingly large number of drug formulations consist of drug-loaded nanoparticles of controlled size, composition, and surface chemistry. Field-flow fractionation (FFF) has emerged as a powerful tool for the physico-chemical characterization of nanoparticulate drug and gene delivery systems. The enabling features and technical difficulties of FFF are assessed in the specific context of drug formulations. The FFF analysis of various classes of drug and gene delivery systems are described, including microspheres, solid lipid nanoparticles, melt extrudates, emulsions, dendrimers, nanogels, lipid/DNA complexes, and polycation/DNA complexes.

Keywords Drug delivery systems • Drug loading • Dynamic light scattering • Field-flow fractionation • Gene delivery systems • Microparticle • Nanoparticle • Size characterization

13.1 Analytical Approaches in Pharmaceutics: A Brief Overview

Various pharmaceutical carriers, such as nanospheres, nanocapsules, micelles, liposomes and dendrimers, are currently used for the delivery of therapeutic or diagnostic agents. For a carrier to be effective it is critical that it evades capture by the reticuloendothelial system (RES), circulates in the blood for a prolonged period, and accumulates at the desired sites, where it is retained by the enhanced permeability and retention (EPR) effect, unobserved in normal tissues. The biophysical characteristics of nanoparticles (NPs) are controlled to a large extent by physico-chemical features, such as size, shape and interface chemistry. In general terms,

A. Moquin • F.M. Winnik (✉)
Department of Chemistry and Faculty of Pharmacy, University of Montreal, Montreal, QC, Canada
e-mail: francoise.winnik@umontreal.ca

S.K.R. Williams and K.D. Caldwell (eds.), *Field-Flow Fractionation in Biopolymer Analysis*, DOI 10.1007/978-3-7091-0154-4_13,

drug delivery systems are colloidal suspensions of NPs ranging in size from ~10 nm to ~1 μm stabilized via electrostatic interactions in the case of charged NPs or by steric repulsion for neutral NPs, such as the very effective NPs decorated with poly (ethylene glycol) (PEG) chains. Dissolved components, present in addition to the suspended nanoparticles, also affect NP performances, for example by guiding their internalization into cells [1].

Nanomedicine relies strongly on the fine balance between the in vivo performance of NPs and their physico-chemical properties, increasing the demand for fast and reliable methods to analyze NP suspensions. Most current techniques yield the bulk (ensemble) properties of a suspension. The size and size distribution of NPs is accessible via dynamic light scattering (DLS), microscopy, and analytical ultracentrifugation (AUC). DLS measures the time-dependent fluctuations of the light scattered by the particles to derive their hydrodynamic sizes. For samples having a broad polydispersity in size, DLS may not be able to detect small changes in the size distributions. The presence of large particles and small amounts of aggregates can mask the light scattered by the smaller particles, limiting their detection. Microscopic techniques such as atomic force microscopy (AFM), scanning electron microscopy (SEM), and transmission electron microscopy (TEM) permit direct visualization of the particles, but they often require sample drying and the use of contrast staining agents that can influence the properties of the particles. The hydrodynamic size and size distribution can be obtained also with AUC if one knows the specific volume of the hydrated particles. Spectroscopic techniques can provide the drug loading in a NP suspension, but measurements yielding the drug concentrations within the nanoparticles can be difficult or tedious. Size exclusion chromatography (SEC) can separate the components of a suspension according to their size, but it is fraught with technical difficulties, such as irreversible adsorption of NPs on the column packing material or clogging of frits placed on the column inlet.

Over the last 10 years, a number of research groups have turned to field-flow fractionation chromatography for the characterization of drug and gene delivery systems. Their pioneering work has stimulated further advances in the design of instruments adapted to the special needs of nanomedicine. Hence FFF under its various forms is poised to take increasing importance in this field. The use of FFF in pharmaceutics was reviewed in 2004 by Fraunhofer and Winter [2], with special emphasis on the use of asymmetrical flow field-flow fractionation (AF4). Since then, a number of reviews have appeared on related topics, such as bioanalysis [3], analysis of macromolecules and of nanoparticles of biological interest [4, 5], and on the place of FFF in the "nanoworld" [6]. In this chapter, we will focus on the use of FFF in the characterization of nanoparticular drug and gene delivery systems and assess the impact of this technique in the development of this field. The chapter starts with a brief review of the enabling features and the technical difficulties of FFF in the characterization of nanoparticles for drug and gene vectorization, compared to conventional methods. In following sections, we describe reports on the analysis of drug and gene delivery systems, mostly those published since 2004. The reader is referred to the review by Fraunhofer and Winter for earlier publications [2].

13.2 Advantages and Technical Difficulties of FFF Analysis in Pharmaceutics and Nanomedicine

13.2.1 Strengths of FFF Technologies

The advantages of FFF for the analysis of colloidal aqueous suspensions derive from the fact that fractionation takes place in a flowing stream of liquid in the absence of any packing material. The retention time of the components is determined primarily by their hydrodynamic volume and to a lesser extent by charge effects or by the tendency of particles to adsorb on the accumulation wall. The mass and hydrodynamic volume of each component can be determined, after fractionation, by multiangle laser light scattering (MALS) and dynamic light scattering (DLS) detectors, respectively, connected to the FFF channel outlet. This set-up provides in a single analysis a complete size profile of eluting components, including the radius of gyration (R_g), hydrodynamic radius (R_h) and size distribution of each NP population as well as the absolute molar mass of soluble components (biopolymers or drugs). Simultaneous analysis by a concentration detector (UV-Vis, RI) generates a complete fingerprint of a suspension that can be correlated to in vitro or in vivo results generated using the collected fractions. Uniform fractions can be collected as they elute and analyzed off-line by standard techniques. The importance of suspension fractionation into components of uniform size distribution prior to size determination cannot be overstated. Ensemble particle sizes are derived from light scattering data (either MALS or DLS) on the basis of various calculation methodologies that work well for the analysis of data collected from samples monodisperse in size. Analysis of data gathered from polydisperse samples is notoriously unreliable, or at best biased towards larger sizes.

Another useful characteristic of FFF for applications in therapeutics is its exceptionally wide range in terms of analyte size (a few nm to microns). Thus it is possible to monitor in situ the fate of drug delivery systems in complex matrices such as serum or even whole blood, as demonstrated in the case of perfluorocarbon emulsions used as synthetic oxygen carriers for temporary maintenance of oxygen delivery to tissues during surgery [7]. Not to be overlooked also is the relatively simple miniaturization of FFF via modifications of the separation channel, such as downscaling of the channel volume or the use of permeable hollow fibers. While downsized systems are not yet commercially available, research prototypes gave promising results (see refs. [5–7], etc in Qureshi et al. [4]). FFF coupled with concentration detectors (UV-Vis or RI) gives ready access to the concentration of drug incorporated in NPs. If the drug is sufficiently large to be retained within the channel, one can use FFF to determine the efficiency of drug entrapment in the NPs during manufacture or to monitor the release of drug from NPs, for example upon treatment with blood serum. Other tests may be envisaged as well, such as monitoring the erosion of biodegradable NPs [8] or assessing the interactions of NPs with serum proteins.

13.2.2 Limitations of FFF Technologies

When establishing a suitable protocol for FFF analysis of drug and gene delivery systems, one needs to avoid several pitfalls inherent to the technique. The choice of the semipermeable membrane that forms the accumulation wall of the flow channel is critical: the components of the suspension must not adsorb irreversibly on it. Meeting this requirement can be a challenge in the case of samples heterogeneous in amphiphilicity and charge. This problem can be exacerbated by the limited choice of well-characterized membranes currently available. The carrier liquid as well needs to be selected carefully. Several types of drug and gene delivery NPs are held together by electrostatic interactions. They may disintegrate rapidly under conditions of high ionic strength or if the carrier pH promotes neutralization of one of the components. Deionized water should not be used as a carrier since it can promote interparticulate and particle-wall repulsion, causing the particles to be insufficiently driven towards their equilibrium position [9]. Factors inherent to specific FFF techniques also limit the choice of carrier. When performing SdFFF, one needs to keep in mind that in order to obtain size information, the density of the particles has to be known and it should be different from that of the solvent in order to obtain sufficient retention of the particles without having to use extremely high rotation rates. In the case of FlFFF, precautions should be taken to avoid carriers interacting with the membrane, for example by inducing it to swell, which affects the separation conditions. Ideally, the carrier should resemble as closely as possible the physiological media, since the drug delivery systems to be analyzed will eventually be administered in vivo and since it allows one to monitor drug release under relevant conditions.

13.3 FFF Analysis of Drug Delivery Formulations

13.3.1 Microspheres, Solid Lipid Nanoparticles and Melt Extrudates

In this section, we will describe applications of FFF for the characterization of colloidal drug carriers in clinical use or under pre-clinical assessment. The objectives here are to demonstrate that FFF analysis can be performed readily on standard pharmaceutical formulations and that the information gathered brings new insights not only on the composition of the formulations, but also on their stability upon storage, and their pharmacological activity.

Biodegradable nanoparticles consisting of poly(lactic acid) (PLA) or its copolymers, are commonly used for the delivery of hydrophobic drugs because their degradation in vivo leads to pharmacologically inactive substances, which are absorbed by the body or removed metabolically. They improve the efficacy of drugs

and alleviate their side effects [10]. The particle dimensions are controlled by adjusting various parameters during their preparation. Drug-loaded PLA microspheres having a diameter of 1 μm or more have been characterized by FFF in the late 1990s [11]. Due to their size, such microspheres have a weak diffusion coefficient. In the FlFFF channel, they are subjected to steric inversion, a phrase coined to describe the change from the normal elution mode to the steric mode, which occurs for particles larger than 1 μm. In this FFF mode (Fl/Hy FFF), the applied field is used to drive the particles to the channel wall. The particles are equilibrated above the wall due to the existence of hydrodynamic lift forces. Under such conditions, it is not possible to predict precisely the size/retention time dependence from the flow rates used in the channel. In addition, light scattering data cannot be analyzed reliably for particles larger than ~1 μm. Therefore, it is necessary to calibrate the instrument with monodisperse samples of known hydrodynamic sizes, such as polystyrene latexes. An Fl/Hy FFF system was used by Moon et al. for the separation of core-shell poly(L-lactide) (PLLA) microspheres stabilized by poly(ethylene glycol) copolymer used for the encapsulation of retinoic acid [11]. Polystyrene latexes (six samples from 2 to 10 μm in diameter) were used to calibrate the system. Eluting polystyrene fractions were collected and imaged by SEM, confirming that the largest particles eluted first and that each fraction had a nearly uniform size distribution. Fractionation of the polystyrene samples occurred in less than 6 min with adequate resolution, although baseline separation was not achieved between the larger samples. The log/log plot of the elution times of the standards versus their known sizes was constructed. It was linear with high correlation and its validity was confirmed by EM imaging of collected fractions. Fl/Hy FFF characterization of series of PLLA microspheres gave important insight into the impact of their composition on their size. The size was shown to increase with increasing retinoic acid content whereas the addition of PEG-PLLA copolymer did not affect the size of the microspheres.

Flow- and sedimentation-FFF were employed to analyze PLA nanoparticles that encapsulate a prodrug of the anti-ischemic agent N6-cyclopentyladenosine (CPA) [12]. The drug loaded nanoparticles were prepared using an evaporation method in the presence of two different surfactants: sodium dodecyl sulfate and Pluronic F68. They were purified by dialysis, gel filtration or ultracentrifugation. Visualization of the NPs by SEM revealed that all samples were polydisperse in size, with a mean diameter ranging from 90 to 400 nm depending on the preparation/purification conditions. Flow FFF protocols were established using polystyrene latex standards (92 nm, 240 nm, 350 nm) to cover the expected elution range of the PLA nanospheres. Fractograms recorded for the PLA samples were broad, independently of the preparation method. Nonetheless, since the geometrical dimensions of the channel were well established by the use of standards, the authors were able to retrieve particle size distributions without on-line MALS capability. The nanoparticles were analyzed also by sedimentation FFF. The resolution of the separation was higher than in the case of FlFFF, possibly due to the enhanced flexibility in the choice of carrier that can be used in SdFFF.

Gelatin nanoparticles loaded with oligonucleotides (ODN) were analyzed by an AF4 system fitted with regenerated cellulose membranes (1, 5 or 10 kDa cutoff) and coupled to MALS and UV detectors [13]. This system was employed first to characterize the gelatin samples prior to nanoparticle formation. The gelatin ranged in molecular weight from ~20 to 10,000 kDa. The authors demonstrate experimentally the superiority of AF4 over SEC for the characterization of gelatin, in terms of range (SEC: <1,000 kDa), reliability, sample recovery, and reduced damage to fragile samples. Gelatin nanoparticles crosslinked with glutaraldehyde were prepared and loaded with ODNs. Imaging of the resulting samples by SEM revealed that the nanoparticles were of broad polydispersity in size, from ~150 to 300 nm in diameter. AF4 separation was optimized for maximum sample recovery by testing various membranes, changing the carrier pH, and applying various cross-flow rates. The experimental approach leading to the best separation process is described in great detail, offering excellent guidance to readers entering this field. It was established that the nanoparticle concentrations correlate well with the area under the curve (AUC_{UV}) values measured from the fractograms monitored by UV. Hence, the ODN loading efficiency could be assessed from AUC_{UV}, after ascertaining that unbound ODNs are separated during elution from ODN-loaded gelatin nanoparticles.

Gelatin nanoparticles were PEGylated in order to protect them against rapid clearance from the blood stream. AF4 separation coupled with refractive index detection was employed to quantify the PEGylation [14]. First, baseline separation of PEG and gelatin nanoparticles was achieved by adjusting the cross-flow. Second, a calibration curve correlating the refractive index detector signal intensity (AUC_{RI}) with PEG concentration was obtained by AF4 analysis of PEG solutions of increasing concentration. Third, gelatin nanoparticles were subjected to PEGylation by addition of different PEG concentrations to a constant amount of nanoparticles. The mixtures were analyzed to determine the amount of unreacted PEG during the reaction and after saturation, based on the previously established calibration curve. The maximum mass of PEG bound to the gelatin nanoparticles was ~0.350 mg of PEG/mg of gelatin. PEGylation of the nanoparticles was ascertained by AFM visualization of gelatin nanoparticles before and after PEGylation.

Lipidic particles for use as drug carriers were subjected to AF4 analysis coupled with MALS detection in an effort to correlate their size and shape with functional features, such as drug loading efficiency and in vivo performance. The nanoparticles analyzed were solid lipid nanoparticles (SLN), oil-loaded solid lipids nanoparticles (NLC, nanostructured lipid nanoparticles), and nanoemulsions (NEmu) [15]. The separation was achieved using a system in which the channel was fitted with a regenerated cellulose membrane (10 kDa cutoff) and the eluate was analyzed by MALS. Since FFF separates particles on the basis of their Stokes radius, particles of equal volume but different shape will elute at different times: isometric particles elute earlier than asymmetric particles. This effect was observed by comparing fractograms of round NEmu droplets and anisometric SLN platelets of comparable volumes.

Melt extrudates dispersed in aqueous media are promising carriers for the oral delivery of poorly-water soluble drugs. They are complex mixtures difficult to characterize by standard techniques, but amenable to AF4 analysis as shown in a study by Kanzer et al. who used a system with triple detection (MALS, RI and UV) [16]. The formulations analyzed contained drugs (the HIV protease inhibitors ritonavir and lopinavir), a hydrophilic carrier (vinylpyrrolidone-vinylacetate copolymer, PVP/VA), a non-ionic lipophilic surfactant (sorbitan monolaurate), and hydrophilic fumed silica. Fractograms presented several eluting bands: a fast eluting band (~10 min), assigned to PVP/VA by comparison with the fractogram of a known sample of PVP/VA, with a tail between 12 and 18 min shown, by ex situ analysis of collected eluate, to contain a significant fraction of the drugs. The fractograms also featured a strong peak between 20 and 40 min, attributed to large associates in the dispersion, as seen in Fig. 13.1. This fraction contained some drug, but its composition could not be resolved from the data. The authors concluded that the formulations were incompletely dissolved and that even after extensive dilution the mixture contained primarily nanoparticles (R_h ~ 50 to 100 nm).

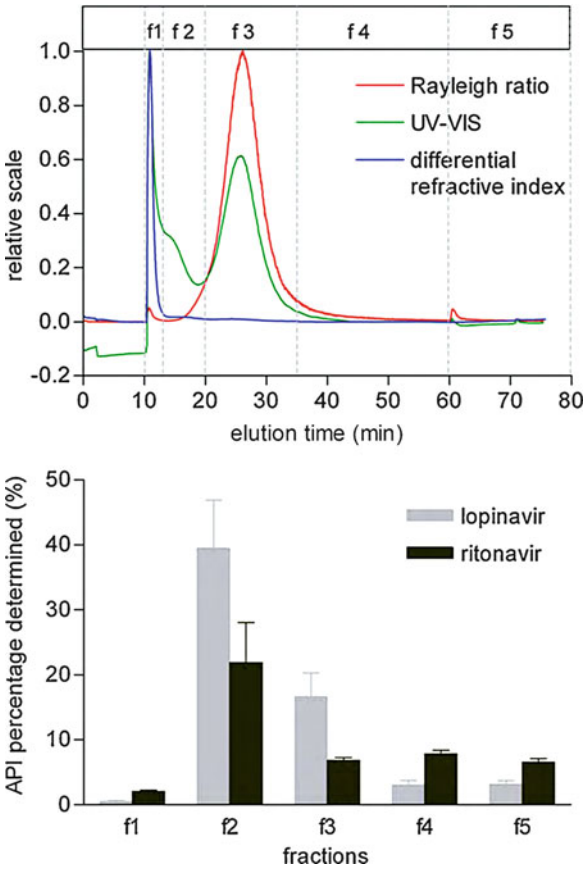

Fig. 13.1 Elution profiles of carriers with fraction borders (*top*) for determination (amount in %) of the active pharmaceutical ingredients (API) lopanivir and ritonavir of composition API in fractions of channel flow (mean ± SD, n = 3) (Reprinted from [16], © 2010, with permission from Elsevier)

Kang et al. designed a delivery system for hydrophobic drugs, such as the mitotic inhibitor Paclitaxel used as a chemotherapy agent, consisting of a lipidic core made of Lecithin surrounded by a hydrophilic shell formed by Pluronic F 127 (PEO_{99}-PPO_{67}-PEO_{99}) [17]. The formulations contained also smaller nanoparticles identified as Pluronic micelles without lecithin by TEM imaging. The core/shell structures were of broad size distribution ranging from 100 to 600 nm in diameter estimated from TEM and DLS measurements. Measurements by batch-mode dynamic light scattering (DLS) of the multimodal population led to size distributions biased towards larger particles. Analysis of the formulations was carried out also on an AF4 system coupled to a UV-detector at 254 nm calibrated with polystyrene particles (diameters: 20, 40, 80 and 150 nm). Separation conditions were established by adjusting the composition of the carrier with added salts and surfactants. AF4 analysis confirmed the co-existence of two particle populations: (1) small coreless Pluronic micelles (20–50 nm in diameter) with a narrow size distribution and (2) core/shell structures which were of much larger sizes and broader size distribution (100–600 nm in diameter). This study is a nice example of the use of this instrument to fully characterize a formulation heterogeneous in NP composition and size distribution.

Virus-like particles (VLP) are formed by self-assembly of viral structural proteins. They are safe but highly immunogenic. They are under assessment in various vaccine formulations. Prior to regulatory acceptance, the samples must be fully characterized to ensure batch-to-batch reproducibility. The VLPs are disassembled and re-assembled during vaccine manufacture. Each step of the manipulation must be monitored by a sensitive, fast and reliable quality control tool in order to ascertain the integrity of the VLPs and the purity of the formulations, which, in addition to VLPs, may contain protein fragments, monomers or dimers, as well as large aggregates. An AF4 analysis of murine polyomavirus VLPs was performed by Chuan et al., who optimized the separation parameters to monitor batch-to-batch reproducibility [18]. Prior results from TEM and DLS measurements indicate that the samples contain nanoparticles ranging in diameter from 16 to 48 nm (distribution mean from TEM: 33 nm). Fractograms of VLPs (monitored by MALS and UV) presented a main band (20–26 min) with a tail (up to ~ 34 min) and a highly retained band, which eluted only when the cross-flow was reduced to 0 (see Fig. 13.2). Collected fractions were imaged by TEM, the main band corresponded to VLPs with diameters from 35 to 45 nm, while the late-eluting fraction contained nanoparticles with radii up to 90 nm. Relative amounts of the VLP components were quantified by UV absorbance, yielding size distributions of the VLPs. The authors recorded fractograms of VLPs from different sources (insect cells or E. coli). The variability in the quaternary structure was readily detected in fractograms obtained by an optimized protocol for which aggregation of the VLPs during separation did not occur to a significant extent.

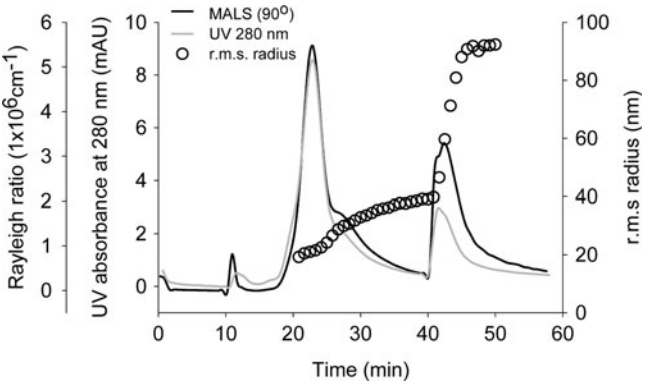

Fig. 13.2 AF4 analysis of virus-like particles (VLPs) under optimal fractionation conditions. AF4-MALS-UV fractograms of VLPs from insect cells purified by ultracentrifugation. Rayleigh ratio shown was calculated from detector signal at 90° (Reprinted in part from [18], © 2008, with permission from John Wiley and Sons)

13.3.2 Dendrimers

Poly(amidoamine) dendrimers (PAMAM) are well defined macromolecules containing tertiary amines in their core and primary amines as surface moieties [19]. They are used for drug or gene delivery purposes, as reaction catalysts or as diagnostic reagents. Because of the large number of protonable sites, dendrimers exhibit complex solution properties that are greatly dependent on pH and salt concentration. This situation renders their analysis by conventional chromatography techniques, such as SEC, quite difficult. In neutral and alkaline solutions, PAMAM dendrimers are neutral; therefore hydrophobic interactions dominate and cause adsorption of dendrimers to the packing material and/or interparticle aggregation. In acidic media, dendrimers bear strong positive charges that stabilize them against aggregation and promote electrostatic repulsion between dendrimers and cationic packing material. Hence, separations of dendrimers by SEC can be performed only when the eluent is sufficiently acidic. This constraint limits the choice of packing materials and prevents SEC analysis of dendrimers in physiological conditions. Lee et al. have shown that AF4 using a channel fitted with regenerated cellulose, allows one to separate from one another PAMAM dendrimers of increasing generation number (G4 to G9) using a neutral or basic carrier. The separation of neutral dendrimers was achieved by decreasing the ratio of the cross-flow to flow rate at the channel outlet (F_c/F_{out}), thus preventing contact between the dendrimers and the membrane, which would lead to their aggregation. The system was calibrated with pullulan standards of known molecular weight and polydispersity, allowing the authors to determine from retention times the diffusion coefficients and hydrodynamic diameters of the various dendrimers. The authors have shown that AF4 offers a relevant solution to the fractionation of pH sensitive, small ($\leq$10 nm) particles of

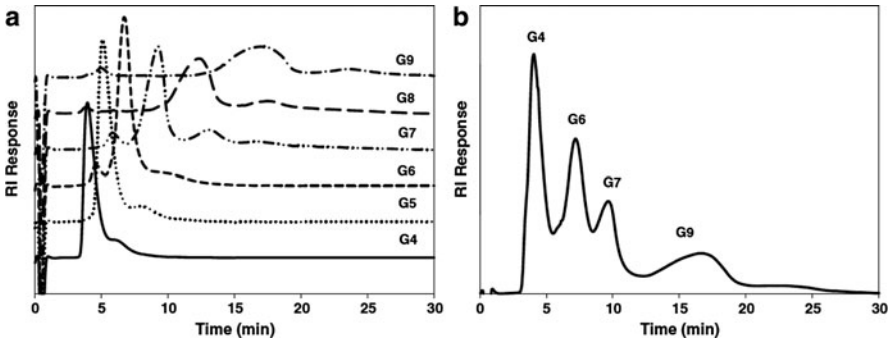

Fig. 13.3 (**a**) AF4 fractograms of PAMAM dendrimers of generations G4 to G9 and (**b**) separation of four dendrimers (G4, G6, G7, G9) obtained at pH of 3.1 (With kind permission from Springer Science + Business Media: [19] Fig. 13.2, © 2010)

well-known characteristics, Fig. 13.3 shows the resolution power during the separation of dendrimers of increasing generation. They have tested the limitations of the instrument and have laid down a sustainable approach for studying similarly sized pH-sensitive particles. They also demonstrated that this technique can be applied to studies of dendrimer-protein interactions under conditions imposed by the properties of the protein, simply by optimizing the separation conditions, a tribute to the versatility of AF4. This article gives a good tutorial for diagnosing sample-membrane interactions by observing the elution "behavior".

13.3.3 Perfluorocarbon-in-Water Emulsions

Perfluorocarbons (PFC) have an exceptionally large capacity to dissolve gases, which together with their non-toxicity, justifies their use as synthetic oxygen carriers (blood substitutes), as well as in certain therapeutic formulations and in vivo imaging applications. To prevent formation of fatal emboli upon intravascular administration, PFC must be emulsified in a water continuous phase. Control of the emulsion particle size distribution upon storage is critical for safe use of blood substitutes, since they can trigger serious flulike symptoms if their size is too small [20]. The particle size is usually measured by DLS, but several reports have indicated that DLS measurements fail to detect small particle fractions, which tend to trigger undesired side effects upon injection. SdFFF was shown to be an excellent method to characterize the composition of PFC-in-water emulsions and to fractionate the particulates as a function of their size, thus allowing collection of monosized fractions that can be further characterized by DLS or gas chromatography, as seen in Fig. 13.4. Weers et al. [7, 21] reported the SdFFF analysis of an emulsion in water of perfluorooctyl bromide (PFOB, 90%), egg yolk phospholipid (EYP, 4%) and long chain triglyceride (LCT, 6%), for which DLS analysis yielded a unimodal size

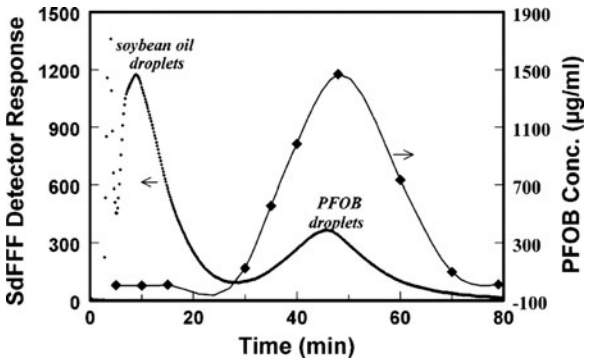

Fig. 13.4 SdFFF fractogram obtained for an emulsion comprised of 90% w/v PFOB, 4% w/v EYP, and 5% w/v soybean oil. Also shown is the PFOB concentration in fractions collected across the particle size distribution (as determined by gas chromatography) (Reprinted with permission from [21], © 2004, American Chemical Society)

distribution. The fractograms monitored with UV detection presented three distinct bands: a shoulder to the longer retention time side of the void volume signal, assigned to small unilamellar vesicles, and bands eluting at ~20 min (~180 nm) and ~50 min (~270 nm) assigned, respectively, to LCT and PFOB emulsions. The latter two bands were characterized by GC analysis of collected fractions. SdFFF was employed also to monitor the fate of PFC emulsions upon intravascular injection. Collected blood samples were diluted (2/1) with phosphate buffer prior to SdFFF analysis. Blood components elute in the void volume due to steric exclusion. A broad peak from 10 to 50 min was assigned to the PFC emulsion. It is shifted to longer time and broadened post-infusion, compared to the original emulsion. These experiments illustrate the versatility and power of SdFFF, a technique capable of monitoring changes in particle size following intravenous infusion from whole blood.

13.3.4 Nanogels

Hydrogel nanoparticles with radii in the 20–100 nm range, or nanogels, are developed currently for use as injectable drug delivery systems. The nanogels size, size distribution and shape, are readily obtained from AF4/MALS analysis, as in the case of other nanoparticles. The technique also provides means to monitor the stepwise outcome of nanogel engineering, e.g., the controlled assembly of nanogels into higher order structure [22] or, conversely, to follow the erosion of hydrolytically-degradable nanogels, as described by Smith et al. [8], who prepared nanogels (NGs) of poly(N-isopropylmethacrylamide)-(N,O-(dimethacryloyl) hydroxylamine (pNIPMAm-DMHA) that are pH- and thermo-sensitive. The authors determined the size of the NGs by batch-mode DLS and MALS to determine the hydrodynamic radius (R_h) (66 nm) and the radius of gyration (R_{rms}) (40 nm), respectively. Using

AF4 separation coupled to light scattering detection, the authors determined that degradation of the nanogels is accelerated in neutral to basic pH, compared to acidic pH or higher temperatures. Upon degradation, the NG size increased as a consequence of the hydrolysis of the DMHA groups responsible for the network connectivity. Degradation was also accompanied by a decrease in the molar mass of the NG fractions implied from the observed decrease of the light scattering intensity. Furthermore, samples were collected at the outlet of the instrument and the recovered fractions were analyzed using the NanoSight particle tracking analysis system, a technique yielding the particle number density and R_h. AF4 proved to be adequate to separate the degradation products from the nanogels, however the authors did not quantify the fraction of degradation products, possibly because their size was too small for them to be retained by the membrane on the accumulation wall.

13.3.5 Liposomes

Liposomes form an important class of drug delivery systems currently in clinical use [23]. Their size and size distribution in suspension is an important factor that will determine the amount of drug encapsulated, the particle sedimentation behavior, as well as their circulation time in the blood-stream and biodistribution [24].

FFF fraction proved to be an excellent tool for the characterization of the liposomes. The reader is referred to Chap. 14 in this book for detailed information on this topic.

13.4 Gene Delivery Systems

The delivery of plasmid DNA to cell nuclei for therapeutic applications offers numerous opportunities for vaccines and for the treatment of hereditary diseases and cancer. Much research has been devoted to the design of safe delivery systems endowed with high in vivo transfection efficiency. Less attention has been paid so far to the design of analytical methods well adapted to control the preparation of the gene delivery vectors and to assure the quality and purity of the final product. Such methods are needed in order to correlate structure and activity of the vectors, in particular in cases of complex mixtures where subsets of particles may greatly differ in transfection efficiency. A limited number of studies on the use of FFF techniques have been reported, covering the three main classes of gene delivery vectors: cationic lipid/DNA complexes, virus-like nanoparticles and polycation/DNA complexes. They are described in the next sections as they lay down the basis for the design of FFF separation of DNA and its complexes.

13.4.1 Cationic Lipid/DNA Complexes

The first application of FFF to gene delivery systems was reported by Lee et al. who established design rules for the separation of DNA complexes, specifically lipofectamine/DNA nanoparticles [25]. Two factors need to be considered at the onset: (1) DNA/cationic lipid complexes can dissociate if the carrier ionic strength is too high and (2) neither the particles nor the other components of the formulations should adsorb on the membrane forming the accumulation wall of the channel. The authors evaluated three membranes (regenerated cellulose, polycarbonate, and polypropylene) for the analysis of DNA, condensed DNA and cationic lipid/DNA complexes of various charge ratios (+/−). Both polypropylene and polycarbonate membranes were found to be suitable; the choice of one over the other depended on the sample type and separation conditions. Regenerated cellulose was rejected since sample adsorption hampered the separation under certain conditions. Fractograms of cobalt-DNA complexes, DNA and lipofectamine/DNA complexes of varying charge ratios were recorded using UV and MALS detectors. MALS fractograms indicated that cationic lipid/DNA complexes are polydisperse in size and contain large species at every charge ratio. The relative proportion of particles of large diameter (200 nm) was largest for complexes with +/− ratios of 1.4 and 2.0. FFF analysis was applied also to assess the effect of sample ageing on the size and size distribution of the complexes.

13.4.2 Virus-Like Particles for DNA Delivery

Virus-based gene delivery systems are the focus of intensive research, in view of their high in vivo transfection efficiency, but their commercial production remains problematic, in part due to the lack of reliable analytical methods. An AF4/MALS/UV method for the analysis of virus-like particles (VLP) derived from the human polyoma JC virus was reported by Citkowicz et al. who demonstrated that the technique is particularly helpful to monitor the VLPs purification and the production scale-up process [26]. The VLPs studied consisted of the recombinant VP1 protein and were obtained from insect cells. Prior to purification, the isolated proteins consisted of two components, with molar masses of 2,500 kDa, ascribed to protein aggregates, and 17,000 kDa (rms radius of 20 nm), corresponding to the VLPs. The protein aggregates proved to be incapable of entrapping DNA and needed to be removed prior to DNA packaging. The VLPs were purified on DEAE Sepharose. The successful outcome of the purification was readily confirmed by AF4/MALS. The authors note that, in contrast, SEC failed to provide any information on the protein during purification. Five standard SEC supports were tested. They all retained the protein irreversibly.

The packaging of a 1.6 kB linear DNA into VLPs was also monitored by AF4/MALS. Packaged VLPs were smaller, by ~1400 kDa, than virgin VLPs, yet the two objects had similar hydrodynamic radii (~24 nm) and the rms radius (obtained from

MALS) of the packaged VLPs was larger than that of the virgin VLPs. The paradox that the packaged VLPs have a larger rms radius than the VLPs, although they are heavier, can be understood if one remembers that the radius calculated from the angular dependence of the scattered light reflects the mass distribution about the particle center of gravity.

13.4.3 Polycation/DNA Complexes

Cationic polymers condense DNA through electrostatic interactions to form nanoparticles that can be internalized by cells and transferred to the nucleus. Although the transfection efficiency of DNA/polycation complexes is usually lower than that of VLPs, the use of synthetic polymers is often favored on the basis of safety considerations. The complexes are prepared by simple mixing of DNA with an excess polycation, so that the ratio of positive to negative charges (+/−) exceeds one. The role of the excess polycation is to ensure overcharging of the particles so that they resist aggregation, as a consequence of interparticle electrostatic repulsion. In addition, excess polycation seems to enhance transfection efficiency, although the mechanism of this effect remains poorly understood. A study by Ma et al. demonstrates that AF4 with MALS and UV-Vis detectors can yield in a single experiment the size and size distribution of DNA/polycation particles and the amount of polycation free in solution [26, 27]. The analysis was performed on complexes between DNA and chitosan, a cationic polysaccharide, which was labeled lightly with the dye rhodamine-B to facilitate UV-Vis detection of the polycation. Optimization of the AF4 separation included (1) selection of the membrane, a special regenerated cellulose membrane designed for the separation of amphiphilic polycations, (2) choice of the aqueous carrier, a pH 4 acetic acid/acetate buffer of low ionic strength known to keep DNA/chitosan complexes intact and to solubilize chitosan; and (3) a four-step gradient cross-flow. The free chitosan content in a sample prepared by mixing DNA and chitosan in a +/− ratio of 5 was determined from fractograms monitored by UV-Vis detection, which presented a band eluting between 1 and 9 min attributed to free chitosan. The chitosan concentration extracted from AF4 fractograms was validated by an independent method involving ultracentrifugation of the dispersions prepared with unlabelled chitosan followed by analysis of the supernatant by the Orange II dye depletion method. The fractograms of DNA/chitosan-rhodamine presented a second elution band between 9 and 32 min, detected by UV-Vis absorption at $\lambda = 250$ nm (DNA) and $\lambda = 556$ nm (chitosan-rhodamine) and also by the MALS and DLS detectors. This band was attributed to the elution of the DNA/chitosan complexes, which had a broad size distribution and a hydrodynamic radius ranging from 20 to 160 nm. Cumulative weight fraction distributions of the hydrodynamic radii of the particles indicate that ~80% of the particles had a R_h ranging from 30 to 50 nm. Batch DLS analysis of the same sample yielded a z-averaged R_h of 130 nm, calculated from the Stokes-Einstein equation and the zero-angle extrapolated diffusion coefficient. Hence,

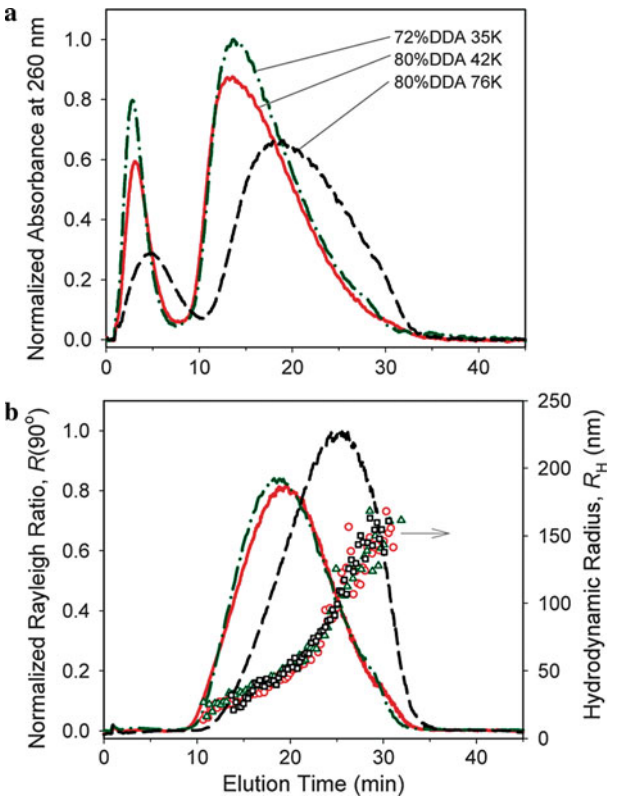

Fig. 13.5 AF4/UV/MALS + DLS fractograms of dispersion of DNA complexed with Ch-rho having different values of DDA and Mn (N/P = 5), showing (**a**) the absorbance at 260 nm, (**b**) the Rayleigh ratio at 90° (*lines*) and the hydrodynamic radius of the nanoparticles with Ch-rho DDA 72% and 35 kDa (Δ), Ch-rho DDA 80% and 42 kDa (○), and Ch-rho DDA 80% and 76 kDa (□). The added DNA concentration was 41 μg/mL (Reprinted with permission from [27], © 2010, American Chemical Society)

although the overall range of hydrodynamic radii determined by on-line DLS and by batch DLS is the same, the contribution of the larger particles to the scattered light is over-emphasized in the batch-mode analysis, as seen in Fig. 13.5.

The authors analyzed chitosan/DNA particles obtained by varying experimental parameters known to influence their transfection efficiency, including the DNA concentration at mixing, the +/− ratio, and the chitosan molecular weight. All dispersions contained free chitosan in addition to nanoparticles. The +/− ratio of the complexes was shown to be constant (~1.3 to 1.6), independently of the polycation and DNA concentrations upon mixing. In all preparations, the DNA/chitosan complexes had hydrodynamic radii ranging from 15 to 160 nm, but the size distribution of the complexes was influenced by the chitosan molecular weight and the DNA concentration at mixing. The ready availability of a detailed description of DNA/polycation complexes will facilitate quality control during preparation

Table 13.1 Review of FFF analysis of drug and gene delivery systems

Sample type	Technique	Year	Results
Drug delivery systems			
Microspheres	Fl/Hy-FFF	1999	Rapid size characterization of micrometer sized core/shell PLLA particles with varying amount of drug encapsulated [11]
Nanospheres	Fl-FFF + Sd-FFF	2007	Complementarity of the techniques, rapid size determination of PLA NPs, effect of surfactant and carrier solution [12]
	AF4+ SLS,DLS, SEM, AFM	2010	Effect of solvents observed. Comparison with other size determination techniques [28]
Core-shell nanoparticles	AF4 + TEM	2008	Separation of coreless micelles from core-shell nanoparticles and size determination [17]
Gelatin nanoparticles	AF4/MALS + SEM&PCS	2004	Determination size, size distribution, MW and loading efficiencies of gelatin NP [13]
	AF4/RI	2007	Quantification of PEG [14]
SLN and oil-loaded SLN	FFF/MALS + PCS/TEM	2004	Analysis of different shapes and of incorporation capacity [15]
Melt extrudates nanoparticles	AF4	2010	Distinction between colloidal polymer, API-rich NPs and surfactant or silica NPs [16]
Poly(amidoamine) dendrimers	AF4	2010	Fractionation between generations, separation from impurities. Interaction with BSA [19]
Perfluorocarbon emulsions in water	Sd-FFF	2004	Assessment of size distribution change of PFC in whole blood samples [7]
Nanogels	AF4/MALS/dRI	2010	Effect of pH and temperature on erosion kinetic of hydrolysable nanogels [8]
Liposomes	Fl-FFF	1993	Size and size distribution [24]
	Fl-FFF/PCS	1998	Effect of ionic strength and pH of carrier solutions on elution time of liposomes [29]
	AF4/MALS	2003	Size, size distribution, and encapsulation efficiency of tetrameric hemoglobin in liposomes + effect of extrusion pore sizes [30]
	SEC + FFF/DLS/MALS	2006	Advantage of fractionation [31]
	AF4	2009	Optimization of the fractionation conditions and importance of concentration monitoring [32, 33]
	AF4/MALS	2010	Influence of carrier ionic strength and osmostic pressure on the fractionation [9]

(continued)

Table 13.1 (continued)

Sample type	Technique	Year	Results
Vesicles	Fl-FFF/MALS	1998	Determination of number and mass weighted vesicle size distributions [34]
Virus-like particles	FFF	2008	Size and size distribution of heterogeneous samples, without adsorption [18]
Gene Delivery Systems			
Cationic lipid-DNA complexes	Fl-FFF/MALS/ UV + RI	2001	Study of heterogeneous particles in size and in charge, and observation of aggregates [25]
Virus-like particles	AF4/MALS/DLS + UV, fluo. RI	2008	Complete characterization of VLPs (MM, rms, Rh) throughout upscaling process [26]
	ES-DMA, AF4, TEM	2009	Comparison of techniques, quantitative size distributions of VLPs [35]
Linear and circular DNA	Fl-FFF	1993	Separation of linear versus single and double circular DNAs based on diffusion values [36]
Polyelectrolyte complexes	AF4/DLS	2005	Influence of ionic strength and mixing ratios on incorporation and elution behaviour [37]
Chitosan/DNA	AF4/UV/MALS/ DLS + SEM	2010	Information on amount of unbound chitosan, size and size distribution of chitosan/DNA complexes [27, 38]

scale up. Moreover, the correlation of the physico-chemical properties of DNA/polycation complexes with their transfection efficiencies is perceived as an important step towards the production of effective synthetic gene delivery systems (Table 13.1) [38].

13.5 Conclusion

The overview of the current bioanalytical literature concerned with pharmaceutical applications presented here provides convincing evidence that FFF techniques are currently applied on a routine basis in biomedical studies, quality control analysis of complex, heterogeneous commercial drug formulation, as well as in the development and characterization of new drug and gene delivery systems. FFF can be used also to great advantage to monitor carrier degradation under physiological conditions. Future applications include monitoring the interactions of NPs with serum proteins or with cells. Miniaturization will increase the use of FFF as a pre-analytical technique.

Conversely, larger scale instruments with preparative or semi-preparative capability may further enhance the scope of this versatile analytical tool.

References

1. Gaumet M, Vargas A, Gurny R, Delie F (2008) Nanoparticles for drug delivery: the need for precision in reporting particle size parameters. Eur J Pharm Biopharm 69(1):1–9
2. Fraunhofer W, Winter G (2004) The use of asymmetrical flow field-flow fractionation in pharmaceutics and biopharmaceutics. Eur J Pharm Biopharm 58(2):369–383
3. Roda B, Zattoni A, Reschiglian P, Moon MH, Mirasoli M, Michelini E, Roda A (2009) Field-flow fractionation in bioanalysis: a review of recent trends. Anal Chim Acta 635(2):132–143
4. Qureshi RN, Kok WT (2011) Application of flow field-flow fractionation for the characterization of macromolecules of biological interest: a review. Anal Bioanal Chem 399(4):1401–1411
5. Williams SK, Lee D (2006) Field-flow fractionation of proteins, polysaccharides, synthetic polymers, and supramolecular assemblies. J Sep Sci 29(12):1720–1732
6. Williams SK, Runyon JR, Ashames AA (2010) Field-flow fractionation: addressing the nano challenge. Anal Chem 83(3):634–642
7. Weers JG, Arlauskas RA (2004) Particle size analysis of perfluorocarbon emulsions in a complex whole blood matrix by sedimentation field-flow fractionation. Colloids Surf B Biointerfaces 33(3–4):265–269
8. Smith MH, South AB, Gaulding JC, Lyon LA (2010) Monitoring the erosion of hydrolytically-degradable nanogels via multiangle light scattering coupled to asymmetrical flow field-flow fractionation. Anal Chem 82(2):523–530
9. Hupfeld S, Moen HH, Ausbacher D, Haas H, Brandl M (2010) Liposome fractionation and size analysis by asymmetrical flow field-flow fractionation/multi-angle light scattering: influence of ionic strength and osmotic pressure of the carrier liquid. Chem Phys Lipids 163(2):141–147
10. Zhao Y, Fu J, Ng DKP, Wu C (2004) Formation and degradation of poly(D, L-lactide) nanoparticles and their potential application as controllable releasing devices. Macromol Biosci 4(9):901–906
11. Moon MH, Kim K, Byun Y, Pyo D (1999) Size characterization of core-shell poly(l-lactide) microspheres by flow/hyperlayer field-flow fractionation. J Liquid Chromatogr R T 22 (18):2729–2740
12. Contado C, Dalpiaz A, Leo E, Zborowski M, Williams PS (2007) Complementary use of flow and sedimentation field-flow fractionation techniques for size characterizing biodegradable poly(lactic acid) nanospheres. J Chromatogr A 1157(1–2):321–335
13. Fraunhofer W, Winter G, Coester C (2004) Asymmetrical flow field-flow fractionation and multiangle light scattering for analysis of gelatin nanoparticle drug carrier systems. Anal Chem 76(7):1909–1920
14. Zillies JC, Zwiorek K, Winter G, Coester C (2007) Method for quantifying the PEGylation of gelatin nanoparticle drug carrier systems using asymmetrical flow field-flow fractionation and refractive index detection. Anal Chem 79(12):4574–4580
15. Jores K, Mehnert W, Drechsler M, Bunjes H, Johann C, Mader K (2004) Investigations on the structure of solid lipid nanoparticles (SLN) and oil-loaded solid lipid nanoparticles by photon correlation spectroscopy, field-flow fractionation and transmission electron microscopy. J Control Release 95(2):217–227
16. Kanzer J, Hupfeld S, Vasskog T, Tho I, Holig P, Magerlein M, Fricker G, Brandl M (2010) In situ formation of nanoparticles upon dispersion of melt extrudate formulations in aqueous

medium assessed by asymmetrical flow field-flow fractionation. J Pharmaceut Biomed 53 (3):359–365
17. Kang D, Kim M, Kim S, Oh K, Yuk S, Lee S (2008) Size characterization of drug-loaded polymeric core/shell nanoparticles using asymmetrical flow field-flow fractionation. Anal Bioanal Chem 390(8):2183–2188
18. Chuan YP, Fan YY, Lua L, Middelberg AP (2008) Quantitative analysis of virus-like particle size and distribution by field-flow fractionation. Biotechnol Bioeng 99(6):1425–1433
19. Lee S, Kwen HD, Lee SK, Nehete SV (2010) Study on elution behavior of poly(amidoamine) dendrimers and their interaction with bovine serum albumin in asymmetrical flow field-flow fractionation. Anal Bioanal Chem 396(4):1581–1588
20. Flaim SF (1994) Pharmacokinetics and side effects of perfluorocarbon-based blood substitutes. Artif Cells Blood Substit Immobil Biotechnol 22(4):1043–1054
21. Weers JG, Arlauskas RA, Tarara TE, Pelura TJ (2004) Characterization of fluorocarbon-in-water emulsions with added triglyceride. Langmuir 20(18):7430–7435
22. Hasegawa U, Sawada S, Shimizu T, Kishida T, Otsuji E, Mazda O, Akiyoshi K (2009) Raspberry-like assembly of cross-linked nanogels for protein delivery. J Control Release 140(3):312–317
23. Wang X, Zheng H, Zhu Z, Wei Y, Chen L (2010) Clinical pharmacokinetics of paclitaxel liposome with a new route of administration in human based on the analysis with ultra performance liquid chromatography. J Pharm Sci 99(11):4746–4752
24. Moon MH, Giddings JC (1993) Size distribution of liposomes by flow field-flow fractionation. J Pharmaceut Biomed 11(10):911–920
25. Lee H, Williams SKR, Allison SD, Anchordoquy TJ (2001) Analysis of self-assembled cationic lipid – DNA gene carrier complexes using flow field-flow fractionation and light scattering. Anal Chem 73(4):837–843
26. Citkowicz A, Petry H, Harkins RN, Ast O, Cashion L, Goldmarm C, Bringmarm P, Plummer K, Larsen BR (2008) Characterization of virus-like particle assembly for DNA delivery using asymmetrical flow field-flow fractionation and light scattering. Anal Biochem 376(2):163–172
27. Ma PL, Buschmann MD, Winnik FM (2010) Complete physicochemical characterization of DNA/chitosan complexes by multiple detection using asymmetrical flow field-flow fractionation. Anal Chem 82(23):9636–9643
28. Scherer C, Noskov S, Utech S, Bantz C, Mueller W, Krohne K, Maskos M (2010) Characterization of polymer nanoparticles by asymmetrical flow field-flow fractionation (AF-FFF). J Nanosci Nanotechnol 10(10):6834–6839
29. Moon MH, Park I, Kim YH (1998) Size characterization of liposomes by flow field-flow fractionation and photon correlation spectroscopy – Effect of ionic strength and pH of carrier solutions. J Chromatogr A 813(1):91–100
30. Arifin DR, Palmer AF (2003) Determination of size distribution and encapsulation efficiency of liposome-encapsulated hemoglobin blood substitutes using asymmetric flow field-flow fractionation coupled with multi-angle static light scattering. Biotechnol Progr 19(6):1798–1811
31. Hupfeld S, Holsaeter AM, Skar M, Frantzen CB, Brandl M (2006) Liposome size analysis by dynamic/static light scattering upon size exclusion-/field-flow-fractionation. J Nanosci Nanotechno 6(9–10):3025–3031
32. Hupfeld S, Ausbacher D, Brandl M (2009) Asymmetric flow field-flow fractionation of liposomes: 2. Concentration detection and adsorptive loss phenomena. J Sep Sci 32(20):3555–3561
33. Hupfeld S, Ausbacher D, Brandl M (2009) Asymmetric flow field-flow fractionation of liposomes: optimization of fractionation variables. J Sep Sci 32(9):1465–1470
34. Korgel BA, van Zanten JH, Monbouquette HG (1998) Vesicle size distributions measured by flow field-flow fractionation coupled with multiangle light scattering. Biophys J 74(6):3264–3272

35. Pease LF, Lipin DI, Tsai DH, Zachariah MR, Lua LHL, Tarlov MJ, Middelberg APJ (2009) Quantitative characterization of virus-like particles by asymmetrical flow field-flow fractionation, electrospray differential mobility analysis, and transmission electron microscopy. Biotechnol Bioeng 102(3):845–855
36. Liu MK, Giddings JC (1993) Separation and measurement of diffusion coefficients of linear and circular DNAs by flow field-flow fractionation. Macromolecules 26(14):3576–3588
37. Yohannes G, Holappa S, Wiedmer SK, Andersson T, Tenhu H, Riekkola ML (2005) Polyelectrolyte complexes of poly(methacryloxyethyl trimethylammonium chloride) and poly(ethylene oxide)-block-poly(sodium methacrylate) studied by asymmetrical flow field-flow fractionation and dynamic light scattering. Anal Chim Acta 542(2):222–229
38. Ma PL, Buschmann MD, Winnik FM (2010) One-step analysis of DNA/chitosan complexes by field-flow fractionation reveals particle size and free chitosan content. Biomacromolecules 11(3):549–554

Chapter 14
Characterization of Liposomes by FFF

Susanne K. Wiedmer and Gebrenegus Yohannes

Abstract Lipids are the main constituent of biological membranes and these semi-permeable lipid layers have many features such as controllable flexibility and water impermeability. The use of liposomes and vesicles as biocompatible targeted drug carriers in pharmaceutical, cosmetic, and biotechnological applications was introduced already in the seventies', and a decade later the use of vesicles as skin drug delivery systems started to become popular. This chapter describes FFF in comparison to other analytical methods in studies of vesicle sizes, size distribution, and stability, when developing pharmacutical formulations for efficient delivery of liposomes, drug release, and transfection. The experimental parameters affecting retention and particle size distribution required for FFF are discussed including selection of the types of membranes, ionic strength and pH of carrier solution, flow rates, and injected mass.

Keywords Dynamic light scattering • FFF • Lipidomics • Lipids • Liposomes • Multiangle light scattering • Refractive index • UV • Vesicles

14.1 Introduction

Biological membranes are built up of a highly diverse mixture of phospholipids, glycolipids, sterols, integral and peripheral proteins. The specific distribution of components of the biological membrane is strongly dependent on the surrounding environment; the membrane fronting the cytoplasm is much different from the part of the membrane fronting the extracellular fluid. This asymmetry of the membrane (inside or outside the cell) is of key importance when studying in vivo membrane

S.K. Wiedmer (✉) • G. Yohannes
Laboratory of Analytical Chemistry, Department of Chemistry, University of Helsinki, Helsinki, Finland
e-mail: susanne.wiedmer@helsinki.fi

S.K.R. Williams and K.D. Caldwell (eds.), *Field-Flow Fractionation in Biopolymer Analysis*, DOI 10.1007/978-3-7091-0154-4_14,

models. The biological cell membrane can be seen as a fluid, semi-permeable bilayer that separates the content of the cell from the environment. This semi-permeable nature of the membrane permits the cell to maintain the composition of the cytosol independent of the external environment.

In addition to providing a semi-permeable wall around the cell, the biological membrane is the site for signal recognition, transduction and amplification, and it provides an essential structural environment for metabolism and photosynthesis. The complexity of biological membranes makes in vivo research on membranes very demanding, and because of this much of the understanding and knowledge that we have about biological membranes are a result of in vitro research. Typical in vitro phospholipid bilayer systems that are used in research are Langmuir Blodgett films, supported phospholipid bilayers, vesicles, discoidal micelles (disks), microbubbles, and suspended phospholipid bilayers.

The use of vesicles and liposomes as biocompatible targeted drug carriers in pharmaceutical, cosmetic, and biotechnological applications was introduced already in the 1970s, and a decade later the use of vesicles as skin drug delivery systems started to become popular. The correct lipid composition, vesicle size and surface charge, membrane fluidity, and vesicle stability is of key importance when developing such formulations for efficient delivery of liposomes, drug release, and transfection. Because of this much research has been carried out on the development of new techniques and methods for size distribution analyses.

Field-flow fractionation (FFF) is one of the most versatile separation techniques in the field of analytical separation sciences, capable of separating macromolecular colloidal and particulate materials [1]. The major sub techniques are sedimentation FFF, thermal FFF, electric FFF, and flow FFF. Depending on the field applied (centrifugal, thermal, electrical, hydrodynamic), each of the FFF sub techniques are different one from another. In terms of biological applications, these methods can be used to separate particles that range in size from a protein to an entire cell. DNA, viruses, and other bioparticles, such as lipoproteins, ribosomes, and liposomes have all been separated using these techniques.

In the following sections we will describe FFF studies carried out on liposomes and other types of lipid aggregates. Focus is mainly on asymmetrical flow FFF (AsFlFFF) but also sedimentation FFF (SdFFF) has been applied to some extent. Comparison of FFF with other techniques for the characterization of particle sizes will be made and important parameters to consider when applying FFF for studies on liposomes and lipid aggregates or on lipid-protein complexes will be discussed.

14.2 Lipids and Liposomes

Lipidomics has become an emerging field among natural sciences, covering the broad study of routes and complex systems of cellular lipids in biological systems. Generally lipidomics can be divided into two subcategories; global lipidomics, that tend to identify all lipids within a certain matrix, and targeted lipidomics, which heads at

quantitative determination of selected (one or many) lipids. Lipids constitute up to about 50% of the mass of most animal cell membranes. A rough estimation is that the theoretical number of lipids, covering the most abundant lipid classes, is close to 200,000. The major lipid classes found in eukaryotic membranes are glycerophospholipids, sphingolipids, and cholesterol. The fundamental role of phospholipids is to maintain the structure of the cellular membranes, to ensure membrane fluidity and a suitable environment and topology for attached proteins. In addition, the lipid composition is of importance to ensure the activity of membrane-bound enzymes and the mobility (lateral) of receptors and the activation of particular signaling trails (Fig. 14.1).

Cholesterol, having both structural and regulatory roles, is the most abundant sterol in biological membranes. It is a steroid metabolite that has received much attention because it is strongly associated with the progression of atherosclerosis. Depending on the type of cell membranes, the cholesterol concentrations vary typically between 25% and 50%. The maximum solubility of cholesterol in phosphatidylcholine (PC) bilayers is 66%, and exceeding this concentration results in

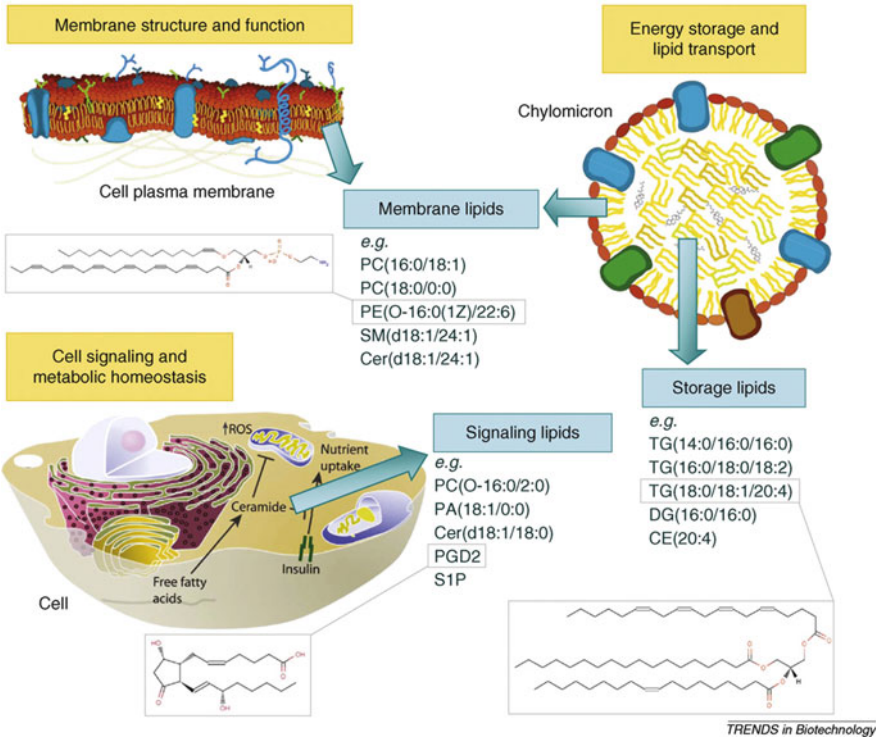

Fig. 14.1 Biological functions of lipids. The chemical structures are shown for ethanolamine plasmalogen PE(O-16:0(1Z)/22:6), prostaglandin D2 (PGD2) and triacylglycerol TG(18:0/18:1/20:4). PC, phosphatidylcholine; PE, phosphatidylethanolamine; PA, phosphatidic acid; DG, diacylglycerol; Cer, ceramide; SM, sphingomyelin; ChoE, cholesterol ester; S1P, sphingosine-1-phosphate (Reprinted from [2], © 2008, with permission of Elsevier)

separation of crystalline cholesterol. Due to the important roles of cholesterol in biological membranes, much in vitro research on biomimicking lipid bilayers comprise cholesterol.

When lipids are dispersed in aqueous solution aggregates are formed due to the amphiphilic properties of the molecule; the hydrophobic chains are screened from the surrounding water phase, with the hydrophilic polar head groups pointing outwards. The types of lipid aggregates that are formed depend on the molecular structure, the concentration of the molecule, and the surrounding properties, such as temperature, solvent composition, and ionic strength. Typical phospholipid aggregates formed under aqueous conditions are lipid vesicles, so called liposomes. The general classification of liposomes is according to the sizes of the aggregates, and these vary in general between 20 nm and 200 μm (Fig. 14.2).

Small, large, and giant unilamellar vesicles are the most important types of liposomes used for analytical applications. On the other hand, multilamellar vesicles are frequently used in pharmaceutical and cosmetic applications. Multivesicular vesicles are giant vesicles encapsulating smaller liposomes that have been used in nanoreactor assemblies and as drug delivery tools (vesosomes).

Unilamellar vesicles for analytical purposes can be prepared from multilamellar vesicles by different approaches. The choice of method will to some extent determine what type of unilamellar vesicles are formed, e.g., sonication typically produces small unilamellar vesicles, whereas extrusion is one of the most popular methods for preparing large unilamellar vesicles.

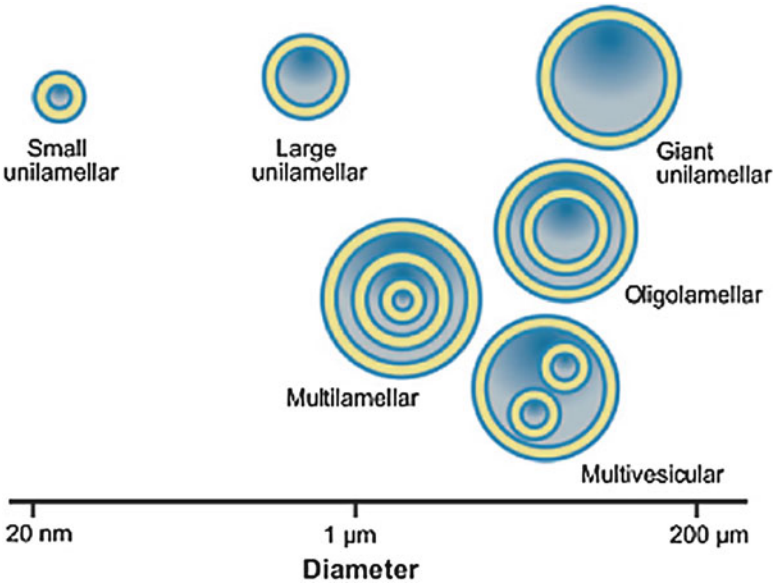

Fig. 14.2 Schematic drawing of liposomes. Small unilamellar vesicles (~20 nm to 100 μm), large unilamellar vesicles (~100 nm to ~1 μm), and giant unilamellar vesicles (>1 μm). The drawings are not to scale (Reprinted with permission from [3], © 2008)

14.3 Types of FFF Techniques

The first publication demonstrating the suitability of FFF in the characterization of lipid aggregates was published in 1981 [4]. In that work SdFFF was used, and two other studies on the use of SdFFF for the characterization of vesicles were published in the 1980s as well [5, 6]. In all these studies the liposomes were dispersed in pH 7.4 buffer solutions and detection was made by UV. The effective mass and mass distribution of particles is determined in SdFFF, but the technique requires a rather complex centrifugation device. In the nineties' flow FFF (FlFFF) started to be the method of choice because, in contrast to SdFFF, FlFFF provides the direct determination of the size and size distribution of vesicles because the separation is based on the differences in the hydrodynamic radius of particles. UV-detection combined with FlFFF was used for the size characterization of negatively charged liposomes prepared by sonicating or extruding multilamellar vesicles [7, 8]. In the first study, published in 1993, the authors used both SdFFF-UV and FlFFF-UV to compare the sizes of liposomes [9]. The liposome samples comprised distearoyl phosphatidylcholine (DSPC) and disteroyl phosphatidic acid (DSPA). The dispersions were sonicated for 5, 15, and 35 min. Both FlFFF and SdFFF showed the same trends for reduction of sizes; the longer the sonication time, the smaller were the particle sizes.

In 1994 [9] the first report on multiangle light scattering (MALS) detection on-line combined with FlFFF was published and some years later [10, 11] vesicle size distributions were studied by FlFFF-MALS. The presence of MALS in addition to UV helps to correct for the effect of light scattering from UV. Korgel et al. described the theoretical basis for use of MALS to measure simultaneously the size and concentration of eluting vesicles such that both absolute number (Fig. 14.3) and mass-weighted vesicle size distributions can be determined without having an RI detector, prior calibration using particle size standards, or assumptions about the nature of the size distribution [10].

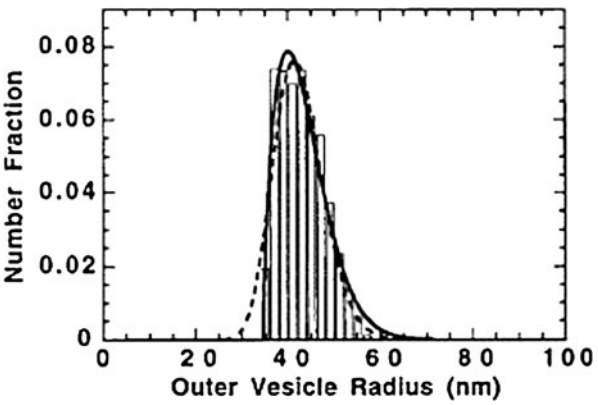

Fig. 14.3 Number-weighted size distribution of vesicles formed by extrusion through a 100-nm pore membrane. The solid curve corresponds to the Weibull distribution fit, whereas the dashed curve represents the best log-normal distribution fit (Reprinted from [10], © 1998, with permission of Elsevier)

At the beginning of the twenty-first century there was some increment in the number of FFF-related publications. Research on lipid-DNA [12] and lipid-protein [13, 14] complexes has successfully been carried out using AsFlFFF. Self-assembled cationic lipid–DNA complexes are capable to carry DNA across the cell membranes and applied in gene therapy. However, the preparations of DNA-lipid complexes with defined sizes and charges are tedious. In the work by Lee et al. heterogeneous mixtures containing lipids, DNA, liposomes, and lipid–DNA complexes were characterized by FlFFF-MALS [12]. FlFFF-MALS measurements showed that different lipid:DNA ratios resulted in different size profiles. In another type of AsFlFFF work the molecular mechanism behind the transfer of lipids between small unilamellar vesicles and high density lipoproteins, by the aid of a phospholipid transfer protein, was studied [15]. Radiolabeled lipids and proteins were used to follow the lipid transferring properties of the protein. Much good research has lately been carried out on the effect of various experimental parameters on the FFF characterization of liposomes [16–18]. These will be described in more details in the following sections.

The long-term stability and circulation persistence of liposomes is of utmost importance in drug delivery for encapsulation, storage, and release of molecules. Even though synthetic liposomes comprising egg phosphatidyl choline and phosphatidyl serine was shown to have excellent long-term stability, studied by FlFFF [19], generally liposomes tend to aggregate in aqueous solution. Accordingly, much research has been done on the development of new stabilized particle/polymer/protein-covered liposomes. FlFFF has been utilized to characterize the sizes of liposomes encapsulating hemoglobin [20], stabilized by polyethylene glycol (PEG); polyoxyethylene (POE), polyethylene oxide (PEO)-lipids [21] and actin [22, 23], and of PEG-lipid aggregates containing various types of PEG-functionalized lipids [24].

To date, however, the stability issue has already been partly solved and the critical aspects on the use of liposomes for drug delivery purposes are currently more related to the efficient release of drugs. A rather novel type of stabilized lipid assemblies is targeted microbubbles used for example in molecular imaging and ultrasound-triggered drug and gene delivery [25–27]. Microbubbles are efficient reflectors of ultrasound energy, and this is the reason for their popularity as contrast agents for medical ultrasound imaging.

In addition to the aforementioned detectors (UV and MALS), other types of detection systems that have been combined with flow FFF for characterization of liposomes or lipid aggregates include dynamic (quasi-elastic) light scattering (DLS) [28, 29] or refractive index detectors (RI) [12, 21, 23, 29]. The use of on-line mass spectrometric detection (matrix-assisted laser desorption/ionization time-of-flight mass spectrometry) with FFF was published already in 2003 [30, 31], however, until now there has been no data published on the use of that system for the characterization of lipid aggregates or lipid-protein complexes. The number of FFF papers is still rather limited and by far the most popular FFF sub-technique for the characterization of lipid aggregates and lipid-protein complexes has been flow FFF. MALS has undoubtedly started to be the detector of choice.

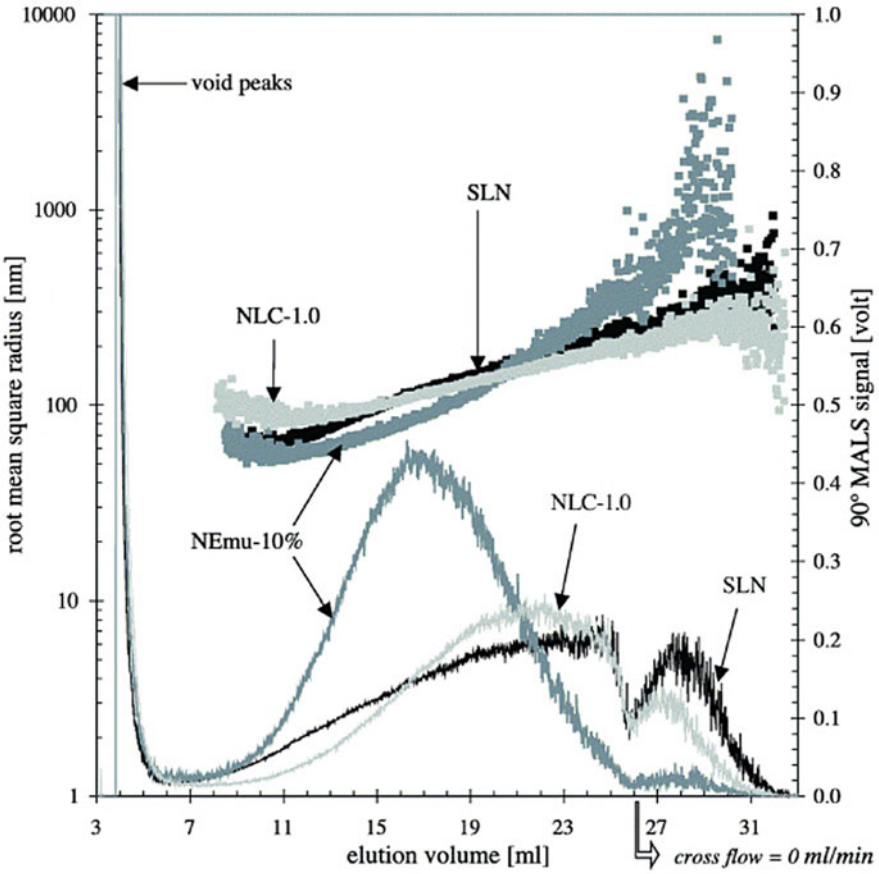

Formulation	Z-average radius [nm] (elution by FFF and subsequent LS measurements of eluates gained in between 8th and 26th minute)	Z-average radius [nm] (elution by FFF and subsequent LS measurements of eluates gained in between 8th and 32th minute)
SLN	185 +/– 4	300 +/– 9
NLC-1.0	160 +/– 3	198 +/– 5
NEmu-10%	273 +/– 9	723 +/– 18

Fig. 14.4 Elution behavior of lipid nanodispersions by AsFlFFF with subsequent detection by LS (*top curves*: root mean square radii; *bottom curves*: intensities of scattered light) (Table at the *bottom*: *z*-average particle sizes of the nanodispersions obtained from the *upper* graphs [32], © 2004, with permission of Elsevier)

Rather recently, solid lipid nanoparticles (SLNs) and oil loaded solid lipid nanoparticles (also named nanostructured lipid carriers or NLCs) were introduced as novel carrier systems for cosmetic active ingredients and

pharmaceutical drugs [32]. In that study AsFlFFF-MALS in combination with DLS, laser diffraction (LD), and cryo TEM was used to characterize the physical behaviors of SLNs and NLCs. DLS results indicated that SLN and NLC differ from a nanoemulsion with respect to Brownian motion due to asymmetric particle shapes. Non-spherical particles, in the case of SLN and NLC, lead to higher polydispersity indices compared to the nanoemulsion. In AsFlFFF, the nanodroplets eluted much earlier than the SLN- and NLC-platelets, even though the DLS and LD data showed similar particle sizes (Fig. 14.4). Platelet (for SLN), oil loaded platelet ("nanospoons"; for NLC), and droplet (for nanoemulsion) structures were observed by TEM. In contrast to literature reports, the investigated SLN appeared as thin platelets. NLC were found to be lipid platelets with oil spots sticking on the surface.

14.4 FFF in Comparison with Other Techniques

Liposomes are biocompatible, completely biodegradable, non-toxic, flexible, and non-immunogenic for systemic and non-systemic administrations. One of the key parameters that need to be considered when developing liposomes and emulsions for pharmaceutical use is determination of particle size and zeta potential. The dispersion should have a narrow particle size distribution in the submicron range. Since intravenous injection of particles with average diameters above 5 μm may cause death due to embolism, the size control and avoidance of particle aggregation is of great importance. DLS (also known as photon correlation spectroscopy, PCS), which measures variations in the intensity of the scattered light, caused by particle movement, is together with LD one of the most applied techniques for determination of particle sizes. In contrast to DLS, a broad range of particle sizes can be detected by LD. The major limitations of light scattering techniques are that they cannot differentiate between subpopulations of different sizes in (size) heterogeneous particle mixtures. Microscopic techniques like atomic force microscopy (AFM) and electron microscopy (EM) (freeze fracture and negative stain EM) are attractive tools for obtaining information on both particle sizes and shapes. However, the major limitations of these are expensive instrumental and running costs and rather complicated sample preparation methods.

Size exclusion chromatography (SEC) is by far the most popular chromatographic technique for size determination of particles. However, for size determination of particles from retention times, standard samples of known diameters are needed or the use of light scattering detectors is required.

Size distributions of lipid nanoparticles were investigated by AsFlFFF and the data were compared with that obtained by cryo transmission EM and DLS [33]. The results showed AsFlFFF to be much more useful than the other studied techniques for the characterization of particles with broad size distributions. Kang et al. studied size characterization of drug-loaded polymeric core/shell nanoparticles having broad and bimodal size distributions [33]. The lipid core

was made up of lecithin, and the shell was a pluronic composed of a self-assembled amphiphilic PEO–polypropyleneoxide–PEO polymer. These amphiphilic diblock or triblock copolymers have been used as carriers for hydrophobic drugs [33]. AsFlFFF provided size characterizations of two populations. The first population was related to an early eluting compound that was made up of non-drug loaded free polymeric micelles with diameters of around 23–31 nm. The second population corresponded to drug-loaded core/shell nanoparticles, having a broad size distribution ranging from about 100–600 nm in diameter. Size analysis by TEM was not easy because only a limited number of particles were measured and sizes measured by DLS were not reliable for samples with broad size distributions. The sizes of PEG-stabilized lipid aggregates were studied by AsFlFFF and data were compared with results obtained by DLS, cryo-TEM, and AFM techniques [24]. The PEGylated lipid aggregates were made of POPC and 1,2-distearoyl-sn-glycero-3-phosphoethanolamine-N-[methoxyPEG] (DSPEGs) with PEG molar masses of 1,000, 2,000, and 3,000. Depending on the molar mass of DSPEG, liposomes or discoidal micelles (disks) or mixtures of these were formed. AsFlFFF revealed two peaks for the POPC/DSPEG2000 sample demonstrating that the dispersion contained both liposomes and disks, and the result was confirmed by cryo-TEM.

14.5 Factors Affecting FFF Separation

In all FFF sub-techniques, sample separation is performed inside a narrow ribbon-like channel with dimensions of 10–50 cm in length, 2–3 cm in width, and 0.01–0.05 cm in thickness. From the inlet, a carrier liquid is pumped through the channel, establishing a parabolic flow profile (laminar Newtonian flow) as in a capillary tube, propelling the samples towards the outlet. An external field (force) is applied perpendicular to the direction of the carrier liquid flow, forcing the sample components to accumulate at one of the channel walls, termed accumulation wall. The experimental parameters affecting retention and particle size distribution generally include selection of the types of membranes, ionic strength and pH of carrier solution, and the injected mass.

14.5.1 Type of Membranes

The most commonly used membrane in FFF liposome research has been regenerated cellulose (RC) with a 10 K molecular weight cut-off (MWCO). Other possible membranes were reported by Lee, et al., in 2001 (*12*). The main goal of their study was to determine combinations of carrier liquid and membrane materials that result in minimal interaction between lipid − DNA complexes and the separation system. The carrier liquid used in the separation was Tris-borate buffer at pH 8.6. Three membranes, i.e., regenerated cellulose (RC, 30 K MWCO),

polycarbonate (PC, 0.03 μm pore size), and polypropylene (PP, 0.05 × 0.125 μm pore dimensions), were investigated. The investigated samples included DNA, condensed DNA, and cationic lipid − DNA complexes of varying average charge ratios. The RC membrane yielded good sample recoveries for the negative lipid − DNA samples. However, less than 5% of the neutral and positively charged samples were recovered. The PC membrane yielded good recovery of the negative and positively charged complexes (90% and 60%, respectively), but severe sample loss was observed for the neutral charge ratio complexes. The PP membrane demonstrated good recovery (90%) of all complexes, as long as the cross-flow rate was ≤0.5 mL/min, whereas higher cross-flow rates resulted in sample loss through the membrane pores as well as adsorption on the membrane. Using a 1.0 mL/min flow rate, the sample recoveries were less than 10%. In summary, each of the three membranes studied had its limitations, with the PC and PP membranes demonstrating good potential for the studied lipid − DNA complexes. In general, the choice of the membrane depends on the type of sample and conditions employed. Recently, Hupfeld investigated egg PC liposomes, and reported that even RC membranes are prone to adsorption when the sample load is less than 0.5 μg [17]. However, this effect can be overcome by pre-saturation of the RC membrane with a sample load of >2 μg. For high sample load, adsorption becomes minimal and the recovery is improved.

14.5.2 Carrier and Running Conditions

One critical parameter in FFF separations is the choice of the buffer system. Moon et al. [8] studied the influence of ionic strength and pH of carrier solutions on the separation of liposomes with subsequent (off-line) DLS size-analysis. Retention behaviors of liposomes that were stabilized by the addition of cholesterol – the liposome samples comprised phosphatidylcholine/phosphatidylglycerol/cholesterol (1:4:5 molar ratio) – were examined in different buffer solutions. The electrolyte solutions were Tris-HCl buffer (pH 7.8, I = 100 mM,), PBS buffer (pH 7.4, I = 160 mM), 0.02% NaN_3 solution (I = 3 mM), and 23.6 mM lactose with 4.62 mM NaCl (I = 4.6 mM). After sonication the liposomes were extruded through 400, 200, and 100 nm membranes for five times each. When NaN_3 or lactose (NaCl were used for dispersing the liposomes and as a carrier for the FFF separation) the retention times were shorter and the particle sizes were smaller as compared to results obtained with Tris and PBS buffer (Fig. 14.5a). The reason for this was the ionic strength, which has a strong effect on particle migration at the vicinity of the accumulation wall. DLS demonstrated that the particle sizes were about the same for all collected fractions. At low ionic strengths, vesicles are not sufficiently driven to their equilibrium positions and are eluted at elevated positions either due to an increase in the double layer thickness or due to strong electrostatic repulsion between the channel wall and the charged particles. Recently, Hupfeld, et al. investigated not only the ionic strength of the buffer solution but also the

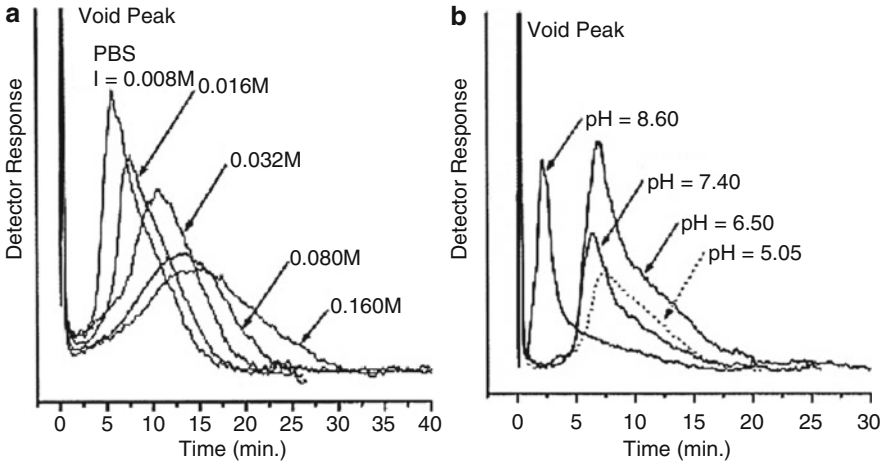

Fig. 14.5 Influence of ionic strength and pH of the carrier solution on the separation of liposomes prepared in PBS at different ionic strengths (**a**) and pH values (I = 16 mM) (**b**). The channel flow-rate was 6.44 mL/min and the cross flow-rate 1.15 mL/min (Reprinted from [8], ©1998, with permission of Elsevier)

osmotic stress-induced effects to increase or decrease particle sizes of vesicles [16, 18]. The authors used large unilamellar vesicles of egg PC and studied the influence of ionic strength of the carrier solution on the retention behavior. The ionic strength was adjusted with 5–50 mM of $NaNO_3$. Much shorter retention times were observed using distilled water as compared to $NaNO_3$ eluents. Zeta potential measurements confirmed that the surface charges (zeta potentials) of the vesicles were higher at lower ionic strengths, resulting in stronger repulsive electrostatic interactions between the vesicles and the accumulation wall.

Moon et al. examined the effect of pH on the retention of liposomes by using PBS carrier at pH values 8.6, 7.4, 6.5, and 5.5 [8]. The ionic strength was fixed at 16 mM. Retention of liposomes at pH 8.6 was shorter than at lower pH values (Fig. 14.5b). The reason was due to increased charge interactions between the vesicles and the channel surfaces at more basic conditions, thus leading to faster elution.

The overloading effect in flow FFF was first recognized by Giddings et al. [34]. It is still an important experimental requirement imposed on practical FFF operation to find a proper balance of factors that provide an adequate detector signal while avoiding observable overloading. Recently, Hupfeld et al. described the overload effect on liposomes [16]. The authors made experiments on different concentration with 1, 10, and 100 μg of mass injections. For the load of 1 and 10 μg, the Rayleigh curve appeared smooth and almost symmetrical, where as for the 100 μg mass injection the shape was distorted, causing frontal tailing, which is a typical indication of the overload effect for particles (Fig. 14.6). The main reason is that, at higher particle concentration, i.e., during the time of focusing, a portion of

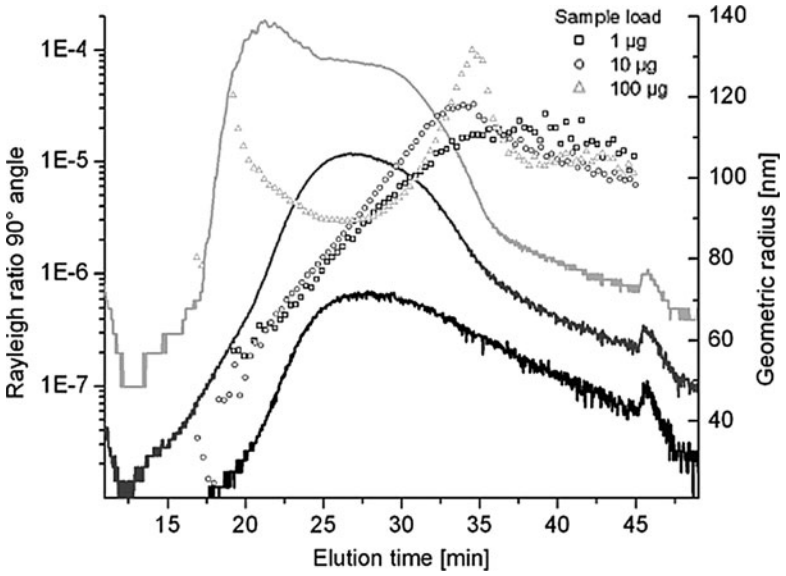

Fig. 14.6 Influence of different sample loads. *Lines*: Rayleigh ratio at 90° angle in log-scale; *scattered dots*: calculated geometric radii. Sample load: 1 µg = *black line*, 10 µg = *gray line*, 100 µg = *light gray line*. The flow rates were 1.0 mL/min at channel flow to detectors, and cross flow gradient of 1.0–0.1 mL/min over 35 min (Reprinted from [16] by permission of John Wiley and Sons, © 2009)

the particles may be hindered from reaching their equilibrium steady state from the position of the accumulation wall. As a result these particles end up in a layer that migrates at a higher velocity within the parabolic flow profile. The calculated geometric radii follow a straight line in accordance with the FFF theory. In contrast, the 100 µg load resulted in a distorted light scattering signal with expressed tailing and the geometric radius curve deviated from linearity. The retention time also decreased with increase in sample load.

Finally, proper flow rates, especially the cross flow rate, must be selected in order to fractionate liposomes and to avoid interactions with the accumulation wall. In many applications of AsFlFFF the components of the sample that have to be separated comprise a wide range of particle sizes. For such samples it is difficult to find an optimal cross flow rate. On one hand a high cross flow is required to obtain enough retention and selectivity for the smaller particle sizes, whereas on the other hand, at high cross flow rates, i.e., at high field strengths, larger particles can be compressed at the accumulation wall, promoting sample loss through the membrane pores and adsorption on the membrane, resulting in long elution times [12]. A valuable tool for AsFlFFF separations is cross flow rate programming. For this, the cross flow is gradually decreased during elution of the sample components. Application of cross flow gradients also prevents sample adsorption and results in reasonable elution times [16].

14.6 Future Perspectives

The increasing interest in liposomes as drug carriers and models for biological membranes has resulted in extensive studies on the characterization of liposomes. Various sub-techniques of FFF have been used for the separation and characterization of liposomes, however, the most applied FFF technique in the future for the characterization of lipid aggregates (including liposomes, disks, mixed surfactant/lipid vesicles) will most probably be AsFlFFF with on-line MALS, DLS, or MS detection. The high detection sensitivity of using fluorescence detection is an attractive future tool for liposomes, however, this would demand fluorescently labeled lipids. With the increasing number of commercial FFF devices, the technique will most probably also slowly start to become even more popular in industrial, pharmaceutical, and clinical laboratories. Another area of big improvements will definitely be the development of new types of membrane materials that would be highly suitable for all types of liposomes (including positively charged vesicles). The fast progress in the development of microscale devices (miniaturization) will certainly also be beneficial in the future for the analysis of liposomes by FFF.

References

1. Giddings JC (1993) Field-flow fractionation: analysis of macromolecular, colloidal, and particulate materials. Science 260:1456–1465
2. Oresic M, Hanninen VA, Vidal-Puig A (2008) Lipidomics: a new window to biomedical frontiers. Trends Biotechnol 26:647–652
3. Jesorka A, Orwar O (2008) Liposomes: technologies and analytical applications. Annu Rev Anal Chem 1:801–832
4. Caldwell KD, Karaiskakis G, Giddings JC (1981) Characterization of liposomes by sedimentation field-flow fractionation. Colloid Surface 3:233–238
5. Kirkland JJ, Yau WW, Szoka FC (1982) Sedimentation field-flow fractionation of liposomes. Science 215:296–298
6. Dreyer R, Hawrot E, Sartorelli AC, Constantinides PP (1988) Sedimentation field-flow fractionation of fused unilamellar vesicles – comparison with electron-microscopy and gel-filtration. Anal Biochem 175:433–441
7. Moon MH, Giddings JC (1993) Size distribution of liposomes by flow field-flow fractionation. J Pharm Biomed Anal 11:911–920
8. Moon MH, Park I, Kim YH (1998) Size characterization of liposomes by flow field-flow fractionation and photon correlation spectroscopy – Effect of ionic strength and pH of carrier solutions. J Chromatogr A 813:91–100
9. Roessner D, Kulicke W-M (1994) On-line coupling of flow field-flow fractionation and multi-angle laser light scattering. J Chromatogr A 687:249–258
10. Korgel BA, van Zanten JH, Monbouquette HG (1998) Vesicle size distributions measured by flow field-flow fractionation coupled with multiangle light scattering. Biophys J 74:3264–3272
11. Wyatt PJ (1998) Submicrometer particle sizing by multiangle light scattering following fractionation. J Colloid Interface Sci 197:9–20

12. Lee H, Williams SKR, Allison SD, Anchordoquy TJ (2001) Analysis of self-assembled cationic lipid-DNA gene carrier complexes using flow field-flow fractionation and light scattering. Anal Chem 73:837–843
13. Yohannes G, Wiedmer SK, Tuominen EKJ, Kinnunen PKJ, Riekkola ML (2004) Cytochrome c-dimyristoylphosphatidylglycerol interactions studied by asymmetrical flow field-flow fractionation. Anal Bioanal Chem 380:757–766
14. Muhonen J, Vidgren J, Helle A, Yohannes G, Viitala T, Holopainen JM, Wiedmer SK (2008) Interactions of fusidic acid and elongation factor G with lipid membranes. Anal Biochem 374:133–142
15. Setala NL, Holopainen JM, Metso J, Wiedmer SK, Yohannes G, Kinnunen PKJ, Ehnholm C, Jauhiainen M (2007) Interfacial and lipid transfer properties of human phospholipid transfer protein: implications for the transfer mechanism of phospholipids. Biochemistry 46:1312–1319
16. Hupfeld S, Ausbacher D, Brandl M (2009) Asymmetric flow field-flow fractionation of liposomes: optimization of fractionation variables. J Sep Sci 32:1465–1470
17. Hupfeld S, Ausbacher D, Brandl M (2009) Asymmetric flow field-flow fractionation of liposomes: 2. Concentration detection and adsorptive loss phenomena. J Sep Sci 32:3555–3561
18. Hupfeld S, Moen HH, Ausbacher D, Haas H, Brandl M (2010) Liposome fractionation and size analysis by asymmetrical flow field-flow fractionation/multi-angle light scattering: influence of ionic strength and osmotic pressure of the carrier liquid. Chem Phys Lipids 163:141–147
19. Yohannes G, Pystynen KH, Riekkola ML, Wiedmer SK (2006) Stability of phospholipid vesicles studied by asymmetrical flow field-flow fractionation and capillary electrophoresis. Anal Chim Acta 560:50–56
20. Arifin DR, Palmer AF (2005) Stability of liposome encapsulated hemoglobin dispersions. Artif Cells Blood Substit Immobil Biotechnol 33:113–136
21. Arifin DR, Palmer AF (2005) Physical properties and stability mechanisms of poly(ethylene glycol) conjugated liposome encapsulated hemoglobin dispersions. Artif Cells Blood Substit Immobil Biotechnol 33:137–162
22. Li SL, Nickels J, Palmer AF (2005) Liposome-encapsulated actin-hemoglobin (LEAcHb) artificial blood substitutes. Biomaterials 26:3759–3769
23. Arifin DR, Palmer AF (2005) Polymersome encapsulated hemoglobin: a novel type of oxygen carrier. Biomacromolecules 6:2172–2181
24. Linden MV, Meinander K, Helle A, Yohannes G, Riekkola ML, Butcher SJ, Viitala T, Wiedmer SK (2008) Characterization of phosphatidylcholine/polyethylene glycol-lipid aggregates and their use as coatings and carriers in capillary electrophoresis. Electrophoresis 29:852–862
25. Unger EC, Porter T, Culp W, Labell R, Matsunaga T, Zutshi R (2004) Therapeutic applications of lipid-coated microbubbles. Adv Drug Deliv Rev 56:1291–1314
26. Feinstein SB (2004) The powerful microbubble: from bench to bedside, from intravascular indicator to therapeutic delivery system, and beyond. Am J Physiol-Heart C 287:H450–H457
27. Lindner JR (2004) Microbubbles in medical imaging: current applications and future directions. Nat Rev Drug Discov 3:527–532
28. Jahn A, Vreeland WN, DeVoe DL, Locascio LE, Gaitan M (2007) Microfluidic directed formation of liposomes of controlled size. Langmuir 23:6289–6293
29. Hupfeld S, Holsaeter AM, Skar M, Frantzen CB, Brandl M (2006) Liposome size analysis by dynamic/static light scattering upon size exclusion-/field-flow-fractionation. J Nanosci Nanotechnol 6:3025–3031
30. Lee H, Williams SK, Wahl KL, Valentine NB (2003) Analysis of whole bacterial cells by flow field-flow fractionation and matrix-assisted laser desorption/ionization time-of-flight mass spectrometry. Anal Chem 75:2746–2752

31. Kassalainen GE, Williams SK (2003) Coupling thermal field-flow fractionation with matrix-assisted laser desorption/ionization time-of-flight mass spectrometry for the analysis of synthetic polymers. Anal Chem 75:1887–1894
32. Jores K, Mehnert W, Drechsler M, Bunjes H, Johann C, Mader K (2004) Investigations on the structure of solid lipid nanoparticles (SLN) and oil-loaded solid lipid nanoparticles by photon correlation spectroscopy, field-flow fractionation and transmission electron microscopy. J Control Release 95:217–227
33. Kang DY, Kim MJ, Kim ST, Oh KS, Yuk SH, Lee S (2008) Size characterization of drug-loaded polymeric core/shell nanoparticles using asymmetrical flow field-flow fractionation. Anal Bioanal Chem 390:2183–2188
34. Giddings JC, Lin GC, Myers MN (1978) Fractionation and size distribution of water-soluble polymers by flow field-flow fractionation. J Liquid Chromatogr 1:1–20

Chapter 15
Mammalian Cell Sorting with Sedimentation Field-Flow Fractionation

G. Bégaud-Grimaud, S. Battu, D. Leger, and P.J.P. Cardot

Abstract Thirty years after the first work on mammalian cells, Sedimentation Field-Flow Fractionation (SdFFF) can be now described as a mature cell sorting method. By simply taking advantage of biophysical properties of cells (size, density, shape, etc.), SdFFF is a gentle, non-invasive and tagless technique respecting cell integrity. This macro-scaled method prepares specific subpopulations with a high degree of purity, viability and sterility for functional investigations (metabolic specificities, cell cycle dependent activities, apoptosis and differentiation, etc.); biotechnological applications or in vivo studies and cellular therapy. This simple, fast and inexpensive technique presented a large panel of applications in many domains such as microbiology, hematology, neurology, cancer and stem cell research. This report is focused on methodological and instrumental strategies, and on applications concerning mammalian cell sorting.

Keywords Cancer cells • Cell sorting • SdFFF • Stem cells

Dedicated to Professor Joseph Chmelik who passed away in July 2007

G. Bégaud-Grimaud • S. Battu (✉) • P.J.P. Cardot
Biomolécules et thérapies anti-tumorales, Laboratoire de Biochimie, Université de Limoges, Institut GEIST, EA 4021, 87025 Limoges Cedex, France
e-mail: serge.battu@unilim.fr

D. Leger
Homéostasie cellulaire et pathologies, Laboratoire de Chimie Analytique et Bromatologie, Université de Limoges, Institut GEIST, EA 3842, 87025 Limoges Cedex, France

S.K.R. Williams and K.D. Caldwell (eds.), *Field-Flow Fractionation in Biopolymer Analysis*, DOI 10.1007/978-3-7091-0154-4_15,

15.1 Introduction

Cell separation methods allowing isolation and purification of specific subpopulations from a complex cellular matrix (tissues, cell lines, etc.) have played an increased role in many life science domains such as cell biology, molecular genetics (genomics, proteomics, etc.) and cellulomic, biotechnology engineering, drug discovery, chemical and cellular therapies (stem cell research), and clinical diagnosis [1–15].

The Field-Flow Fractionation (FFF) family is a community of separation methods based on the differential elution of species submitted to the combined action of (1) a parabolic profile generated by flowing the mobile phase through a ribbon-like capillary channel; and (2) an external field applied perpendicularly to the flow direction. The ability to implement different types of external field such as gravitational (GrFFF, gravitational splitt) and multi-gravitational (Sedimentation or SdFFF), cross flow (Flow FFF, Asymmetrical Flow FFF or ASF_4), electrical (ElFFF), magnetic (MgFFF), thermal (ThFFF) or acoustic field; defined each FFF subfamily [7,14,16]. The implication of FFF in life sciences has recently been reviewed, pointing out the increasing role of this technique [7,8,14,17,18]. FFF and related technologies have been successfully used in many biological applications including nucleic acids [7,8,17–36], proteins [7,18,23,37–65], organelles [22,27,66–70], microorganisms (environmental or biotechnology purposes) [38,40,52,71–94] and eukaryotic cells separations [1,3,10,36,45,64,83,95–119].

Cell separation methods can be classified on the basis of their application scales and separation principles. Classically, Flow-FFF, Hollow-Fiber FFF, GrFFF and SdFFF are defined as macroscaled methods which take advantage of biophysical parameters such as size, density, shape or rigidity [1,4,5,7,14,15,17,18,99,120,121]. Magnetic-, electrical- and DEP-FFF take advantage of electrical and magnetic properties, and have been developed as micro or nano-scaled technologies [6,10,37,44,45,101,104,105,122–132].

SdFFF was a pioneering technology in many application fields such as cell sorting with the work of Caldwell and coworkers in 1984 [95]. SdFFF was then quickly described as a promising method for mammalian cell separation [133,134]. Nevertheless, the next studies published 10 years later were also by the same group [135]. In parallel, important methodological developments in Gravitational FFF (GrFFF) arrived, leading to many studies in hematology ranging from population characterization [97,136,137], pathologies or transfusion monitoring [97,138,139], to bone marrow stem cell preparation [98]. GrFFF appeared as a more accessible FFF device using natural earth gravity as an external field while less effective in comparison to SdFFF [140]. From a general cellular point of view, SdFFF separation has also been successfully achieved for microorganisms such as viruses, bacteria, yeasts and parasites for diagnostic, bioengineering and environmental applications [7,18,38,40,52,71–90,141]. As also described below, other FFF technologies such as flow-FFF, hollow fiber-FFF, hybrid-FFF, magnetic FFF or DEP-FFF, have been also successfully used to sort mammalian cells in the fields of hematology or cancer research [3,10,36,45,83,96,101–105,107,108]. For SdFFF, hematology has been

progressively replaced by new fields such as neurology, oncology and stem cell research [106,142–148]. The pioneering work in neurology [142] demonstrated the capacity of SdFFF to sort viable, sterile and useable populations of cortical neurons from complex mixtures of E15 rat embryonic cortices.

15.2 Methodology for SdFFF Cell Separation

SdFFF is described as a gentle, noninvasive and tagless method, allowing the macroscaled preparation of functional cell populations for analytical and preparative applications.

15.2.1 Noninvasive Method

The major advantage of SdFFF, and all physical criteria based separation methods, is linked to the drastic limitation of cell-solid phase interaction by the use of a (1) specific separation device : empty ribbon-like channel without stationary phase; and (2) device setup allowing the "Hyperlayer" elution mode, a size/density driven separation mechanism. In the "Hyperlayer" mode, the flow velocity/channel thickness balance generates a hydrodynamic lift force which drives the particles away from the accumulation wall (Fig. 15.1). Species are then focused into a thin layer which corresponds to an equilibrium position in the channel thickness where the external field is exactly balanced by the hydrodynamic lift forces [17,99,121,135,149–157]. At this equilibrium position, the risk of cell-wall interactions is negligible, providing better cell separation. At equivalent density, large cells generate more lift forces and are focused in faster streamlines to be eluted first. Then, specific instrumentations and methodologies have been developed to protect cell functional integrity [5,156].

The first part of the development process concerns device design and setup [156,158,159] such as (1) channel wall material: biocompatible hydrophobic surface (polystyrene); biocompatible tubing and screwing (Peek® from Upchurch®); (2) injection mode determined by the specific channel inlet/outlet tubing position. Sample was introduced through the accumulation wall via a "flow" injection procedure [156,158,159]; (3) the mobile phase: sterile isoosmotic PBS pH = 7.4, allowing simple, fast and low cost cell suspension preparation; (4) a simplified cleaning and decontamination method [5,160]: total device flushing at 2–5 mL/min flow rate, for 15 min each, of the following solutions: sterile distilled water/Clenz®/ sterile distilled water/sodium hypochlorite 3°/sterile distilled water. The system is then ready for a new separation by replacing sterile distilled water by sterile PBS. This end-day/end run cleaning-decontamination procedure avoids channel poisoning, sample cross-contamination and microorganism proliferation. This enhances cell recovery, viability and sterility.

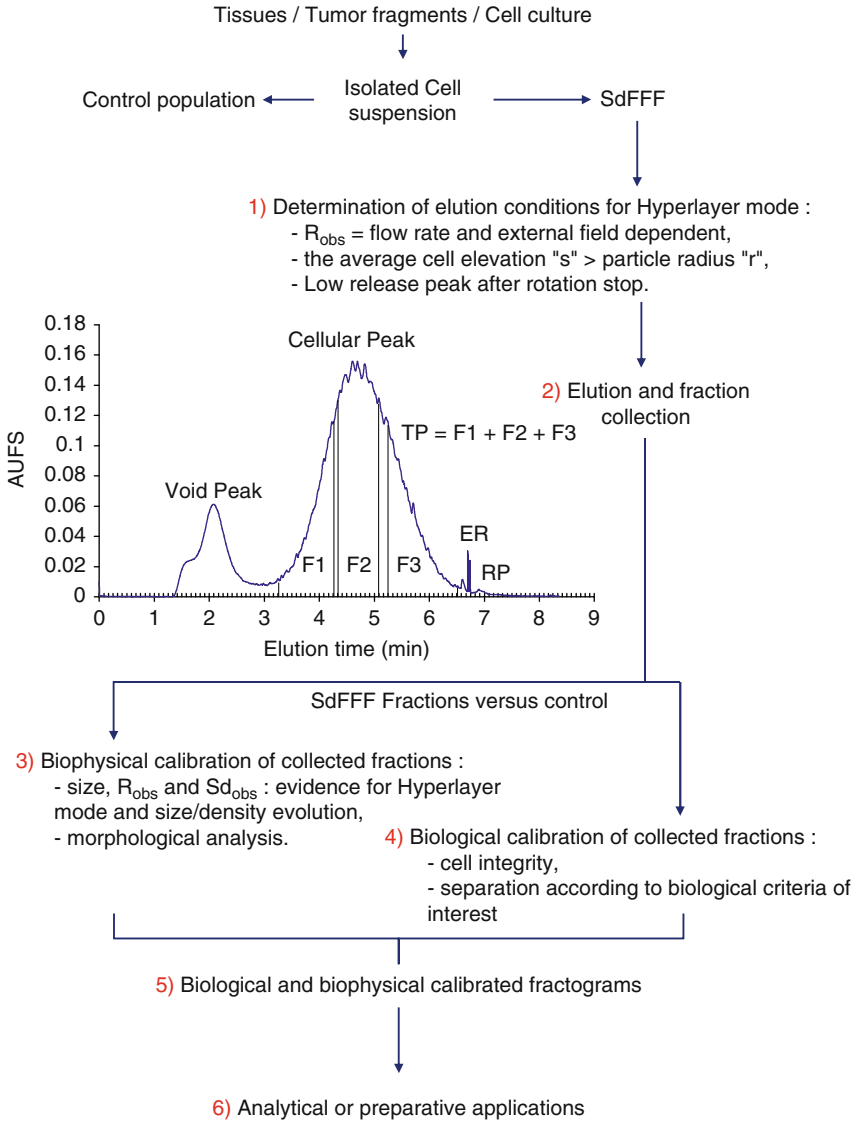

Fig. 15.1 Organization of SdFFF cell sorting. Schematic representation of the different operations leading to calibrated fractograms and possible application of SdFFF cell separation from cell cultures or tissues. Illustration of "Hyperlayer" elution mode (1.1), and example of a SdFFF cell elution fractogram (1.2). Elution conditions: flow injection of 100 µL K562 cells (3.5×10^6 cells/mL); channel thickness: 175 µm; flow rate: 0.80 mL/min (sterile PBS pH 7.4); external multi-gravitational field: 8.00 ± 0.01 g, spectrophotometric detection at $\lambda = 254$ nm. TP and Fn represent the collected fractions. **ER** corresponds to the end of channel rotation, in this case the mean externally applied field strength was equal to zero gravity, thus **RP**, a residual signal, corresponds to the release peak of reversible cell-accumulation wall adherence

The second part concerns the elution mode. Tuning of the flow rate/external multigravitational field balance enhances cell elution under the "Hyperlayer" elution mode.

Historically [16,17,120], FFF was defined and used as a measurement technique of particle properties [157,161–167]. As particle retention depends on field induced forces, the experimental retention parameters such as retention ratio (R_{obs} = void volume/retention volume, [168]) can be used to calculate the values of exerted forces with equations depending on the retention mechanism. These results could be used, after suitable calibration, to measure particle properties: size, density, diffusivity, electrical charge, and their distribution in poly-dispersed populations [4,5,16,156]. When cell separation is performed, determination of elution mode is of little interest to explore particle size or density distribution if it is not correlated with biological properties [106,144,146,147]. In addition, since no standards can be used for a multi-polydispersed cellular population (size, density, shape,. . .), suitable calibration cannot be established. On the other hand, as "Hyperlayer" is the only biocompatible elution mode, it is of primary importance to demonstrate that cells are eluted via this mode [4,5,16,156]. A first set of experiments is performed to determine optimal flow rate/external field setup (Fig. 15.1, 1).

According to the elution theory [17,99,121,135,149–157], a "Hyperlayer" mode is demonstrated (1) by dependence of R_{obs} on flow rate/external field balance. As described, at constant external field, the increase in flow rate increases lift forces, particle velocity, and then R_{obs} value. The increase in external field, at constant flow rate, decreases lift forces, particle velocity, and then the R_{obs} value. As a limit case, complete lifting force offset occurring in the "Steric" elution mode, results in elution of particles in close contact with the accumulation wall. Then the R_{obs} value becomes constant and only dependent on particle size. This leads to harmful particle-solid phase interactions causing a dramatic decrease in cell functional integrity, as well as repeatability, reproducibility and recovery by channel poisoning [17,41,99,121,135,149–157]; (2) by determination of the approximate average cell elevation parameter "**s**". As predicted with the "Hyperlayer" mode, particles are focused away from the accumulation wall in a thin layer at their equilibrium position where external field strength is exactly balanced by lift forces [17,41,149–152,154,155,157].

By using the following equation [152]:

$$R = \frac{6s}{\omega} \tag{15.1}$$

in which R is the retention ratio, ω is the channel thickness, and s the distance from the center of the focused zone to the channel wall. The approximate average cell elevation "**s**" is calculated by using experimental R_{obs} values. Particles are eluted away from the accumulation wall if "**s**" is greater than average particle radius. If "**s**" is equal to particle radius, particles are eluted under the "Steric" elution mode; (3) by a low level of reversible cell sticking. At the end of elution, channel rotation is stopped (ER, Fig. 15.1, 2) leading to zero mean gravity. A residual signal is

observed (RP, Fig. 15.1, 2), corresponding to cell release from channel. This reversible cell sticking is due to low interactions between cells and the hydrophobic accumulation wall (polystyrene), easily disrupted by the mobile phase flowing under the weak external field. As they are not collected, these cells do not have an impact on functional cell integrity. To obtain a sufficient quantity of cells in collected fractions, successive injections and collections (5–15/run) are needed. In the absence of end-day, or better, end-run cleaning-decontamination procedures, the cell release peak increases while retention parameters dramatically change [5,156,160,169,170]. This is an indirect proof of channel poisoning. It corresponds to all particles: cells, cell residues (membranes, organelles, proteins. . .), and residual culture medium which will finally be adsorbed on the accumulation wall. This strong interaction is not easily reversed by the mobile phase flowing alone, and leads to a modification of channel wall surface properties, changing particle retention by reducing repeatability, reproducibility and recovery [5,156,160,169,170]. This increases the risk of apoptosis or necrosis (the most common phenomena), or differentiation activation.

According to the FFF theory [17,41,149–152,154,155,157], when all these conditions are fulfilled, we can assume that the cell population is eluted under the biocompatible "Hyperlayer" elution mode. Optimal elution conditions are achieved when external field strength/flow rate balance lead to effective subpopulation isolation and characterization. As described [5,156], a cell sample can be defined as a polydispersed population in many biophysical (size, density, shape,. . .) and biological parameters, and only be described through a matrix of polydispersity. In this case, the fractogram always appears as a broad peak (Fig. 15.2). Optimal elution is a balance between a sufficient retention time to collect subpopulations of interest and reduced cell trapping and plate height. If fast and resolutive separations can be performed by using high flow rate and field strength [171,172], allowing minute scale monitoring of biological events [117], gentle conditions using low flow rate and external field (0.4–1.0 mL/min – 10–50 g) have to be selected to avoid mechanical cell injury in the case of large scale population preparations [95,142,148,169].

15.2.2 Respect of Cellular Integrity

After optimizing device setup and elution conditions to reduce cell-solid phase interactions and enhancing subpopulations separation, SdFFF has to demonstrate its ability to take into account and respect cell properties (Figs. 15.1, 3 and 15.1, 4): (1) *viability*: a high viability (>90%), similar to a control population, is usually obtained after elution (short term viability) [142,144]. This is proof of optimal elution without any mechanical obstacles in the mobile phase flow (in rotating seals or the detector). Further uses of cells such as characterization and functional investigations need sub-culture and transplantation. Long term viability should be maintained without nonspecific or uncontrolled cell death induction leading to necrosis, apoptosis or autophagy. This is achieved by overcoming channel poisoning ("Hyperlayer" elution and cleaning-decontamination procedures) [5,142,148,160]; (2) *cell functional*

integrity: for example : growing capabilities; if short-term separation must respect growing potential, separation should only depend on specific biophysical and biological criteria, and not only depend on growing possibilities [10,142]; cell adhesion properties; genomic, phenotypic and proteomic properties with specific expression of receptors and surface antigens [10,106,115,116,142,147]; (3) *maturation, differentiation and apoptosis* [106,143,144,146,147]: characterization of any of these processes (metabolic and signaling pathways, antigen expression), as well as the routine preparation of specific sub-populations, requires that elution respects either the maturation-differentiation stages (from immature to differentiated cells) or the degree of apoptosis [106,143,147,148]. Moreover, long-term uses also require that cells do not receive any activation, differentiation or apoptotic signals during separation. The untransformed populations retain their capacities to differentiate or to become apoptotic [106,143,147,148]. They will constitute an effective model for mechanism and kinetics studies. This also appears as an essential criterion when immature cells, precursor, progenitor or stem cells, must be sorted [143,148]. As described above, this corresponds to the second main advantage of a non-invasive and tagless method such as SdFFF or GrFFF [7,14,109]; (4) *Sterility*: Sub-culturing and transplantation require absolute sterility and apyrogenecity of samples. This is achieved by sterile preparation and manipulation of samples (sterile flow hood, sterile disposable medium, gloves and mask) as well as by always running SdFFF devices with sterile mobile phases and respecting cleaning-decontamination procedures.

15.2.3 Analytical Requirements

As for other analytical and separation methods, SdFFF has to also fulfill the following requirements: (1) *high repeatability and reproducibility*: these criteria have been validated with biological samples (RBC, red blood cells) using the "Hyperlayer" mode [160,173]. Hyperlayer mode (reduced channel aging) gives repeatable replicate sample injections (10–20) leading to similar fractograms either in terms of retention time (R_{obs} CV $< 5\%$, $n > 10$) or peak shape [117]. Concerning reproducibility, or more precisely the intermediate fidelity measured with the same operator and device, but with new samples of identical biological species (major source of variability), comparable fractograms are obtained (R_{obs} CV $< 5\%$, $n > 10$), permitting the use of constant elution conditions [106,117,144,146,147]. Nevertheless, as described [106,115,144,146,147,174], for one and the same cell line, the absolute R_{obs} value depends on time and condition of culture; (2) *maximal recovery*: this criterion, as well as the repeatability, depends on the application of the "Hyperlayer" elution mode under low external field [106,147,148] enhancing cell viability and recovery which classically range from 75% to 90%. This is of prime importance in sorting rare cells from complex biological samples [142,143,148]. Decreased recovery could be due to reversible/irreversible sticking to the accumulation wall [147]. Additionally the "stopless" injection mode could be another reason [175,176]. The classical injection procedure

is described as "stop-flow" [5,175,177]. Sample is driven to the channel inlet, the flow is stopped while the external field is maintained. This leaves sub-micron sized particles in a "primary relaxation step". They reach their equilibrium position before flow resumes, leading to separation with optimal selectivity. For micron-sized particles (cells) with negligible diffusivity, offset of the lift-force drives them onto close contact with the accumulation wall with the risk of cell trapping or activation (differentiation or apoptosis). A "stopless" or direct flow injection method is more convenient even if it can decrease the selectivity by the absence of a "primary relaxation step". Different strategies have been proposed to operate direct injection without loss of selectivity such as pinched inlet [175,177], split inlet [178], frit inlet and specific inlet triangle design [131,179]. As described [1,158], our specific device design solves this problem by direct injection of the sample through the accumulation wall, preserving selectivity and elution time. Nevertheless, a non-specific part of sample never reaches its equilibrium position and is eluted in the void volume, decreasing sample recovery but maintaining, on the other hand, cell viability, integrity and functionality.

15.2.4 Simple, Fast and "Tagless" Method

Separation selectivity is only based on intrinsic cellular biophysical properties (size, density, shape, etc.) and experimental parameters, such as channel geometry and external field strength/flow rate balance, making SdFFF a simple, fast and inexpensive method [7,14]: (1) *device setup and elution*: for each new separation problem, the device is easily and rapidly set up to obtain "Hyperlayer" elution conditions. Elution time for each injection is usually very short (5–10 min, Figs. 15.1, 2 and 15.2), leading to limited cell stress especially since smooth field and flow conditions are applied to achieve "Hyperlayer" elution; (2) *mobile phase*: the use of a hydrophobic material as the channel wall (i.e. polystyrene) permits the employment of the simplest mobile phase: PBS pH 7.4 (without Ca^{2+} and Mg^{2+}) classically used for cell experiments. If some sample types (tissues) require addition of specific antibiotic-antifungal combinations to ensure sterility [110,142,148], no other complement such as BSA is needed, simplifying preparation. Since separation devices do not contain any selective channel wall coating, this reduces the risk of channel poisoning and enhances cleaning-decontamination procedure and channel shelf-life (6–12 months with daily use); (3) *Sample preparation*: SdFFF only requires the preparation of a suspension of isolated cells [156]. This is obtained by chemical-enzymatic release from culture plates for adherent cells [147], or by centrifugation for suspended cells [106]. Cells from tissues such as olfactory epithelium are prepared after classical steps of mechanical and enzymatic dissection and dissociation [148]. In all cases, isolated cells should finally be diluted in the mobile phase to a density somewhere between 1×10^6 and 3×10^6/mL depending on channel capacity [147]. Sample concentration is important as it affects subpopulation separation effectiveness and cell-cell or cell-solid phase interactions [46,147,173,180–182].

As described below, the second advantage of a size-density based approach is that it does not require using either specific cell expression markers, such as specific fluorescent nor magnetic prelabeling, to achieve separation; in this respect it provides advantages over FACS or MACS methods [5,7,10]. Tagless methods such as SdFFF became interesting for applications in which (1) specific markers do not exist (animal models, stem cells); (2) labeling interferes with further cell uses such as in vitro expansion, in vivo transplantation or immunological characterizations; (3) labeling could activate differentiation which is very critical for rare or immature cells [3,5,7,10,116,143,148,156].

15.2.5 From Fraction Collection to Fractogram Calibration

15.2.5.1 Elution and Fraction Collection

As explained below, even the most apparently homogenous cultured cell lines can only be described through biophysical (size, density, shape,...) and biological (metabolic activity, cell cycle position,...) matrices of polydispersity [5,156,176]. Thus "Hyperlayer" elution of such populations leads to broad peaks composed of the juxtaposition of the multiple/different subpopulations. This peak might be calibrated as a function of particle size or density distribution [157,183,184] (Fig. 15.1, 3). As previously described [81,117,147,185], size selectivity has been experimentally established, by using the following equation [185,186]:

$$\log\ t_R = -S_d \cdot \log\ d + \log\ t_{R1} \tag{15.2}$$

where $-S_d$, the slope of the graph, represents the selectivity coefficient, t_r is the retention time, d the mean cell diameter and t_{R1} a constant value, equal to the retention time of a 1 µm particle. It has been demonstrated [186] that in the case of elution of a population containing particles of different sizes, but analogous density profiles, the size selectivity curve is a straight line. After calibrating the SdFFF device with standard particles (calibrated latex beads), the size-based selectivity curve can be used to establish the particle size distribution of an eluted sample.

Unfortunately, equivalent cell standards do not exist. As previously described [81,106,117,147,185], by using fraction collections and size measurement (by Coulter Counter, Flow Cytometry or FC), experimental size selectivity curves can be established in order to calculate an observed Sd_{obs} value.

$$\log\ t_R = -Sd_{obs} \cdot \log\ d + \log\ t_{R1} \tag{15.3}$$

According to the "Hyperlayer" theory [17,41,149–152,154,155,157], high Sd_{obs} values suggest effective cell separation with regards to their biophysical properties. Furthermore, Sd_{obs} determination allows comparison between elution conditions, device setup and demonstrates density changes during induction of biological events

[106,147]. Nevertheless, an effective biophysical cell separation does not give any information concerning effective biological isolation. This justifies time dependent fraction collection (Fig. 15.1, 2) and biological characterization (Fig. 15.1, 4).

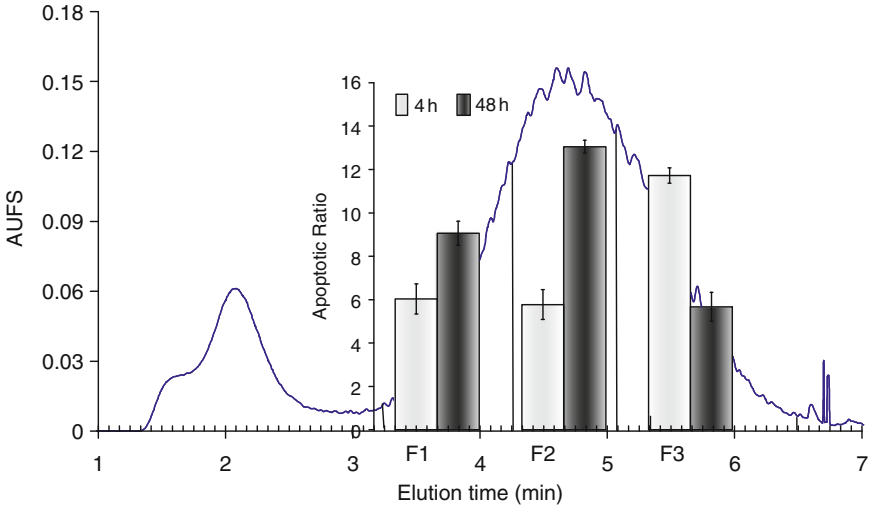

Fig. 15.2 Example of a calibrated fractogram. SdFFF K562 cell elution was calibrated as a function of elution time and apoptotic kinetics. Cells were incubated for 12 h with 40 µM diosgenin before SdFFF elution. Early apoptosis was measured by flow cytometry [174] after 4 and 48 h sub-culturing without diosgenin. Elution conditions: see Fig. 15.1

15.2.5.2 Biological Calibration

SdFFF elution has been associated with many analytical tools for cell biology investigations such as (1) cell culture, morphological and particle size distribution (PSD) studies; (2) cellular viability (MTT) and proliferation (EdU/BrdU incorporation) assays; (3) immunological characterization of antigen expression and metabolic activities by Western Blotting, Elisa assays, immunohistochemistry, flow cytometry or Amnys analysis; and (4) molecular biology (semi-quantitative PCR) [106,115,116,144,146–148,174,187,188].

These studies have been performed on collected fractions, named Fn and representing a part of the total population, versus a control population (not eluted crude extract) and the total peak fraction (TP) which is the whole eluted population minus the void volume and the release peak (Fig. 15.1, 2). They answered many questions concerning (1) *cell integrity*. This is demonstrated by short and long term viability analysis, adhesion, cultural, morphological and phenotypic properties, proteomic and antigenic expression, genomic capacities as well as maturation or apoptotic stage determinations. The TP fraction must behave similarly to the control, demonstrating that any differences between Fn and control are due to separation efficacy and not to nonspecific phenomena such as selective subpopulation death,

trapping or sticking. Similar TP and control behavior also assesses that separation only depends on intrinsic biophysical properties of cells as predicted by the "Hyperlayer" model; (2) *isolation of subpopulations*. This is determined by differential analyses of Fn properties, depending on the biological criteria of interest on which studies are based [106]. Association of retention parameters with the distribution of biological markers led to the concept of the multidimensional hyphenated fractogram (Figs. 15.1, 5, and 15.2 [156].

From this point (Fig. 15.1, 6), two different sets of applications can be performed (1) *analytical applications*. Complete subpopulation characterization gives an accurate sample description, corresponding to the "cellulomic" concept earlier developed [156]. This could be done either in steady state culture conditions (ecology and phenotypic relationship), or in dynamic motion after induction of biological events allowing both monitoring and mechanistic-kinetic descriptions [106,115–117,142–144,146–148,174,187,189]; (2) *preparative applications*. The proper biological calibration of fractograms, as well as the high level of reproducibility, permits systematic preparation of specific subpopulations. The routinely prepared populations can be used, for example, as models for anticancer therapy research [106,147]. Preparative separation of immature or stem cells opened the field of cellular therapies and biotechnologies [115,116,143,145,148,174,187,189].

15.3 Recent Applications and Perspectives in Mammalian Cell Separation

Since the initial work of Caldwell et al. [95] on the HeLa cell line, cell separation and sorting is one of the principal applications of SdFFF and GrFFF in life sciences, including first microbiology, and hematology while new fields such as neurology, cancer and stem cell research have recently emerged [5,7,11,79–81,87,95,98–100,109–111,115,116,119,138,142,145,146,148,189–193]. The pioneering work in neurology [142] demonstrated the capacity of SdFFF to sort viable, sterile and useable population of cortical neurons from complex mixtures of E15 rat embryonic cortices.

15.3.1 Cancer Research

In normal conditions, cell growth, proliferation, differentiation and maturation processes are controlled leading from stem cells or progenitors to normal functional and mature cells. [194]. Normal cell death is usually the consequence of a natural process called apoptosis (programmed cell death). This fundamental process for development and homeostasis of tissues and organs in pluricellular organisms [195], is regulated by a large variety of receptors, signaling and active proteins

including caspases which direct the last step resulting in morphological changes and DNA fragmentation [196,197].

Cancer etiology is multi-factorial and involves the action of genes throughout the complex multi-step process of carcinogenesis. At a molecular level, cell transformation results from the occurrence of genetic events that uncouple the cell from its normal regulatory mechanisms of proliferation, differentiation and maturation. Cancer cells continuously sense a message to undergo tomitosis without response to normal regulatory signals (maturation or apoptosis) leading to the growth of a clone of proliferative, immature and immortal cells [196]. To limit or stop cancer spreading, two strategies have been suggested. The first corresponds to apoptosis induction which is the action of the most common therapeutic agents. Nevertheless, hormonal and differentiation therapies play an increasing role [106,198–202]. Differentiation is also a complex, multistep and highly regulated phenomenon. As a clonal disease, cancer is initiated at the level of individual early progenitor cells leading to possible reversible defects in differentiation [106,196,198–202]. Differentiation therapy reprograms tumor cells resulting in loss of proliferating capacity and induction of terminal maturation enhancing natural or induced apoptosis [106,196,198–202]. Then apoptosis and differentiation therapies are two ways to achieve the same goal: cancer cell arrest.

Over the last few years, two aspects of SdFFF in oncology have been explored. The first point concerns the studies of chemical apoptosis or differentiation induction and are (1) monitoring the induction of biological events (BE); (2) the separation of specific subpopulations of interest; (3) mechanistic and kinetic studies including the exploration of potential links between the kinetics and extent of a BE and cell status (i.e. cell cycle position).

The second point concerns the isolation of specific phenotypes from the original crude population (culture cell line, tumor fragment) in order to study phenotypical relationships, or for cancer stem cell sorting.

15.3.1.1 Monitoring Biological Events (BE)

Pioneering reports concerning the monitoring of BE used microorganisms to follow cell growth, protein or rRNA production as a function of culture time and condition [67,74,77,80]. Studies on red blood cells (RBC) monitored the emergence of pathologies as well as followed age-dependent properties [138,139].

As apoptosis and differentiation led to morphological changes, it was supposed that they could be monitored by SdFFF. After proper characterization of BE induction, cells were eluted by SdFFF. Mean cell diameter was also measured on crude populations (treated and control) and on collected fractions [106,147]. Mean size determination was used to calculate Sd_{obs} allowing the evaluation of size and density evolution associated with BE induction [106,147]. Finally, elution profiles of control (reference profile) and treated populations were compared as a function of inducer, incubation time and concentration [106,144,146,147].

Figure 15.3 shows characteristic fractograms obtained with HEL cells (Human Erythroleukemia cell line) incubated with various diosgenin concentrations. With a

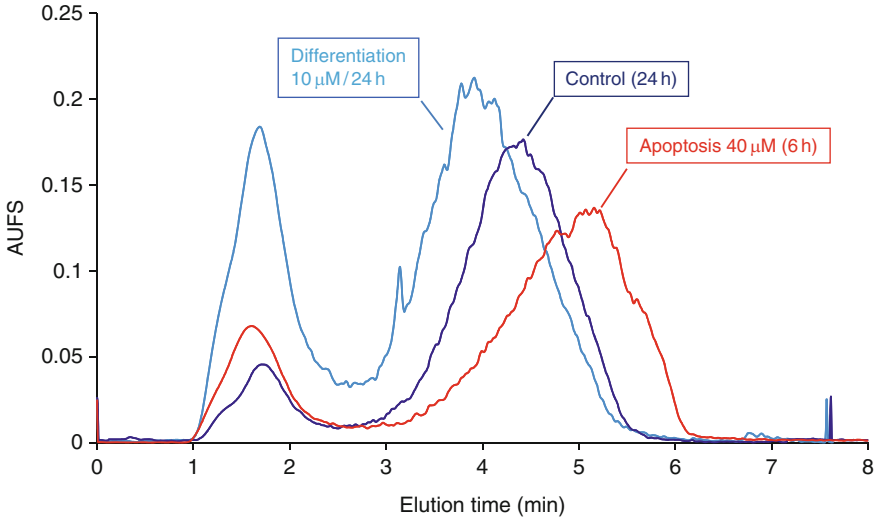

Fig. 15.3 Apoptosis and differentiation monitoring of HEL cells by SdFFF. After acquisition of a reference profile, 40 µM diosgenin induced HEL apoptosis. As early as after 6 h incubation, an evolution of fractograms with an increase in retention time was observed. In contrast, 10 µM diosgenin induced megakaryocytic differentiation was associated with a decrease in retention time. Elution conditions: flow injection of 100 µL cell suspension (2×10^6 cells/mL); channel thickness: 125 µm; flow rate: 0.5 mL/min (sterile PBS, pH 7.4); external multi-gravitational field: 40.00 ± 0.03 g, spectrophotometric detection at $\lambda = 254$ nm

40 µM concentration, diosgenin induced apoptosis with complete cell death after 48 h incubation [144,146]. As early as 6 h incubation, an increase in retention time was observed (Fig. 15.3). By using a downscales device [117], apoptosis detection time was reduced to 3 h for only 10^3 injected cells. In contrast, 10 µM diosgenin induced megakaryocytic differentiation associated with a decrease in retention time as early as after 24 h incubation (Fig. 15.3) [106,146]. Table 15.1 summarizes results published for different cell lines [115,117,144,146,147,174,187,188,199]. Results showed a correlation between BE induction and fractogram changes regardless of the inducer and incubation time. With weak apoptosis inducers (heco-and tigogenin), only very few changes were recorded [144]. With the exception of 40 µM diosgenin (apoptotic dose), an increase in R_{obs} (decreased retention time) was always observed, which is in agreement with the "Hyperlayer" model as an increase in cell size was measured. A linear correlation between cell size increase and R_{obs} evolution could not be established [106,117,144,146,174]. Size criteria alone are not sufficient to discriminate BE. Mean size and Sd_{obs} measurements demonstrate that BE are always associated with major and complex changes in the size/density balance, parameters highly influencing SdFFF elution [117,144,146,199]. Cell rigidity and shape have a secondary influence and are more difficult to study. For example [144,146], 40 µM diosgenin, MG-132 or staurosporin, which all induced significant apoptosis, provoked different morphological modifications.

Fractogram changes are also connected with the kinetics of BE. Apoptosis, which is a fast and short process leading to rapid and total cell death (24–48 h), can be detected quite early by SdFFF while many biological methods usually employed for characterization are not yet sufficiently sensitive (Western Blotting, Elisa detection kit or Tunnel methods) [144,146,147,174]. In contrast, differentiation is a longer and slower process only starting after many hours of incubation. Again, SdFFF is able to detect the early stages of megakaryocytic differentiation of HEL cells where specific markers such as cell ploïdy increase or CD41 and GpV expressions are not significant [106,146]. Time-dependent monitoring is essential to identify a BE.

In conclusion, by taking into account changes in major biophysical parameters (size, density, shape, rigidity) occurring during BE induction, SdFFF alone appears to be an effective monitoring tool for different BE in their early stages. Many applications arise from these results such as: (1) screening series of molecules and doses; (2) monitoring new BE models used in various life science fields. For example, SdFFF has been used to explore native starch amylolysis [203,204]. The association of monitoring and fraction collection permitted the study of the complex enzymatic action as a function of granule size and incubation time; and (3) the preparation of specific subpopulations [203,204].

15.3.1.2 Cell Separation of Specific Subpopulations

Apoptosis and differentiation are multi-parameter and multi-step processes with complex regulation mechanisms. The use of a noninvasive separation method can prepare an enriched subpopulation of interest which could be further used as a model of BE mechanism and kinetic studies [189].

In apoptosis, pre-apoptotic cells, cells in the early stage of apoptosis, are the population of interest [147]. Based on monitoring results [144], 1547 cells (human osteosarcoma cell line) incubated 6 h with 40 μM diosgenin were eluted. Microscopic observations, proliferation and apoptosis characterization demonstrated the isolation of a pre-apoptotic population which led to a higher apoptotic ratio (16.8 versus control) in comparison to the whole treated population (1.7) [147]. This separation was obtained with a 175 μm thick channel which better takes into account density variations associated with early apoptosis signaling compared to a 125 μm channel, as demonstrated by Sd_{obs} analysis [147]. Such results were confirmed on K562 cells, where SdFFF elution isolated different apoptotic stages in the same population [174]. Each subpopulation could then be used as a model to study the specific mechanisms and kinetics of induced apoptosis [174].

Comparable studies have been realized to purify differentiated cells from HEL cells incubated with 10 μM diosgenin for 96 h. Table 15.2 summarizes the distribution of biological properties in collected fractions. SdFFF appeared to be an effective method to sort populations having specific degrees of maturation ranging from undifferentiated cells (F3) to differentiated cells (F1) corresponding to large non-proliferative cells with high ploïdy and CD41 expression [106].

Table 15.1 Apoptosis and differentiation monitoring by SdFFF in 1547, HEL and K562 human cell lines [117,144,146,174,187,188]. Regardless of the inducer and incubation time, a correlation between induction of a biological event (BE) and fractogram changes was observed. SdFFF elution profile changes were associated with the evolution of cell biophysical parameters (size or density), and kinetics of biological events in a cell population

	Inducers							
	Diosgenin (40 μM)	Staurosporin (1 μM)	MG 132 (3 μM)	Tigogenin (40 μM)	Hecogenin (40 μM)	Diosgenin (10 μM)	PMA (50 nM)	SU6656 (5 μM)
Expected BE	Apoptosis					Differentiation		
Observed BE	++	++	++	−	−	++	++	+++
Effect on fractograms	++	++	++	−	−	++	++	+++
R_{obs}	↘	↗	↗	↔	↔	↗	↗	↗
Cell diameter increase	++	+/−	+/−			++++	++++	++++
Minimal incubation time	3 h	6 h	6 h			24 h	96 h	12 h

Table 15.2 SdFFF sorting of HEL cells incubated for 96 h with 10 µM diosgenin [106,187,188]. SdFFF appeared to be an effective method to sort an enriched population of megakaryocytic cells as shown by the results of the biological properties studied: in comparison to a crude population, cells eluted in the first fraction led to the culture of large cells having maximal ploïdy and CD41/GpA ratios. Therefore, cells eluted in F1 could be defined as differentiated cells compared to cells eluted in F3 which behaved just like the control HEL population

	Control	Treated cells (10 µM diosgenin for 96 h)				
		Crude	TP	F1	F2	F3
Mean diameter (µm) (Coulter Coulter)	12.70	15.08	15.28	17.15	13.57	11.82
Sd	2.932	1.219	_	_	_	_
Ploidy (%) (flow cytometry)	98%	56%	59%	15%	57%	95%
2–4 N	2%	44%	41%	85%	43%	5%
8–64 N						
Ratio CD41/GpA (flow cytometry)	0.32	0.62	0.90	2.26	0.95	0.34
Cell culture and cell species	UD	M	M	D	M	UD

UD undifferentiated cells, *M* mixture of UD and D cells, *D* megakaryocytic differentiated cells

In all cases [106,147,174,187–189], associating cell separation under the Hyperlayer mode to the characterization method leads to elution profile calibration from biophysical (size, density) and biological (e.g. morphology, proliferation, antigen expression, DNA content and fragmentation,..) points of view. Calibrated conditions allow routine preparation of specific subpopulations of interest which

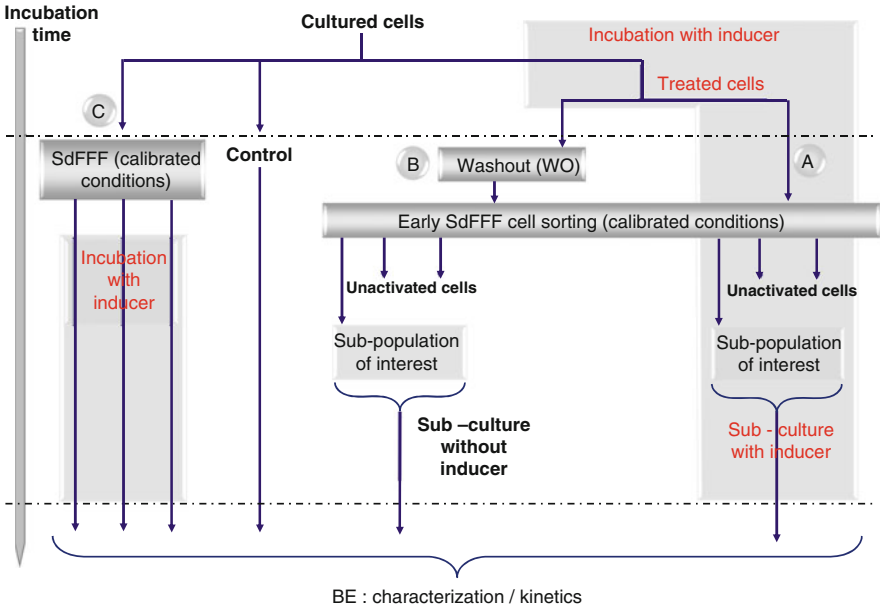

Fig. 15.4 Protocol to study mechanisms and kinetics of induced biological events. Strategies combining cell treatment and early SdFFF elution (calibrated elution conditions). (**a**) Populations of interest are continuously sub-cultured with inducer. (**b**) After inducer washout, populations of interest are sub-cultured without inducer; (**c**) Crude population, before any treatment, is used to sort cells having same status (i.e. cell cycle), to study a link between the kinetics and extent of a BE and cell status at the start of induction

can be used in turn as models for the further investigation of different processes such as mechanisms, kinetics or cancer therapy [174,187,189] (Figs. 15.1, 4 and 15.1, 5).

15.3.1.3 Mechanism and Kinetic Studies

These studies are based on the monitoring and cell sorting ability of SdFFF. The use of a whole population as a cell model for BE, usually demonstrates global induction. Nevertheless, in many cases, as some parts of the population (apparently homogeneous) are not concerned or involved in the process, a mixed population of activated and inactivated cells is obtained leading to difficult interpretation [174,189,205,206]. Then, continuous chemical exposure to inducer is needed. As shown below, early SdFFF separation can prepare enriched subpopulations of interest, and different strategies can be proposed (Fig. 15.4).

In the first (Fig. 15.4a,) cells are incubated for the minimal time necessary to process induction and significant SdFFF monitoring. SdFFF elution performed on the basis of previously calibrated conditions, allowing the preparation of subpopulations of interest which are subcultured with inducers leading to an enriched population of desired cells to accurately monitor BE process and kinetics. This protocol elucidates the apparent contradiction between keratinocytic differentiation and extensive proliferation in HaCat cells submitted to high level Ca^{2+} concentration [189].

The second protocol is identical to the first until fraction collection (Fig. 15.4b). Then, subpopulations are this time subcultured in the absence of inducer = washout (WO). These types of strategies have been successfully used to study HEL megakaryocytic differentiation and apoptosis in 1547 (human osteosarcoma) and K562 cells (human erythroleukemia cell lines) [147,174,187,199]. The association of WO and early SdFFF elution answers many questions such as (1) does the inducer have to be continuously present to provide BE; (2) if not, what is the minimal time needed to observe and monitor BE induction; (3) then, how does a cell culture behave without continuous exposure to inducer? In particular, does the BE lead to similar final stages or kinetics in enriched populations, and are the remaining unselected cells resistant to therapy, or only unreceptive at the time of inducer exposure? This last point is critical in the goal of chemotherapy research. If a part of the cells are resistant, what could be the involved mechanism, and if they are not resistant, in which cellular stage should cells be to obtain optimal induction?

To answer this crucial question: what is the potential link between the kinetics and extent of a BE and cell status at the start of induction; SdFFF can be used (Fig. 15.4c) to sort a crude population to prepare cells having same status (i.e. cell cycle), demonstrating a direct link between sensitivity to molecules and cell cycle position either for apoptosis or differentiation induction [115,188]. With these types of protocols, the monitoring of R_{obs} evolution, in particular the ratio between fraction and control (normalized R_{obs} or ΔR_{obs}) can be used to follow evolution of BE in the different fractions and not only on the total population, showing the correlation between BE induction and SdFFF signal changes [174,188].

The second set of experiments in Oncology concerning the isolation of specific phenotypes from the original crude population (culture cell line, tumor fragment) and performed in order to study phenotypic relationships, or for cancer stem cell sorting, is developed in the next section.

15.3.2 Immature Cells: From Normal to Cancer Stem Cells

FFF in stem cell research started in the middle 90s with the work of Urbankova et al. [98]. GrFFF was used to isolate mouse bone marrow stem cells before transplantation to irradiated mice. DEP-FFF has also been proposed to eliminate cancer cells from a mixture containing CD34+ hemathopoietic stem cells [207]. Important studies have also been carried out using GrFFF. Hematopoietic and mesenchymal stem cells, two important stem cell populations, were purified, with and without stop-flow injection methods [14,109–111]. DEP-FFF was also successfully used in the isolation of rare (circulating) tumor cells and stem cells from peripheral blood or from adipose tissue [103,113,118].

The pioneering work in neurology [142] demonstrated the capacity of SdFFF to sort viable, sterile and useable populations of cortical neurons from complex mixtures of E17 rat embryonic cortices. This study has been used as a model for the isolation of embryonic neural stem cells from avian olfactory epithelium [148]. In the nervous system, the olfactory epithelium (OE) provides an interesting tool to study stem cells and set up isolation from different cell types. The OE consists of four cell types: (1) Sustentacular cells, (2) Olfactory Receptor Neurons (ORNs), and two basal populations of proliferative cells. ORNs are continuously replaced in both immature and adult animals. Several pieces of evidence suggest that the basal cells are a self renewing source of new sensory neurons and act as stem cells [208–210].

"Hyperlayer" elution gave an enriched population of immature cells which led to the subculture of cells having many stem cell properties: undifferentiating, self-renewal capability and multipotentiality by regeneration of all olfactory epithelium cell types [148]. These results open many perspectives concerning neurogenesis and neuroregeneration after extension to a mammalian model (rodent).

Original applications in stem cell biotechnology have also been reported [145]. SdFFF elution of genetically modified mouse embryonic stem cells (ES cells) results in, after proper biological fractogram calibration based on in vitro developmental potential and cell cycle correlation, the isolation of ES cells having the most in vivo potential to obtain transgenic mice with a high degree of chimerism and germinal transmission of gene modification.

At the same time, reports on cancer cell lines showed the capacity of SdFFF to sort populations according to the degree of differentiation. Like neuroblastomas (NB) and glioblastomas (GB), many tumors and derived cell lines, are composed of heterogeneous populations with cells in various stages of differentiation. Heterogeneity affects treatment outcome, in particular response to apoptotic chemotherapy.

It is of utmost importance to understand the natural process of differentiation in order to improve treatment response.

The SH-SY5Y cell line (human neuroblastoma) is heterogeneous with the presence of distinct morphological cell types. Large Stromal cells (S-type cells) eluted first and appeared as adherent differentiated cells expressing N-CAM. In contrast, the last eluted cells were small Neuroblastic undifferentiated Fas-expressing cells (N-type) [143]. These non-adherent cells formed neurosphere-like structures as described in the case of neural stem cells. Similar results were obtained with IMR-32, another human neuroblastoma cell line. SdFFF subpopulation enrichment demonstrated [211] (1) the presence of two distinct populations of undifferentiated cells (N-type cells); and (2) the kinetics of population differentiation. One N-type population was composed of quiescent cells present in large aggregates. The second contained proliferative cells forming small aggregates which released cells in intermediate stages of differentiation at their periphery, which then migrated to the culture flask surface where they finished maturating into S-type cells or stromal cells expressing neuron markers [211]. From this model, the role of each population in tumorigenicity and malignancy has to be defined by in vitro and in vivo studies, after routine preparation by SdFFF.

These results are linked to immature cancer cell isolation [143,211]. Increasing bibliographic data describe the presence of immature and cancer stem cells in tumors and derivative cell lines [212–217]. They appear to be responsible for malignancy and resistance to therapy (radio- and chemotherapies) [216,217]. Gentle separation of these populations should be of great interest from various points of view such as (1) enrichment of subpopulations [116,143,211]; (2) phenotypic relationship and differentiation kinetic studies [211]; (3) studies of specific sensitivity to apoptosis or differentiation chemotherapies and therapeutic trials using combined induction [116]; and (4) in vivo studies of tumorigenicity, metastatic development and drug efficacy after transplantation. In recent work on glioblastoma U87-MG cells, SdFFF separated two major cell subpopulations, a more differentiated cell fraction, containing large and adherent cells, sensitive to Fas-induced apoptosis and another one, characterized by small cells forming aggregates, expressing CD133, a marker of stem cells and more resistant to Fas-activated apoptosis [217]. These results suggest that these immature stem cells in gliomas could be a major factor implicated in resistance to chemotherapy requiring apoptosis through the Fas signaling system. Indeed, future strategies of treatment, inducing differentiation of these stem cells need to be considered to enhance therapeutic efficacy [116]. Actually, these results have been exported to a colorectal cancer model.

15.4 Conclusion

Early defined as a promising method for cell sorting and biological applications, SdFFF played a pioneering role in many separation fields. Used originally as a cell sorter 30 years ago by Caldwell and co-workers, this macro-scaled method can now

be described as a mature technique. Based on cell biophysical properties, SdFFF gives a gentle, non-invasive and "tagless" elution/separation, respecting cell integrity and function in order to investigate many important aspects of cell biology which include cell death and differentiation (development and oncology), or stem cell research. Recently, Roda et al. [14] described FFF as the "Best-kept-secret" in bio-separation sciences. SdFFF and GrFFF can be defined as "the secret in the secret" in the field of cell separation. There are many reasons for that, such as (1) the development of SdFFF inside a framework mainly devoted to chemistry like separation concerning macromolecules and colloids with principal applications in environmental sciences, as observed with the major emergence of AsF4; (2) the efficacy of SdFFF as measurement tool for sample properties (size, density, diffusivity) and forces; (3) the device complexity and until now poor commercial availability of upgradable equipment allowing a rapid change of channels (material, geometry,. . .); and finally (4) the lack of on line hyphenation with very selective detectors, as in the case of MALS for AsF4. Nevertheless, recent reviews on cell separation methods, produced by non-FFF specialists, have started to reference FFF devices and applications [13,15], leading to discovery of the secret? On the other hand, many instrumental developments still need to occur concerning scale reduction, sample dilution, output capacity and hyphenation with cell characterization methods such as specific noninvasive detectors.

References

1. Chianea T, Assidjo NE, Cardot PJP (2000) Sedimentation field-flow-fractionation: emergence of a new cell separation methodology. Talanta 51(5):835–847
2. Yang J, Huang Y, Wang X-B, Becker FF, Gascoyne PRC (2000) Differential analysis of human leukocytes by dielectrophoretic field-flow-fractionation. Biophys J 78(5):2680–2689
3. Wang X-B, Yang J, Huang Y, Vykoukal J, Becker FF, Gascoyne PRC (2000) Cell separation by dielectrophoretic field-flow-fractionation. Anal Chem 72(4):832–839
4. Cardot PJP, Chianea T, Battu S (2001) Sedimentation field-flow fractionation of living cells. In: Cazes J (ed) Encyclopedia of chromatography, vol Chapter 265. M. Dekker Inc, New York, pp 742–747
5. Battu S, Cook-Moreau J, Cardot PJP (2002) Sedimentation field-flow fractionation: methodological basis and application for cell sorting. J Liq Chromatogr Relat Technol 25(13–15):2193–2210
6. Pethig R, Lee RS, Talary MS (2004) Cell physiometry tools based on dielectrophoresis. J Assoc Lab Autom 9(5):324–330
7. Reschiglian P, Zattoni A, Roda B, Michelini E, Roda A (2005) Field-flow fractionation and biotechnology. Trends Biotechnol 23(9):475–483
8. Kowalkowski T, Buszewski B, Cantado C, Dondi F (2006) Field-flow fractionation: theory, techniques, applications and the challenges. Crit Rev Anal Chem 36(2):129–135
9. Mattanovich D, Borth N (2006) Applications of cell sorting in biotechnology. Microb Cell Fact 5:1–12
10. Radisic M, Lyer RK, Murthy SK (2006) Micro- and nanotechnology in cell separation. Int J Nanomedicine 1(1):3–14
11. Liu B-F, Xu B, Zhang G, Du W, Luo Q (2006) Micro-separation toward systems biology. J Chromatogr A 1106(1–2):19–28

12. Borland LM, Kottegoda S, Phillips KS, Allbritton NL (2008) Chemical analysis of single cells. Annu Rev Anal Chem 1:191–227
13. Pappas D, Wang K (2007) Cellular separations: a review of new challenges in analytical chemistry. Anal Chim Acta 601(1):26–35
14. Roda B, Zattoni A, Reschiglian P, Moon MH, Mirasoli M, Michelini E, Roda A (2009) Field-flow fractionation in bioanalysis: a review of recent trends. Anal Chim Acta 635(2):132–143
15. Gossett DR, Weaver WM, Mach AJ, Hur SC, Tse HTK, Lee W, Amini H, Di Carlo D (2010) Label-free cell separation and sorting in microfluidic systems. Anal Bioanal Chem:1–19. doi:10.1007/s00216-010-3721-9
16. Giddings JC (1993) Field-flow fractionation: analysis of macromolecular, colloidal, and particulate materials. Science 260(5113):1456–1465
17. Giddings JC (2000) The field-flow fractionation family: underlying principles. In: Schimpf ME, Caldwell K, Giddings JC (eds) Field-flow fractionation handbook. Wiley, New York, pp 3–30
18. Williams SKR, Lee D (2006) Field-flow fractionation of proteins, polysaccharides, synthetic polymers, and supramolecular assemblies. J Sep Sci 29(12):1720–1732
19. Schallinger LE, Yau WW, Kirkland JJ (1984) Sedimentation field-flow fractionation of DNA's. Science (Washington, DC, 1883) 225(4660):434–437
20. Schallinger LE, Gray JE, Wagner LW, Knowlton S, Kirkland JJ (1985) Preparative isolation of plasmid DNA with sedimentation field-flow fractionation. J Chromatogr 342(1):67–77
21. Liu MK, Giddings JC (1993) Separation and measurement of diffusion coefficients of linear and circular DNAs by flow field-flow fractionation. Macromolecules 26(14):3576–3588
22. Nilsson M, Wahlund K-G, Bulow L (1998) Monitoring of ribosomes and subunits in Escherichia coli during production of glucose isomerase using flow field-flow fractionation. Biotechnol Tech 12(6):477–480
23. Nilsson M, Kallio PT, Bailey JE, Buelow L, Wahlund K-G (1999) Expression of vitreoscilla hemoglobin in Escherichia coli enhances ribosome and tRNA levels: a flow fieldflow fractionation study. Biotechnol Prog 15(2):158–163
24. Cole KD, Tellez CM, Blakesley RW (2000) Separation of different physical forms of plasmid DNA using a combination of low electric field strength and flow in porous media: effect of different field gradients and porosity of the media. Electrophoresis 21(5):1010–1017
25. Eaton MAW, Baker TS, Catterall CF, Crook K, Macaulay GS, Mason B, Norman TJ, Parker D, Perry JJB, Taylor RJ, Turner A, Weir AN (2000) A new self-assembling system for targeted gene delivery. Angew Chem Int Ed 39(22):4063–4067
26. Lee H, Williams SKR, Allison SD, Anchordoquy TJ (2001) Analysis of self-assembled cationic lipid-DNA gene carrier complexes using flow field-flow fractionation and light scattering. Anal Chem 73(4):837–843
27. Arfvidsson C, Wahlund K-G (2003) Time-minimized determination of ribosome and tRNA levels in bacterial cells using flow field-flow fractionation. Anal Biochem 313(1):76–85
28. Chen Z, Chauhan A (2005) DNA separation by EFFF in a microchannel. J Colloid Interface Sci 285(2):834–844
29. Cotts PM, Zheng M (2005) Light scattering of DNA-carbon nanotubes in aqueous suspension. In: Abstracts of papers, 230th ACS national meeting, Washington, DC, 28 Aug–1 Sept 2005:PMSE-027
30. Lao AIK, Hsing IM (2005) Flow-based and sieving matrix-free DNA differentiation by a miniaturized field-flow fractionation device. Lab Chip 5(6):687–690
31. Smith JE, Wang L, Tan W (2006) Bioconjugated silica-coated nanoparticles for bioseparation and bioanalysis. TrAC 25(9):848–855
32. Nour AA, Huggett J, Pfaffl MW (2010) qPCR: current technologies and future applications. Eur Pharm Rev (2)
33. Ma PL, Buschmann MD, Winnik FM (2010) One-step analysis of DNA/chitosan complexes by field-flow fractionation reveals particle size and free chitosan content. Biomacromolecules 11(3):549–554. doi:10.1021/bm901345q

34. Lipin DI, Chuan YP, Lua LHL, Middelberg APJ (2008) Encapsulation of DNA and non-viral protein changes the structure of murine polyomavirus virus-like particles. Arch Virol 153 (11):2027–2039
35. Citkowicz A, Petry H, Harkins RN, Ast O, Cashion L, Goldmann C, Bringmann P, Plummer K, Larsen BR (2008) Characterization of virus-like particle assembly for DNA delivery using asymmetrical flow field-flow fractionation and light scattering. Anal Biochem 376(2):163–172
36. Tong X, Yang L, Lang JC, Zborowski M, Chalmers JJ (2007) Application of immunomagnetic cell enrichment in combination with RT-PCR for the detection of rare circulating head and neck tumor cells in human peripheral blood. Cytometry B Clin Cytom 72:310–323
37. Caldwell KD, Kesner LF, Myers MN, Giddings JC (1972) Electrical field-flow fractionation of proteins. Science 176(32):296–298
38. Litzen A, Wahlund KG (1989) Improved separation speed and efficiency for proteins, nucleic acids and viruses in asymmetrical flow field-flow fractionation. J Chromatogr 476:413–421
39. Litzen A, Garn MB, Widmer HM (1994) Determination of acid phosphatase in cultivation medium using asymmetrical flow field-flow fractionation. J Biotechnol 37(3):291–295
40. Sklaviadis T, Dreyer R, Manuelidis L (1992) Analysis of Creutzfeldt-Jakob disease infectious fractions by gel permeation chromatography and sedimentation field-flow fractionation. Virus Res 26(3):241–254
41. Giddings JC (1993) Field-flow fractionation of macromolecules. J Chromatogr 470 (2):327–335
42. Wahlund KG, Gustavsson M, MacRitchie F, Nylander T, Wannerberger L (1996) Size characterization of wheat proteins, particularly glutenin, by asymmetrical flow field-flow fractionation. J Cereal Sci 23(2):113–119
43. Li P, Hansen M, Giddings JC (1997) Separation of lipoproteins from human plasma by flow field-flow fractionation. J Liq Chromatogr Relat Technol 20(16 & 17):2777–2802
44. Gale BK, Caldwell KD, Frazier AB (1998) A micromachined electrical field-flow fractionation (mu-EFFF) system. IEEE Trans BioMed Eng 45(12):1459–1469
45. Gale BK, Caldwell K, Frazier AB (2000) Blood and protein separations using a micromachined electrical field-flow fractionation (.mu.-EFFF) system. Micro total analysis systems 2000, Proceedings of the muTAS symposium, 4th, Enschede, 14–18 May 2000:399–402
46. Yohannes G, Sneck M, Varjo SJO, Jussila M, Wiedmer SK, Kovanen PT, Oeoerni K, Riekkola M-L (2006) Miniaturization of asymmetrical flow field-flow fractionation and application to studies on lipoprotein aggregation and fusion. Anal Biochem 354(2):255–265
47. Yohannes G, Pystynen K-H, Riekkola M-L, Wiedmer SK (2006) Stability of phospholipid vesicles studied by asymmetrical flow field-flow fractionation and capillary electrophoresis. Anal Chim Acta 560(1–2):50–56
48. Sangsawong S, Shiowatana J, Siripinyanond A (2006) Matrix removal before inductively coupled plasma spectrometric detection: another capability of flow field-flow fractionation. J Anal At Spectrom 21(11):1336–1339
49. Saeseaw S, Shiowatana J, Siripinyanond A (2006) Observation of salt-induced b-lactoglobulin aggregation using sedimentation field-flow fractionation. Anal Bioanal Chem 386(6): 1681–1688
50. Roda A, Parisi D, Guardigli M, Zattoni A, Reschiglian P (2006) Combined approach to the analysis of recombinant protein drugs using hollow-fiber flow field-flow fractionation, mass spectrometry, and chemiluminescence detection. Anal Chem 78(4):1085–1092
51. Reschiglian P, Zattoni A, Roda B, Roda A, Parisi D, Moon M-H, Min B-R (2006) Hollow-fiber flow field-flow fractionation: a gentle separation method for mass spectrometry of native proteins. Anal Chim 96(5–6):253–277
52. Magliulo M, Roda B, Zattoni A, Michelini E, Luciani M, Lelli R, Reschiglian P, Roda A (2006) An innovative, flow-assisted, noncompetitive chemiluminescent immunoassay for the detection of pathogenic bacteria. Clin Chem 52(11):2151–2155

53. Liu J, Andya JD, Shire SJ (2006) A critical review of analytical ultracentrifugation and field-flow fractionation methods for measuring protein aggregation. AAPS J 8(3):E580–E589
54. Luo J, Leeman M, Ballagi A, Elfwing A, Su Z, Janson J-C, Wahlund K-G (2006) Size characterization of green fluorescent protein inclusion bodies in E. coli using asymmetrical flow field-flow fractionation-multi-angle light scattering. J Chromatogr A 1120(1–2):158–164
55. Lee S, Kwen HD, Lee SK, Nehete SV (2010) Study on elution behavior of poly(amidoamine) dendrimers and their interaction with bovine serum albumin in asymmetrical flow field-flow fractionation. Anal Bioanal Chem 396(4):1581–1588. doi:10.1007/s00216-009-3353-0
56. Lee JY, Min HK, Choi D, Moon MH (2010) Profiling of phospholipids in lipoproteins by multiplexed hollow fiber flow field-flow fractionation and nanoflow liquid chromatography-tandem mass spectrometry. J Chromatogr A 1217(10):1660–1666. doi:10.1016/j.chroma.2010.01.006
57. Rambaldi DC, Reschiglian P, Zattoni A, Johann C (2009) Enzymatic determination of cholesterol and triglycerides in serum lipoprotein profiles by asymmetrical flow field-flow fractionation with on-line, dual detection. Anal Chim Acta 654(1):64–70
58. Qureshi RN, Kok WT, Schoenmakers PJ (2009) Fractionation of human serum lipoproteins and simultaneous enzymatic determination of cholesterol and triglycerides. Anal Chim Acta 654(1):85–91
59. Pease Iii LF, Lipin DI, Tsai DH, Zachariah MR, Lua LHL, Tarlov MJ, Middelberg APJ (2009) Quantitative characterization of virus-like particles by asymmetrical flow field-flow fractionation, electrospray differential mobility analysis, and transmission electron microscopy. Biotechnol Bioeng 102(3):845–855
60. Lang R, Vogt L, Zürcher A, Winter G (2009) Asymmetrical flow FFF as an analytical tool for the investigation of the physical stability of virus-like particles. LC GC North Am 27 (9):844–852
61. Kang D, Yoo JS, Kim MO, Moon MH (2009) A soft preparative method for membrane proteome analysis using frit inlet asymmetrical flow field-flow fractionation: application in a prostatic cancer cell line. J Proteome Res 8(2):982–991
62. Reschiglian P, Moon MH (2008) Flow field-flow fractionation: a pre-analytical method for proteomics. J Proteomics 71(3):265–276
63. Lipin DI, Lua LHL, Middelberg APJ (2008) Quaternary size distribution of soluble aggregates of glutathione-S-transferase-purified viral protein as determined by asymmetrical flow field-flow fractionation and dynamic light scattering. J Chromatogr A 1190 (1–2):204–214
64. Kang D, Oh S, Ahn S-M, Lee B-H, Moon MH (2008) Proteomic analysis of exosomes from human neural stem cells by flow field-flow fractionation and nanoflow liquid chromatography-tandem mass spectrometry. J Proteome Res 7(8):3475–3480
65. Henry MB, Gao Y-s, Blake RC, Blake DA (2008) Conformational change detected using asymmetric flow field-flow fractionation in a monoclonal antibody upon binding to its ligand. In: Abstracts of papers, 235th ACS national meeting, New Orleans, 6–10 April 2008:BIOL-051
66. Mozersky SM, Caldwell KD, Jones SB, Maleeff BE, Barford RA (1988) Sedimentation field-flow fractionation of mitochondrial and microsomal membranes from corn roots. Anal Biochem 172(1):113–123
67. Nilsson M, Bulow L, Wahlund K-G (1997) Use of flow field-flow fractionation for the rapid quantitation of ribosome and ribosomal subunits in Escherichia coli at different protein production conditions. Biotechnol Bioeng 54(5):461–467
68. Lu H, Gaudet S, Schmidt MA, Jensen KF (2004) A microfabricated device for subcellular organelle sorting. Anal Chem 76(19):5705–5712
69. Fettke J, Eckermann N, Tiessen A, Geigenberger P, Steup M (2005) Identification, subcellular localization and biochemical characterization of water-soluble heteroglycans (SHG) in leaves of Arabidopsis thaliana L.: distinct SHG reside in the cytosol and in the apoplast. Plant J 43(4):568–585

70. Kang D, Oh S, Reschiglian P, Moon MH (2008) Separation of mitochondria by flow field-flow fractionation for proteomic analysis. Analyst 133(4):505–515
71. Giddings JC, Yang FJ, Myers MN (1977) Flow field-flow fractionation: new method for separating, purifying, and characterizing the diffusivity of viruses. J Virol 21(1):131–138
72. Caldwell KD, Nguyen TT, Giddings JC, Mazzone HM (1980) Field-flow fractionation of alkali-liberated nuclear polyhedrosis virus from gypsy moth Lymantria dispar Linnaeus. J Virol Methods 1(5):241–256
73. Yonker CR, Caldwell KD, Giddings JC, Van Etten JL (1985) Physical characterization of PBCV virus by sedimentation field-flow fractionation. J Virol Methods 11(2):145–160
74. Hoffstetter-Kuhn S, Rosler T, Ehrat M, Widmer HM (1992) Characterization of yeast cultivations by steric sedimentation field-flow fractionation. Anal Biochem 206(2):300–308
75. Sharma RV, Edwards RT, Beckett R (1993) Physical characterization and quantification of bacteria by sedimentation field-flow fractionation. Appl Environ Microbiol 59(6):1864–1875
76. Gao Y-S, Lorbach SC, Blake R II (1997) Separation of bacteria by sedimentation field-flow fractionation. J Microcolumn Sep 9(6):497–501
77. Sharma RV, Edwards RT, Beckett R (1998) Analysis of bacteria in aquatic environments using sedimentation field-flow fractionation: (I) biomass determination. Water Res 32(5):1497–1507
78. Yager P, Afromowitz MA, Bell D, Forster FK, Holl JP, Kamholz A, Weigla B (1998) Design of microfluidic sample preconditioning systems for detection of biological agents in environmental samples. Proc SPIE Int Soc Opt Eng 3515(Microfluidic Devices and Systems):252–259
79. Saenton S, Lee H, Gao Y-S, Ranville JF, Williams SKR (2000) Evaluation of different field-flow fractionation techniques for separating bacteria. Sep Sci Technol 35(11):1761–1775
80. Khoshmanesh A, Sharma R, Beckett R (2001) Biomass of sediment bacteria by sedimentation field-flow fractionation. J Environ Eng 127(1):19–25
81. Sanz R, Cardot P, Battu S, Galceran MT (2002) Steric-hyperlayer sedimentation field-flow fractionation and flow cytometry analysis applied to the study of Saccharomyces cerevisiae. Anal Chem 74(17):4496–4504
82. Lee H, Williams SKR, Wahl KL, Valentine NB (2003) Analysis of whole bacterial cells by flow field-flow fractionation and matrix-assisted laser desorption/ionization time-of-flight mass spectrometry. Anal Chem 75(11):2746–2752
83. Reschiglian P, Zattoni A, Roda B, Cinque L, Melucci D, Min BR, Moon MH (2003) Hyperlayer hollow-fiber flow field-flow fractionation of cells. J Chromatogr A 985 (1–2):519–529
84. Sanz R, Puignou L, Galceran MT, Reschiglian P, Zattoni A, Melucci D (2004) Coupling gravitational and flow field-flow fractionation, and size-distribution analysis of whole yeast cells. Anal Bioanal Chem 379(7–8):1068–1075
85. Jackson BP, Ranville JF, Neal AL (2005) Application of flow field-flow fractionation-ICPMS for the study of uranium binding in bacterial cell suspensions. Anal Chem 77(5):1393–1397
86. Reschiglian P, Zattoni A, Cinque L, Roda B, Dal Piaz F, Roda A, Moon Myeong H, Min Byung R (2004) Hollow-fiber flow field-flow fractionation for whole bacteria analysis by matrix-assisted laser desorption/ionization time-of-flight mass spectrometry. Anal Chem 76 (7):2103–2111
87. Farmakis L, Koliadima A (2005) Kinetic Study of Cell Proliferation of Saccharomyces cerevisiae Strains by Sedimentation/Steric Field Flow Fractionation in Situ. Biotechnol Progr 21(3):971–977
88. Cho SK, Shim SH, Park KR, Choi S-H, Lee S (2006) Purification and characterization of a biosurfactant produced by Pseudomonas sp. G11 by asymmetrical flow field-flow fractionation (AsFlFFF). Anal Bioanal Chem 386(7–8):2027–2033
89. Chon K, Moon J, Kim S, Kim S-D, Cho J (2007) Bio-particle separation using microfluidic porous plug for environmental monitoring. Desalination 202(1–3):215–223

90. Garcia MT, Sanz R, Galceran MT, Puignou L (2006) Use of fluorescent probes for determination of yeast cell viability by gravitational field-flow fractionation. Biotechnol Progr 22(3):847–852
91. Moncada-Hernandez H, Lapizco-Encinas BH (2010) Simultaneous concentration and separation of microorganisms: insulator-based dielectrophoretic approach. Anal Bioanal Chem 396(5):1805–1816. doi:10.1007/s00216-009-3422-4
92. Lim S, Lee S, Choi S, Moon J, Hong S (2010) Evaluation of biofouling potential of microorganism using flow field-flow fractionation (Fl-FFF). Desalination. doi:10.1016/j.desal.2010.05.042
93. Lee E, Shon HK, Cho J (2010) Biofouling characteristics using flow field-flow fractionation: effect of bacteria and membrane properties. Bioresour Technol 101(5):1487–1493
94. Lainioti GC, Kapolos J, Koliadima A, Karaiskakis G (2010) New separation methodologies for the distinction of the growth phases of Saccharomyces cerevisiae cell cycle. J Chromatogr A 1217(11):1813–1820
95. Caldwell KD, Cheng ZQ, Hradecky P, Giddings JC (1984) Separation of human and animal cells by steric field-flow fractionation. Cell Biophys 6(4):233–251
96. Bigelow JC, Giddings JC, Nabeshima Y, Tsuruta T, Kataoka K, Okano T, Yui N, Sakurai Y (1989) Separation of B and T lymphocytes by a hybrid field-flow fractionation/adhesion chromatography technique. J Immunol Methods 117(2):289–293
97. Cardot PJ, Gerota J, Martin M (1991) Separation of living red blood cells by gravitational field-flow fractionation. J Chromatogr 568(1):93–103
98. Urbankova E, Vacek A, Chmelik J (1996) Micropreparation of hemopoietic stem cells from the mouse bone marrow suspension by gravitational field-flow fractionation. J Chromatogr B 687(2):449–452
99. Tong X, Ash JF, Caldwell KD (1997) Rapid swelling of a CHO-K1 aspartate/glutamate transport mutant in hypo-osmotic medium. J Membr Biol 156(2):131–139
100. Metreau JM, Gallet S, Cardot PJP, Le Maire V, Dumas F, Hernvann A, Loric S (1997) Sedimentation field-flow fractionation of cellular species. Anal Biochem 251(2):178–186
101. Chalmers JJ, Zborowski M, Sun L, Moore L (1998) Flow through, immunomagnetic cell separation. Biotechnol Prog 14(1):141–148
102. Ikeya T, Kataoka K, Okano T, Sakurai Y (1998) Selective adhesion of rat lymphocyte subpopulation on the polymer surface with phenylboronic acid moieties: evaluation by field-flow fractionation/adhesion chromatography FFF/AC) method. React Funct Polym 37 (1–3):251–261
103. Huang Y, Yang J, Wang XB, Becker FF, Gascoyne PR (1999) The removal of human breast cancer cells from hematopoietic CD34+ stem cells by dielectrophoretic field-flow-fractionation. J Hematother Stem Cell Res 8(5):481–490
104. Williams PS, Moore LR, Leigh D, Zborowski M (2003) Use of quadrupole magnetic fields for separation of biological cells. In: Abstracts of papers, 225th ACS national meeting, New Orleans, 23–27 March 2003:ANYL-197
105. Zborowski M, Chalmers JJ (2005) Magnetic cell sorting. Methods Mol Biol 295:291–300
106. Leger DY, Battu S, Liagre B, Beneytout JL, Cardot PJP (2006) Megakaryocyte cell sorting from diosgenin-differentiated human erythroleukemia cells by sedimentation field-flow fractionation. Anal Biochem 355(1):19–28
107. Cinque L, Williams PS, Zborowski M (2006) Sorting of unmodified human progenitor cells. In: Abstracts of papers, 232nd ACS national meeting, San Francisco, 10–14 Sept 2006:ANYL-286
108. Jing Y, Moore LR, Schneider T, Williams PS, Chalmers JJ, Farag SS, Bolwell B, Zborowski M (2007) Negative selection of hematopoietic progenitor cells by continuous magnetophoresis. Exp Hematol 35(4):662–672
109. Roda B, Lanzoni G, Alviano F, Zattoni A, Costa R, Di Carlo A, Marchionni C, Franchina M, Ricci F, Tazzari PL, Pagliaro P, Scalinci SZ, Bonsi L, Reschiglian P, Bagnara GP (2010) A novel stem cell tag-less sorting method. Stem Cell Rev Rep 5(4):420–427. doi:10.1007/s12015-009-9088-7

110. Roda B, Reschiglian P, Zattoni A, Alviano F, Lanzoni G, Costa R, Di Carlo A, Marchionni C, Franchina M, Bonsi L, Bagnara GP (2009) A tag-less method of sorting stem cells from clinical specimens and separating mesenchymal from epithelial progenitor cells. Cytometry B Clin Cytom 76(4):285–290
111. Roda B, Reschiglian P, Alviano F, Lanzoni G, Bagnara GP, Ricci F, Buzzi M, Tazzari PL, Pagliaro P, Michelini E, Roda A (2009) Gravitational field-flow fractionation of human hemopoietic stem cells. J Chromatogr A 1216(52):9081–9087
112. Leu TS, Weng CY (2009) Dynamics of dielectrophoretic field-flow fractionation (dep-fff) based micro sorter for cell separation. Mod Phys Lett B 23(3):389–392
113. Gascoyne PRC, Noshari J, Anderson TJ, Becker FF (2009) Isolation of rare cells from cell mixtures by dielectrophoresis. Electrophoresis 30(8):1388–1398
114. Gascoyne PRC (2009) Dielectrophoretic-field-flow fractionation analysis of dielectric, density, and deformability characteristics of cells and particles. Anal Chem 81(21):8878–8885
115. Bertrand J, Liagre B, Bégaud-Grimaud G, Jauberteau MO, Beneytout JL, Cardot PJP, Battu S (2009) Analysis of relationship between cell cycle stage and apoptosis induction in K562 cells by sedimentation field-flow fractionation. J Chromatogr B 877(11–12):1155–1161
116. Bertrand J, Begaud-Grimaud G, Bessette B, Verdier M, Battu S, Jauberteau MO (2009) Cancer stem cells from human glioma cell line are resistant to Fas-induced apoptosis. Int J Oncol 34:717–727
117. Bégaud-Grimaud G, Battu S, Liagre B, Beneytout JL, Jauberteau MO, Cardot PJP (2009) Development of a downscale sedimentation field-flow fractionation device for biological event monitoring. J Chromatogr A 1216(52):9125–9133
118. Vykoukal J, Vykoukal DM, Freyberg S, Alt EU, Gascoyne PRC (2008) Enrichment of putative stem cells from adipose tissue using dielectrophoretic field-flow fractionation. Lab Chip 8(8):1386–1393
119. Roda B, Reschiglian P, Zattoni A, Tazzari PL, Buzzi M, Ricci F, Bontadini A (2008) Human lymphocyte sorting by gravitational field-flow fractionation. Anal Bioanal Chem 392 (1–2):137–145
120. Giddings JC (1966) New separation concept based on a coupling of concentration and flow nonuniformities. Sep Sci 1(1):123–125
121. Caldwell KD, Nguyen TT, Murray TM, Myers MN, Giddings JC (1979) Observations on anomalous retention in steric field-flow fractionation. Sep Sci Technol 14(10):935–946
122. Dunkel M, Tri N, Beckett R, Caldwell KD (1997) Electrical field-flow fractionation: a tool for characterization of colloidal adsorption complexes. J Microcolumn Sep 9(3):177–183
123. Williams SKR, Lee H, Turner MM (1999) Size characterization of magnetic cell sorting microbeads using flow field-flow fractionation and photon correlation spectroscopy. J Magn Magn Mater 194(1–3):248–253
124. Gale BK, Caldwell KD, Frazier AB (2001) Geometric scaling effects in electrical field-flow fractionation. 1. Theoretical analysis. Anal Chem 73(10):2345–2352
125. Gale BK, Caldwell KD, Frazier AB (2002) Geometric scaling effects in electrical field-flow fractionation. 2. Experimental results. Anal Chem 74(5):1024–1030
126. Gascoyne PC, Das C, Vykoukal J, Weinstein R, Gandini A, Parks D, Sawh R (2003) Magnetophoretic-dielectrophoretic field-flow fractionation. In: Abstracts of papers, 225th ACS national meeting, New Orleans, 23–27 March 2003:ANYL-198
127. Gale BK (2003) Novel techniques and instruments for field-flow fractionation of biological materials. In: Abstracts of papers, 225th ACS national meeting, New Orleans, 23–27 March 2003:ANYL-199
128. Latham AH, Freitas RS, Schiffer P, Williams ME (2005) Capillary magnetic field-flow fractionation and analysis of magnetic nanoparticles. Anal Chem 77(15):5055–5062
129. Carpino F, Zborowski M, Williams PS (2006) Quadrupole magnetic field-flow fractionation: a novel technique for the characterization of magnetic nanoparticles. In: Paper presented at the abstracts of papers, 232nd ACS national meeting, San Francisco 10–14 Sept 2006

130. Sant Himanshu J, Gale Bruce K (2006) Geometric scaling effects on instrumental plate height in field-flow fractionation. J Chromatogr A 1104(1–2):282–290
131. Sant HJ, Kim JW, Gale BK (2006) Reduction of end effect-induced zone broadening in field-flow fractionation channels. Anal Chem 78(23):7978–7985
132. Narayanan N, Saldanha A, Gale BK (2006) A microfabricated electrical SPLITT system. Lab Chip 6(1):105–114
133. Caldwell KD (1986) Field-flow fractionation in biomedical analysis. Chem Sep, Dev Sel Pap Int Conf Sep Sci Technol 1st 1:41–57
134. Schallinger LE, Kaminski LA (1985) Sedimentation field-flow fractionation: a promising new bioseparations technique. Biotechniques 3(2):124–128, 130–121, 134–125
135. Tong X, Caldwell KD (1995) Separation and characterization of red blood cells with different membrane deformability using steric field-flow fractionation. J Chromatogr B 674(1):39–47
136. Urbankova E, Vacek A, Novakova N, Matulik F, Chmelik J (1992) Investigation of red blood cell fractionation by gravitational field-flow fractionation. J Chromatogr 583(1):27–34
137. Yue V, Kowal R, Neargarder L, Bond L, Muetterties A, Parsons R (1994) Miniature field-flow fractionation system for analysis of blood cells. Clin Chem 40(9):1810–1814
138. Merino-Dugay A, Cardot PJP, Czok M, Guernet M, Andreux JP (1992) Monitoring of an experimental red blood cell pathology with gravitational field-flow fractionation. J Chromatogr 579(1):73–83
139. Cardot PJP, Elgea C, Guernet M, Godet D, Andreux JP (1994) Size- and density-dependent elution of normal and pathological red blood cells by gravitational field-flow fractionation. J Chromatogr B 654(2):193–203
140. Cardot PJP, Battu S, Chianea T, Rasouli S (2000) Cells and cell organelles: field-flow fractionation. In: Wilson ID, Adlard ER, Cooke M, Poole CF (eds) Encyclopedia of separation science, vol 5. Academic, London, pp 2267–2271
141. Bouamrane F, Assidjo NE, Bouteille B, Dreyfuss MF, Darde ML, Cardot PJP (1999) Sedimentation field-flow fractionation application to toxoplasma gondii separation and purification. J Pharm Biomed Anal 20(3):503–512
142. Battu S, Elyaman W, Hugon J, Cardot PJP (2001) Cortical cell elution by sedimentation field-flow fractionation. Biochim Biophys Acta 1528(2–3):89–96
143. Lautrette C, Cardot PJP, Vermot-Desroches C, Wijdenes J, Jauberteau MO, Battu S (2003) Sedimentation field-flow fractionation purification of immature neural cells from a human tumor neuroblastoma cell line. J Chromatogr B 791(1–2):149–160
144. Corbiere C, Battu S, Liagre B, Cardot PJP, Beneytout JL (2004) SdFFF monitoring of cellular apoptosis induction by diosgenin and different inducers in the human 1547 osteosarcoma cell line. J Chromatogr B 808(2):255–262
145. Guglielmi L, Battu S, Le Bert M, Faucher JL, Cardot PJP, Denizot Y (2004) Mouse embryonic stem cell sorting for the generation of transgenic mice by sedimentation field-flow fractionation. Anal Chem 76(6):1580–1585
146. Leger DY, Liagre B, Cardot PJP, Beneytout JL, Battu S (2004) Diosgenin dose-dependent apoptosis and differentiation induction in HEL cell line and SdFFF monitoring. Anal Biochem 335:267–278
147. Begaud-Grimaud G, Battu S, Liagre B, Leger DY, Beneytout JL, Cardot PJP (2006) Pre-apoptotic sub-population cell sorting from diosgenin apoptosis induced 1547 cells by sedimentation field-flow fractionation. J Chromatogr A 1128(1–2):194–202
148. Comte I, Battu S, Mathonnet M, Bessette B, Lalloue F, Cardot P, Ayer-Le Lievre C (2006) Neural stem cell separation from the embryonic avian olfactory epithelium by sedimentation field-flow fractionation. J Chromatogr B 843(2):175–182
149. Schure MR, Caldwell KD, Giddings JC (1986) Theory of sedimentation hyperlayer field-flow fractionation. Anal Chem 58(7):1509–1516
150. Martin M, Williams PS (1992) Theoretical basis of field-flow fractionation. In: Dondi F, Guiochon G (eds) Theoretical advancement in chromatography and related separation

techniques, 383rd edn, NATO ASI Ser., Ser. C: mathematical and physical sciences. Kluwer, Dordrecht, pp 513–580
151. Williams PS, Lee S, Giddings JC (1994) Characterization of hydrodynamic lift forces by field-flow fractionation. Inertial and near-wall lift forces. Chem Eng Commun 130:143–166
152. Chmelik J (1999) Different elution modes and field programming in gravitational field-flow fractionation; I. A theoretical approach. J Chromatogr A 845(1–2):285–291
153. Caldwell KD (2000) Steric field-flow fractionation and steric transition. In: Schimpf ME, Caldwell KD, Giddings JC (eds) Field-flow fractionation handbook. Wiley, New York, pp 79–94
154. Plockova J, Matulik F, Chmelik J (2002) Different elution modes and field programming in gravitational field-flow fractionation IV. Field programming achieved with channels of non-constant cross-sections. J Chromatogr A 955(1):95–103
155. Williams PS, Moon MH, Xu Y, Giddings JC (1996) Effect of viscosity on retention time and hydrodynamic lift forces in sedimentation/steric field-flow fractionation. Chem Eng Sci 51(19):4477–4488
156. Cardot PJP, Denizot Y, Battu S (2005) Cell sorting using sedimentation field-flow fractionation: methodologies, problems, and solutions – A "Cellulomics" Concept. In: Cazes J (ed) Encyclopedia of chromatography, vol Chap. 265. M. Dekker Inc., New York, pp 282–291
157. Williams PS, Moon MH, Giddings JC (1996) Influence of accumulation wall and carrier solution composition on lift force in sedimentation/steric field-flow fractionation. Colloids Surf A 113(3):215–228
158. Cardot P, Battu S, Sarrazin R (2006) Field-flow fractionation separation device with a separation channel and a counter channel. Ep Patent 1679124
159. Cardot P, Battu S, Sarrazin R (2006) Swivel joint for conduits used in analytical chemistry. Fr Patent 2880669
160. Battu S, Roux A, Delebasee S, Bosgiraud C, Cardot PJP (2001) Sedimentation field-flow fractionation device cleaning, decontamination and sterilization procedures for cellular analysis. J Chromatogr B 751(1):131–141
161. Masudo T, Okada T (2006) Low-capacity channel designed for particle separation with controlled electric fields and evaluation of involved forces. J Chromatogr A 1106(1–2):196–204
162. Pasti L, Ventosa EA, Mingozzi I, Dondi F (2006) Determination of calibration function in thermal field-flow fractionation under thermal field programming. J Sep Sci 29(8):1088–1101
163. Kronholm J, Vastamaeki P, Raesaenen R, Ahonen A, Hartonen K, Riekkola ML (2006) Thermal field-flow fractionation and gas chromatography-mass spectrometry in determination of decomposition products of expandable polystyrene after reactions in pressurized hot water and supercritical water. Ind Eng Chem Res 45(9):3029–3035
164. Kim H-J, Oh S, Moon MH (2006) Hollow-fiber flow/hyperlayer field-flow fractionation for the size characterization of airborne particle fractions obtained by SPLITT fractionation. J Sep Sci 29(3):423–428
165. Kim W-S, Eum CH, Molnar A, Yu J-S, Lee S (2006) Repeatability and reproducibility of thermal field-flow fractionation in molecular weight determination of processed natural rubber. Analyst 131(3):429–433
166. Contado C, Wahlund K-G (2006) High-speed separation and size characterization of wheat and barley starch granules by lift-hyperlayer asymmetrical flow field-flow fractionation in synergy with SPLITT fractionation. Starch/Staerke 58(3–4):140–154
167. Cho J, Park Y-J, Sun H, Kim S, Yoon Y (2006) Measurements of effective sizes and diffusivities of nano-colloids and micro-particles. Colloids Surf A 274(1–3):43–47
168. Williams PS, Lee S, Giddings JC (1994) Characterization of hydrodynamic lift forces by field-flow fractionation. Inertial and near-wall lift forces. Chem Eng Commun 130:143–166
169. Chianea T, Cardot PJP, Assidjo E, Monteil J, Clarot I, Krausz P (1999) Field- and flow-dependent trapping of red blood cells on polycarbonate accumulation wall in sedimentation field-flow fractionation. J Chromatogr B 734(1):91–99

170. Andreev VP, Stefanovich LA (1993) Theory of field-flow fractionation with the reversible adsorption on channel walls. Chromatographia 37(5–6):325–328
171. Koch T, Giddings JC (1986) High-speed separation of large (>1 .mu.m) particles by steric field-flow fractionation. Anal Chem 58(6):994–997
172. Giddings JC, Chen X, Wahlund KG, Myers MN (1987) Fast particle separation by flow/steric field-flow fractionation. Anal Chem 59(15):1957–1962
173. Assidjo E, Chianea T, Dreyfuss M-F, Cardot PJP (1998) Validation procedures of sedimentation field-flow fractionation techniques for biological applications. J Chromatogr B 709 (2):197–207
174. Bertrand J, Liagre B, Bégaud-Grimaud G, Jauberteau MO, Cardot P, Beneytout JL, Battu S (2008) Study of diosgenin-induced apoptosis kinetics in K562 cells by sedimentation field-flow fractionation. J Chromatogr B 869:75–78
175. Giddings JC (1989) A pinched inlet system for reduced relaxation effects and stopless flow injection in field-flow fractionation. Sep Sci Technol 24(9–10):755–768
176. Assidjo NE, Chianea T, Clarot I, Dreyfuss MF, Cardot PJP (1999) Osmolarity effects on red blood cell elution in sedimentation field-flow fractionation. J Chromatogr Sci 37(7):229–236
177. Moon MH, Myers MN, Giddings JC (1990) Evaluation of pinched inlet channel for stopless flow injection in steric field-flow fractionation. J Chromatogr 517:423–433
178. Lee SH, Myers MN, Giddings JC (1989) Hydrodynamic relaxation using stopless flow injection in split inlet sedimentation field-flow fractionation. Anal Chem 61(21):2439–2444
179. Martin M (2006) Onset of non-linearity in zonal elution separators: the concept of effective analyte concentration. J Chromatogr A 1126(1–2):129–142
180. Caldwell KD, Brimhall SL, Gao Y, Giddings JC (1988) Sample overloading effects in polymer characterization by field-flow fractionation. J Appl Polym Sci 36(3):703–719
181. Carlshaf A, Jonsson JA (1992) Perturbations of the retention parameter due to sample overloading in hollow-fiber flow field-flow fractionation. Sep Sci Technol 28(5):1191–1201
182. Reschiglian P, Martin M, Contado C, Dondi F (1997) Assessment of linearity conditions in thermal field-flow fractionation by peak shape analysis. Int J Polym Anal Charact 3(2):107–130
183. Moon MH, Giddings JC (1993) Size distribution of liposomes by flow field-flow fractionation. J Pharm Biomed Anal 11(10):911–920
184. Moon MH, Giddings JC (1993) Rapid separation and measurement of particle size distribution of starch granules by sedimentation/steric field-flow fractionation. J Food Sci 58 (5):1166–1171
185. Clédat D, Battu S, Mokrini R, Cardot PJP (2004) Rice starch granule characterization by flow cytometry scattering techniques hyphenated with sedimentation field–flow fractionation. J Chromatogr A 1049:131–138
186. Schimpf ME (2000) Resolution and fractionating power. In: Schimpf ME, Caldwell KD, Giddings JC (eds) Field-flow fractionation handbook. Wiley, New York, pp 71–79
187. Cailleteau C, Liagre B, Battu S, Jayat-Vignoles C, Beneytout JL (2008) Increased cyclooxygenase-2 and thromboxane synthase expression is implicated in diosgenin-induced megakaryocytic differentiation in human erythroleukemia cells. Anal Biochem 380(1):26–34
188. Cailleteau C, Micallef L, Lepage C, Cardot PJP, Beneytout JL, Liagre B, Battu S (2010) Relationship between cell cycle stage and diosgenin-induced megakaryocytic differentiation of HEL cells using sedimentation field-flow fractionation. Anal Bioanal Chem. doi:10.1007/s00216-010-4062-4
189. Micallef L, Battu S, Pinon A, Cook-Moreau J, Cardot PJP, Delage C, Simon A (2010) Sedimentation field-flow fractionation separation of proliferative and differentiated subpopulations during Ca^{2+}-induced differentiation in HaCaT cells. J Chromatogr B 878 (15–16):1051–1058

190. Parsons R, Yue V, Tong X, Cardot P, Bernard A, Andreux JP, Caldwell K (1996) Comparative study of human red blood cell analysis with three different field-flow fractionation systems. J Chromatogr B 686(2):177–187
191. Cardot PJP, Launay J-M, Martin M (1997) Age-dependent elution of human red blood cells in gravitational field-flow fractionation. J Liq Chromatogr Relat Technol 20(16 & 17):2543–2553
192. Weers JG, Arlauskas RA (2004) Particle size analysis of perfluorocarbon emulsions in a complex whole blood matrix by sedimentation field-flow fractionation. Colloids Surf B 33(3–4):265–269
193. Arifin DR, Palmer AF (2005) Stability of liposome encapsulated hemoglobin dispersions. Artif Cells Blood Substit Immobil Biotechnol 33(2):113–136
194. Singh S, Dirks PB (2007) Brain tumor stem cells: identification and concepts. Neurosurg Clin N Am 18(1):31–38
195. Thompson CB (1995) Apoptosis in the pathogenesis and treatment of disease. Science 267:1456–1462
196. Hanahan D, Weinberg RA (2000) The hallmarks of cancer. Cell Adhes Commun 100(1):57–70
197. Rensing-Ehl A, Frei K, Flury R, Matiba B, Mariani SM, Weller M, Aebischer P, Krammer PH, Fontana A (1995) Local Fas/APO-1 (CD95) ligand-mediated tumor cell killing in vivo. Eur J Immunol 25(8):2253–2258
198. Cailleteau C, Liagre B, Beneytout JL (2009) A proteomic approach to the identification of molecular targets in subsequent apoptosis of HEL cells after diosgenin-induced megakaryocytic differentiation. J Cell Biochem 107(4):785–796
199. Leger DY, Battu S, Liagre B, Cardot PJP, Beneytout JL (2007) Sedimentation field-flow fractionation to study human erythroleukemia cell megakaryocytic differentiation after short period diosgenin induction. J Chromatogr A 1157(1–2):309–320
200. Leszczyniecka M, Roberts T, Dent P, Grant S, Fisher PB (2001) Differentiation therapy of human cancer: basic science and clinical applications. Pharmacol Ther 90:105–156
201. Sachs L (1978) The differentiation of myeloid leukaemia cells: new possibilities for therapy. Br J Haematol 40(4):509–517
202. Blagosklonny MV (2003) Hormonal and differentiation agents in cancer growth suppression. Methods Mol Biol 223:505–522
203. Salesse C, Battu S, Begaud-Grimaud G, Cledat D, Cook-Moreau J, Cardot PJP (2006) Sedimentation field-flow fractionation monitoring of bimodal wheat starch amylolysis. J Chromatogr A 1129(2):247–254
204. Morelon X, Battu S, Salesse C, Begaud-Grimaud G, Cledat D, Cardot PJP (2005) Sedimentation field-flow fractionation monitoring of rice starch amylolysis. J Chromatogr A 1093(1–2):147–155
205. Liagre B, Bertrand J, Leger DY, Beneytout JL (2005) Diosgenin, a plant steroid, induces apoptosis in COX-2 deficient K562 cells with activation of the p38 MAP kinase signalling and inhibition of NF-kappaB binding. Int J Mol Med 16(6):1095–1101
206. Micallef L, Belaubre F, Pinon A, Jayat-Vignoles C, Delage C, Charveron M, Simon A (2008) Effects of extracellular calcium on the growth differentiation switch in immortalized keratinocyte HaCaT cells compared with normal human keratinocytes. Exp Dermatol 18(2):143–151
207. Yang J, Huang Y, Wang X-B, Becker FF, Gascoyne PRC (1999) Cell separation on microfabricated electrodes using dielectrophoretic/gravitational field-flow fractionation. Anal Chem 71(5):911–918
208. Graziadei PP, Metcalf JF (1971) Autoradiographic and ultrastructural observations on the frog's olfactory mucosa. Z Zellforsch Mikrosk Anat 116(3):305–318
209. Graziadei PP, Graziadei GA (1979) Neurogenesis and neuron regeneration in the olfactory system of mammals. I. Morphological aspects of differentiation and structural organization of the olfactory sensory neurons. J Neurocytol 8:1–18

210. Moulton DG (1974) Dynamics of cell populations in the olfactory epithelium. Ann N Y Acad Sci 237:52–61
211. Bégaud-Grimaud G, Battu S, Lazcoz P, Castresana JS, Jauberteau MO, Cardot PJP (2007) Study of the phenotypic relationship in the IMR-32 human neuroblastoma cell line by sedimentation field-flow fractionation. Int J Oncol 31:883–892
212. Allan AL, Vantyghem SA, Tuck AB, Chambers AF (2007) Tumor dormancy and cancer stem cells: implications for the biology and treatment of breast cancer metastasis. Breast Dis 26:87–98
213. Krause M, Prager J, Zhou X, Yaromina A, Dörfler A, Eicheler W, Baumann M (2007) EGFR-TK inhibition before radiotherapy reduces tumour volume but does not improve local control: differential response of cancer stem cells and nontumourigenic cells? Radiother Oncol 83(3):316–325
214. Ponti D, Costa A, Zaffaroni N, Pratesi G, Petrangolini G, Coradini D, Pilotti S, Pierotti MA, Daidone MG (2005) Isolation and in vitro propagation of tumorigenic breast cancer cells with stem/progenitor cell properties. Cancer Res 65(13):5506–5511
215. Ponti D, Zaffaroni N, Capelli C, Daidone MG (2006) Breast cancer stem cells: an overview. Eur J Cancer 42(9):1219–1224
216. Gilbert CA, Ross AH (2009) Cancer stem cells: cell culture, markers, and targets for new therapies. J Cell Biochem 108(5):1031–1038
217. Hermann PC, Bhaskar S, Cioffi M, Heeschen C (2010) Cancer stem cells in solid tumors. Semin Cancer Biol 20(2):77–84

Chapter 16
Isolation and Characterization of Cells by Dielectrophoretic Field-Flow Fractionation

Peter R.C. Gascoyne

Abstract Dielectrophoresis (DEP) is a spatially inhomogeneous force field phenomenon that arises when dielectrically-polarizable particles are subjected to a spatially inhomogeneous, alternating electric field. DEP may be applied by a microelectrode array and, with appropriate choices of suspending medium and electric field voltage and frequency conditions, can be used to impose differential forces according to the properties of different microparticle types in a mixture. Because the intensity and direction of the DEP force may be controlled electronically, it is versatile in FFF applications. The physical principles of DEP-FFF fractionation involving the balance of DEP, sedimentation and hydrodynamic lift forces, are described with special emphasis on applications to living cells. It is shown how batch-mode DEP-FFF elution profiles obtained under appropriate operating conditions may be used to profile the density, mechanical flexibility and membrane capacitance properties of cells. Finally, the principles of high throughput isolation of target particle types by continuous-flow DEP-FFF are treated. This method is applicable to clinical applications including the antigen-independent isolation of rare circulating tumor cells from blood.

Keywords Cell density • Cell membrane capacitance • Cytoplasm conductivity • Deformability • DEP-FFF of normal and cancer cells • Dielectrophoresis (DEP) • inhomogeneous electric fields • Throughput capacity

P.R.C. Gascoyne (✉)
Department of Imaging Physics, Unit 951, The University of Texas M.D. Anderson Cancer Center, Houston, TX, USA
e-mail: pgascoyn@mdanderson.org

S.K.R. Williams and K.D. Caldwell (eds.), *Field-Flow Fractionation in Biopolymer Analysis*, DOI 10.1007/978-3-7091-0154-4_16,

16.1 Introduction

The imposed forces determining the elution behavior of dissimilar particle types in field-flow fractionation (FFF) balance at unique equilibrium positions only if at least one varies spatially relative to the accumulation wall. Therefore, considerable interest lies in inhomogeneous field types that are easy to manipulate. Dielectrophoresis (DEP) is a spatially-variant field effect that is instantly controllable by programming the voltage and/or frequency of an electric excitation signal. DEP forces may be positive or negative depending on the particle dielectric and conductivity characteristics relative to the suspending medium and the chosen frequency of the applied electric field. Therefore, programmed DEP allows smooth transitions from steric to hyperlayer FFF modes to be achieved and enables either or both modes to be used during a single run to fractionate particles according to their dielectric properties.

As with many field types, Giddings was the first to apply DEP to FFF [1, 2]. However the complexities of creating appropriate field patterns and the dominant role of the charge double layer, rather than intrinsic molecular properties, in controlling DEP forces on molecules in aqueous suspensions led the technique of DEP-FFF to languish in physical chemistry. Greater interest in DEP was kindled by physicist Herb Pohl [3] who used it to manipulate living cells based on their dielectric properties. Several laboratories subsequently played key roles in elucidating the theory and practice of DEP [4–7], lending an understanding of the biophysical basis for cellular responses [8–10] and inventing methods to apply field patterns to enable the DEP characterization, manipulation, and isolation of cells [11–14]. Subsequent efforts, especially in micro-fluidic and micro-total analysis systems, have applied DEP for cell sorting and isolation based on these early developments [15–19]. An outstanding review of DEP has been given recently by Pethig [17]. Unfortunately, most DEP embodiments suffer from extremely low throughput rates with no feasible route to scale-up, making them unrealistic for real-world preparative and specimen analysis applications.

Following early demonstrations of the DEP discrimination of normal and cancer cells in micro-devices [20, 21], our laboratory addressed this central issue of realizing higher throughput by moving from a single step sorting concept employing a small group of electrodes to a chromatographic approach that integrated the effect of passing cells rapidly over thousands of microelectrodes covering a long flow path in a much larger device [22, 23]. Similar reasoning led Markx, Pethig and Rousselet independently to an almost identical approach [24]. The result was the development of DEP-FFF on large microelectrode arrays, a method that can be used to process millions of cells at much faster rates than microchips yet exploit the same microscale physical principles. This chapter describes the application of the DEP-FFF method to mammalian cell mixtures and demonstrates how it can be employed to derive population profiles for cell density, membrane capacitance and cell mechanical properties in a batch implementation and to prepare cell isolates from large samples including the extraction of very rare cells from clinical blood specimens in a continuous flow

implementation. Despite the emphasis on mammalian cell mixtures in this chapter, the theory and methods are adaptable to other types of particle mixtures where dielectric differences are a useful discriminant – including plant cells, bacteria, cell organelles, as well as industrial microparticles.

16.2 The Force Fields in DEP-FFF

In hyperlayer mode DEP-FFF, the height h above the accumulation wall at which a particle moves through the FFF chamber, and hence its elution behavior, is determined by the balance of vertical DEP, sedimentation and hydrodynamic lift (HDL) forces:

$$F_{sed} + F_{DEP} + F_{HDL} = 0. \tag{16.1}$$

In this case, the particle transit time through the chamber is controlled by the fluid flow rate (Fig. 16.1).

In steric mode DEP-FFF, the particles come into contact with the accumulation wall and a vertical contact force $F_{contact}$ comes into play so that $F_{sed} + F_{DEP} + F_{contact} = 0$. Steric (friction-like) interactions occur between the particle and the wall, slowing the lateral translation, and making the elution process a complex function of particle-wall contact interaction properties (Fig. 16.1).

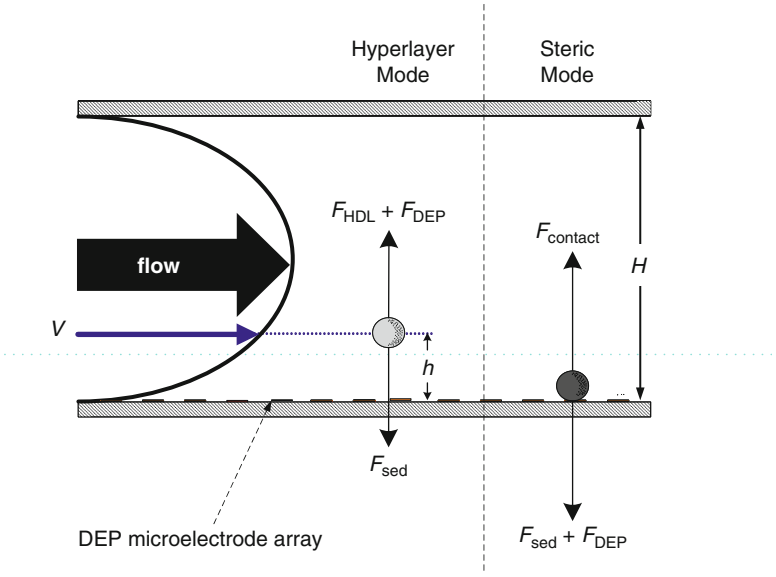

Fig. 16.1 The balance of forces in DEP-FFF in hyperlayer mode and steric mode. The DEP force is applied by a microelectrode array covering the accumulation wall of the chamber

In normal mode FFF, the distribution of particles is dominated by diffusion and particle distributions in the flow stream must be described thermodynamically. DEP-FFF may be applied for normal mode fractionation of molecules and sufficiently small cell organelles and nanoparticles for which diffusion is significant on the time scale of the elution. However, because biological cells, including bacteria, exceed ~1 μm in diameter, their diffusion at temperatures compatible with cell viability is extremely weak and does not contribute significantly to FFF elution behavior; therefore it will not be treated here.

16.2.1 Sedimentation Force

F_{sed} is the sedimentation force $\frac{4}{3}\pi \cdot R^3\left(\rho_p - \rho_s\right)g$, where ρ_p and ρ_s are the densities of the particle and the DEP-FFF elutant medium, respectively, and g is the acceleration due to gravity. The cell density for a given particle is usually considered to be a fixed parameter, but alterations in suspension conditions such as osmolarity may impact it dynamically.

16.2.2 Dielectrophoretic Force

F_{DEP} arises from the dielectric response of a particle to an imposed inhomogeneous electric field [3, 4, 25]. The field induces electric polarization whereby equal and opposite charges build up on opposite sides of the particle to form an electric dipole. Because the electric field varies spatially, the field intensities on the opposing charges on either side of the particle are different, imposing coulombic forces that do not balance. The residual net force, called the dielectrophoretic force, acts on the particle even though it retains zero net charge. Because reversal of the field also causes reversal of the particle polarization, the DEP force direction is independent of the field sense. These properties of independence to net particle charge and field direction distinguish the dipolar DEP phenomenon from electrophoresis, its better known monopolar cousin. The buildup of charges in DEP is not spontaneous but depends on both particle dielectric and geometric characteristic and the medium [3, 4]. Particle DEP responses to fields of different frequencies may be used to infer the particle properties and to impose separation forces on different particle types.

Suitable inhomogeneous electric fields for DEP can be created by an array of phased electrodes and, depending on the configuration and excitation phases, the electric field pattern may move through space (a so-called traveling wave) or form a fixed field pattern [14, 24]. Although DEP forces for many field types have been explored, in FFF F_{DEP} is usually produced by a fixed electric field distribution created by energizing, in anti-phase, two interdigitated arrays of microelectrodes patterned all over the accumulation wall of the FFF chamber. Pethig's group was the first to

introduce microlithography for the fabrication of precise arrays in DEP [26]. When the electrode array consists of parallel plain microelectrode strips (Fig. 16.2a) of equal width and spacing s, the vertical component of the DEP force due to fringing fields above the electrode plane may be written (adapted from [23]) as

$$F_{DEP} = 2\pi\varepsilon_s\varepsilon_0 R^3 \cdot \mathrm{Re}[f_{CM}(f)] \cdot q(h) \cdot \left[P_{eff}(f) \cdot V\right]^2, \tag{16.2}$$

where $V$is the AC voltage of frequency $f$that energizes the microelectrode array to provide the electric field. V and f may be adjusted to program the DEP response. The geometric scaling function

$$q(h) = -\left(\frac{176}{d^3}\right).\exp\left(-\frac{4\pi h}{d}\right) \tag{16.3}$$

defines the height dependency of the intensity of the DEP field above the electrode plane (Adapted from [23]) and depends on the electrode periodicity, $d = 4s$ (Fig. 16.2a). $P_{eff}(f)$, which ideally approaches unity, defines the proportion of the applied excitation voltage that is effective in imposing a DEP force on particles within the eluate. As defined here, it accounts for frequency-dependent voltage drops caused not only by electrode polarization at the electrode-eluate interface [23] but also by electrode imperfections and stray impedance in the leads, buses and electrodes downstream of the voltage measurement point. Therefore, $P_{eff}(f)$ lumps together all the unknowns of the DEP configuration into a single parameter that can be readily determined experimentally from the DEP-FFF elution characteristics of standard particles such as

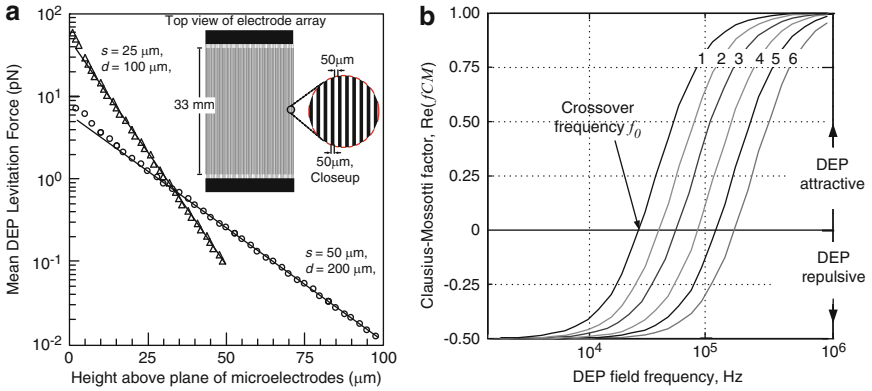

Fig. 16.2 (**a**) The maximum DEP force generated on particles as a function of height above the accumulation wall for microelectrode spacings of $s = 25$ μm and $s = 50$ μm. Inset: a 15 mm length of the microelectrode array showing a close-up of individual microelectrodes with $s = 50$ μm and $d = 200$ μm; (**b**) The frequency dependency of the Clausius-Mossotti factor at a suspension conductivity of 30 mS.m^{-1} according to the single-shell model for mammalian cells [9, 10]. Tumor cells typically respond as curves 1 & 2; granulocytes as curve 5; lymphocytes as curve 6

polystyrene beads (described in Sect. 16.3.1). It is the only calibration term needed to define the performance of a practical DEP-FFF instrument and, although it may alter over time, it can remain stable for many months of operation with good electrode care.

$\mathrm{Re}[f_{CM}(f)]$, the real part of the Clausius-Mossotti factor [3, 4], describes the frequency-dependent dielectric polarization properties of the particle of radius R within its eluate medium, which is assumed to have a dielectric permittivity $\varepsilon_s\varepsilon_0$. This factor for mammalian cells has been the subject of numerous papers [8–10, 14, 25]. If mammalian cells are suspended in a medium having a much lower conductivity than their cytoplasm and they have an intact membrane barrier function, then their dielectric responses are dominated by the membrane. Over the approximate frequency range 1 kHz $< f <$ 1 MHz, the real part of the Claussius-Mossotti factor can then be defined in terms of a single "crossover" frequency f_0 at which cells exhibit a null DEP response [8–10]:

$$\mathrm{Re}[f_{CM}(f)] = \frac{f^2 - {f_0}^2}{f^2 + 2\,{f_0}^2}. \tag{16.4}$$

Cells then exhibit three regimes of behavior:

1. When $f << f_0$, the polarizability of the cell is smaller than the suspending medium, $\mathrm{Re}[f_{CM}(f)]$ is negative and the DEP force is repulsive. The factor approaches –½ when $f << f_0$ and maximum DEP repulsion occurs.
2. When $f = f_0$, the effective polarizability of the cell matches that of the suspending medium, $\mathrm{Re}[f_{CM}(f)]$ equals zero and the DEP force vanishes. Cells undergoing DEP-FFF revert to conventional sedimentation FFF behavior at this frequency. (Note that the DEP force can also vanish over a wide range of frequencies for cell debris having an ineffective plasma membrane barrier.)
3. When $f >> f_0$, the cell polarizability exceeds that of the medium, $\mathrm{Re}[f_{CM}(f)]$ is positive and the DEP force is attractive towards the accumulation wall. The factor approaches +1 when $f >> f_0$, resulting in maximum steric interaction between cells and the accumulation wall in DEP-FFF.

16.2.3 Cell Suspension Conditions for Dielectrophoresis

Under physiological conditions, the conductivity of the cytoplasm of a mammalian cell exceeds 1 $\mathrm{S.m^{-1}}$ and has an osmolarity of ~300 mOs. So that the cell is suspended in a medium having a lower conductivity than this to allow attractive DEP forces to be applied, the eluate is usually chosen with a conductivity in the range 30–100 $\mathrm{mS.\,m^{-1}}$. An ionic solution with this conductivity has low osmolarity and the eluate is supplemented with a non-ionic osmolyte to avoid inflicting osmotic stress on the cells. This osmolyte is usually a cell membrane-impermeant sugar such as 9.5% sucrose or 5.1% mannitol. The requirement of using a low

conductivity eluate also demands that steps be taken to reduce the ionic conductivity of clinical specimens as they are interfaced to DEP-FFF fractionation. If cells are left in low conductivity eluate for > ~1,000 s, their DEP behavior alters because changes occur in their dielectric properties, probably as a result of ion leakage from the cytoplasm and non-ideal osmotic responses of the cell membrane towards the sugars. Therefore, DEP-FFF runs should be designed to be completed in <1,000 s.

16.2.4 Hydrodynamic Lift Force (HDLF)

In our early DEP-FFF studies, flow shear rates were kept low enough that HDLF was negligible compared with other applied forces. However, low flow rates result in slow elution times, low throughput, and long exposures of cells to low conductivity eluate. Therefore faster flow rates that introduce concomitant HDLF responses are now used. A body of work has considered HDLF effects and identified contributing factors including wall effects, particle rotation, and particle deformation [27, 28]. Importantly, FFF retention times of mammalian cells depend on cell shape and rigidity [29, 30], indicating that cell structural and mechanical properties may be accessible though FFF measurements.

The velocity profile for a flow of rate B through a channel of height H and width W is parabolic at low Reynolds numbers and the fluid at height h above the accumulation wall moves with a velocity v_f given by

$$v_f = \dot{v}_0 h\left(1 - \frac{h}{H}\right) \tag{16.5}$$

where $\dot{v}_0 = \frac{6v_0}{H}$ is the flow shear rate at the wall and $v_0 = B/(HW)$ is the mean fluid flow velocity. Abkarian and Viallat [31] and Mader et al. [32] showed that the lift force on deformable lipid vesicles, the most cell-like synthetic particles for which HDLF-shape correlations have been reported, depended on vesicle geometry according to the relationship

$$F_{HDL} = -\eta\dot{v}_0 \frac{R^3}{h} \cdot \Phi(V) \tag{16.6}$$

where η is the dynamic viscosity of the eluate and $\Phi(V)$ is a dimensionless geometry function ($0<\Phi(V)<1$). This function was found to increase for increasing deviations from vesicle sphericity with even a relatively small change resulting in a 30-fold variation in $\Phi(V)$. Both stable and shear-induced asphericity contributed to increases in $\Phi(V)$ [31, 32]. Membrane heterogeneity and linkages between the membrane, the sub-membrane matrix and the cytoskeleton imbue cells with a richer pallet of mechanical responses than lipid vesicles. It is therefore helpful to

recognize the mechanical contributions to HDLF of the cytoskeleton and plasma membrane, M_{cyt} and M_{mem}, explicitly, and express the force on mammalian cells as

$$F_{HDL} = -\eta \dot{v}_0 \frac{R^3}{h} \cdot \Phi\left(M_{cyt}, M_{mem}\right) \tag{16.7}$$

16.3 Characterizing Cell Properties by Batch DEP-FFF

The expressions for F_{sed}, F_{DEP} and F_{HDL} indicate that the DEP-FFF force balance condition depends on particle density ρ_p, radius R, crossover frequency f_0, and mechanical deformability, M_{cyt} & M_{mem}. Therefore, height differences of particles during DEP-FFF may be exploited to investigate these parameters or to achieve fractionation. Batch and continuous flow implementations of FFF may be used.

In batch FFF, an aliquot of particle mixture is loaded onto one end of the separation chamber and allowed to relax onto the accumulation wall without eluate flowing. Eluate flow is then initiated with the fractionation fields applied. Particles reach equilibrium heights according to their physical properties in the applied fields and are transported through the chamber at corresponding velocities. Different particle properties are thereby mapped into different elution times. Discrimination depends on the effective plate height, which can be increased up to some limit by lengthening the chamber. While the particles are in transit, the fields may be programmed allowing great flexibility for particle characterization experiments. Throughput of batch methods is limited by the allowable loading capacity for each batch and the time taken for the slowest particles to elute (see Sect. 16.3.6).

By undertaking batch DEP-FFF on multiple aliquots of the same cell mixture under different, carefully chosen field conditions, it is possible to deduce the profiles of the cell physical properties shown earlier to contribute to the forces [33]. Because the force balance expressions are highly non-linear, this can be achieved most readily by mapping the cell elution profiles to the cell parameter domains computationally. To determine the appropriate mappings, it is necessary to know the relationship between the velocity v_p at which a cell is carried in an FFF chamber and its height h above the accumulation wall in the hydrodynamic flow stream. A combination of torque, wall, and lateral forces modifies v_p from the eluate velocity v_f (Eq. 16.5) at the same height. Empirical equations derived from experimental data [27, 28] allow the particle velocity to be written as:

$$\frac{v_p}{R\dot{v}_0} = \frac{0.7431(1 + h/R)}{0.6376 - 0.2000\log(h/R)} \; for\; h<<R,\; and \tag{16.8a}$$

$$\frac{v_p}{R\dot{v}_0} = (1 + h/R)\left[1 - \frac{5}{16}\left(\frac{1}{(1 + h/R)}\right)^3\right] \text{ for } h>>R. \tag{16.8b}$$

Conveniently, the blended function

$$v_p(h) = R\dot{v}_0(1 + h/R)\ \min\left(\frac{0.7431}{0.6376 - 0.2000\log(h/R)}, 1 - \frac{5}{16}\left(\frac{1}{(1 + h/R)}\right)^3\right) \tag{16.8c}$$

transitions smoothly between the two cases and may be used for computational purposes [33].

16.3.1 Cell and Particle Density

As shown earlier, the Claussius-Mossotti factor approaches –½ when the applied electric field frequency is well below the cell crossover frequency f_0, leading to maximum DEP levitation above the accumulation wall. The levitation may be arranged to be so high that HDLF becomes negligible. For example, for a micro-electrode width and spacing $s = 50$ μm, an applied voltage $V = 3\ V_{p\text{-}p}$ at 15 kHz, a chamber height $H = 350$ μm, and using an eluate of 9.5% sucrose at a conductivity 30 $mS.m^{-1}$, the levitation height is in the range 20 μm $< h <$ 40 μm for most mammalian cell types. This is well above the height range for which HDLF is significant for mean flow velocities as long as $v_0 < 5$ $mm.s^{-1}$. Under these conditions, the force balance condition simplifies to $F_{sed} + F_{DEP} \approx 0$ and by substituting the expressions given earlier, and rearranging, we obtain

$$h = \frac{d}{4\pi}\ln\left(\frac{132 \cdot \varepsilon_s\varepsilon_0 \cdot \left[P_{eff}(f) \cdot V\right]^2}{(\rho_p - \rho_s)g \cdot d^3}\right) \text{ for } (f << f_0) \tag{16.9}$$

This is a variant of the expression used to describe DEP-FFF behavior in our early studies in which HDLF was neglected [22, 23] and it may be used in conjunction with Eq. 16.8c to allow particle transit times to be mapped directly to particle densities ρ_p. The only unknown in Eq. 16.9 is the calibration term $P_{eff}(f)$. Fortunately, polymer microbeads of different known densities are readily available and these have dielectric properties that satisfy Eq. 16.9 at all frequencies used for cell DEP-FFF. Therefore, $P_{eff}(f)$ may be measured and periodically checked using the elution times of one or more known bead types. After calibration, DEP-FFF elution profiles for cells may be mapped exactly to high resolution cell density profiles [33]. Figure 16.3a shows DEP-FFF elution profiles for blood and tumor cells mapped to density profiles in Figure 16.3c using calibration results for hollow glass beads of different, known densities that were prepared by isopycnic focusing on a sucrose stepwise density gradient.

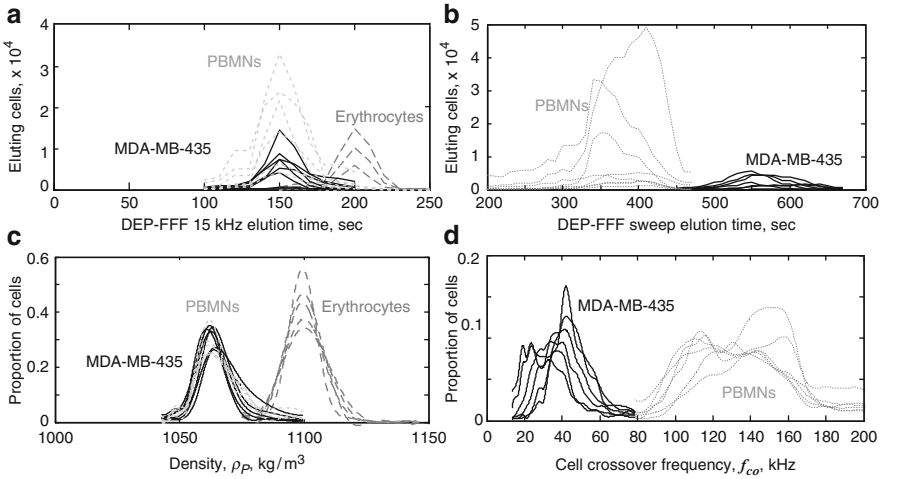

Fig. 16.3 DEP-FFF elution profiles for MDA-MB-435 breast cancer cells, PBMNs and erythrocytes for (**a**) 15 kHz applied frequency; (**b**) 200 kHz to 15 kHz logarithmic frequency sweep over 600 s. The profiles are mapped, using the methods described in the text, to derive the distributions of (**c**) cell densities and (**d**) DEP crossover frequencies for the cells

Because a typical cell DEP-FFF run under density measurement conditions is completed in less than 5 min, this method is faster and provides higher resolution than conventional centrifugation or sedimentation methods and can also be used for rapid, high resolution fractionation based on density. It is noteworthy that this method does not depend on dielectric properties that are unique to cells and it may be applied to characterize or fractionate any non-conductive particle type by density.

16.3.2 Cell Shape and Deformability

When the DEP force is zero, the force balance condition simplifies to $F_{sed}+F_{HDL}=0$ under flow conditions that are sufficiently fast for steric interactions between particles and the accumulation wall to be negligible, so that

$$\eta\dot{v}_0\frac{R^3}{h}\cdot\Phi\left(M_{cyt},M_{mem}\right)=\tfrac{4}{3}\pi R^3\left(\rho_p-\rho_s\right)g, \tag{16.10}$$

giving

$$\Phi\left(M_{cyt},M_{mem}\right)=\frac{2\pi H\left(\rho_p-\rho_s\right)g}{9v_0\eta}h. \tag{16.11}$$

To examine the form of dependency of $\Phi(M_{cyt}, M_{mem})$ on flow rate explicitly, the particle velocity can be approximated as being the same as the fluid velocity at the same height, to yield

$$v = \frac{27\eta}{\pi H^2(\rho_p - \rho_s)g} \cdot \Phi(M_{cyt}, M_{mem}) \cdot {v_0}^2 \; for \; h << H. \tag{16.12}$$

This shows that a plot of cell velocity v versus ${v_0}^2$ has intercept zero and slope $\frac{27\eta}{\pi H^2(\rho_p - \rho_s)g} \cdot \Phi(M_{cyt}, M_{mem})$.

More properly, the slope is computed by regression analysis of the cell elution times using Eq. 16.8c. It follows that conventional sedimentation FFF conducted as a function of eluate flow rate may be used to determine the ratio of cell mechanical properties to density $\frac{\Phi(M_{cyt}, M_{mem})}{(\rho_p - \rho_s)}$ for particles and cells.

ρ_p can be determined in the same apparatus as described in Sect. 16.3.1 though, unfortunately, ρ_p and $\Phi(M_{cyt}, M_{mem})$ cannot be determined *simultaneously* for each cell. Rather, from the precise distribution obtained for ρ_p, an estimate of the distribution of $\Phi(M_{cyt}, M_{mem})$ may be derived from the sedimentation FFF data. Nevertheless, in all cases examined, mammalian cells of a given type have a much narrower distribution of densities than of mechanical properties, making the derived distributions of $\Phi(M_{cyt}, M_{mem})$ reasonably accurate [33].

Most mammalian cells relax into a spherical shape following harvest and in this case $\Phi(M_{cyt}, M_{mem})$ can be expected to depend on cell deformability in the FFF shear field. However, if the cell shape under non-shear conditions is non-spherical, both shape and deformability characteristics need to be deduced from the dependency of $\Phi(M_{cyt}, M_{mem})$ on ${v_0}^2$. The non-zero intercept reveals the shape parameter under non-shear conditions and the slope gives the deformability response as before. Tong & Caldwell [30] showed that erythrocytes, which have discoid morphology under non-shear conditions, exhibited a significant increase in retention times following chemical fixation as a result of their reduced deformability under shear conditions in sedimentation FFF, a finding that is consistent with this analysis.

16.3.3 Cell DEP Crossover Frequency

To determine the profile of cell crossover frequencies f_0, the electric field frequency can be programmed to sweep downwards during a DEP-FFF run from f_{start} to f_{end}, where $f_{start} >> f_0$ and $f_{end} << f_0$ [33]. Initially DEP will attract cells strongly to the accumulation wall and impose large steric forces that will keep cell velocities close to zero. As the frequency sweeps downwards, DEP attraction will decrease until it reaches zero at $f = f_0$ and sedimentation FFF conditions prevail. Still further into

the sweep, cells will be levitated and finally approach the conditions used to determine cell density in Sect. 16.3.1.

Providing the cell velocity is negligible during the steric phase of the sweep and cells approach their maximum velocity soon after lift off from the accumulation wall then the elution time is dominated by two factors, namely the time at which the sweep reached $f = f_0$ and the maximum velocity determined by the cell density in Sect. 16.3.1. By using this concept together with the deformability properties determined in Sect. 16.3.2, reasonably accurate distributions for f_0 of cells may be computed. Examples calculated by computer analysis of 15 kHz elution profiles for density, no DEP profiles for HDLF, and sweep frequency DEP profiles results for distributions of crossover frequencies for human blood and cancer cells are shown in Fig. 16.3d. The mean f_0 results compare favorably with those obtained for similar cell types by direct DEP crossover frequency [34] and electrorotation [10] measurements performed one cell at a time.

16.3.4 Cell Membrane Capacitance

The crossover frequencies f_0 derived in Sect. 16.3.3 may be expressed in terms of the effective conductivities σ_s and σ_p and the electric permittivities ε_s and ε_p of the suspending medium and cells, respectively [35], as

$$f_o = \frac{1}{2\pi}\left\{\frac{(\sigma_s - \sigma_p)(\sigma_p + 2\sigma_s)}{(\varepsilon_p - \varepsilon_s)(\varepsilon_p + 2\varepsilon_s)}\right\}^{1/2}. \tag{16.13}$$

showing that cells have a crossover frequency as long as $\sigma_p < \sigma_s$ and $\varepsilon_p > \varepsilon_s$. The parameters ε_p and σ_p may be understood in terms of cell biophysical properties by applying a suitable dielectric model such as the single shell model [9] that is appropriate for most mammalian cell types. This model shows that

$$f_{co} \approx \frac{\sigma_s}{\pi\sqrt{2} \cdot RC_{mem}} \quad for\ \sigma_p << \sigma_s \tag{16.14}$$

where C_{mem} is the effective capacitance per unit area of the cell plasma membrane [10]. For *viable* mammalian cells, this approximation is usually valid as long as $\sigma_s >> 3\text{mS.m}^{-1}$.

Equation 16.14 shows that f_{co} depends linearly on the eluate conductivity σ_s. For practical purposes, it is useful to write the cell DEP properties in the form

$$\Lambda_{cell} = \frac{f_{co}}{\sigma_s} = \left(\pi\sqrt{2} \cdot RC_{mem}\right)^{-1}. \tag{16.15}$$

where Λ_{cell} is the *crossover frequency per unit conductivity* for the given cell type. The crossover frequency expected for the cell in an arbitrary eluate is then $f_{co} = \Lambda_{cell} \cdot \sigma_s$, allowing the required frequency setting to be calculated to obtain the desired DEP-FFF behavior in that eluate.

The total cell membrane capacitance of the cell is $C_{tot} = 4\pi R^2 \cdot C_{mem}$ and therefore the membrane capacitance per unit area and the cell total capacitance distributions for cell mixtures can be derived directly from the f_0 distributions obtained in Sect. 16.3.3. Unlike conventional electrophysiological determination of cell capacitance that demand insertion of microelectrodes and several minutes of measurements for each individual cell, DEP requires no cell contact and provides cell capacitance population profiles for up to 10^6 cells within 15 min.

16.3.5 Combined Computational Approach

If a series of sequential DEP-FFF experiments is conducted on aliquots of a cell mixture using DEP settings (1) $f << f_0$ (e.g. 15 kHz); (2) no DEP at 2 or 3 flow rates; and (3) a sweep $f_{start} \rightarrow f_{end}$, where $f_{start} >> f_0$ and $f_{end} << f_0$ (e.g. 200 kHz to 15 kHz); then the resulting elution profiles may be processed computationally using the concepts described above and taking into account the exact form of the forces [33], to yield (1) the exact distribution of cell densities; (2) an extremely good approximation for the distribution shape and of cell deformability properties; (3) a very good approximation for the distribution of cell membrane capacitance.

We have applied these methods to a number of different cell types, using an eluate of 9.5% sucrose and 30 m.Sm-1, s = 50 um, and chamber dimensions of L = 300 mm, W = 24 mm and H = 0.47 mm. Density measurements were conducted at f=15 kHz, V = 2.8Vp-p and a flow rate of 3 mL/min. FFF measurements used V = 0 and flow rates of 3, 6 and 9 ml.min-1. DEP-FFF sweep measurements used settings of V = 2.8Vp-p, f_{start} = 200 kHz, f_{end} = 15 kHz and a logarithmic sweep over 600 s at a flow rate of 3 mL/min.

Figure 16.4 shows a log-log plot of mean cell total capacitance C_{tot} versus mean cell radius R for 26 different cell types. Because C_{tot} reflects total plasma membrane area, this plot reveals the power law relationship between total membrane area and cell size. Conventional wisdom might dictate that the membrane area should vary with the square of the cell radius, as it does for a smooth sphere, so that that the slope of the plot should be 2. However, the cell total membrane area is found to depend on the cube of the cell radius (slope = 3). This suggests that mammalian cells develop as much surface area as is needed to exchange nutrients and metabolites between the cell interior and the extracellular space in accordance with a total metabolic exchange that occurs on a *per volume* basis. This result is reasonable if cell activity is not diffusion-limited, meaning that the extracellular space has an abundance of nutrients and can rapidly absorb the metabolic byproducts from the cell. This result in turn suggests that, in general, mammalian

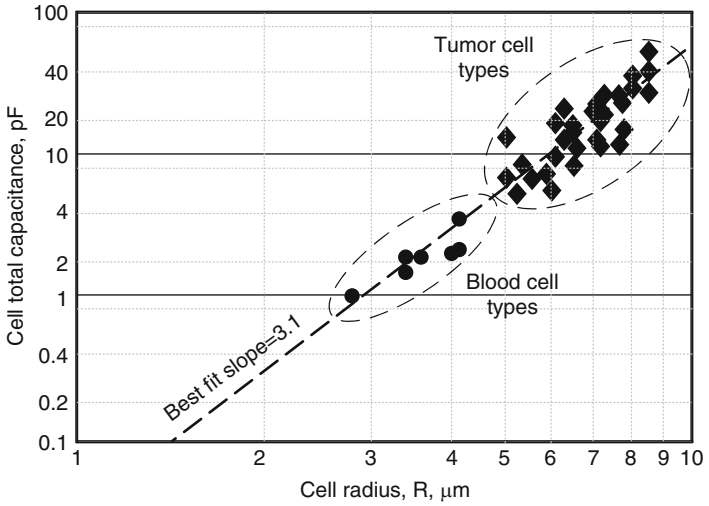

Fig. 16.4 Plot showing the relationship between cell total plasma membrane capacitance and cell radius derived for the major subpopulations of normal peripheral blood mononuclear cells (PBMNs) and for 26 different cultured tumor cell lines available from the American type culture collection of human breast, colon, ovary, liver and brain origin

cell size is not determined by ambient nutrient conditions, unlike single-celled organisms such as phytoplankton that exhibit nutrient-dependent size [36, 37].

This dependency of C_{tot} on R^3 has important implications for cell sorting applications. Circulating cancer cells are significantly larger than other cells in the peripheral blood and in addition their high glycolytic activity causes their membrane capacitance to be much higher than that of peripheral blood cells. DEP is able to exploit this biophysical characteristic to improve the discrimination between tumor and blood cells. An important upshot is that the DEP crossover frequencies for all tumor cell types we have measured are well below those of blood cells, allowing similar DEP settings to be used to isolate any type of CTC from blood by DEP-FFF (Fig. 16.4).

16.3.6 Batch DEP-FFF Loading and Throughput Capacity

It is important to note that the expressions given above to describe the DEP force on particles (Eq. 16.2) and to derive the Claussius-Mossotti factor for individual cells (Eq 16.4) are based on dipolar considerations only. Jones has analyzed the conditions under which dipolar assumptions are valid and finds that particles begin to experience dipole-dipole interactions that can affect their dielectric behavior when they are less than about 5 diameters apart [4]. It follows that to ensure ideal

operation according to the expressions given earlier, the loading concentration for DEP-FFF needs to be controlled to achieve adequate particle separation.

To compute the spacing of particles for a given injection concentration, it can be considered that they settle into a 2-D layer during relaxation. Acrivos et al. [38] have shown that high concentrations of particles in an electric field can undergo a dielectrically-induced phase change in which the particles accumulate into a separate phase from the suspending medium and we have shown that DEP-FFF becomes much less efficient as such concentrations are approached [39].

If, in a batch run, the front end of a DEP-FFF chamber of height H is filled with a particle concentration N m^{-3} then, after relaxation, the mean particle spacing at the accumulation wall is $D = (HC)^{-\frac{1}{2}}$. To achieve a spacing of at least 5 diameters, the maximum concentration of particles in the mixture is $N_{\max} = (25d^2H)^{-1}$, or $N \leq \sim 10^6$ particles of 10 μm diameter per mL. If the DEP-FFF chamber has a volume of 5 mL and the chamber load is 10% of its volume, then a maximum of 5×10^5 particles can be processed per batch to satisfy the spacing requirement. If the turnaround time per batch is 15 min then this sets the maximum throughput rate at around 2×10^6 particles per hour for batch mode operation under these conditions. This maximum loading capacity is not a problem for analytical applications but it is very low in most clinical situations. For example, it is at least 20 times lower than is needed for analysis of peripheral blood mononuclear cells (PBMNs).

16.4 Continuous Flow DEP-FFF

In continuous FFF implementations, differences in the heights above the accumulation wall at which different particle types arrive at the chamber outlet are exploited by skimming off the eluate laminae that contain the desired types. The first such implementation, developed by Giddings [40] and termed Split-Flow Lateral-Transport Thin (SPLITT) separation, injects the particle mixture at the top of the chamber at the inlet end. During transit, different particle types move downwards towards the chamber bottom at different rates under the influence of the applied fields. Particles are not required to reach equilibrium heights in SPLITT as long as they attain sufficient height differences to be skimmed off in different flow laminae at the exit end.

In continuous flow DEP-FFF, on the other hand, the particle mixture is injected slowly as a laminar flow through a slot at the bottom of the inlet end of the chamber while a much faster laminar flow of eluate is injected to join it from above. The two flows combine so that the particle mixture is confined to a very thin layer near the accumulation wall with eluate filling the chamber above it. Because the particles are injected, and remain, close to the accumulation wall as they flow through the chamber, they attain their equilibrium heights over the DEP electrode as described for batch operation within a few seconds of injection and prior to reaching the exit end of the chamber.

Fractionation is achieved by withdrawing fluid from a precision slot across the bottom of the exit end of the chamber. This skims off fluid containing particles up to a well-defined height above the accumulation wall. Particles that are traveling above that predefined height flow past the exit slot and leave the chamber through a downstream port along with the bulk of the flow. For fractionation to operate effectively in this scheme, the transit time through the DEP-FFF chamber must be long enough for the particles to attain their equilibrium heights before they reach the exit slot. Otherwise, the transit time is not important and particles may be injected and skimmed continuously, allowing huge samples to be processed given a long enough period of operation. The skimming process must be precise enough to split the flow to a consistent height across the separation chamber. Adjustment of the field parameters during such processing would change the particle types that would emerge through the exit slot, causing particles to be mixed up again. Therefore, field programming is not usually helpful for continuous DEP-FFF operation.

A continuous-flow DEP-FFF system based on a π-chamber design is shown in Fig. 16.5. Cell mixture is slowly injected at a flow rate B_{spec} into the bottom inlet slot and joins the faster eluate flow rate B_{eluate} from the top inlet. The proportion of the chamber height $\frac{h}{H}$ that is filled by specimen during this continuous injection process (see Fig. 16.5) can be found from

$$\frac{B_{spec}}{B_{eluate}} = \frac{3h^2}{H^2} - \frac{2h^3}{H^3}, \tag{16.16}$$

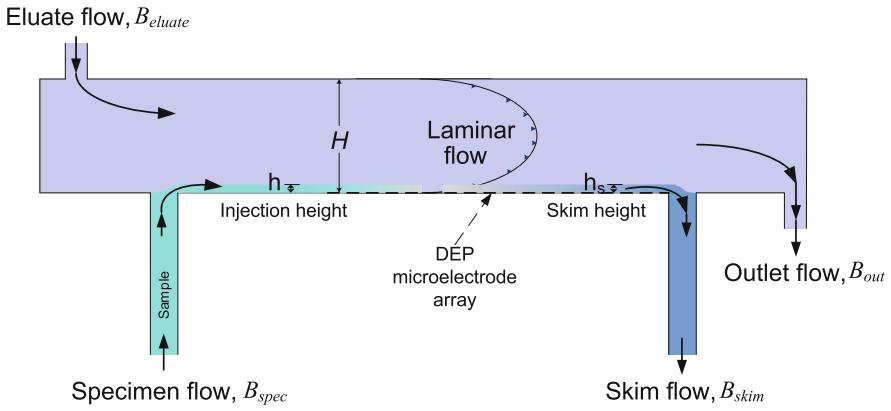

Fig. 16.5 A "π configuration" chamber for continuous-flow DEP-FFF processing of large batches of particle mixtures showing the port flows that determine the height above the accumulation wall to which sample is injected at the inlet and the height to which the collected fraction is skimmed at the outlet

showing that the height to which specimen fills the chamber is

$$h \approx H \cdot \sqrt{\frac{B_{spec}}{3F}} \; when \; \frac{h}{H} \text{ is small.} \tag{16.17}$$

An analogous expression describes the height h_s up to which fluid is skimmed by a flow rate B_{skim}through the first outlet slot. The cell population targeted by the continuous DEP-FFF method therefore depends on the DEP frequency and voltage and the specimen injection, skimming and eluate flow rates. For proper discrimination, the eluate flow rate needs to be small for the injected cells to reach equilibrium FFF heights before reaching the skimming port. Clearly, it is advisable to know the cell properties prior to running separation so that the DEP and flow conditions can be selected appropriately. This can be accomplished by using batch DEP-FFF to characterize small aliquots of cells prior to using the continuous method.

16.4.1 Continuous DEP-FFF Throughput Capacity

To assure that particle-particle dielectric interactions are negligible in continuous DEP-FFF, the same particle spacing criterion applies as was discussed in Sect. 16.3.6 for batch DEP-FFF operation. If, in a continuous run, the particle concentration is N m^{-3} and the particle suspension is injected up to a heigh h, then the mean particle spacing after settling towards the accumulation wall is $D = (hC)^{-\frac{1}{2}}$. For a particle mixture injection rate of 25 μL min^{-1}, an eluate flow rate of 1500 μL min^{-1}, and a chamber height H of 300 μm, Eq. 16.17 shows that the height of the chamber filled with particles h is 22 μm. For a particle spacing of at least 5 diameters to be achieved, the maximum concentration of particles in the mixture is $N_{\max} = (25d^2h)^{-1}$, or $N \leq \sim 4 \times 10^7$ particles of 10 μm diameter per mL. At the given particle injection rate, this corresponds to a throughput of 10^6 particles per minute, or 6×10^7 particles per hour. This is about 30 times faster than batch DEP-FFF and is sufficient for challenging cell sorting applications such as the isolation of circulating tumor cells from PBMNs.

16.4.2 Isolating Circulating Tumor Cells(CTCs) from Blood

The isolation of CTCs from the peripheral blood of cancer patients is considered to be of importance for the prognosis and treatment of breast, prostate, ovarian, colon, and other cancers [41–43]. The CTC concentrations in the peripheral blood of patients vary in relation to the stage of the disease but are always extremely low

compared with the background count of PBMNs. It has been concluded that a concentration above five CTCs per 7.5 mL of peripheral blood correlates to worsening outcome in breast cancer [44]. A number of methods exist for isolating CTCs from blood but most rely on the cell surface marker EpCAM that targets epithelial cells. Because not all cancers, even of the same type, express EpCAM, those methods are not universally applicable. Furthermore, to derive detailed information about the metastatic potential of CTCs, it is desirable to collect them in an intact and viable state to allow for complete morphological, phenotypic, cytokinetic and molecular characterization. Most methods cannot achieve this. As shown above in Fig. 16.4, the DEP characteristics of all tumor cell types examined so far allow them to be isolated from blood cells by DEP-FFF. Because DEP exploits the membrane capacitance of the tumor cells as an intrinsic property without the need for antibody or other labeling and maintains cell viability during sorting without the need to modify the cell, it appears to be an ideal tool for CTC recovery.

To isolate CTCs in the continuous flow implementation, 10 mL of blood is first subjected to centrifugation on a histopaque density gradient to remove erythrocytes. The supernanant layer of cells consisting of peripheral blood mononuclear cells (PBMNs) and rare CTCs is suspended in 1 mL of RPMI medium whose density has been adjusted to 1036 $kg.m^{-3}$ with iodixanol (Optiprep, Axis-Shield, Norway). This suspension is injected into the bottom inlet port of a continuous DEP-FFF chamber at a rate of 25 uL/min (see Fig. 16.5). Eluate consisting of 9.5% sucrose at 30 mS/m flows from the inlet to the outlet end of the chamber at a rate of 1 mL/min and meets the influx of cell suspension to form a laminar junction. Under these conditions, the blood cell suspension has the same density as the eluate and fills the bottom 40 um of the chamber while the eluate flows above it. Although the cell suspension flows over a DEP electrode from the moment it enters the chamber, the first 40 mm of the electrode is not energized. This is because the cell suspension has a physiological concentration of ions and a conductivity of ~1.4 S/m. As the suspension moves along the chamber floor, ions diffuse throughout the chamber height, bringing the conductivity to ~60 mS/m while the cells sediment to equilibrium heights based on the balance of sedimentation and HDLF alone. The next 40 mm of DEP electrode leading to the first skimming port is energized with a DEP signal of 95 kHz and 3.5 Vp-p. Once cells reach this region, the CTCs experience a positive DEP force because the applied signal is above their crossover frequency. This pulls the CTCs closer to the electrode but is not sufficient to overcome HDLF and they therefore move slowly towards the exit about 5 μm from the chamber floor. Conversely, the DEP frequency is well below the crossover frequency for PBMNs and these are levitated about 22 um above the chamber floor where they move rapidly towards the exit. Fluid is withdrawn through the skimmer port at 15 uL/min by a syringe pump and collected on a filter. The CTCs are thereby captured while the vast majority of PBMNs pass over the skimming port and are carried out of the far exit to waste.

16.5 Other Applications

The DEP-FFF principles and basic equations provided here apply to any particle mixture for which diffusion is negligible on the time scale of separation, namely particles of the order of 1 μm in diameter and larger. Such particles include many types of cells, bacteria, large organelles, cell nuclei, sedimentary particles and silts, minerals, ores, conductive versus nonconductive versus semiconducting particles, plastics, glasses, etc. For microparticles that are surrounded by a thin membrane, the single shell model described here is applicable together with the analytical methods presented for deriving particle physical parameters. In particular, living organisms normally depend on membrane barriers to control the flux of nutrients and metabolites and constrain the locality of biomolecules. Therefore DEP, which can be used to characterize and exploit the properties of membrane barriers, would appear to offer possibilities for as yet unknown applications in the life sciences also. For more complex particle types, a different form of dielectric model (e.g., multi-shell) might be applicable.

Diffusion considerations have not been included in the present analysis and normal mode FFF, which depends on diffusion, is not treated. This limits the applicability of the approaches described here to micro- and larger particles. DEP-FFF is certainly applicable to small particles including nanoparticles and molecules but these applications would require different approaches to apparatus and theory than are dealt with here.

References

1. Davis JM, Giddings JC (1986) Feasibility study of dielectrical field-flow fractionation. Separation Sci Tech 21:969–989
2. Giddings JC (1993) Field-flow fractionation: analysis of macromolecular, colloidal, and particulate materials. Science 260:1456–1465
3. Pohl HA (1978) Dielectrophoresis. Cambridge University Press, Cambridge
4. Jones TB (1995) Electromechanics of particles. Cambridge University Press, Cambridge
5. Clague DS, Wheeler EK (2001) Dielectrophoretic manipulation of macromolecules: the electric field. Phys Rev E Stat Nonlin Soft Matter Phys 64:026605
6. Wang X-B, Hughes MP, Huang Y, Becker FF, Gascoyne PRC (1995) Non-uniform spatial distributions of both the magnitude and phase of AC electric fields determine dielectrophoretic forces. Biochim Biophys Acta 1243:185–194
7. Wang X-B, Becker FF, Gascoyne PRC (1996) A theoretical method of electrical field analysis for dielectrophoretic electrode arrays using Greens theorem. J Phys D: Appl Phys 29:1649–1660
8. Wang XB, Huang Y, Gascoyne PRC, Becker FF, Holzel R, Pethig R (1994) Changes in Friend murine erythroleukaemia cell membranes during induced differentiation determined by electrorotation. Biochim Biophys Acta 1193:330–344
9. Irimajiri A, Hanai T, Inouye A (1979) A dielectric theory of "multi-stratified shell model" with its application to a lymphoma cell. J Theor Biol 78:251–269
10. Chan KL, Gascoyne PRC, Becker FF, Pethig R (1997) Electrorotation of liposomes: verification of dielectric multi-shell model for cells. Biochim Biophys Acta 1349:182–96

11. Fuhr G, Muller T, Schnelle T, Hagedorn R, Voigt A, Fiedler S, Arnold WM, Zimmermann U, Wagner B, Heuberger A (1994) Radiofrequency microtools for particle and live cell manipulation. Naturwissenschaften 81:528–535
12. Green NG, Morgan H, Milner JJ (1997) Manipulation and trapping of sub-micron bioparticles using dielectrophoresis. J Biochem Biophys Methods 35:89–102
13. Markx GH, Pethig R (1995) Dielectrophoretic separation of cells: continuous separation. Biotechnol Bioeng 45:337–343
14. Gascoyne PR, Vykoukal J (2002) Particle separation by dielectrophoresis. Electrophoresis 23(13):1973–83
15. Holmes D, Morgan H, Holmes D (2000) Cell positioning and sorting using dielectrophoresis. Eur Cell Mater 4(suppl 2):120–122
16. Medoro G, Guerrieri R, Manaresi N, Nastruzzi C, Gambari R (2007) Lab on a chip for live-cell manipulation. IEEE Design Test Comput 24:26–36
17. Pethig R, Menachery A, Heart E, Sanger RH, Smith PJS (2008) Dielectrophoretic assembly of insulinoma cells and fluorescent nanosensors into three-dimensional 'pseudo-islet' constructs. IET Nanobiotechn 2:31–38
18. Valero A, Braschler T, Demierre N, Renaud P (2010) A miniaturized continuous dielectrophoretic cell sorter and its applications. Biomicrofluidics 4:022807
19. Lewpiriyawong N, Yang C, Lam YC (2008) Dielectrophoretic manipulation of particles in a modified microfluidic H filter with multi-insulating blocks. Biomicrofluidics 2:034105
20. Becker FF, Wang XB, Huang Y, Pethig R, Vykoukal J, Gascoyne PRC (1995) Separation of human breast cancer cells from blood by differential dielectric affinity. Proc Natl Acad Sci USA 92(3):860–4
21. Gascoyne PRC, Wang X-B, Huang Y, Becker FF (1997) Dielectrophoretic separation of cancer cells from blood. IEEE Indus Appl Soc 33:670–678
22. Huang Y, Wang XB, Becker FF, Gascoyne PR (1997) Introducing dielectrophoresis as a new force field for field-flow fractionation. Biophys J 73:1118–29
23. Wang XB, Vykoukal J, Becker FF, Gascoyne PR (1998) Separation of polystyrene microbeads using dielectrophoretic/gravitational field-flow-fractionation. Biophys J 12:3846
24. Markx GH, Pethig R, Rousselet J (1997) Field-flow fractionation using non-uniform electric fields. J Liq Chromatogr Technol 20:2857
25. Pethig R (2010) Dielectrophoresis: status of the theory, technology, and applications. Biomicrofluidics 4:022811
26. Price JAR, Burt JPH, Pethig R (1988) Applications of a new optical technique for measuring the dielectrophoretic behaviour of microorganisms. Biochim Biophys Acta 964:221–230
27. Goldman AJ, Rox RG, Brenner H (1967) Slow viscous motion of a sphere parallel to a plane wall. II. Couette flow. Chem Eng Sci 22:653–660
28. Williams PS, Koch T, Giddings JC (1992) Characterization of near-wall hydrodynamic lift forces using sedimentation field-flow fractionation. Chem Eng Comm 111:121–147
29. Qing D, Schimpf ME (2002) Correction for particle – wall interactions in the separation of colloids by flow field-flow fractionation. Anal Chem 74:2478–2485
30. Tong X, Caldwell KDJ (1995) Separation and characterization of red blood cells with different membrane deformability using steric field-flow fractionation. Chromatogr B: Biomed Appl 674:39–47
31. Abkarian M, Viallat A (2005) Dynamics of vesicles under a bounded shear flow: role of the deformability. Biophys J 89:1055–1066
32. Mader MA, Vitkova V, Abkarian M, Viallat A, Podgorski T (2006) Dynamics of viscous vesicles in shear flow. Eur Phys J E Soft Matter 19:389–397
33. Gascoyne PRC (2009) Dielectrophoretic-field-flow fractionation analysis of dielectric, density and deformability characteristics of cells and particles. Anal Chem 81:8878–85
34. Vykoukal DM, Gascoyne PR, Vykoukal J (2009) Dielectric characterization of complete mononuclear and polymorphonuclear blood cell subpopulations for label-free discrimination. Integr Biol 1:477–484

35. Jones TB, Kallio GA (1979) Dielectrophoretic levitation of spheres and shells. J Electrostat 6:207–224
36. Kiørboe T (2008) A mechanistic approach to plankton ecology. Princeton University Press, Princeton
37. Irwin AJ, Finkel ZV, Schofield OME, Falkowski PG (2006) Scaling-up from nutrient physiology to the size-structure of phytoplankton communities. J Plankton Res 28:459–471
38. Kumar A, Qiu Z, Acrivos A, Khusid B, Jacqmin D (2004) Combined negative dielectrophoresis and phase separation in nondilute suspensions subject to a high-gradient ac electric field. Phys Rev E Stat Nonlin Soft Matter Phys 69:021402
39. Gascoyne PR, Noshari J, Anderson TJ, Becker FF (2009) Isolation of rare cells from cell mixtures by dielectrophoresis. Electrophoresis 30:1388–1398
40. Giddings JC (1985) A system based on split-flow lateral-transport thin (SPLITT) separation cells for rapid and continuous particle fractionation. Sep Sci Technol 20:749–768
41. Cristofanilli M (2005) The "microscopic" revolution in breast carcinoma. Cancer 103:877–880
42. Riethdorf S, Fritsche H, Muller V et al (2007) Detection of circulating tumor cells in peripheral blood of patients with metastatic breast cancer: a validation study of the Cell Search system. Clin Cancer Res 13:920–8
43. Apostolaki S, Perraki M, Pallis A, Bozionelou V, Agelaki S, Kanellou P, Kotsakis A et al (2007) Ann Oncol 18:851–858
44. Hayes DF, Cristofanilli M, Budd GT et al (2006) Circulating tumor cells at each follow-up time point during therapy of metastatic breast cancer patients predict progression-free and overall survival. Clin Cancer Res 12:4218–24

Chapter 17
Field-Flow Fractionation Coupled to Inductively Coupled Plasma-Mass Spectrometry (FFF-ICP-MS): Methodology and Application to Environmental Nanoparticle Research

Emily K. Lesher, Aimee R. Poda, Anthony J. Bednar, and James F. Ranville

Abstract Nanoparticles, particles less than 100 nm in diameter, play an important role in hydrobiogeochemical systems due to their high specific surface area and ability to bind metals. Particles in this size range, especially highly engineered nanoparticles, also often display unique characteristics (biocidal, optical, catalytic, etc.) that result from their size. For these reasons, there is often a need to characterize size dependent elemental concentrations in environmental and toxicity research. Since their inception, flow and sedimentation FFF methods have demonstrated the capacity to separate and size material in the nanometer size-range. Current and future nanoparticle research also requires quantitative information on nanoparticle concentration and composition. When hyphenated with a sensitive, selective elemental detector such as ICP-MS, metal distributions can be measured making FFF-ICP-MS a useful tool for characterizing both engineered and naturally occurring nanoparticles and their interactions with soluble species (trace metals). Quantitative FFF measurements of complex nanoparticle dispersions rely heavily on factors affecting separation and recovery – including flow rates, membrane material, and carrier composition – the latter also affecting ICP-MS performance. Recovery, even with an optimized system, is often less than 100% and can be size dependent. The interface between the FFF and the ICP-MS, methods for metals calibration, and a means of conceptualizing the sample-dependent detection limit is discussed. This chapter also highlights recent applications of FFF-ICP-MS to environmental

E.K. Lesher
Environmental Science and Engineering Division, Colorado School of Mines, Golden, CO, USA
e-mail: emily.lesher@gmail.com

A.R. Poda • A.J. Bednar
U.S. Army Corps of Engineers, Vicksburg, MS, USA

J.F. Ranville (✉)
Department of Chemistry and Geochemistry, Colorado School of Mines, Golden, CO, USA
e-mail: jranvill@mines.edu

S.K.R. Williams and K.D. Caldwell (eds.), *Field-Flow Fractionation in Biopolymer Analysis*, DOI 10.1007/978-3-7091-0154-4_17,

research, including characterization, stability, toxicity, adsorption, and metal transport studies.

Keywords Concentration and toxicity • Elemental composition of nanoparticles • engineered nanoparticles • Environmental health and safety (EHS) • Flow FFF • nanoecotoxicity • Nanometrology • Sample recovery • Sedimentation FFF • Single particle ICP-MS

17.1 Introduction

Although the study of finely dispersed matter (colloids) was first systematically investigated by Francesco Selmi in 1845, and colloid and polymer chemistry flourished throughout the twentieth (and twenty-first) century, two recent advances have truly redefined this field of study and have led to the development of "nanotechnology", a term first introduced in 1974 [1]. The first advance is the increased control over the synthesis of nanomaterials and the creation of structures having dimensions in the range of 10^{-9}–10^{-6} m. Only recently have we been able to carefully control characteristics such as size distribution, surface coatings, particle shape, and molecular self-assembly. The second advance lies in the improvement of our measurement tools, which allow us to better quantify and characterize nanomaterials. From the first use of the "ultramicroscope" to visualize nanoparticles (NP) smaller than the wavelength of light [2] to techniques that allow visualization of individual atoms [3], the field of nanometrology is a critical development.

Nanometrology is central to all aspects of nanotechnology. In the field of environmental health and safety (EHS) it has become particularly apparent that "complete" characterization of nanomaterials is key to interpreting the results of toxicological, human health, and environmental fate studies [4]. Often improper, or incomplete, characterization is cited as the weak link in the interpretation of the implications of the study [5].

The focus of this chapter is the use of field-flow fractionation (FFF) coupled to elemental analysis, most commonly inductively coupled plasma-mass spectrometry (ICP-MS) [6, 7] for the characterization of metal-containing nanomaterials. Metal-containing NPs form a particularly significant class, as their use in consumer products and industrial applications make them the fastest growing category of engineered NPs (ENPs). Several life cycle assessments conclude that metal bearing NP could enter aquatic systems at potentially harmful concentrations [8–13].

Many analytical techniques are available for nanometrology, only some of which can be successfully applied to nano-EHS studies [14]. Summaries of methods are given in Table 17.1. These methods differ in part by the properties measured: average size, size distribution (polydispersity), surface characteristics (zeta potential, etc.), shape, and chemical composition. Methods for assessing particle concentration and particle size distributions include: microscopy

Table 17.1 Comparison of different techniques for detecting and characterizing nanoparticles

Characterization techniques	Features	Applicability to environmental systems
Scanning and/or transmission electron microscopy	Visualization and semi-quantitative chemical analysis	Very useful for number distributions, can discriminate among particle shapes and types, laborious without automation, possible artifacts from high vacuum
Dynamic light scattering	Non intrusive, rapid and accurate measurement of particle size for monodispersed NPs	Generally unsuitable as it cannot discriminate among particle types, gives average size that is heavily biased to large particles
Filtration and/or centrifugation	Provides elemental size distribution when coupled to chemical analysis	Filtration is very widely used but data is often over-interpreted, incomplete passage of particles through filters bias results to larger size, centrifugation is procedurally difficult and has low resolution for size separation
UV-Vis and fluorescence spectroscopy	UV absorbance and fluorescence are widely used for size analysis of quantum dots and other semi-conductor NPs	Generally unsuitable as other species present in most natural waters interfere.
Field-flow fractionation	High resolution size separation with wide dynamic range, when coupled with specific detectors can provide size distributions of chemical properties	Very applicable for polydisperse, heterogeneous systems when coupled to ICP or TEM, generally requires sample pre-concentration and size pre-fractionation
Single particle ICP (SP-ICP)	Element specific particle sizing and counting	Very useful due to low detection limit, potential of ICP-AES to discriminate among particles

[15, 16], chromatography [17, 18], centrifugation [19], laser light scattering [20], filtration [21–23], and spectroscopy [24, 25]. Difficulties generally arise due to a lack of sensitivity for characterizing and quantifying particles at environmentally relevant concentrations (low μg/L) or in complex environmental matrices that may introduce polydisperse particle size distributions having heterogeneous compositions [26].

Electron microscopy (EM) and dynamic light scattering (DLS) are the most commonly applied methods, but have advantages and disadvantages [27]. EM gives the most direct information on the size distribution and shapes of the primary particles, however, agglomeration artifacts may be introduced by the sample preparation steps (drying, exposure to vacuum). In addition, organic coatings are not visible without staining, giving a smaller diameter compared to measurements of hydrodynamic diameter [28]. Broad distributions require some form of image analysis/particle counting to obtain quantitative data.

Dynamic Light Scattering (DLS) measures the particle hydrodynamic diameter, but limitations include: poor sensitivity at dilute concentrations, non-selective material detection, inability to distinguish mixtures or complex matrices and no capability to count particles to resolve the dominant size in multi-modal particle or aggregate size distributions. The presence of a small number of aggregates can skew the effective diameter toward a larger particle size distribution. DLS remains, nevertheless, a rapid technique to quickly determine average particle hydrodynamic diameter for a wide range of particle types.

A very new method, single particle ICP-MS (SP-ICP-MS), has been developed and applied for detecting and determining concentrations of silver nanoparticles [29]. While this method is in its infancy, it shows promise for detecting and sizing metallic nanoparticles at environmentally relevant concentrations (sub-ppb) [30].

Traditional FFF analysis, incorporating UV absorbance detection, is generally limited to particle concentrations in the mg/L level and lacks particle specificity. Furthermore, UV response is not a direct measure of particle mass concentration, but rather depends on particle size, shape, and optical characteristics. Use of the sensitive and selective ICP-MS lowers detection capabilities by approximately three orders of magnitude, into the microgram/L range [31], and provides indirect information on particle mass concentration. It is becoming clear that due to its elemental specificity, high size resolution, and low detection limit FFF-ICP-MS is a promising method for nano-EHS (Fig. 17.1).

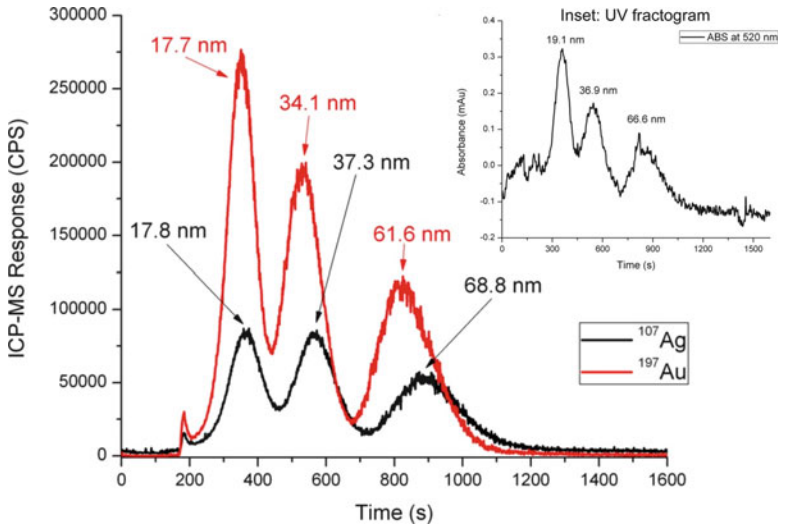

Fig. 17.1 Flow FFF fractograms of mixed nominal 10, 30, 60 nm Ag and Au NPs. Inset: UV absorbance fractogram of the mixture, showing no ability to discriminate between the Ag and Au NPs

17.2 FFF-ICP-MS Methodology

Effectively detecting, quantifying, and characterizing nanoparticles in environmental samples requires sufficient method sensitivity and selectivity, while avoiding the potential interference of natural particles, also frequently present in environmental samples. ICP-MS has become the premier method for low-level quantitation of metals in environmental matrices, with multi-element capability similar to that of ICP-atomic emission spectroscopy (ICP-AES), with the sensitivity equal to or greater than that of graphite furnace atomic absorption spectroscopy.

17.2.1 Particle Size Calibration

FFF theory is well developed for sizing of dispersed particles in simple matrices [32–34] using retention time, if the dimensions of the channel are measured. Furthermore, simple external calibration approaches can be applied if well-behaved size calibration standards are used. Often, FFF employs stable dispersions of National Institute of Standards and Technology (NIST)-traceable polystyrene (PS) bead standards. Unfortunately, ICP-MS detection of carbon is not possible. When external size calibration is needed, an in-line UV detector prior to the ICP-MS detector is a simple addition. As new reference nanomaterials become commonplace, PS bead standards can be supplemented or replaced with metallic nanoparticles. Currently NIST provides monodisperse gold nanoparticles, suitable for sizing at low μg/L Au levels. External size calibration requires stable particle dispersions and minimal membrane interactions. Depending on the nanoparticles to be separated, and their surface charges, a neutral or cationic surfactant may be needed, which might not be compatible with PS standards, thus requiring different size calibration standards. For example, PS standards are poorly separated in carrier fluid containing 0.01% CTAB, a cationic surfactant which was found to be best for the iron oxide NP under study [35]. In addition, the proper selection of the membrane will depend on particle properties as well as the solution matrices.

When using ICP-MS online detection, other considerations need be made with respect to carriers. For example the carrier can cause salt formation on the ICP-MS cones, leading to a decrease in ICP-MS signal intensity over time. Polyatomic interferences can be created in the plasma by carrier components. For example, use of chloride-based salts will result in polyatomic interferences on elements such as vanadium, chromium, arsenic, and selenium, among others. Therefore, optimization of FFF separation conditions must consider the impact on the ICP-MS detector. Use of carbon and nitrogen based carrier fluids (e.g. ammonium nitrate, sodium azide, and organic acids/surfactants) generally produce the least additional interferences, as these elements are present in the atmosphere.

17.2.2 Quantitative Analysis

Proper interfacing of ICP-MS to field-flow fractionation enables quantitative fractionation analysis. It is possible to couple FFF to ICP-MS due to the similarity of the FFF outlet flow rate (0.5–2.0 mL/min) and sample introduction rate of the ICP. However, serious challenges exist in accurately quantifying metal concentrations in FFF fractionated samples. Introduction of both internal and external calibration standards, and sample recovery need to be carefully considered.

Due to the nature of metal solubility, traditional ICP-MS internal standards are prepared in 1–5% acid solutions. Unfortunately, the introduction of a dissolved metal standard into a near neutral pH FFF mobile phase can result in precipitation of analytes resulting in inaccurate metal quantification of fractionated samples. While numerous studies do not use internal standards, an alternative is to use split flows that allow the introduction of acidified internal standards directly to the ICP nebulizer after elution from the FFF channel. Internal standards have also been mixed directly into the carrier fluid and simultaneously used for external calibration by comparison of elemental response factors to the internal standard [36, 37].

Methods for converting metal intensities to concentrations/masses were presented in a recent review by Dubascoux and coauthors [38]. In brief, there are two commonly used methods for external calibration: (1) injecting a known mass of metal, and comparing the area of the known mass to the area of the sample elution peak, and (2) analyzing a continuous flow (usually delivered by flow rate-matched peristaltic pump) of known concentrations of metal, developing a calibration curve, and then converting each fractogram intensity reading to a concentration.

Quantitative applications of the FFF-ICP-MS coupling are often complicated by recovery issues. When reported, the ratio between recovered mass after analysis and injected mass is often well below 100%. Analyte loss within the FFF channel can be attributed to several mechanisms. Membrane ‘stickiness’ is generally recognized as a major analyte sink, arising from physical interaction with the membrane surface, as well as ionic sorption mechanisms. In addition, losses through the accumulation wall based on membrane cut off values are noted for samples containing dissolved and macromolecular constituents. Analyte loss can also occur in the sample tubing and ICP-MS nebulizer and spray chamber. Typically these losses are relatively small in comparison to those due to membrane interactions.

Quantitative analyte recovery experiments performed by Poda et al. examined the loss of silver NPs in the system. [31]. Recoveries of the three silver nanoparticle sizes tested (10, 40, and 70 nm) at different concentrations are illustrated in Fig. 17.2, which with the cross flow field on, cross flow field off, and bypassing the FFF entirely, yielded recoveries of 88–98% based on integrated peak areas.

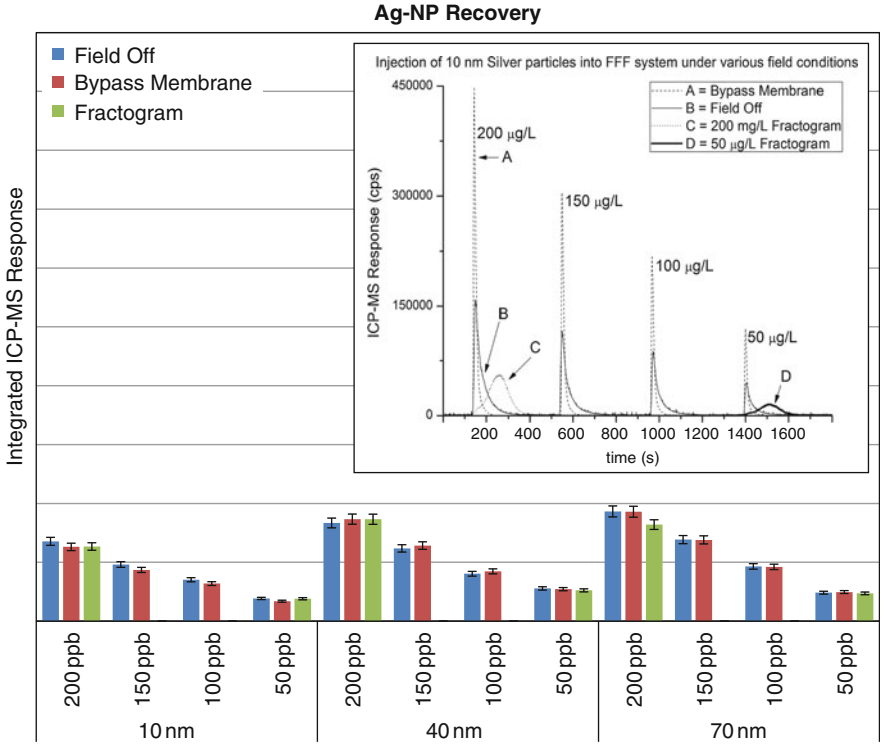

Fig. 17.2 Measurement of the recovery of 10 nm Ag NPs by integrating Ag response in field off, bypassing the membrane, and fractionated flow FFF fractograms. Masses are generally within 5% of each other, as represented by the bars. Inset: fractograms; response as a function of time

17.2.3 Detection Limit

Traditional ICP-MS analysis generally has instrumental detection limits for dissolved metals in the range of 1–100 ng/L, depending on the specific metal and the abundance of the isotope measured. However, in FFF applications, the mass of metal nanoparticles being detected is distributed over a size range, which is diluted as the mass is spread out over the effluent volume. Spreading is a function of sample polydispersity, non-ideal membrane interactions, and band broadening. Thus, the detection limit is more appropriately conceptualized as a mass, where as shown in Fig. 17.3a, the mass-based detection limit (mDL) is the product of the instrument detection limit and the peak width. This example shows the uranium elution profile during measurement of U binding to monodisperse nano-hematite (data presented in [39]), along with fractograms mathematically scaled down by factors of 2 and 10. The test of significance is the comparison of the area (mass) under the elution peak with the area (mass) defined by the mDL. While there are no outstanding rules on

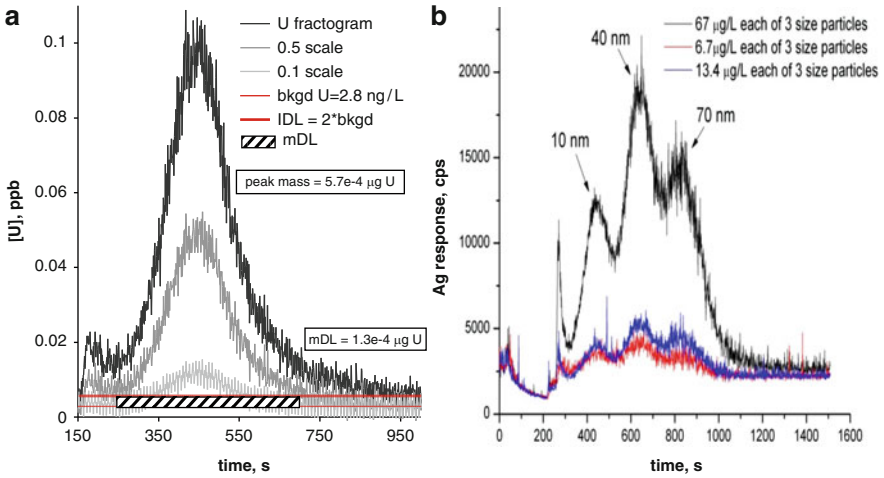

Fig. 17.3 Effect of polydispersity on detection limit for FFF-ICP-MS methods. (**a**) Uranium fractogram at 1, 0.5 and 0.1 scale in relation to the mass-based detection limit (mDL), which is the product of the instrument detection limit (IDL) and peak width. (**b**) Serial dilutions of a mixture of 10, 40, and 70 nm Ag NPs

significance, it is clear in the figure that the 0.1 scale fractogram is roughly the same area of the mDL and the mass of U would not be accurately quantifiable. In mixtures the effect of polydispersity is more drastic. Figure 17.3b depicts serial dilutions of a mixture of three sizes of silver NPs (Ag NPs) [31]. While, for example, 20.1 µg/L of only the 40 nm particles would have provided a quantifiable peak, the mixture of 6.7 µg/L (20.1 µg/L total) of 10, 40, and 70 nm particles results in a fractogram that is only slightly above background.

Finally, the multi-element capability of ICP-MS further enhances the utility of FFF determinations of nanoparticles when investigating multicomponent or mixtures of materials, as was discussed in relation to Fig. 17.1. Metal salt semiconductors, such as cadmium selenide quantum dots represent an excellent test case. Dissolution of the cadmium selenide core is inhibited by addition of an outer shell of zinc sulfide or similar material. Traditional ICP-MS technology can easily detect these metals, with the exception of sulfur, thereby allowing size-dependent dissolution or aggregation of these particles to be studied.

17.3 Applications: Characterizing Nanoparticles with FFF-ICP-MS

Despite intense interest in using FFF with elemental detection, especially ICP-MS, to characterize ENPs, there are still few published reports of its application. The number is sure to rise quickly in the next few years as many research groups are

investing in the technology and testing its applicability for studies into nanoparticle stability (aggregation, dissolution, persistence of coatings) in general and during toxicity, transport, and exposure tests. As noted in the Dubascoux et al. review [38], perhaps the earliest application of the method to engineered nanoparticles was reported in 2002 by Siripinyanond and Barnes [40]. The samples were alumina and silica particles used for polishing integrated circuit chips. Diameters of the particles ranged from 28 to 680 nm. Also reviewed by Dubascoux et al. was a size and elemental characterization of Cd-Se/Zn-S quantum dots by Bouby and co-authors [41].

Four more papers reporting characterizations of engineered nanoparticles using FFF-ICP-MS, and an additional three using FFF with off-line elemental analysis have been published since the Dubascoux review. A summary of all of these, plus recent papers characterizing natural nanoparticles (NNP) and colloids with FFF-ICP-MS can be found in Table 17.2, and are described below. When comparing studies, it should be noted that recovery and detection limit are defined and measured differently by different authors, and are not always directly comparable.

17.3.1 Engineered NP – FFF with Offline Elemental Detection

Although the primary focus of this review is online coupling of FFF with ICP-MS, two recent papers present FFF separations with offline ICP-AES analysis, which could be applied on-line [42]; moreover Contado and Pagnoni describe that as a goal of their FFF optimizations for the separation of TiO_2 nanoparticles [43]. Despite the superior detection limit for most metals by ICP-MS, ICP-AES may have an advantage in that there may be fewer interferences, all isotopes contribute to the emission, and the fact that there are no cones or vacuum interface that could be affected by carrier fluid constituents.

Contado and Pagnoni presented the first detection, separation, and quantification of TiO_2 NP by FFF, by analyzing TiO_2 from two commercial powders and a sunblock [43]. The recovery of the extraction procedure, up to 21% depending on sonication conditions, was measured by comparison to acid digested Ti concentrations. FFF sizing results were compared to SEM imaging, with good agreement. Ti concentration in the elution fractions is compared against the UV fractogram, with good agreement and recoveries of 85–107%. Fractograms and results are given for a variety of flow parameters, and the discussion traces their optimization of FFF operating parameters to achieve good resolution and recovery. This discussion is often omitted, making this paper useful for a new FFF user.

In a newer paper, Contado and Pagnoni revisit TiO_2 particles by measuring six different TiO_2-bearing cosmetics with Sd FFF and symmetrical flow FFF and offline ICP-AES [44]. An important outcome is the extraction and identification of the TiO_2 particles, which are mostly in the micro- size range as opposed to nano-, and the recognition of the variation in particle shape and size distribution between samples. In some of the Sd FFF fractograms, there is a very good overlap between

Table 17.2 Summary of reviewed papers employing FFF with elemental detection

Study/Ref #	Type of samples	Type of FFF, model	Elemental detector	Elements analyzed	Approx. size range, nm	Detail codes[a]
Contado and Pagnoni 2008, [43]	TiO_2 NP	Sy F-1000 PN	PE Optima 3100 XL, offline ICP-AES	Ti	20–500	2, 3, 7, 9
Contado and Pagnoni 2010, [44]	TiO_2 NP	Sy F-1000 PN	PE Optima 3100 XL, offline ICP-AES	Ti	5–500	2
Contado and Pagnoni 2010, [44]	TiO_2 NP	sedimentation S-101, PN	PE Optima 3100 XL, offline ICP-AES	Ti, Fe, Bi, Zn	50–500	2
Songsilawat et al. 2011, [45]	Ag NPs	Sy PN-1201-FO, PN	PE Model A Analyst 100, off-line electro-thermal AAS	Ag	5–90	2, 3,
Poda et al. 2010, [31]	Ag NPs	Sy F-1000, PN	PE Elan DRC II	Ag	10–100	2, 3, 7, 8
Pace et al. 2010, [28]	CdSe/ZnS quantum dots	Sy F-1000, PN	PE Elan 6100	Cd, Se, Zn	7–80	1, 2, 3, 4, 6
Schmidt et al. 2009, [50]	Biopolymer composite w/synthetic nano-clay	As Eclipse 3, Wyatt	Agilent 7500ce	Mg, Zr	50–800	1, 2, 3
Lesher et al. 2009, [39]	Synthesized nano-hematite	Sy flow F-1000, PN	PE Elan 6100	U, Fe	10–160	1, 2, 3, 4, 6, 8, 9
Trenfield et al. 2011, [51]	Bog OM isolates	Sy F-1000, PN	PE Elan 6100	U	0.5–5	1, 2, 3, 4, 5, 6
Claveranne-Lamoiere et al. 2009, [53]	Soil leachates	As Eclipse 3, Wyatt	Agilent 7500ce	Fe, Al, Ca, Mg, Mn, U	1–450	1, 2, 3, 4, 6, 7
Huang et al. 2011, [37]	Dissolution and recrystallization products from Be ore dust	As AF2000, PN	Agilent 7500ce	Be, Si, Al	3–450	1, 2, 3, 4, 5, 6, 7, 9
Worms et al. 2010, [55]	WWTP OM and effluent impacted lake water	As AF2000, PN	No ICP-MS detection	n/a	1–456 kDa	2, 3

Worms et al. 2010, [55]	WWTP OM and effluent impacted lake water	As Eclipse 3, Wyatt	Agilent 7500ce	Pb, Cd, Ag, Zn, Cu, Fe, MN, Cr, Al	1–100	4
Bolea et al. 2010, [56]	Compost leachate	As AF2000, PN (normal and steric modes)	PE Elan DRC-e	many	1–17	1, 2, 3, 5, 7, 10
Laborda et al. 2011, [57]	Compost leachates	As AF2000, PN	PE Elan DRC-e	Cu, Pb	<5 kDa-115 nm	1, 2, 3, 7, 10
Diaz et al. 2009, [36]	Lake water	As, PN	Agilent 7500ce	many	0.9–250	2, 3, 4, 5, 6
Plathe et al. 2010, [58]	Stream waters and sediments	As 2000 Focus, PN	Thermo ELEMENT 2	many	20–500	1, 2, 3, 4, 5, 6, 7, 10
Stolpe et al. 2010, [60]	Stream, estuary, and seawater	Sy F-1000, PN	Thermo ELEMENT 2	Fe, P, Mn, Cu, Zn, Pb, U	0.5–40	2, 3, 4
Gelting et al. 2009, [66]	Seawater	Sy F-1000, PN	n/s	Fe	2–40	2
Krachler et al. 2010, [67]	Peat bog water	As AF2000, PN	PE Elan 6100	Fe	0.1–100 kDa	2, 3, 4, 7
Stolpe and Hassellov, 2010, [68]	Seawater	As AF 2000 Focus, PN	Thermo ELEMENT 2	Fe, Cu, Ag, La, Pb	0.5–40	2, 3, 4, 6, 9

PE Perkin Elmer, *PN* Postnova, *Sy* Symmetrical FFF, *As* Asymmetrical FFF, *n/s* not specified in paper, *n/a* not applicable

[a]Details codes column. Each numeral indicates that the paper has carried out a quantification and/or includes a discussion of the step: 1 indicates details provided on interface setup, 2 indicates that size was determined, 3 indicates details provided on how size was determined, 4 indicates that metals were calibrated, 5 indicates that an internal standard was used for calibration, 6 indicates details provided on how calibrations were carried out, 7 indicates information provided on recovery, 8 indicates discussion provided on detection limit, 9 indicates discussion of potential artifacts/problems, 10 indicates details of optimization of carrier fluid and/or membrane and/or flow rates and/or ICP-MS presented

the UV and Ti signals. However, two samples displayed a strong Ti peak at 45 min while the UV showed a much earlier peak followed by a slow decline. Particles with diameter ~300 nm are visible in the SEM and likely created the Ti peak. No explanation of the lack of UV absorbance is given; it is perhaps a result of varying UV absorbance characteristics with size and shape.

Silver nanoparticles (Ag NPs) are predicted by life cycle assessments to be one of the most likely engineered nanomaterials to enter the environment at concentrations capable of causing environmental effects [8, 9, 11]. Songsilawat et al. studied the effect of different coatings and the presence of humic acid on the stability of Ag NPs [45]. The Ag NPs were separated by flow FFF and silver content measured by electrothermal atomic absorption spectrometry (ETAAS). Citrate-stabilized Ag NPs aggregated quickly in environmental waters (tap, ground, and seawaters), however 200 mg/L humic acid reduced aggregation. Alginate and pectin coated Ag NPs were less susceptible to aggregation. The study was an excellent demonstration of the applicability of FFF for aggregation studies.

17.3.2 Engineered NP – Online FFF-ICP-MS

A recent study on Ag NPs by Poda et al. [31] makes FFF-UV more powerful by adding the elemental discrimination of ICP-MS. The authors achieved excellent separation and sizing of monodisperse Ag NPs down to concentrations of 6.7 μg/L with 88–98% recovery. The optimized method was then employed to characterize the Ag NPs extracted from worms (*Lumbriculus variegates*) that had been exposed to Ag NP spiked sediments. When solid matrices are involved, extraction and preservation of the physicochemical form of particles can be quite challenging. Analysis of total metals, for example, often involves digestion of the matrix with concentrated acids, which can produce a liquid solution for metals analysis, but will have little similarity to the original form in the starting material. To preserve the physicochemical form of any nanoparticle, a less aggressive method of extraction must be used. Only a few methods of particle extraction from tissue have been previously proposed [46]. The Ag NPs were liberated from worm tissue by sonication using deionized water, but extraction efficiency was not reported. FFF-ICP-MS of the original Ag NPs and the extractant showed an increase in diameter from 31 to 46 nm.

Nanoecotoxicity is a growing field, and one that would benefit from greater characterization of engineered nanoparticles. There have been persistent calls for better characterization of the ENPs studied in toxicity tests [47, 48] because the particles are not standardized and are likely to change in size, aggregation state, and coating integrity upon introduction to an organism (as shown in the Poda et al. study [31]). Even before introduction, the character of the ENP may not be exactly as is represented by the manufacturer. This is demonstrated by Pace et al. [28]. In this study four types of Cd-Se/Zn-S quantum dots (QD, two core sizes and two types of coatings: mercaptoundecanoic acid, MUA, and polyethylene oxide, PEO) were

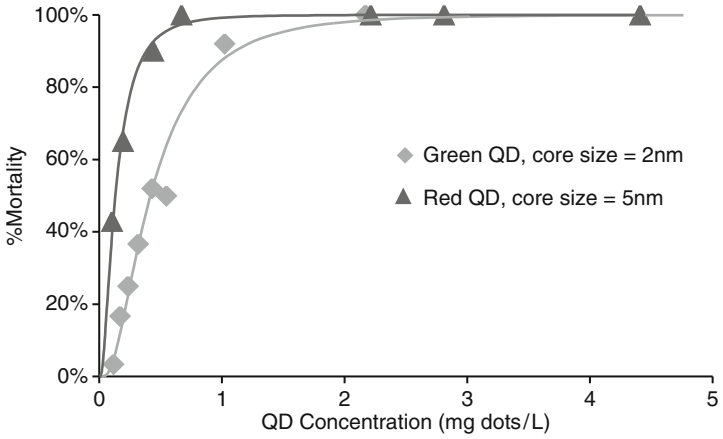

Fig. 17.4 Dose–response curves for *D. magna* exposed to two different-sized, MUA-coated quantum dots. The larger (5 nm core size) quantum dot showed greater toxicity than the smaller (2 nm core size) quantum dot on a mass concentration basis (Used with permission from [28], © 2010 American Chemical Society)

dosed to *Daphnia magna*. A finding of the study was that for the MUA coated QDs, the larger QD demonstrated higher toxicity than the smaller QD (Fig. 17.4), a result that is contradictory to the general sense that smaller NPs have great effects on organisms. FFF has been used previously to size [49], and with ICP-MS, to quantify metals [41] in QD, but this is perhaps the first application to interpretation of toxicity results. The authors found that the MUA coated QD had a much greater Cd:Se ratio than the 1:1 M ratio expected (7:1 and 9:1 for green and red, respectively), and importantly, that the excess Cd was integral to the QD, not a dissolved or particulate impurity, as shown in the FFF fractogram in Fig. 17.5. The MUA coated dots were significantly more toxic than the PEO coated QD, presumably due to the greater quantity of Cd released to solution over the 48 h toxicity test, as shown in Fig. 17.4, inset. The authors hypothesize that the excess Cd is retained in the MUA polymer coating during synthesis and is more readily released to solution than Cd in the QD core.

Schmidt et al. examined an engineered nanoclay, which when added at a 1:20 ratio, strengthens a biopolymer material (polylactide, PLA) that has been proposed as a green alternative to petroleum-based plastics for food packaging [50]. The nanomaterial is Cloisite30B, a derivatized montmorillonite clay sold commercially. The experiment contacted the 95% PLA/5% Cloisite30B with ethanol, representing a food substance, and then looked for NP in the ethanol. The authors also replicated the experiment in controls: 100% PLA + ethanol, 100% Cloisite30B + ethanol, and ethanol alone. The ethanol extracts were then analyzed by asymmetrical flow FFF with multi-angle light scattering (MALS) and ICP-MS detection. Particles were sized by MALS, and Zr and Mg were chosen as signatures of the Cloisite30B. MALS indicated that particles do leave the packaging material, but the particles did

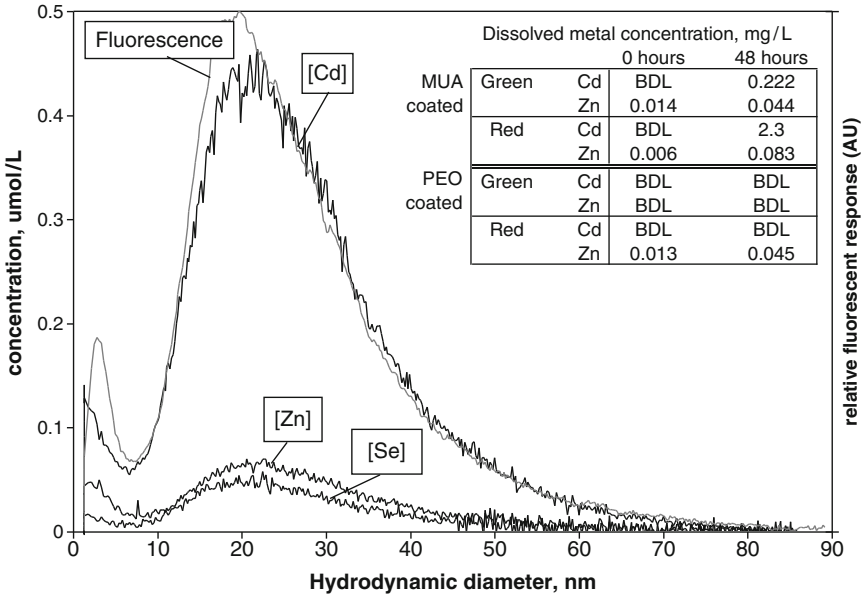

Fig. 17.5 Metals and fluorescence fractograms for red MUA-coated quantum dots (core size = 5 nm). Inset: Dissolution data for 48 h exposure of QD in hard water. The red MUA QD released 34% of the total Cd content, but without a shift in the fluorescence peak. FFF-ICP-MS confirmed that excess Cd is associated with the QD, leading to the hypothesis that there is also Cd associated with the MUA coating (Used with permission from [28], © 2010 American Chemical Society)

not include Zr or Mg in the PLA, or PLA + Cloisite30B experiments. Nanoparticles containing Zr and Mg were only released during the 100% Cloisite30B test, indicating that the nanocomposite does not release NP to food.

A final study on "engineered" nanoparticles examined iron oxides [39]. In this study, Lesher et al. attempted to determine the degree to which quantitative adsorption measurements can be made using FFF-ICP-MS. Samples with variable pH and containing constant concentrations of hematite and uranium were created, and symmetrical flow FFF-ICP-MS was used to measure the mass of U associated with the mass of Fe. These results allowed for calculation of the percent U sorbed at each pH. The FFF method was compared against a combination of centrifugation, filtration, and total analysis of the filtrate, assumed to contain only the truly dissolved U. A sorption edge was created with the results; the two methods showed relatively good agreement, as shown in Fig. 17.6a. The authors note that while there are a great number of outstanding papers studying metal speciation and phase distribution on natural samples, FFF-ICP-MS still needs to be vetted in more controlled laboratory studies before it may be accepted as the preeminent tool for measuring metal speciation in complex, natural samples.

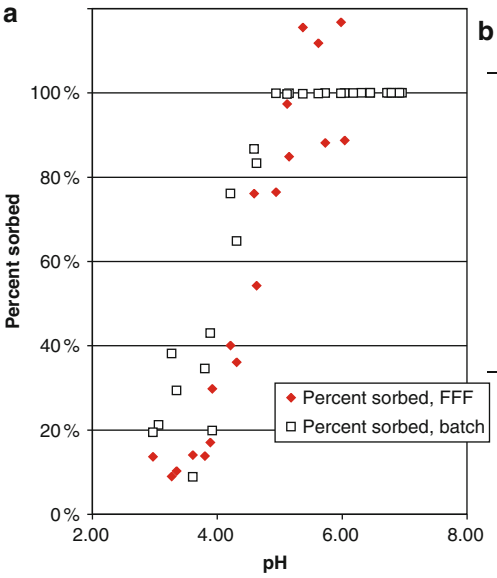

b

U (µg L^{-1})	U-DOC complex	
	HARPHRQ	FFF-ICPMS
	%	%
89	8.1	12
957	3.5	3
1900	2.5	1.7

Fig. 17.6 Comparison of FFF-ICP-MS measurements of U complexation against alternate techniques. (**a**) comparison of the sorption edge of U in the presence of nanoparticulate hematite measured by FFF-ICP-MS vs. centrifugation and filtration (Lesher et al. [39], used with permission). (**b**) comparison of computed (HARPHRQ computer code) vs FFF-ICP-MS measured complexation of U with Billabong fulvic acid (Used with permission from [51], © 2011 American Chemical Society)

17.3.3 Natural NP- Online FFF-ICP-MS

In another paper looking for insights on U speciation, but in the context of a toxicity study, Trenfield et al. used symmetrical flow FFF-ICP-MS to measure U complexation with a natural fulvic acid isolated via XAD-8 resin from Sandy Billabong, Australia (SBFA) [51]. The results indicated that little of the U was actually present as the U-SBFA complex. Potentiometric titrations showed that SBFA had weaker binding sites (dissociated acidic groups) compared to a standard fulvic acid, and would therefore not bind U as effectively. Accordingly, an adjusted binding constant was derived from the titrations and used in speciation modeling. The modeled concentration and FFF-ICP-MS measured concentration of U-SBFA complex were within 4% (Fig. 17.6b). Furthermore, in associated U aquatic toxicity tests, less protection was observed than expected for a "typical" DOC [52].

Claveranne-Lamolère et al. used two asymmetrical flow FFF-ICP-MS protocols to characterize rendosol (a French soil type characterized as rich organic material overlaying limestone) leachates for their capability of transporting uranium [53]. The methodologies employed, including the different protocols for low and high MW ranges, are based on the work by Dubascoux et al. [54]. The work identified

two colloidal populations. The first was lower molecular weight (1,500 ± 300 Da, confirmed by SEC), high in organic carbon, associated with some Fe, Al, and was likely composed of humic substances. The authors gave a 60% recovery on this fraction, but that value was based on recovery of PSS beads, not the sample itself. The second population was inorganic with no UV absorbance, but a strong MALS signal. These particles ranged from 30 to 450 nm diameter, and 97% were recovered. These colloids were characterized by a strong Ca signal, and 40% of the carbon is inorganic, therefore the colloids were likely to be composed of calcite, perhaps coated with humic substances. Only 1% of the total U was equally distributed between the two colloidal populations.

Another study seeking toxicological perspective on NNPs used asymmetrical flow FFF-ICP-MS to examine the dissolution and recrystallization of beryllium containing microparticles in an effort to explain statistically different rates of chronic beryllium disease among workers at four Be processing plants [37]. Huang et al. hypothesized that it was the differences in properties among the various facilities' source ore materials (BeO versus bertandite and beryl) that caused differences in rates of disease. The authors examined the behavior of the different Be-containing source materials in synthetic lung fluid (SLF). This is perhaps the first direct application of FFF-ICP-MS to a human health study. The authors found that BeO contact with SLF resulted in fewer nanoparticles, and a greater amount of truly dissolved Be, perhaps suggesting a mechanism of disease. Recovery was quantified at two points in the analysis to differentiate between recovery of particles in the FFF, and recovery during ICP-MS. Loss during the FFF fractionation is mostly low, ranging from 0% to 50%, but loss due to ICP inefficiencies (nebulization, particle ablation and ionization) is high, 70–95%. The effluent was not acidified prior to entering the spray chamber. The low recovery on the ICP-MS cast doubts on the size distributions because size itself may be a variable affecting efficiency. Nevertheless, the paper is an important benchmark in the use of FFF-ICP-MS for human health applications. Furthermore, their efforts to measure recoveries could lead to approaches for quantifying recovery.

A study on wastewater treatment plant (WWTP) colloidal organic matter (COM) presented tandem characterizations utilizing two separate asymmetrical flow FFF systems, one of which was hyphenated with ICP-MS [55]. Worms et al. observed that WWTP effluent organic matter is sometimes the primary contributor to the pool of organic matter in urban water systems, and that there is little information on how it differs from natural organic matter in terms of reactivity and metal complexation. The effluent COM (EfCOM) was characterized for composition, chemical properties, molar mass distributions, and metal associations and additional metal binding capacity, and compared to lake NOM. While an asymmetrical flow FFF-MALS-UV system measured the COM size distributions, the metal binding was measured by the second FFF-MALS-UV-ICP-MS. Metal binding was measured before and after spiking EfCOM samples with Cd, Cu, and Pb. The spikes increased the Cd-OM complex signal, but not the Cu or Pb complexes. Further characterizations (LC with online TOC, UV, and FL detectors) showed a humic-like fraction with low aromaticity that was most of the EfCOM. In general,

Ag, Cd, Cu, Cr, Mn and Zn associated with low molecular weight COM and Al, Fe, and Pb with low to high molecular weight fractions.

Bolea et al. used asymmetrical flow FFF-ICP-MS in both steric and normal modes to measure metal binding to a compost leachate derived from urban solid residues [56]. By taking advantage of two separation modes, the authors were able to analyze microparticles (greater than 1 μm), colloids (15 nm to 1 μm), and macromolecules (less than 1,000 kDa). For most of the analyzed elements (all but Ag, Co, Cu, Mo, and Ni), more than 50% was associated with the particulate fraction. Less than 10% of every element was associated with the nanocolloidal fraction. The remainder of the mass was associated with the macromolecular fraction; for the elements noted as exceptions to the general trend, the amount complexed to macromolecules was more than half. The authors also note an advantage of the normal/steric combination method: eliminating the need for prefiltering, which can create artifacts and precludes quantification of the particulate fraction by FFF-ICP-MS.

Laborda et al. use similar methods to Bolea et al., but applied the asymmetrical FFF-ICP-MS to establish isotope ratios in an isotope dilution study [57]. Isotope dilution allows for the measurement of the exchangeability of metals between the aqueous phase and in this case that bound to the organic matter of a compost leachate. This is the first application of FFF-ICP-MS to an isotope dilution study, and it required significant optimization of ICP-MS to capture the transient isotope ratios. The authors did not see a difference in the Pb or Cu isotope ratios across the size range, but show that it is feasible to measure this effect.

Diaz et al. investigated nanoparticles in the Great Salt Lake, Utah, where due to high TDS, one might expect a substantial colloidal fraction [36]. These natural nanoparticles may act as vectors, transporting trace elements through the food web eventually to the large population of birds. The hypersaline environment creates permanent layers in the lake: an oxic and an anoxic zone. The authors hypothesized the two layers would support different colloidal populations. The hypothesis was tested by asymmetrical flow FFF-ICP-MS, using two fractionation protocols: one with a stronger field for the 0.9–7.5 nm range, and a second with a weaker field for the 10–250 nm range. More than 50% of the mass of Al, Fe, and Pb was particle-associated. Cu, Zn, Mn, Co, Au, Hg, and U were also associated with particles to a lesser degree. Interesting size-related trends were uncovered, such as that Hg was mostly associated with <2 nm NPs, and concentrations increased with depth, indicating possible complexation with DOC. Arsenic was also associated with <2 nm NP, but did not increase with depth, possibly pointing towards the presence of arsenite NP.

Plathe et al. characterized the NNP present in the sediments associated with the polluted Clark Fork River Superfund Site by asymmetrical flow FFF-MALS-UV-ICP-MS [58]. Beyond the very thorough characterization, an important outcome of this paper is the publication of a method to extract colloids from sediment that builds on the dissertation work of von der Kammer [59]. Here, the internal standard and nitric acid met the FFF effluent at a T before entering the ICP. This interface also served as an introduction port for the calibration standards.

The study found that toxic trace metals are bound to Fe- and Ti- containing nanoparticles.

Samples from the lower Mississippi region were characterized by symmetrical flow FFF-ICP-MS with UV and fluorescence (FL) detectors by Stolpe et al.; the result was the identification of four unique colloidal populations with varying degrees of metal binding capacity [60]. Monitoring a variety of FL excitation/emission wavelengths allowed for the distinction between humic substances of terrestrial origin and biogenic protein-like colloids. The authors observed that colloidal concentrations decreased gulf-ward, and size distributions of protein-like colloids and Fe colloids vary from river to river, likely a result of different influences of allochthonous and autochthonous colloidal inputs. Most metals peak in the humic region, indicating metallo-organic complexes, although Fe, P, Mn, and Pb associate with larger colloids, likely Fe bearing ones. In summation, the authors note that high-DOC, low alkalinity systems support a greater concentration of Fe-colloids, though they are smaller in size, when compared to moderate DOC, high alkalinity rivers. The work builds on similar characterizations and methods of European streams and estuaries by Stolpe, Hassellov, and coworkers [61–65].

A paper by Gelting et al. also builds on the older FFF-ICP-MS work cited above, but further incorporates iron isotope data, numerous sampling time points, and a sediment trapping experiment to put together a comprehensive story on the transport of Fe-colloids, association with trace metals, and the effect of salinity gradients in marine systems [66]. The authors measured aggregation as a function of salinity by sampling in various locations in the Baltic Sea. The research was motivated by the ecological concerns: nitrogen fixing cyanobacteria have been shown to have high Fe requirements, and thus algal blooms may be dependent to some degree on Fe-colloid transformations. Gelting et al. also relied on the methods developed by Hassellov, Stolpe, and coworkers [61, 63]. The results show that Fe and fulvic acids co-occurred and were the most significant colloids.

Krachler et al. asked the question, "can peat bog-derived colloidal iron endure estuarine flocculation to contribute significantly to the oceanic dissolved Fe pool?" [67]. A number of papers have looked at riverine and terrestrial Fe-colloids, but the authors hypothesized the dramatically greater fulvic content of bog water induces the Fe to exist bound as ions or very small nanoparticles to bog humic substances. They used asymmetrical flow FFF-ICP-MS to measure the distribution of Fe colloids, and perform field mixing experiments to mimic the effect of increasing salinity on the bog water. The FFF-ICP-MS results showed that most of the Fe is indeed in the humic region in contrast to rivers where a large fraction of the Fe exists as $>$10 kDa inorganic particles. The mixing experiment showed that these Fe-organic colloids are less susceptible to flocculation. Projecting the mixing experiment results to 100% seawater, they predicted 22% of the iron to stay in solution.

Stolpe and Hassellov also published the first FFF-ICP-MS characterization of environmental nanofibrils, along with three other populations of colloids [68]. Colloidal fibrils are long, string-like polysaccharide-rich particles capable of

binding metals [69]. The populations were characterized by asymmetrical flow FFF-ICP-MS with UV and FL detections, atomic force microscopy, and a staining method to quantify planktonic exudates (transparent exopolymer particles, TEP). An isotope spiking experiment also explained metal partitioning among the colloidal populations.

17.4 Conclusion

The recent increase in publications (18 reviewed here in less than 2 years) using FFF with elemental detection, most commonly ICP-MS, shows that the method is practical, effective, and adaptable to many different types of studies. The studies show that FFF methods can be used quantitatively or qualitatively, depending on the goals of the study. FFF methods have fractionated a variety of nano-sized particles and macromolecules: TiO_2, Ag, derivatized clay, synthetic and natural iron oxides, Be minerals, soil and compost leachates, and organic matter from WWTP effluent, lakes, bogs, streams, and seawater. Hyphenated FFF has been used to address questions of NP size distribution, stability, toxicity, migration from composite material, impacts on human health, and effect on metal speciation and transport. Still, there are outstanding questions and issues to be resolved.

Regarding methodology, a number of instrumentation setups, standardization procedures, and choices regarding mobile phase composition and sample preparation, have been presented in the work reviewed. The versatility that defines FFF as a valuable analytical technique can also make optimization for diverse environmental samples a challenge. One set of conditions is not universally superior to another, rather the best conditions depend on the samples and the goals of the study. Still, a goal for environmental FFF researchers should be to communicate best practices and results for optimizing systems, and also determine how to best measure, describe, and communicate detection limits and recoveries (both in the FFF fractionation step, and the ICP-MS analysis), both being critical elements of quantitative analysis by FFF-ICP-MS.

A number of fundamental questions still exist regarding the role FFF methods may play in studies on both engineered and natural nanomaterials. For engineered nanoparticles, future topics of research include the role of coatings in stability and biological effects; the degree to which aggregation and dissolution can be monitored by FFF methods; and investigations into the lowest detectable concentrations for each type of ENP and whether that value is environmentally relevant. For natural nanoparticles, future topics of research include the degree to which the method can be used to quantitatively measure metal-particle interactions and how the measurement itself might affect the sample. As these fundamental questions are addressed, FFF methods will continue to impact a variety of fields via novel applications.

References

1. Taniguchi N (1974) On the basic concept of nanotechnology. Proceedings from the International Conference on Production Engineering, Japan Society of Precision Engineering, Tokyo
2. Zsigmondy R (1914) Colloids and the ultramicroscope: a manual of colloid chemistry and ultramicroscopy, 1st edn. Wiley, New York
3. Binnig G, Rohrer H, Gerber C et al (1982) Surface studies by scanning tunneling microscopy. Phys Rev Lett 49:57–61
4. Burleson DJ, Driessen MD, Penn RL (2005) On the characterization of environmental nanoparticles. J Environ Sci Health A 39:2707–2753
5. Maynard A (2008–2011) Characterization matters. The Minimum Information for Nanomaterial Characterization (MINChar) Initiative. http://characterizationmatters.org/. Accessed 1 Feb 2011
6. Beckett R (1991) Field-flow fractionation-ICP-MS - a powerful new analytical tool for characterizing macromolecules and particles. At Spectrosc 12:228–232
7. Murphy DM, Garbarino JR, Taylor HE et al (1993) Determination of size and element composition distributions of complex colloids by sedimentation field-flow fractionation inductively-coupled plasma-mass spectrometry. J Chromatogr 642:459–467
8. Nowack B, Bucheli TD (2007) Occurrence, behavior and effects of nanoparticles in the environment. Environ Pollut 150:5–22
9. Mueller NC, Nowack B (2008) Exposure modeling of engineered nanoparticles in the environment. Environ Sci Technol 42:4447–4453
10. Gottschalk F, Scholz RW, Nowack B (2010) Probabilistic material flow modeling for assessing the environmental exposure to compounds: methodology and an application to engineered nano-TiO_2 particles. Environ Model Softw 25:320–332
11. Gottschalk F, Sonderer T, Scholz RW et al (2009) Modeled environmental concentrations of engineered nanomaterials (TiO_2, ZnO, Ag, CNT, fullerenes) for different regions. Environ Sci Technol 43:9216–9222
12. Nowack B (2009) Is anything out there?: what life cycle perspectives of nano-products can tell us about nanoparticles in the environment. Nano Today 4:11–12
13. Blaser SA, Scheringer M, MacLeod M et al (2008) Estimation of cumulative aquatic exposure and risk due to silver: contribution of nano-functionalized plastics and textiles. Sci Total Environ 390:396–409
14. Hassellöv M, Readman J, Ranville J et al (2008) Nanoparticle analysis and characterization methodologies in environmental risk assessment of engineered nanoparticles. Ecotoxicology 17:344–361
15. Mavrocordatos D, Perret D (1998) Quantitative and qualitative characterization of aquatic iron oxyhydroxide particles by EF TEM. J Microsc 191:83–90
16. Leppard G, Mavrocordatos D, Perret D (2004) Electron-optical characterization of nano-and micro-particles in raw and treated waters: an overview. Water Sci Technol 50:1
17. Song Y, Jimenez V, McKinney C et al (2003) Estimation of size for 1–2 nm nanoparticles using an HPLC electrochemical detector of double layer charging. Anal Chem 75:5088–5096
18. Scrivens WA, Tour JM, Creek KE et al (1994) Synthesis of 14 C-labeled C60, its suspension in water, and its uptake by human keratinocytes. J Am Chem Soc 116:4517–4518
19. Lyon DY, Adams LK, Falkner JC et al (2006) Antibacterial activity of fullerene water suspensions: effects of preparation method and particle size. Environ Sci Technol 40:4360–4366
20. Powers KW, Palazuelos M, Moudgil BM et al (2007) Characterization of the size, shape, and state of dispersion of nanoparticles for toxicological studies. Nanotoxicology 1:42–51
21. Jamison JA, Krueger KM, Mayo J et al (2009) Applying analytical ultracentrifugation to nanocrystal suspensions. Nanotechnology 20:355702
22. Howell KA, Achterberg EP, Tappin AD et al (2006) Colloidal metals in the Tamar estuary and their influence on metal fractionation by membrane filtration. Environ Chem 3:199–207
23. Akthakul A, Hochbaum AI, Stellacci F et al (2005) Size fractionation of metal nanoparticles by membrane filtration. Adv Mater 17:532–535

24. Powell CJ, Seah MP (1990) Precision, accuracy, and uncertainty in quantitative surface analyses by auger-electron spectroscopy and x-ray photoelectron spectroscopy. J Vac Sci Technol A 8:735–763
25. Liu J (2005) Scanning transmission electron microscopy and its application to the study of nanoparticles and nanoparticle systems. J Electron Microsc 54:251–278
26. Petosa AR, Jaisi DP, Quevedo IR et al (2010) Aggregation and deposition of engineered nanomaterials in aquatic environments: role of physicochemical interactions. Environ Sci Technol 44:6532–6549
27. Bootz A, Vogel V, Schubert D et al (2004) Comparison of scanning electron microscopy, dynamic light scattering and analytical ultracentrifugation for the sizing of poly(butyl cyanoacrylate) nanoparticles. Eur J Pharm Biopharm 57:369–375
28. Pace H, Lesher E, Ranville J (2010) Influence of stability on the acute toxicity of CdSe/ZnS nanocrystals to *Daphnia magna*. Environ Toxicol Chem 29:1338–1344
29. Mitrano DM, Lesher EK, Bednar AJ et al (2011) Detection of nano-Ag using single particle inductively coupled plasma mass spectrometry. Environ Toxicol Chem (in press)
30. Mitrano DM, Pace HE (2011) Sizing of inorganic nanoparticles by SP-ICP-MS (Unpublished work)
31. Poda AR, Bednar AJ, Kennedy AJ et al (2011) Characterization of silver nanoparticles using flow-field-flow fractionation interfaced to inductively coupled plasma mass spectrometry. J Chromatogr 1218:4219–4225
32. Schimpf ME (2000) Resolution and fractionating power. In: Schimpf ME, Caldwell K, Giddings JC (eds) Field-flow fractionation handbook. Wiley-Interscience, New York
33. Giddings C (1968) Nonequilibrium theory of field-flow fractionation. J Chem Phys 49:81–85
34. Giddings J, Caldwell K (1989) Field-flow fractionation. In: Rossiter BW, Hamilton JF (eds) Physical methods of chemistry, volume 3, part b, determination of chemical composition and molecular structure. Wiley-Interscience, New York
35. Lesher E (2009) Carrier fluid optimization for FFF separation of hematite nanoparticles (Unpublished work)
36. Diaz X, Johnson W, Fernandez D et al (2009) Size and elemental distributions of nano-to microparticulates in the geochemically-stratified great salt lake. Appl Geochem 24:1653–1665
37. Huang W, Fernandez D, Rudd A et al (2011) Dissolution and nanoparticle generation behavior of Be-associated materials in synthetic lung fluid using inductively coupled plasma mass spectroscopy and flow field-flow fractionation. J Chromatogr 1218:4149–4159
38. Dubascoux S, Le Hecho I, Hassellov M et al (2010) Field-flow fractionation and inductively coupled plasma mass spectrometer coupling: history, development and applications. J Anal At Spectrom 25:613–623
39. Lesher EK, Ranville JF, Honeyman BD (2009) Analysis of pH dependent uranium(VI) sorption to nanoparticulate hematite by flow field-flow fractionation – inductively coupled plasma mass spectrometry. Environ Sci Technol 43:5403–5409
40. Siripinyanond A, Barnes RM (2002) Flow field-flow fractionation-inductively coupled plasma mass spectrometry of chemical mechanical polishing slurries. Spectrochim Acta B At Spectrosc 57:1885–1896
41. Bouby M, Geckeis H, Geyer F (2008) Application of asymmetric flow field-flow fractionation (AsFlFFF) coupled to inductively coupled plasma mass spectrometry (ICPMS) to the quantitative characterization of natural colloids and synthetic nanoparticles. Anal Bioanal Chem 392:1447–1457
42. Benedetti MF, Ranville JF, Allard T et al (2003) The iron status in colloidal matter from the Rio Negro, Brasil. Colloids Surf Physicochem Eng Aspects 217:1–9
43. Contado C, Pagnoni A (2008) TiO_2 in commercial sunscreen lotion: flow field-flow fractionation and ICP-AES together for size analysis. Anal Chem 80:7594–7608
44. Contado C, Pagnoni A (2010) TiO_2 nano-and micro-particles in commercial foundation creams: field-flow-fractionation techniques together with ICP-AES and SQW voltammetry for their characterization. Anal Methods 2:1112–1124

45. Songsilawat K, Shiowatana J, Siripinyanond A (2011) Flow field-flow fractionation with off-line electrothermal atomic absorption spectrometry for size characterization of silver nanoparticles. J Chromatogr 1218:4213–4218
46. Tadjiki S, Assemi S, Deering C et al (2009) Detection, separation, and quantification of unlabeled silica nanoparticles in biological media using sedimentation field-flow fractionation. J Nanopart Res 11:981–988
47. Stone V, Nowack B, Baun A et al (2010) Nanomaterials for environmental studies: classification, reference material issues, and strategies for physico-chemical characterisation. Sci Total Environ 408:1745–1754
48. Warheit D (2008) How meaningful are the results of nanotoxicity studies in the absence of adequate material characterization? Toxicol Sci 101:183
49. Rameshwar T, Samal S, Lee S et al (2006) Determination of the size of water-soluble nanoparticles and quantum dots by field-flow fractionation. J Nanosci Nanotechnol 6:2461–2467
50. Schmidt B, Petersen J, Bender Koch C et al (2009) Combining asymmetrical flow field-flow fractionation with light-scattering and inductively coupled plasma mass spectrometric detection for characterization of nanoclay used in biopolymer nanocomposites. Food Addit Contam A 26:1619–1627
51. Trenfield MA, McDonald S, Kovacs K et al (2011) Dissolved organic carbon reduces uranium bioavailability and toxicity. Part 1: Characterisation of aquatic fulvic acid and its complexation with uranium[VI]. Environ Sci Technol (accepted)
52. Trenfield MA, Ng JC, Noller BN et al (2011) Dissolved organic carbon reduces uranium bioavailability and toxicity. Part 2: Uranium[VI] speciation and toxicity to three tropical freshwater organisms. Environ Sci Technol 45:3075–3081
53. Claveranne-Lamolère C, Lespes G, Dubascoux S et al (2009) Colloidal transport of uranium in soil: size fractionation and characterization by field-flow fractionation-multi-detection. J Chromatogr 1216:9113–9119
54. Dubascoux S, Le Hecho I, Potin Gautier M et al (2008) On-line and off-line quantification of trace elements associated to colloids by As-Fl-FFF and ICP-MS. Talanta 77:60–65
55. Worms I, Al-Gorani Szigeti Z, Dubascoux S et al (2010) Colloidal organic matter from wastewater treatment plant effluents: characterization and role in metal distribution. Water Res 44:340–350
56. Bolea E, Laborda F, Castillo J (2010) Metal associations to microparticles, nanocolloids and macromolecules in compost leachates: size characterization by asymmetrical flow field-flow fractionation coupled to ICP-MS. Anal Chim Acta 661:206–214
57. Laborda F, Ruiz-Begueria S, Bolea E et al Study of the size-based environmental availability of metals associated to natural organic matter by stable isotope exchange and quadrupole inductively coupled plasma mass spectrometry coupled to asymmetrical flow field-flow fractionation. J Chromatogr (in press, accepted manuscript)
58. Plathe KL, von der Kammer F, Hassellov M et al (2009) Using flfff and atem to determine trace metal-nanoparticle associations in riverbed sediment. Environ Chem 7:82–93
59. von der Kammer F (2004) Characterization of environmental colloids applying field-flow fractionation: multi detection analysis with emphasis on light scattering techniques. Dissertation, Hamburg University of Technology
60. Stolpe B, Guo LD, Shiller AM et al (2010) Size and composition of colloidal organic matter and trace elements in the Mississippi River, Pearl River and the northern Gulf of Mexico, as characterized by flow field-flow fractionation. Mar Chem 118:119–128
61. Hassellov M, Lyven B, Haraldsson C et al (1999) Determination of continuous size and trace element distribution of colloidal material in natural water by on-line coupling of flow field-flow fractionation with ICPMS. Anal Chem 71:3497–3502
62. Stolpe B, Hassellov M (2007) Changes in size distribution of fresh water nanoscale colloidal matter and associated elements on mixing with seawater. Geochim Cosmochim Acta 71:3292–3301

63. Stolpe B, Hassellov M, Andersson K et al (2005) High resolution ICPMS as an on-line detector for flow field-flow fractionation; multi-element determination of colloidal size distributions in a natural water sample. Anal Chim Acta 535:109–121
64. Dahlqvist R, Benedetti MF, Andersson K et al (2004) Association of calcium with colloidal particles and speciation of calcium in the kalix and amazon rivers. Geochim Cosmochim Acta 68:4059–4075
65. Lyven B, Hassellov M, Turner DR et al (2003) Competition between iron- and carbon-based colloidal carriers for trace metals in a freshwater assessed using flow field-flow fractionation coupled to ICPMS. Geochim Cosmochim Acta 67:3791–3802
66. Gelting J, Breitbarth E, Stolpe B et al (2009) Fractionation of iron species and iron isotopes in the Baltic sea euphotic zone. Biogeosci Discuss 6:6491–6537
67. Krachler R, Krachler RF, von der Kammer F et al (2010) Relevance of peat-draining rivers for the riverine input of dissolved iron into the ocean. Sci Total Environ 408:2402–2408
68. Stolpe B, Hassellov M (2010) Nanofibrils and other colloidal biopolymers binding trace elements in coastal seawater: significance for variations in element size distributions. Limnol Oceanogr 55:187–202
69. Leppard GG (1995) The characterization of algal and microbial mucilages and their aggregates in aquatic ecosystems. Sci Total Environ 165:103–131

Index

S.K.R. Williams and K.D. Caldwell (eds.), *Field-Flow Fractionation in Biopolymer Analysis*, DOI 10.1007/978-3-7091-0154-4, © Springer-Verlag/Wien 2012